

**Characterization, Stabilization and Formulation Design of IgG and Secretory IgA  
Monoclonal Antibody Candidates during Storage and Administration**

By

© 2019

Yue Hu

Submitted to the graduate degree program in Pharmaceutical Chemistry and the  
Graduate Faculty of the University of Kansas in partial fulfillment of the requirements for  
the degree of Doctor of Philosophy.

---

Chairperson: David B. Volkin, Ph.D

---

David D. Weis, Ph.D

---

Teruna Siahaan, Ph.D

---

Michael Hageman, Ph.D

---

Roberto N. De Guzman, Ph.D

Date Defended: 02/19/2019

The Dissertation Committee for Yue Hu

certifies that this is the approved version of the following dissertation:

**Characterization, Stabilization and Formulation Design of IgG and Secretory IgA  
Monoclonal Antibody Candidates during Storage and Administration**

---

Chairperson: David B. Volkin, Ph.D

Date Defended: 02/19/2019

## ABSTRACT

Monoclonal antibodies (mAbs) have become a class of therapeutic protein-based drugs of high importance for treating numerous human diseases. As a complex, delicate three dimensional molecule, a mAb can be sensitive to ambient environments and thus often display colloidal/conformational instability during manufacturing, storage, and administration. The use of formulation strategies, such as employing specific excipients and/or particular solution conditions (e.g., pH and buffers), can significantly improve a mAb's pharmaceutical stability properties. In this Ph.D. thesis research work, both formulation/storage stability as well as stability during *in vitro* models of mAb administration *in vivo* are evaluated with two different of classes of immunoglobulin molecules (IgG and IgA). In addition, the effect of specific classes of excipients and solution conditions are examined by using a wide variety of physicochemical and immunological binding analytical techniques.

Specifically, the second and third chapters of the Ph.D. thesis work focus on the formulation development of high-concentration mAb dosage forms for subcutaneous (SC) injections. Reversible self-association (RSA) of mAbs, which is primarily due to intermolecular protein-protein interactions (PPIs) between mAb molecules, has emerged as an important formulation challenge in terms of significantly increasing solution viscosity and turbidity as well as initiating phase separation. In these two chapters, two different human IgG1 molecules (mAb-J and mAb-C), which showed strong RSA propensity at relatively high protein concentrations, were comprehensively studied to better understand their solution properties and molecular behaviors by both biophysical techniques as well as hydrogen-deuterium exchange mass spectrometry (HX-MS). The aim is to not only

characterize mAb molecular properties and solution behavior at relatively high protein concentrations, but also to develop a better mechanistic understanding by identifying peptide segments within the mAb involved PPIs in solution.

In these two studies, both elevated solution viscosity and turbidity as well as reduced relative solubility and increased protein-protein interaction propensity (as measured by light scattering profiles and observations of phase separation) were determined for two different mAbs (mAb-J and mAb-C) at comparatively high protein concentrations. Concomitantly, based on the amino acid sequence of each mAb's RSA sites (as determined by lyophilization-reconstitution-based HX-MS methodology), two different dominant non-covalent forces (electrostatic and hydrophobic) are proposed to be the major driving force for PPIs of the two different mAbs (consistent with previous results). More importantly for this work, varying effects of different excipients were investigated particularly for their ability to promote or disrupt PPIs of each mAb. For mAb-J (electrostatic driven RSA), selected ionic excipients showed the ability to disrupt liquid-liquid phase separation and reduce intermolecular interactions to varying extents, with arginine hydrochloride possessing the highest efficiency. For mAb-C (hydrophobic driven RSA), opposing effects were observed for sodium sulfate versus selected hydrophobic additives (e.g., specific salts, amino acids, solvents), showing both enhanced and reduced PPI propensity, respectively. In both studies, not only was the RSA of mAbs shown to be mAb concentration dependent, but the excipient's ability to mitigate the RSA of mAbs RSA also displayed an excipient concentration dependent pattern.

The fourth chapter focuses on the possibility of using various classes of mAbs, including secretory IgA (sIgA) and IgG1, as potential drug candidates for oral delivery to

prevent enteric diseases in infants. Specifically, the use of mAbs against enterotoxigenic *Escherichia coli* (ETEC) is examined with the idea that passive immunization by pathogen-specific immunoglobulins, by oral delivery to infants, is promising approach to provide “instant” protection against ETEC. Secretory IgA (sIgA) is of particular interest because it is naturally found in the mucosal surfaces within the GI tract, is relatively more resistant to proteolysis by digestive enzymes (vs. IgG), and can protect against enteric bacteria by directly neutralizing virulence factors. In this study, three different mAbs, (sIgA1, sIgA2 and IgG1) against heat labile toxin (LT, one of the major virulence factors of ETEC), were used as a model for developing analytical techniques to characterize the structural integrity of the mAbs and to assess their stability profiles under various solution conditions (using physicochemical and immunochemical binding assays).

In this work, very different total carbohydrate levels and N-linked glycosylation oligosaccharide composition profiles were observed between sIgAs and IgG1 made from CHO cell lines. According to SDS-PAGE, SE-HPLC, and SV-AUC results, heterogeneous mixtures of higher molecular weight species were observed for sIgAs, while IgG1 samples showed less heterogeneity with more than 90% monomer in solution. The overall physical stability results at both pH 7.2 and pH 3.0 demonstrated that both sIgA1 and sIgA2 were more stable than IgG1, with sIgA1 displaying the best stability profile. The relative solubility profile of each molecule was pH dependent with higher solubility noted at the lower pH. Furthermore, an *in vitro* digestion model was adapted in the laboratory to mimic *in vivo* oral gastric degradation conditions using minimal material, and was utilized to monitor the oral delivery stability of the three mAbs. It was shown that F(ab')<sub>2</sub> was the major digestion product by pepsin digestion. Both sIgAs displayed better resistance to

degradation by proteases at low pH compared to IgG1. Moreover, the sIgAs showed greater retention of LT-antigen binding activity than that of IgG1, confirming the superior pharmaceutical properties of sIgAs for oral delivery. In summary, we hope to use the information gained by these preformulation characterization studies for the long-term goal to design stable, low-cost liquid formulations for oral delivery of sIgAs to protect against enteric diseases currently affecting infants in the developing world.

*Lovingly dedicated to*

*my family*

*especially my parents*

*Defu Hu & Rongmei Wang*

*and*

*my beloved wife*

*Xin Hu*

## ACKNOWLEDGEMENTS

Completion of this doctoral research and PhD thesis has been a truly life-changing experience for me and it could not have been possible without tremendous guidance and valuable contributions of a lot of scientists at the University of Kansas (KU) and collaborating companies/institutes.

I would first and foremost like to express my sincere gratitude and extreme thanks to my Ph.D. thesis advisor, Dr. David Volkin. It was really a fruitful time working with him in the past four and half years. My PhD work could not have been finished successfully without his invaluable advice, scholarly inputs, consistent inspiration and encouragement. I am very grateful to him for not only providing me different projects for my thesis, but also inspiring me to collaborate with various companies and institutes, pushing me to do my best, and more importantly, leading me to become a better scientist and researcher. I also want to sincerely thank Dr. David Weis for his scientific guidance and sustained support in last several years. His work ethics, skills on presentation and interpretation of scientific results, and thirst for knowledge set a great example for me and will be useful throughout my scientific career. I would like to thank Dr. Teruna Siahaan, Dr. Michael Hageman, and Dr. Roberto De Guzman for serving as members of my thesis committee and providing their valuable time to review my thesis research. Their insightful feedback and scientific inputs have greatly helped me to complete my thesis dissertation.

I want to extend my sincere appreciation to Dr. Sangeeta Joshi, director of Macromolecular and Vaccine Stabilization Center (MVSC), for her scientific guidance and consistent research inputs, as well as her encouragement, and patience towards me. I



thank her for her enthusiasm, friendship, and great advice. I also thank her for always being there to support me. It was an absolute pleasure to work with her in past few years. I also thank Dr. Russ Middaugh for imparting his scientific knowledge, always encouraging to think outside the box, and his coursework on protein biophysics, advanced technologies and pharmaceutical equilibrium. I have learned a lot from him about protein chemistry and physics, scientific writing, and critical thinking. In addition, I would like to thank Dr. Ozan Kumru and Dr. John Hickey for their scientific feedback, advice, and discussions for my thesis research. I thank Dr. Ronald Toth, Dr. Jian Xiong and Dr. Jayant Arora for their various contributions and suggestions throughout my PhD research. I thank Dr. Yangjie Wei for scientific discussions on varying topics and friendship. I would also like to thank all the present and past MVSC members and Weis's group members for their friendship and direct/indirect contributions to my scientific journey at KU. I want to acknowledge my financial support from MedImmune Inc. and Bill and Melinda Gates Foundation for my thesis research work.

Last but not least, I would love to thank my parents for their incredible support by giving me help, strength, and encouragement. I value their love, best wishes and contributions. I thank them for always being there for me. Without them, I would not have this opportunity to get a better education in the United States. I want to express special appreciation to my wife, Xin Hu, who has been an excellent source of inspiration, encouragement, patience, and help. I very much appreciate her love, company and support through my ups and downs during my scientific career. I dedicate this accomplishment to my parents and my wife.

# TABLE OF CONTENTS

## Chapter 1. Introduction

1.1. Overview of Classes of Immunoglobulin.....	2
1.1.1. General Description of 5 Immunoglobulin classes.....	2
1.1.2. Brief Introduction of IgG and IgA.....	5
1.1.3. Structure and Function of IgM, IgD, and IgE.....	5
1.2. More Detailed Description of Physicochemical and Biological Properties of IgG Class .....	8
1.2.1. Basic Structure.....	8
1.2.1.1. Chain Composition and Molecular Weight .....	9
1.2.1.2. Glycosylation.....	10
1.2.2. Body Distribution and Percentage Level .....	13
1.2.3. IgG Subclasses .....	13
1.2.4. Biological Functions.....	16
1.3. More Detailed Description of Physicochemical and Biological Properties of IgA Class.....	17
1.3.1. Basic Structure.....	17
1.3.1.1. Chain Composition and Molecular Weight .....	17
1.3.1.2. Glycosylation.....	19
1.3.2. Body Distribution and Percentage Level .....	21
1.3.3. IgA Subclasses .....	21
1.3.4. Biological Functions.....	22

1.4. Formulation Development Challenges and Opportunities for IgG as Therapeutic mAb Candidate.....	24
1.4.1. Administration Pathway.....	25
1.4.1.1. Intravenous Injection.....	26
1.4.1.2. Subcutaneous Injection.....	26
1.4.2. Reversible Self-Association Induced by High-Concentration Solution.....	27
1.4.2.1. Viscosity.....	27
1.4.2.2. Opalescence.....	28
1.4.2.3. Aggregation.....	29
1.4.2.4. Phase Separation.....	30
1.4.3. Strategy to Mitigate Reversible Self-Association.....	31
1.4.3.1. Formulation.....	32
1.4.3.2. Engineering.....	33
1.4.3.3. Lyophilization.....	34
1.4.3.4. Use of Recombinant Human Hyaluronidase Enzyme.....	35
1.5. Formulation Development Challenges and Opportunities for sIgA as Therapeutic mAb Candidate.....	36
1.5.1. High Molecular Species Formation in Solution.....	37
1.5.2. Challenges Associated with Oral Protein Delivery.....	37
1.5.2.1. Gastric pH.....	38
1.5.2.2. Proteases .....	39
1.5.2.3. Absorption.....	39
1.5.3. Mucosa Compartment as an “Ideal” Place for sIgA-based Treatments...41	

1.5.3.1. Diarrheal Diseases.....	41
1.5.4. Formulation Approaches for Oral Delivery of sIgA.....	43
1.5.4.1. Protease Inhibitors.....	43
1.5.4.2. Buffers or Reagents for Gastric pH Neutralization.....	44
1.5.4.3. Novel Mucoadhesive Carrier Systems.....	45
1.5.4.4. “Decoy” Protein Protection .....	46
1.6. References.....	47

**Chapter 2. Characterization of Excipient Effects on Reversible Self-association, Backbone Flexibility, and Solution Properties of an IgG1 Monoclonal Antibody at High Concentrations: Part 1**

2.1. Introduction.....	57
2.2. Materials and Methods.....	60
2.2.1. Sample Preparation.....	60
2.2.2. Solution Appearance Study.....	61
2.2.3. Ultraviolet Absorption Spectroscopy.....	61
2.2.4. Turbidity Measurements.....	61
2.2.5. Dynamic Light Scattering.....	62
2.2.6. Viscosity Measurements.....	63
2.2.7. Composition-Gradient Multi-Angle Light Scattering (CG-MALS).....	63
2.2.8. PEG-Induced Precipitation Study.....	64
2.2.9. Lyophilization of mAb-J Samples.....	64
2.2.10. Size Exclusion Chromatography (SEC).....	65
2.2.11. Karl-Fischer Titration.....	66
2.2.12. Deuteration of Excipients (Amino Acids).....	66

2.2.13. Hydrogen Exchange-Mass Spectrometry (HX-MS).....	66
2.2.14. HX-MS Data Processing and Analysis.....	68
2.3. Results.....	68
2.3.1. Solution Properties of mAb-J in the Absence/Presence of Excipients.....	69
2.3.2. Physical Properties of mAb-J in the Absence/Presence of Excipients.....	71
2.3.3. HX-MS Reveals the Effects of Excipients on RSA Disruption and Changes of Local Dynamics for mAb-J.....	74
2.4. Discussion.....	79
2.4.1. Effect of Five Excipients on Solution Properties of mAb-J.....	81
2.4.2. HX-MS Analysis of Effect of Five Excipients on Sites of RSA in mAb-J...83	
2.4.3. Effect of Five Excipients on Properties of mAb-J.....	85
2.4.4. Comparative Results in Companion Paper with Different IgG1 mAb.....	88
2.5. References.....	90
2.6. Figures and Tables.....	96

**Chapter 3. Characterization of Excipient Effects on Reversible Self-association, Backbone Flexibility, and Solution Properties of an IgG1 Monoclonal Antibody at High Concentrations: Part 2**

3.1. Introduction.....	113
3.2. Materials and Methods.....	116
3.2.1. Materials.....	116
3.2.2. Ultraviolet Absorption Spectroscopy.....	117
3.2.3. Viscosity Measurements.....	118
3.2.4. Hydrodynamic Diameter Measurements by DLS.....	118
3.2.5. Protein Interaction Parameter ( $k_{D2}$ ) by DLS .....	119

3.2.6. Composition-Gradient Multi-Angle Light Scattering (CG-MALS).....	120
3.2.7. PEG-Induced Precipitation Assay.....	121
3.2.8. Lyophilization of mAb-C Samples.....	123
3.2.9. Size Exclusion Chromatography (SEC).....	124
3.2.10. Karl-Fischer Titration.....	124
3.2.11. Circular Dichroism (CD).....	125
3.2.12. Excipients Deuteration.....	125
3.2.13. Hydrogen Exchange-Mass Spectrometry (HX-MS).....	126
3.2.14. HX-MS Data Processing and Analysis.....	127
3.2.15. Homology Modeling and Protein-Additive Docking.....	127
3.3. Results.....	128
3.3.1. Excipient Effects on Solution Properties of mAb-C.....	128
3.3.2. Excipient Effects on Molecular Behavior of mAb-C.....	129
3.3.3. Alteration of mAb-C RSA Propensity by Excipients Measured by HX-MS.....	133
3.4. Discussion.....	137
3.4.1. Effects of Hydrophobic (TMPAI and TrpNH <sub>2</sub> HCl) and Chaotropic (GdnHCl) Salts on RSA of mAb-C.....	139
3.4.2. Effects of Ethanol on RSA of mAb-C.....	141
3.4.3. Effects of Na <sub>2</sub> SO <sub>4</sub> on RSA of mAb-C .....	143
3.5. Conclusions.....	144
3.6. References.....	146
3.7. Figures and Tables.....	151

## **Chapter 4. Structure Characterization and Stability Assessments of Secretory IgA Monoclonal Antibodies as Potential Candidates for Passive Immunization by Oral Administration**

4.1. Introduction.....	168
4.2. Materials and Methods.....	170
4.2.1. Sample Preparation.....	171
4.2.2. Sodium Dodecyl Sulfate Polyacrylamide Gel Electrophoresis.....	171
4.2.3. Size Exclusion Chromatography (SEC).....	172
4.2.4. Sedimentation Velocity Analytical Ultracentrifugation (SV-AUC).....	173
4.2.5. LC-MS Peptide Mapping.....	173
4.2.6. Total Carbohydrate Analysis.....	175
4.2.7. N-Glycan Oligosaccharide Analysis.....	175
4.2.8. Conformational Stability Assessments.....	176
4.2.9. Relative Protein Solubility (Polyethylene Glycol Precipitation Assay).....	177
4.2.10. In vitro Model of Gastric Digestion.....	178
4.2.11. Immobilized Pepsin Digestion.....	179
4.2.12. Enzyme-Linked Immunosorbent Assay (ELISA).....	179
4.3. Results.....	180
4.3.1. Characterization of Purity, Primary Structure and Post-translational Modifications of sIgA vs. IgG mAbs.....	180
4.3.2. Characterization of Size and Aggregation Profile of sIgA vs IgG mAbs.....	184

4.3.3. Conformational Stability and Relative Solubility Assessment of sIgA vs IgG mAbs.....	185
4.3.4. Examination of sIgA vs IgG Stability in an In Vitro Gastric Digestion Model to Mimic Oral Administration.....	187
4.3.5. Comparisons of Stability/Solubility Profiles of sIgA1, sIgA2 and IgG under Various Conditions.....	191
4.4. Discussion.....	192
4.5. References.....	201
4.6. Figures and Tables.....	207

## **Chapter 5. Summary, Discussions, and Future Directions**

5.1. Overview.....	220
5.2. Chapter Summaries and Future Work.....	221
5.2.1. Chapter 2.....	221
5.2.2. Chapter 3.....	223
5.2.3. Chapter 4.....	225
5.3. References.....	229



## **Chapter 1**

### Introduction

## 1.1. Overview of Classes of Immunoglobulin

### 1.1.1. General Description of 5 Immunoglobulin Classes

Immunoglobulins (Igs), also known as antibodies, are a key part of the human immune system. These protein molecules specifically recognize and bind to particular pathogens, such as toxins, viruses, and bacteria. They are produced by plasma cells, a specific type of B cell in the immune system, in response to immune challenges. A typical Ig molecule has the following basic molecular structure<sup>1,2</sup>: four polypeptide chains, including two identical light chains (LC) and another two identical heavy chains (HC). There are variable and constant regions to each heavy and light chain. The variable region contains the amino acid sequences responsible for antigen binding (see below). Based on differences in the primary amino acid sequence in the constant regions, the light chains are classified as either the "kappa" ( $\kappa$ ) or "lambda" ( $\lambda$ ), while the heavy chains fall into as "alpha" ( $\alpha$ ), "gamma" ( $\gamma$ ), "delta" ( $\delta$ ), "epsilon" ( $\epsilon$ ), and "mu" ( $\mu$ ) class, representing the IgA, IgG, IgD, IgE, and IgM classes, respectively. Distinct biological functions and physical properties have been discovered for each of the five Ig classes (Table 1). Nonetheless, different types of Ig molecules have same basic structure of four polypeptide chains (Figure 1), including aforementioned two light and two heavy chains, which are connected together by a combination of disulfide bonds as well as non-covalent interactions, forming a Y-shaped structure. The hinge region on the heavy chain divides whole Ig molecule into Fab and Fc parts, meaning antigen-binding and crystallizable fragments, respectively. Just as its name implies, the Fab fragment contains variable sections that determine the specific target that Ig molecule can bind. By contrast, the Fc fragment of Ig molecules (within a specific class) is the same for each species, can be

recognized by particular macrophage receptors for initiating potential immune responses. Based on the variability of primary sequence, heavy chain is further divided into four domains, including variable domain ( $V_H$ ), constant domain one ( $C_H1$ ), constant domain two ( $C_H2$ ), and constant domain three ( $C_H3$ ). Light chain, on the other hand, has two distinct domains, including variable domain ( $V_L$ ) and constant domain ( $C_L$ ). Three complementarity-determining regions (CDRs) are located on each of the variable region, which are the particular places within the antibody that binds to different antigens, usually referred as paratope. Furthermore, albeit varying considerably across types of Ig molecules, post translational modifications such as glycosylation (N-linked, O-linked or both types) can be attached to at least one site on each heavy chain of all Ig molecules.

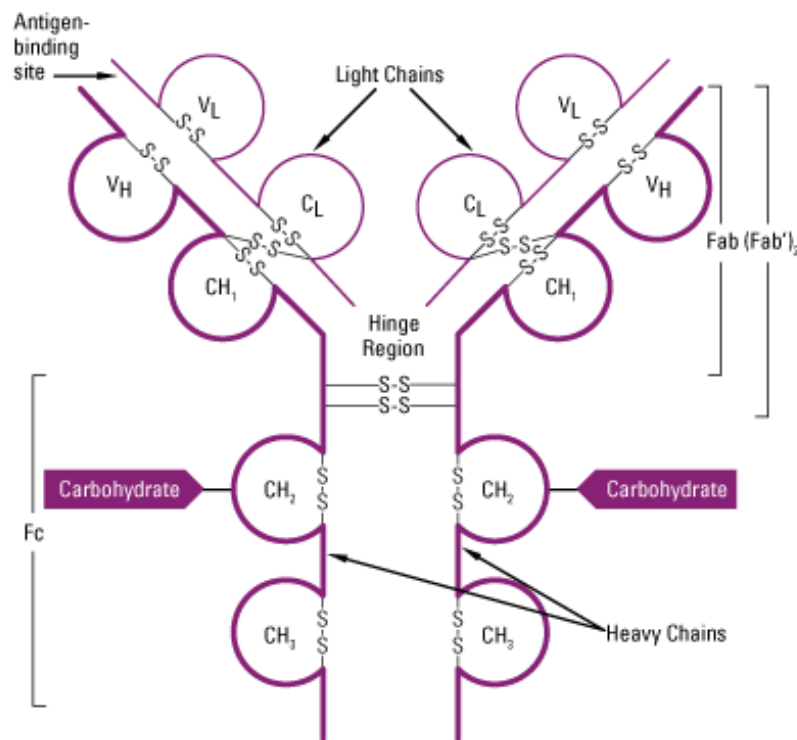
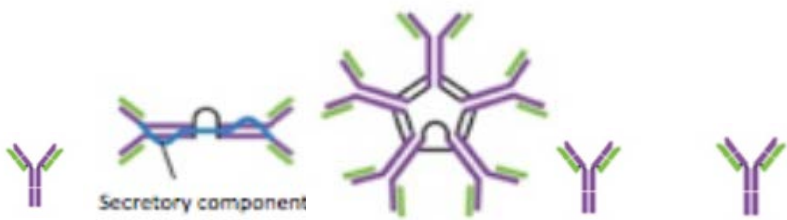


**Figure 1.** The basic structure of immunoglobulin Ig molecules. The distribution of both interchain and intrachain disulfide bonds are shown. Purple-labelled carbohydrate point

to localization of potential N-glycosylation in CH2 domain.<sup>3</sup> (This website was accessed on January 7<sup>th</sup>, 2019, and figure reprinted).

**Table 1.** Biological and physical properties of Ig classes.<sup>2</sup> (Table reprinted)



	IgG	IgA	IgM	IgD	IgE
Molecular formula	$\kappa_2\gamma_2$ $\lambda_2\gamma_2$	$\kappa_2\alpha_2$ $\lambda_2\alpha_2$	$\kappa_5\mu_2$ $\lambda_5\mu_2$	$\kappa_2\delta_2$ $\lambda_2\delta_2$	$\kappa_2\varepsilon_2$ $\lambda_2\varepsilon_2$
	Monomers	Monomers, dimers (+SC, + J chain)	Pentamers (+ J chain), hexamers	Monomers	Monomers
Subclasses	$\gamma$ 1-4	$\alpha$ 1-2	—	—	—
Molecular weight	150,000	160,000	950,000	180,000	190,000
$s_{20, w}$	6.6S	7S, 9S, 11S	19S	7S	8S
Electrophoretic mobility	$\gamma$	Fast $\gamma$ to $\beta$	Fast $\gamma$ to $\beta$	Fast $\gamma$	Fast $\gamma$
Carbohydrates (%)	3	7.5	12	12	12
No. of oligosaccharide chains per constant region	(1)	(5) ( $\alpha$ 1-2, +5 in hinge; $\alpha$ 2-4 or 5)		(3, +4 in hinge)	(6)
Serum level (mg/ml)	~10	~2	~1.2	~0.04	~3 × 10 <sup>-4</sup>
Half life (days)	23 (IgG3: 8)	5-6	5	2.8	2.5
Complement fixation					
Classical	+	-	+	-	-
Alternative	-	+	-	-	-
Transplacental transfer	+	-	-	-	-
Binding to cells	Macrophages, polymorphs	—	—	—	Mast cells, basophils

### **1.1.2. Brief Introduction to IgG and IgA Molecules**

Immunoglobulin G (IgG) is the most common class of immunoglobulins found in blood circulation. Among all serum antibodies, approximately 75% are belonging to this class.<sup>4</sup> IgG has four subclasses (IgG1, 2, 3, 4) in humans, which have the nomenclature based on their relative abundance in serum. By binding and neutralizing different kinds of pathogens such as bacteria, fungi, and viruses, IgG plays a critical role in protecting the human body from infection. More details of IgG structure and biological functions will be described in 1.2. section below.

Immunoglobulin A (IgA), the second most prevalent Ig protein in human serum (after IgG) and the preeminent antibody class (as secretory IgA, sIgA) in the mucosa community that bathes mucosal surfaces, acts as the first line of body defense and plays a crucial role in immune protection. Two subclasses of (s)IgA have been found in human, including (s)IgA1 and (s)IgA2, and (s)IgA2 is also with two allelic variants [A2m(1) and A2m(2)]. Further details about IgA physical structure, body distribution, and biological properties will be discussed in 1.3. section below.

### **1.1.3. Structure and Function of IgM, IgD, and IgE Molecules**

Immunoglobulin M (IgM), among the 5 major antibodies in human serum, is the largest and most complex (macroglobulin). It is not only the first antibody developed during human fetal development at about 5 months, but it also the first to react in the response to initial exposure to a pathogenic antigen. The concentration of IgM in human serum is

about 1.2 mg/mL. Although the basic structure of IgM monomer is same as IgG, IgM usually appears to be pentameric assembly of these monomers (or rarely hexamers) in human serum. Therefore, a pentameric IgM comprises of 10 heavy chains, 10 light chains, and usually a joint chain, called J chain. The polymeric property of IgM is primarily due to J chain mediated connections by disulfide bonds involving cysteines in the tailpieces. However, unlike IgA, it is not necessary to have a J chain to form polymeric IgM, since the tailpiece cysteine of IgM heavy ( $\mu$ ) chain can also form covalent bond with other  $\mu$  chain.<sup>5-8</sup> Although a rare occurrence, two or three J chains can exist in one IgM molecule.<sup>9-12</sup> Hexameric IgM can also be produced by B cells, but usually in the absence of J chain, and only less than 5% of total IgM in human serum are hexamers.<sup>2</sup> Theoretically, 10 antigens can bind to one IgM molecule at the same time because of predominantly pentameric structure. However, due to steric effects, approximately 5 large antigens can bind simultaneously. Both monomeric (like IgG structure) and polymeric (pentameric or hexameric) IgM have significant effects in the immune system. As an antigen-specific component of the antigen receptor, monomeric IgM associates on the B-cell surface and plays key roles on natural development of unstimulated B lymphocytes. The polymeric IgM can activate the classical pathway by binding to complement component (C1qR and Fc $\alpha$ / $\mu$ R), recruiting phagocytic cells for immune responses, and lead to antigen opsonization and cytolytic reactions. Furthermore, IgM can also be secreted to mucosal surfaces by a function of J chain for potential immune reactions, for example secreted into breast milk or gut lumen. In summary, IgM antibodies provide “natural immunity” as the first protection and thus commonly initiate an immune response against invading microorganism.

Immunoglobulin D (IgD) is a minor antibody component that makes up less than 0.25% of total antibody concentration in serum. IgD is usually present in serum in a monomer state, comprising of two heavy ( $2\delta$ ) and two light chains, without any other polypeptide chains involved. The half-life of IgD is relatively short, only about 2.8 days.<sup>13</sup> Because of a highly extended hinge region, IgD is extremely sensitive to proteases.<sup>2</sup> Moreover, as primarily a membrane bound protein, IgD can anchor on B-cell surface by a glycosyl phosphatidylinositol linkage, serving as an antigen-specific part of B-cell receptors. IgD will not be expressed until B cell leaves the bone marrow to further settle down and grow in the peripheral lymphoid tissues. Collaborating with IgM on the surface of B cell, IgD plays certain key roles in the immune signalling cascade. However, it has been found that only repetitive multivalent immunogens can trigger IgD signalling, while both soluble monomeric or multivalent immunogens can initiate IgM immune signalling.<sup>14</sup> The quantity of IgD on B-cell surface, on the other hand, is about one order of magnitude higher than that of IgM.<sup>2</sup> Recently, additional biological functions have been found for IgD which can bind to basophiles and mast cells, activating them to produce antimicrobial factors that control respiratory immune defense.<sup>15</sup> Finally, IgD might also be involved in allergic reactions in humans.

Immunoglobulin E (IgE) is generally synthesized by plasma cells (in mammals only), but as another minor class of antibody in humans, it is present at very low concentration in serum. As a normally monomeric form, IgE is comprised of two heavy chains ( $2\epsilon$ ) and two light chains, where the  $\epsilon$  chain contains four constant domains ( $C\epsilon 1$ - $C\epsilon 4$ ). IgE acts as the most important participants for allergic and inflammatory reactions, in which the Fc part of antibody has very high affinity for mast cells and can bind to  $Fc\epsilon$

receptors, including FcεRI and FcεRII, on the surface of mainly mast cells and basophils. Also, it has been found that monocytes, eosinophils, platelets, and macrophages in humans have such Fc receptors in humans.<sup>16</sup> The binding of multivalent antigens with membrane-bound IgE initiates the release of many active mediators, such as leukotrienes, histamine, prostaglandins, and chemotactic factors, to trigger corresponding allergic and inflammatory reactions. Plasma concentrations of IgE are usually elevated by several hundredfold due to allergic conditions or infection by *Necator americanus* and nematodes.<sup>2,17,18</sup> Elevation of IgE level is also been reported in various autoimmune disorders, including rheumatoid arthritis and psoriasis, leading to hypersensitivity reactions with pathogenic effects.<sup>19,20</sup> Furthermore, the presence of specific IgE molecules can potentially be used in allergy diagnosis when conducting a blood or skin test.<sup>21</sup>

## **1.2. More Detailed Description of Physicochemical and Biological Properties of IgG Class**

Of the five major immunoglobulin classes, IgG is the most abundant one, accounting for approximately 75% of serum antibodies present in humans. It is found in all body fluids and plays a critical role in protecting humans from pathogenic infections due to viruses, bacteria, and other microorganisms. The Y-shaped IgG molecule not only binds antigens via the Fab regions of the protein, but it also possesses many immune triggering properties and functions (after antigen binding) which are dictated by the glycosylation pattern within the Fc region.

### **1.2.1. Basic Structure**



### 1.2.1.1. Chain Composition and Molecular Weight

Two identical polypeptide heavy chains ( $2\gamma$ ) and two identical polypeptide light chains assemble to form a three dimensional Y-shaped IgG molecule with a molecular weight of about 150 kDa (see Figure 2 below). As outlined above,<sup>1,2</sup> four domains are distinguished on the IgG heavy chain including  $V_H$ ,  $C_{H1}$ ,  $C_{H2}$ , and  $C_{H3}$ . The molecular weight of the heavy chain is about 50 kDa, with some minor differences between IgG molecules based on the sequence on the variable region. As for the light chains of IgG, two basic domains have been defined including  $V_L$ , and  $C_L$ . The light chain has a relatively lower molecular weight of about 25 kDa, which also fluctuates between IgG molecules due to various sequences especially on the variable region. These polypeptide chains of IgG are connected by inter-chain disulfide bonds, including the linkages at the hinge region for connecting two heavy chains, and the linkage between  $C_{H1}$  and  $C_L$  domains for connecting between heavy and light chains. Intra-chain disulfide bonds are also formed for IgG, usually one disulfide bond per defined domain.

An important feature revealed by comparing the primary sequence is that only the approximately first 110 amino acids for each polypeptide chain, corresponding to the  $V_H$  or  $V_L$  domain (also called variable region), varies greatly between different IgG antibodies.<sup>2,22</sup> The remaining sequence, however, is essentially constant between antibody chains for each subclass of IgG, called constant region. Complementarity-determining regions (CDRs) are part of both heavy chain and light chain variable chains of IgG molecule, where the sequence differs a lot between IgG molecules in order to bind to different epitopes on various antigens present on pathogenic toxins, bacteria, or viruses. A particular set of CDRs and surrounding sequences constitutes an antibody

paratope, while the region on the antigen where paratope binds is called epitope. Three CDR loops are on each variable domain (heavy or light) of IgG molecule. And total of six CDRs (from both heavy and light chain) can collectively dictate the sequence that defines the three dimensional structure that binds an antigen. Thus, two identical antigen-binding sites are on Y-shaped IgG molecule by two Fab arms, and IgG has ability to bind two identical epitopes simultaneously (see Figure 2). In terms of the hinge region of IgG, it is the most flexible region on the molecule, which allows independent movement of the two Fab arms as well as the Fc fragment. The high flexibility and exposed properties of IgG hinge region also contribute to its susceptibility of proteolysis.<sup>23</sup> Both papain and pepsin can cleave IgG molecules at the hinge region by via proteolysis at the amino-terminal side and carboxy-terminal side, respectively. Fab, F(ab')<sub>2</sub>, and Fc fragments are obtained after cleavage with these two proteases (see Figure 2). Both Fab and F(ab')<sub>2</sub> could be functional fragments in terms of antigen-binding activity,<sup>23</sup> but probably to different extents. Thus, although loss of ability of interacting with any effector molecule due to lack of Fc fragment, Fab domains are of potential value in antibody therapeutic applications, such as direct neutralization of antigens. Several Fab (with/without PEGylation) drugs are currently on market, such as Ranibizumab, abciximab, and certolizumab pegol.<sup>24</sup>

#### **1.2.1.2. Glycosylation**

All IgG antibodies have a conserved N-linked glycosylation site at Asn297 in each of the two heavy chains (C<sub>H</sub>2 domain) within the Fc region of the antibody, with glycosylation accounting for about 3% of total weight of an IgG molecule. There is a core heptasaccharide structure in IgG antibodies from humans consisting of N-acetylglucosamine and mannose units, combined with a varying other monosaccharide

units, that form into a complex biantennary shape. Because of differences in terminal sugars such as galactose and sialic acid, as well as varying levels of fucose, there are a large number post translational glycosylation types that have been identified between various IgG molecules and even within the two sites of the same IgG molecule.<sup>25</sup> There are theoretically 32 potential glycosylation types for IgG molecule, which can be grouped into three subsets, including G0, G1, and G2.<sup>26,27</sup> The two N-linked carbohydrate chains, unlike many other glycoproteins which expose their oligosaccharides on the surface, face inside the cavity between the Fc polypeptide monomers.<sup>28,29</sup> In addition to playing a key biological role<sup>30</sup> (see next section), N-linked glycosylation of Asn297 in IgG molecules is of high importance for stabilizing Fc domain by interacting with a hydrophobic patches and keeping proteins in their native structure.<sup>31,32</sup>

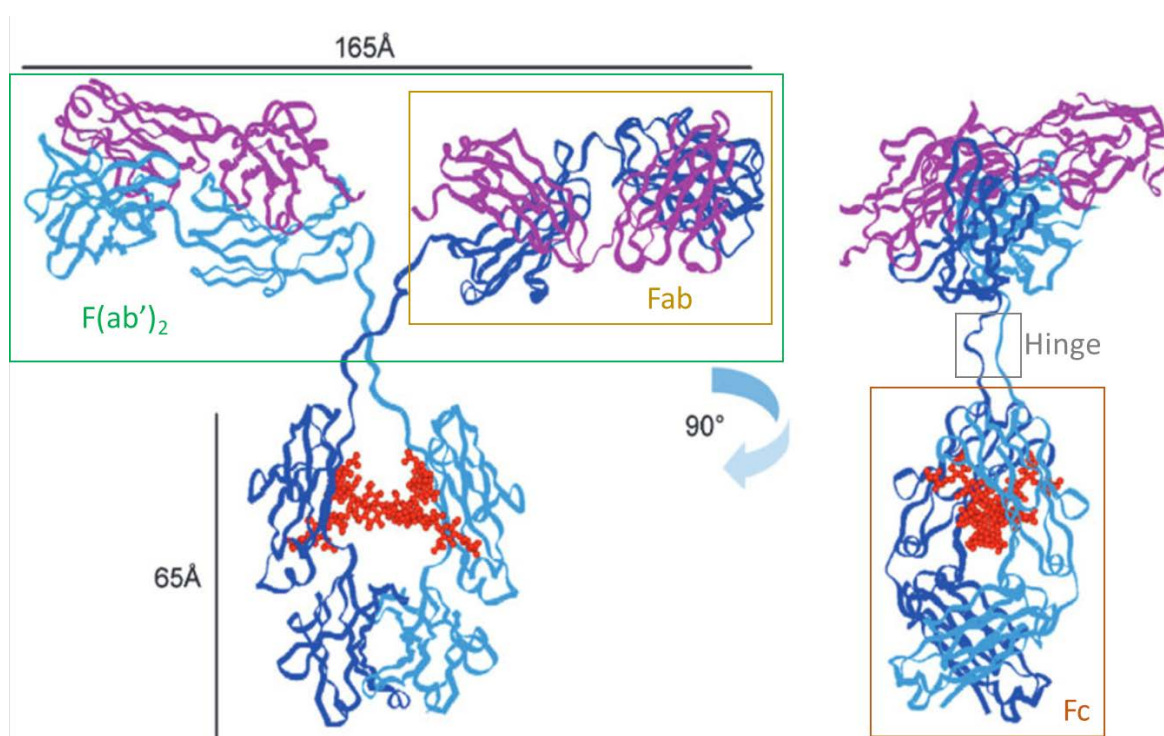


**Figure 2.** Three dimensional structure including glycosylation model of IgG molecules. Red dots show the N-glycans on the C<sub>H2</sub> domain of IgG antibody.<sup>26</sup> (Figure reproduced)

The N-linked glycosylation on Asn297 of IgG molecule profoundly influences the binding activity between Fc domain and Fc receptors, such as FcγR. Such binding plays a critical role in antibody-dependent cellular cytotoxicity (ADCC), where antibody-antigen complexes first bind to the FcγR receptor and then activate immune functional cells such as monocytes and natural killer cells. The type and extent of ADCC activity varies based on the composition of oligosaccharide glycan structure at the Asn297 site. Furthermore, another effector function of IgG has been recognized as complement-dependent cytotoxicity, in which after binding of antigen via the Fab region, the Fc region of IgG binds to the complement protein (C1q) to activate the complement cascade process leading to direct lysis of a pathogen. Glycosylation pattern of the Asn297 in the Fc domain has substantial effect on their binding efficiency, and it is reported that a complicated glycan structure is usually required, including at least 2 N-acetylglucosamines with multiple galactoses and sialic acids.<sup>25</sup> Finally, IgG half-life (the longest serum half-life of all immunoglobulin classes) is also greatly influenced by glycosylation. Fast clearance has been detected for IgG molecule glycosylated with high mannose structures at Asn297.<sup>33</sup> The shorter half-life is presumably due to lower binding affinity between IgG Fc domain and the neonatal Fc receptor (FcRn), in which in turn is due to the high mannose glycan structure.

From a pharmaceutical perspective, controlling and reproducibly producing the Asn297 glycosylation pattern plays a key role in process development for a given monoclonal antibody candidates. In terms of formulation development and stability, as discussed in more detail below, the glycan structures present at Asn297 in IgG antibodies

have been shown to influence solubility, chemical and physical stability, aggregation propensity, etc.<sup>34</sup>

### **1.2.2. Body Distribution and Percentage Level**

The concentration of IgG in human serum is about 10 mg/mL (shown in Table 1), which is the highest among all five immunoglobulins. More than three-quarters of total immunoglobulins are in the IgG class.<sup>4</sup> The body distribution of IgG is determined by both their size and biological functions, which for example, enables them to engage particular transporters for delivery across epithelia. Specifically, IgG is the most dominant antibody species found in the blood and extracellular fluid (in the body tissue with accessory cells and molecules available for immune response). Furthermore, serum IgG levels are related to both age and sex. It has been reported that higher serum IgG level was observed in females than in males, showing a constant difference throughout all age ranges.<sup>35</sup> Interestingly, the serum IgG levels tend to increase with age for both males and females.<sup>35</sup>

### **1.2.3. IgG Subclasses**

Four subclasses of IgG exist in human serum, including IgG1, IgG2, IgG3, and IgG4. The nomenclature is primarily based on the abundance in serum, where approximately ~66%, ~23%, ~7%, and ~3% are determined for IgG1, IgG2, IgG3, and IgG4, respectively. Except for IgG2, the other three subclasses of IgG can cross placenta easily, thereby having biological functions of providing immunity and protecting a new born baby. Furthermore, the half-life of the subclasses is also different, especially IgG3, in which the half-life is about 7 days while others are about 21 days.<sup>36</sup>

Although four IgG subclasses share more than 95% similarity between their Fc regions, substantial variations are observed primarily via the hinge region, molecular weight, and the position and number of disulfide bond. As shown in Table 2, there are 12 amino acid residues in the IgG2 and IgG4 hinge region, whereas IgG1 has 15, while IgG3 has 62 (depends on IgG allotype) residues. Also, there are only 2 inter-heavy chain disulfide bonds for IgG1 and IgG4, but IgG2 and IgG3 have 4 and 11 disulfide bonds, respectively. Moreover, IgG3 has a relatively higher molecular weight (170 kDa), while others have average molecular weight about 146 kDa.

**Table 2.** Physical and biological properties of human IgG subclasses.<sup>37</sup> (Table reproduced)

	IgG1	IgG2	IgG3	IgG4
<b>General</b>				
Molecular mass (kD)	146	146	170	146
Amino acids in hinge region	15	12	62 <sup>a</sup>	12
Inter-heavy chain disulfide bonds	2	4 <sup>b</sup>	11 <sup>a</sup>	2
Mean adult serum level (g/l)	6.98	3.8	0.51	0.56
Relative abundance (%)	60	32	4	4
Half-life (days)	21	21	7/~21 <sup>a</sup>	21
Placental transfer	++++	++	++/++++ <sup>a</sup>	+++
<b>Antibody response to:</b>				
Proteins	++	+/-	++	++ <sup>e</sup>
Polysaccharides	+	+++	+/-	+/-
Allergens	+	(-)	(-)	++
<b>Complement activation</b>				
C1q binding	++	+	+++	-
<b>Fc receptors</b>				
FcγRI	+++ <sup>c</sup>	-	+++	++
FcγRIIIa <sub>H131</sub>	+++	++	+++	34
FcγRIIIa <sub>R131</sub>	+++	+	+++	0.17
FcγRIIb/c	+	-	++	0.21
FcγRIIIa <sub>F158</sub>	++	-	+++	0.20
FcγRIIIa <sub>V158</sub>	+++	+	+++	0.20
FcγRIIIb	+++	-	+++	0.25
FcRn (at pH < 6.5)	+++	+++	+++	-
			++/++++ <sup>a</sup>	+++

<sup>a</sup>Depends on allotype.

<sup>b</sup>For VA isomer.

<sup>c</sup>Multivalent binding to transfected cells. Adapted from Bruhns et al. (2).

<sup>d</sup>Association constant ( $\times 10^6 M^{-1}$ ) for monovalent binding (2).

<sup>e</sup>After repeated encounters with protein antigens, often allergens.

#### 1.2.4. Biological Functions

Varying biological roles have also been identified for different IgG subclasses. Specifically, IgG1 and IgG3 are predominantly responsible for immune responses targeting polypeptide and protein antigens, and IgG1 is also fundamentally involved in opsonization and activation of the complement cascade. As for IgG2, it plays an important role in immune responses against carbohydrate and polysaccharide antigens. The immunological roles of IgG4 are still actively being investigated.<sup>38</sup>

The main role of IgG is to increase the detection efficiency and the promotion of clearance of pathogens toxins, microorganisms, and viruses in human serum and body tissues. IgG molecules can bind and neutralize pathogenic substances to prevent them from performing their biological functions. Furthermore, clearance of pathogens from the body is usually performed via IgG-antigen complexes by FcγRs activating phagocytosis and degradation. Moreover, the surface of pathogenic virus and bacteria can be coated by IgG, in a process named opsonization, in order to optimize complement fixation or phagocytosis. The binding of FcγRs with Fc-antigen complexes will initiate phagocytosis and finally degrade the antigens in endosome. Furthermore, for pathogenic microorganisms, fixation of complement could also be performed by binding of some IgGs, improving efficiency of cell killing by primarily punching holes on the cell membrane via the complement cascade of proteins. The IgG-antigen complex bind to C1q, a protein complex involved in the complement system as part of the innate immune system, to first activate C1q, and thus to initiate the classical complement pathway of the complement system. However, only three IgG subclasses (IgG1, IgG2, and IgG3) are able to interact with C1q, with IgG3 having the highest efficacy. Finally, the pathogen infected cells in



human tissue can also be killed or cleared by IgG-antigen-activated natural killer (NK) cells, called ADCC.

### **1.3. More Detailed Description of Physicochemical and Biological Properties of IgA Class**

IgA is another important antibody class found in human serum as well as mucous membranes, especially in the respiratory and digestive tracts. It is the predominant antibody type in external secretion compartment, acting as the “First Line” of body defense. The major function of IgA is to bind and destroy pathogenic substances, preventing antigens from entering human circulatory system. More complicated structures and glycosylation patterns, compared to IgG, have been identified for IgA molecules.

#### **1.3.1. Basic Structure**

##### **1.3.1.1. Chain Composition and Molecular Weight**

The basic composition of IgA is same as other Ig antibodies, including two identical polypeptide heavy chains (~55 kDa each) and another two identical polypeptide light chains (~25 kDa each), as shown in Figure 3. There are four defined regions for the heavy chain including  $V_H$ ,  $C_{H1}$ ,  $C_{H2}$ , and  $C_{H3}$ . As for the light chain, two domains are described containing  $V_L$  and  $C_L$ . Similar to IgG molecules, IgA also has inter-chain and intro-chain disulfide bonds by cysteine residues to connect the polypeptide chains and rigidify the overall structure. The antigen binding sites on IgA are also located at the variable regions, including three CDRs at each  $V_H$  and  $V_L$  domain. A tailpiece at the C-terminal of heavy

chain is a particular highly conserved polypeptide for IgA (and IgM), which plays important roles in IgA dimerization or even polymerization (Figure 3). The cysteine residue on the tailpiece section of the heavy chain make it possible to form disulfide bond to another IgA component, joint chain or J chain,<sup>39</sup> which is a ~16 kDa cysteine-rich glycoprotein present in dimeric IgA (dIgA) or secretory IgA (sIgA) structures. Two disulfide bonds formed with tailpieces of two IgA monomers connect Fc domains to form a dimeric structure. Higher-order oligomer formation of IgA is thus essentially due to the presence of J chain. Moreover, another important polypeptide chain, as shown in Figure 3 for sIgAs, is the secretory component (SC), a highly glycosylated ligand-binding protein coming from polymeric immunoglobulin receptor (pIgR). There are five Ig-like domains for the SC (~80 kDa) chain, including D1 to D5 from the N-terminus. In an unbound state, SC prefers to form a structure that curves back upon itself.<sup>40</sup> By forming disulfide bonds with Fc part of IgA, SC wraps around two Fc regions of two IgA monomers, functioning to stabilize IgA antibodies, especially the Fc domain. However, SC only binds to polymeric IgA, primarily sIgA, when IgA undergoes transcytosis from epithelial cells to form sIgA in secretion process. The binding of SC and dimeric IgA has critical functions of increasing sIgA resistance to proteolysis.<sup>41</sup> It has been reported that SC delays the digestion of sIgA, slowing down the conversion of sIgA to a potential digestion product F(ab')<sub>2</sub> (an antigen-binding active protein).<sup>42</sup>

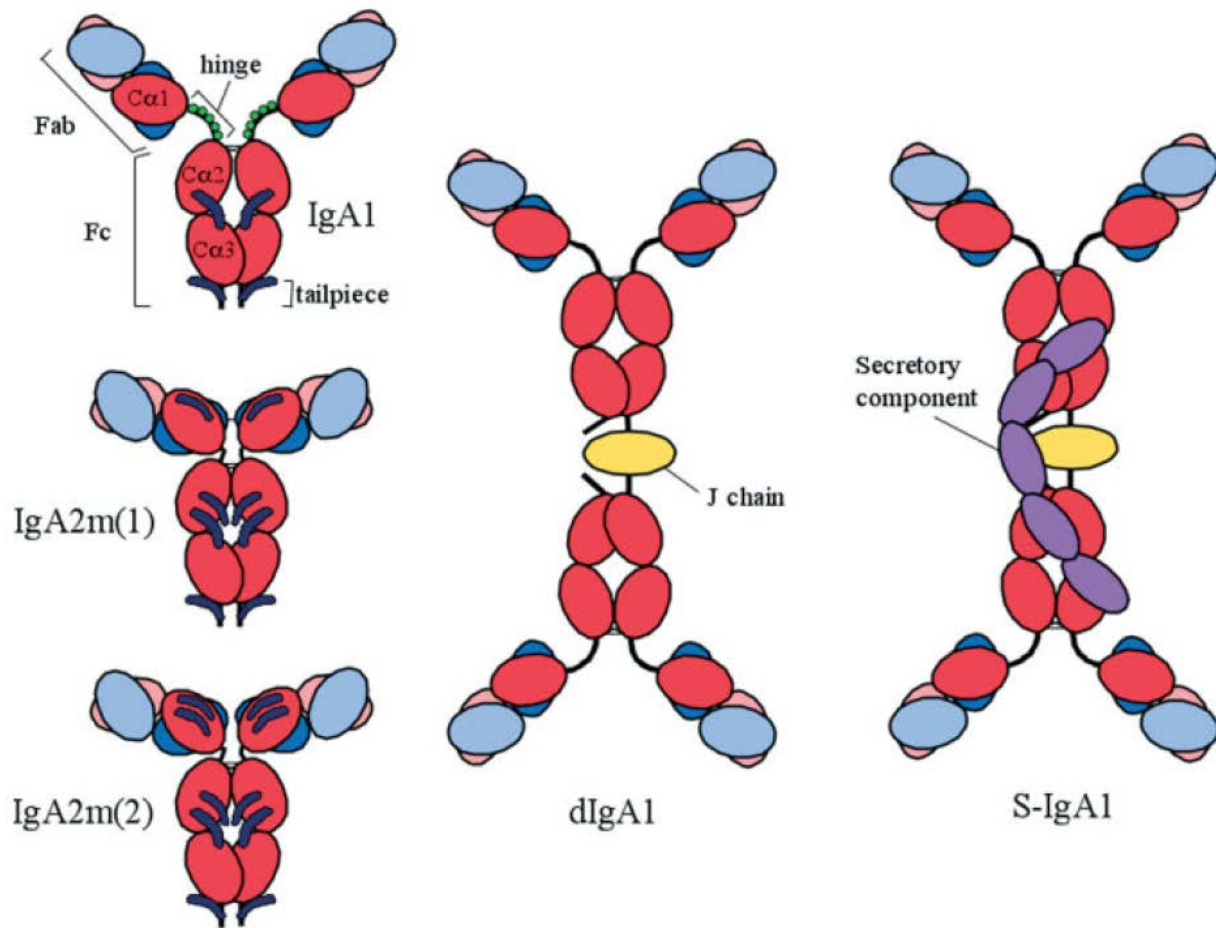


**Figure 3.** Schematic structure of IgA, including monomeric IgA1, IgA2, and dimeric IgA1, such as dIgA1 and sIgA1 (more details of IgA subclasses will be described in 1.3.3. section). N-linked glycosylation is shown in dark blue, and O-linked glycosylation is presented in green circle.<sup>43</sup> (Figure reprinted)

### 1.3.1.2. Glycosylation

In comparison to IgG, IgA has notably higher carbohydrates (18-22% w/w), including N-linked glycosylations as well as O-linked glycosylations.<sup>25,26,39,41,44</sup> There are two conserved N-glycosylation sites within the Fc domain, while IgA1 has five O-linked

glycosylation sites on its elongated hinge region (formed by five serine residues). For IgA2, two or three more conserved N-glycosylation sites have been identified in C<sub>H</sub>1 and C<sub>H</sub>2 domains, depending on the allotype of IgA2m(1) and IgA2m(2), respectively. More than 90% of N-glycans in IgA1 are in sialylated structure, while IgG has less than 10% N-glycans with sialic acids. The N-linked glycosylation of IgA consists of a family of structures with a mannosyl chitobiose as the N-glycan core. High heterogeneity of IgA N-glycans comes from the type and number of terminal sugars, such as galactose and sialic acid.<sup>39,45,46</sup> Moreover, the biantennary glycans are predominant in IgA C<sub>H</sub>2 domain, while N-glycan on the tailpiece has mostly triantennary structure. For sIgAs, both J chain and SC chain are also highly glycosylated. J chain has a single N-glycosylation site, showing a carbohydrate content of ~8% w/w.<sup>41</sup> In terms of the SC chain, up to seven N-glycosylation sites are on different domains, and thus possessing a high amount of carbohydrates (~22% w/w).<sup>41</sup> The N-glycosylation on SC chain promotes the stability profile of sIgAs.<sup>41</sup> Moreover, the N-glycosylation on the heavy chain of IgA has been proposed to enhance antigen binding and clearance.<sup>47</sup> Another report confirms the function of serum IgA glycans to bind the asialoglycoprotein receptor (ASGP-R) for mediating the clearance of IgA from serum.<sup>48,49</sup> Furthermore, the O-glycosylation on IgA1 also have many biological functions including affecting the activity of some of the proteases, and binding to microorganisms (to prevent the attachment of pathogens to epithelial cells in gut and to accelerate the excretion of such pathogens in the feces).<sup>26,50</sup> The one N-linked glycosylation site on J chain helps IgA form dimeric or higher-order structures, and also adjusts the binding affinity between IgA and pIgRs.<sup>26</sup> As for SC chain glycosylation, a series of glycan epitopes could be formed due to high heterogeneity of

SC chain N-glycans, such as various Lewis and sialyl-Lewis epitopes.<sup>45</sup> Competition binding of SC chain N-glycans with lectins or bacterial adhesins inhibits potential attachments or following infections on surface of epithelial cells.<sup>51,52</sup>

### **1.3.2. Body Distribution and Percentage Level**

IgA, primarily in its monomeric form, is the second most abundant antibody in human serum, after IgG, possessing a concentration of about 1-4 mg/mL (Table 1), taking up of 15% of the total serum antibodies. In the mucosa compartment, however, IgA is primarily in its secretory dimeric form (sIgA) and is presents as the predominant antibody. It exists in colostrum, breastmilk, saliva, tears, and other secretions such as respiratory, gastrointestinal, and genitourinary tracts. In human serum, one of the IgA subclass (IgA1, more details will be discussed in 1.3.3. section) accounts for ~ 90% of total amount, and the remaining 10% are IgA2 (the second IgA subclass). However, in mucosa sites, the distribution of sIgA1 and sIgA2 varies a lot, ranging from 60-90% sIgA1 in male genital, hepatic bile, jejunal fluid, bronchial, saliva, or nasal secretions, and ~60% sIgA2 in female genital or colonic secretions.<sup>39</sup> Furthermore, it has been reported that, no matter what age, IgA levels in serum are higher in males than in females, and the levels increase with age.<sup>35</sup>

### **1.3.3. IgA Subclasses**

As already mentioned above, there are two major subclasses of IgA in human serum, including IgA1 and IgA2. Among them, IgA1 accounts for about 90% of total IgA in serum, while the secretory form of IgA2 (sIgA2) is the predominant form (~65%) in the external secretions, such as the mucosa of the airways, eyes, and the gastrointestinal

tract. The major difference of IgA1 and IgA2 comes from their hinge regions. Particularly, IgA1 features an elongated hinge region with 16 amino acids insertion, which comprises a repeat of 8 amino acids enriched with serine, threonine, and proline. In addition, such special region is usually attached with 3-5, or sometimes 6, O-linked glycans.<sup>45,47,53</sup> IgA2, however, lacks of such sequence as well as O-linked glycosylation in hinge region, indicating a relatively shorter exposed and flexible linkage between Fab and Fc domains, which probably renders (s)IgA2 critical biological consequences of resisting cleavage by potential proteases generated by pathogenic bacteria or viruses.<sup>54</sup> In addition, as aforementioned above for IgA2, there are two allotypic variants of IgA2m(1) and IgA2m(2).

Besides the number of N-glycans on the heavy chain, another basic difference between these IgA subclasses is the nature of their disulfide bonds between their polypeptide chains.<sup>55,56</sup> Specifically, IgA2m(1) does not possess disulfide bond between heavy and light chains, but does have disulfide bridge between two light chains, and thus IgA2m(1) usually appears to be heavy or light chain dimer under denaturing conditions. While, IgA2m(2) has same disulfide bond as IgA1 molecule between the heavy and light chains. Furthermore, IgA2m(1) has a hybrid composition of heavy chain constant region, containing a C<sub>H</sub>3 domain (same as IgA1 molecule), but also C<sub>H</sub>1 and C<sub>H</sub>2 domains (same as IgA2m(2) molecule).<sup>56</sup> In terms of potential antigens that IgA antibodies could target, IgA1 mainly performs its immune responses in human serum via binding against essentially protein antigens, while (s)IgA2 plays crucial role in external secretions to bind and fight against polysaccharide and lipopolysaccharide antigens.

#### **1.3.4. Biological Functions**

As the second most abundant antibody type, IgA displays its activities not only in serum, but more importantly in mucosal secretions. Several identified biological mechanisms have been described for IgAs binding to pathogenic bacteria, microorganisms, viruses, or toxins. Particularly, IgA prevents microbial adherence to epithelial surfaces and interacts with antigens on basolateral surfaces to form IgA-antigen complex, facilitating antigen elimination by exocytosis or phagocytosis.<sup>57</sup> Furthermore, IgA can inhibit antigens penetrating across lumen epithelial surface and has functions on forcing salvage pathway especially at interstitial levels.<sup>58,59</sup> There are several receptors that IgA can bind to perform its biological functions. Among them, FcαRI, also known as CD89, is a key mediator that is responsible for immune responses based on IgA-antigen complexes. FcαRI is a receptor located on the surface of many immune cells such as monocytes, eosinophils, neutrophils, and some macrophages as well as interstitial dendritic cells. The engagement of FcαRI with IgA-antigen complex will trigger a series of antigen elimination processes, including cytokine release, phagocytosis, oxygen species activation, calcium mobilization, degranulation, and antigen presentation, and also ADCC.<sup>60,61</sup> Furthermore, another receptor, called Fcα/μR, is an immune mediator that binds to polymeric IgA, such as sIgA.<sup>62</sup> Such receptor also presents at surface of various cells, such as macrophages, plasma cells, Paneth cells, follicular dendritic cells, and B cells.<sup>63,64</sup> Although the functions of Fcα/μR have not been completely studied in humans, it has been discovered that mouse Fcα/μR plays a role of mediating B-cell endocytosis of IgM-opsonized pathogenic bacteria, and probably can trigger uptake of IgA-coated microorganisms.<sup>65</sup> In addition, the pIgR on the basolateral side of mucosal epithelial cell performs critical roles not only in helping polymeric IgA transport cross epithelial cells to

gut lumen, but also in assembling polymeric IgA with SC chain as a secretory IgA molecule (sIgA). This process not only greatly improves the transcytosis of IgA into external secretions, but also enhances the physical and protease digestion stability of sIgA (with SC chain wrapping around Fc part of IgA molecule). In addition, it has been described previously that the polymeric IgA, that is undergoing pIgR-mediated transcytosis in epithelial cells, can neutralized intracellular pathogenic viruses, such as measles, Sendai, and influenza.<sup>66-68</sup> Lastly, unlike IgG and IgM molecules, IgA lacks the ability of activating the classical complement pathway due to poor binding property with C1q. On the contrary, the complement activation can be inhibited by IgA-antigen complex, in a situation of limited antigen existing, due to blocking IgG- or IgM-antigen binding.<sup>39,65,69-71</sup>

#### **1.4. Formulation Development Challenges and Opportunities for IgG as Therapeutic mAb Candidate**

Monoclonal antibodies (mAbs), especially IgG, have been developed over the last 30 years as successful class of therapeutic drugs. They have turned to be a well-deserved mainstream branch of the drug discovery and development pipelines in the pharmaceutical industry. All aspects of mAb pharmaceutical development has matured for over this time period including early R&D research, process development, clinical studies, and commercialization strategies. By the end of 2018, more than 80 mAb therapeutics have been granted marketing approvals.<sup>72</sup> In the year of 2018, a total of 13 therapeutic mAbs were granted first approvals in the United States or the European Union, reaching a record high for a single year (Figure 4).<sup>72</sup> A significant increase of approved mAbs started in 2014, and after that, a steady increase has occurred each year



(Figure 4). A wide range of several diseases can be targeted by mAb therapies, such as the treatment of autoimmune, infectious, and cardiovascular diseases, cancer as well as inflammation. Therapeutic mAbs bring high specificity to antigen target, and thus potentially reduce unwanted effects during therapy. Also, relative prolonged half-life of mAbs substantially reduces dosage frequency.

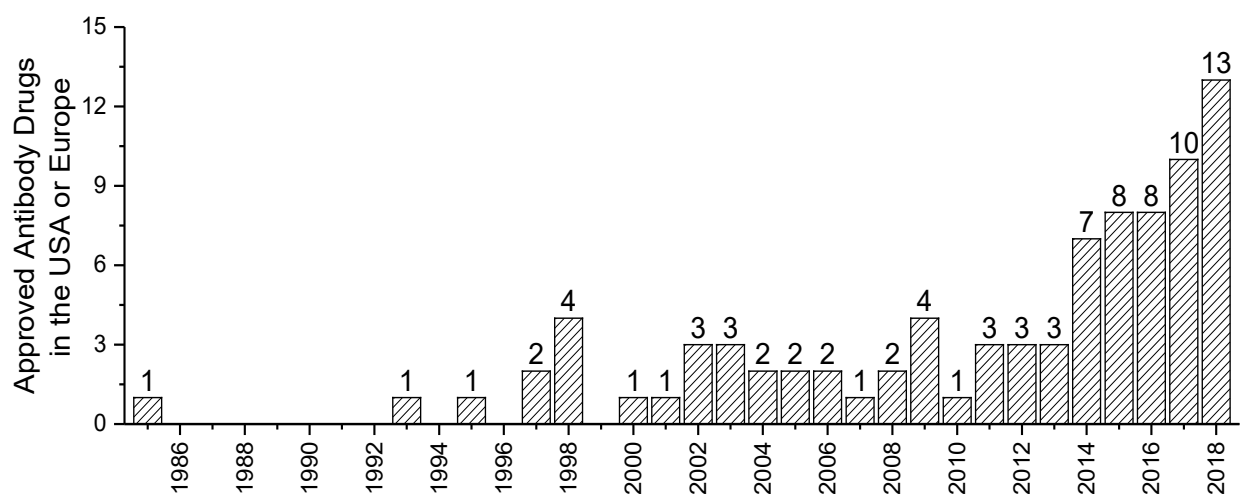


**Figure 4.** Number of antibody therapeutics approval in the USA or Europe.<sup>73,74</sup> (This website was accessed on January 10<sup>th</sup>, 2019)

#### 1.4.1. Administration to Patients

Therapeutic mAbs have been predominantly developed and administered intravenously (IV). Nevertheless, an increasing number of mAbs currently are designed, formulated and injected subcutaneously (SC).<sup>75</sup> Based on the approved antibody drugs in 2018, 10 out of 13 mAbs approved were recommended to be administered by SC dosing,<sup>73</sup> including Ravulizumab, Erenumab, Fremanezumab, Galcanezumab,

Burosumab, Lanadelumab, Caplacizumab, Cemiplimab, Tildrakizumab, and Emapalumab, demonstrating the increasing popularity for antibody drugs to be parenterally administered by the SC route.

#### **1.4.1.1. Intravenous Injection**

After first introduction of mAb administration by intravenous injection (IV) in the 1980s, it has been the preferred route for mAb therapy.<sup>76</sup> Compared to intramuscular (IM) route, which was the first administration pathway attempted for mAb therapy, IV provides a sufficient amount of antibodies upon administration to reach therapeutic window, and greatly reduces injection pain for patients. In addition, ~100% bioavailability is usually obtained by IV injections. However, patients need to go to hospitals or clinics for IV-based mAb therapy, which is time-consuming, costly and inconvenient. A fairly high rate of adverse effects have been observed in some cases, because physiological barriers and systemic distribution substantially reduce the actual mAb concentration obtained in target organs or tissues.<sup>77</sup> Currently, although IV administration is still an important administration route for mAb therapy, other potential parenteral routes are typically evaluated such as the SC or IM administration pathways.

#### **1.4.1.2. Subcutaneous Injection**

The subcutaneous route of administration for mAb therapy was first introduced in the 1980s, but it has been considered only as the second choice (vs. IV) for many years.<sup>76</sup> Due to systemic severe side effects of IV administration in certain cases, more and more attention was taken to utilize alternative administration pathways, such as the SC route. SC brings a lot of benefits for patients such as saving time, reducing cost, more

convenience, and self-administration. For example, SC administration has improved patient compliance by self-administration using pre-filled syringes, especially for treatment of chronic diseases.<sup>75</sup> However, a high concentration mAb solution is usually required for SC administration because of the maximum volume of injection is usually restricted to 1-2 mL.<sup>78-81</sup> Higher injection volume can cause a lot of pains for patients, which is commonly not acceptable (except using tissue-modification enzymes, such as use of hyaluronidase for Herceptin<sup>82</sup>). Therefore, a concentration of >100 mg/mL is often required for SC products.<sup>81</sup> Many challenges exist when formulating such a high concentration mAb solution, such as high viscosity and turbidity, aggregation, and even phase separation, which are essentially due to intermolecular non-covalent protein-protein interactions (PPIs) between mAb molecules in high concentration solutions.

#### **1.4.2. Reversible Self-Association of mAbs Induced by High-Concentration Protein Solutions**

A major formulation problem that can be encountered by high-concentration mAb solution is called reversible self-association (RSA), which is a phenomenon of reversible, non-covalent, concentration and temperature dependent non-native intermolecular interactions of mAb molecules to form oligomeric species of native protein. Poor solution properties and reduced mAb physical stability are often detected due to RSA, influencing the manufacturing, storage, delivery, and even administration processes of mAb candidates during development into commercial products.

##### **1.4.2.1. Viscosity**

As one critical indicator of PPIs of mAbs at high protein concentrations, dynamic solution viscosity has been widely employed to study mAbs RSA under various conditions. Extensive intermolecular interactions of mAb molecules result in the forming of high molecular weight oligomers or even interacting networks, which tightens connections between liquid layers, and thus elevates solution viscosity.<sup>83-85</sup> It has been broadly reported in previous studies that the dynamic viscosity of RSA-mAb solutions increased exponentially as a function of protein concentration.<sup>81,86-89</sup> Such dramatic increased of solution viscosity lead to various challenges and problems involved in pharmaceutical product development of SC formulations at high protein concentrations. Extremely high pressure will be encountered using viscous solutions during tangential flow filtration, or during analyses of samples, causing low filtration efficacy and frequent instrument maintenance, respectively.<sup>90</sup> Also, it is usually difficult to inject viscous solutions employing commonly used needles for parenteral administration, and thus additional design and manufacturing of special needles are sometimes needed.<sup>91</sup> In addition, patients may suffer pain due to time and force required when injecting high-viscosity solutions, which significantly reduces patients' compliance.<sup>92</sup>

#### **1.4.2.2. Opalescence**

PPIs play critical roles in solution opalescence especially at high protein concentrations. For mAb solutions, it is not necessary for them to contain particulates to show opalescence.<sup>80</sup> An IgG1, as reported previously<sup>80</sup>, displays opalescence at high concentration, but it turns out that the antibodies were essentially monomeric in nature, and the opalescence primarily came from Rayleigh scattering. Normally, Rayleigh scattering of visible light occurs when proteins have diameters of less than 30 nm.

However, self-associated antibodies can lead to cloudy appearance as a result of PPIs, indicating solution opalescence, or solution turbidity, where protein oligomers with broader size distributions, exist.<sup>90</sup> Filtration does not help to reduce solution opalescence since it is not due to the presence of particulates, but since PPIs are reversible, dilution of high concentration solution results in lower turbidity values.<sup>93</sup> High opalescent solutions can lead to unacceptable appearance and may fail due to patient compliance issues (instructions dictate to discard dosage forms with cloudy appearance).<sup>94</sup> Also, from a manufacturing perspective, high-concentration mAb solutions with high opalescence potentially increase systemic pressures when undergoing regular protein filtrations of protein solutions. Furthermore, during clinical trials, it can be challenging to match opalescence for clinical placebo solutions as compared to the protein containing formulations.<sup>90</sup> As described below, an increase of solution turbidity may also be achieved as more and more large particulates (irreversible aggregates) are formed in solution.<sup>95</sup>

#### **1.4.2.3. Aggregation**

Reversible self-associated (RSA) mAbs complexes contain protein in their native structures and normally return to their monomeric forms after dilution. Such the RSA process, however, could also lead to instability issues such as the formation of irreversible aggregates. As antibody molecules get closer in solution and interact with each other due to RSA, it presumably enhances the opportunity for any transiently formed, partially unfolded proteins to interact as well via exposed hydrophobic aggregation hot-spots. This is the first step to potentially undergo an irreversible change to form an aggregation “nuclei”.<sup>96</sup> Such nuclei follows an irreversible process to grow by combining with other nuclei species or complexed proteins, forming soluble and insoluble aggregates. These

types of irreversible aggregates are not affected by dilution of the solution. The formation of irreversible aggregates may result in unwanted immunogenicity, loss of mAb potency and/or product viability.<sup>97</sup> Furthermore, pharmacokinetic profiles of mAb products can be greatly altered as protein aggregates can dramatically change overall absorption, distribution, and even clearance or elimination (half-life).<sup>98</sup>

#### **1.4.2.4. Phase Separation**

As another critical phenomenon caused by PPIs, liquid-liquid phase separation, has been observed and studied broadly.<sup>99-101</sup> Phase separation of high concentration mAb solutions is a thermodynamic process in which two distinct liquid phases appear in solution. The top layer is usually the protein-poor phase, possessing protein concentration of <10 mg/mL, while the bottom layer is extreme viscous due to the presence of large amount of proteins (>200-300 mg/mL), called protein-rich phase. The ratio (v/v) of protein-poor/protein-rich phases depends on a variety of factors including net protein concentrations, temperature, and solution conditions (such as pH, buffer composition, or additives). Phase separation is also a reversible process, which can revert back to a single phase by changing temperature, adjusting solution composition, or simply by just diluting to a lower protein concentration. In many studies,<sup>102-104</sup> a phase diagram tool has been used to represent phase separation behaviour of various mAbs, where the phase separation is demonstrated using the binodal curve. Phase separation is occurring in these high concentration solutions mainly because the original protein solution is thermodynamic unstable, and thus it tries to equilibrate to another thermodynamic stable condition. The kinetics of such equilibrium process varies a lot based on properties of particular mAbs, solution conditions, and temperature. Phase separation usually shows

strong opalescence during equilibrium process and even after phase separation has already formed. Therefore, high opalescence and viscosity, especially in the protein-rich phase, brings a lot of challenges during product manufacturing and administration. Furthermore, irreversible aggregation may happen among protein molecules, especially during long-time storage. A summary of the many differences that exist between phase separation and aggregation has been reported (Table 3).<sup>103</sup>

#### **1.4.3. Strategies to Mitigate Reversible Self-Association**

Due to so many challenges and problems caused by RSA of mAbs at high protein concentrations, including mAb manufacturing, storage stability, and delivery to patients, numerous approaches or strategies to mitigate PPIs have been pursued and evaluated in developing high-concentration mAb formulations. Various methods to improve high-concentration solution properties have been studied and are discussed in more detail below including formulation, protein engineering, lyophilization, and use of the enzyme hyaluronidase.

**Table 3.** Difference between aggregation and phase separation for protein solutions<sup>103</sup>

(Table reproduced)

aggregation	liquid–liquid phase separation
reversible and/or irreversible	reversible
native and/or non-native species	native species
high temperature	low temperature
covalent and/or noncovalent interactions	noncovalent interactions
opalescence due to particles in solution	opalescence due to concentration fluctuation in solution

#### 1.4.3.1. Formulation

Different solution parameters such as pH, ionic strength, and addition of excipients have been examined for their ability to reduce mAb PPIs at high protein concentrations and thus improve solution properties.<sup>100,105,106</sup> Based on the various mechanisms of PPIs, different buffer conditions or excipients can be employed to modulate the extent of mAb RSA.<sup>87,89,91</sup> Although formulation screening can be a time-consuming process, for example, sometimes many factors or effects exist at the same time with addition of multiple excipients, it usually gives successful results in terms of identifying conditions for mitigating PPIs for RSA mAbs. Furthermore, a balance between excipient effects on RSA must be balanced against their potential effects on protein conformational and/or colloidal stability. For example, excipients can disrupt the RSA of a specific mAb, but at the same time, conformation stability of the mAb could also be altered. Rational formulation design and selection of specific excipient types and corresponding concentrations are thus an



important consideration in formulating high-concentration protein mAb solutions. Solution pH is another critical factor on controlling PPIs by adjusting the net charge of mAbs.<sup>87,107</sup> Based on the isoelectric point (pI) of a mAb, alteration of solution pH can substantially increase/decrease charge repulsions between protein molecules, playing a key role in PPIs of certain mAbs (e.g., when RSA of a mAb is driven by either electrostatic or hydrophobic forces).<sup>89,107</sup> A recent study of formulation development approach to reduce solution viscosity demonstrates a wealth of knowledge on excipients selection, pH alteration, and provides a potential formulation development platforms on characterizing ultra-high protein concentration solutions.<sup>89</sup> Overall, a formulation strategy is a widely employed and useful approach to mitigate mAb RSA of mAb candidates requiring delivery at high protein concentrations.

#### **1.4.3.2. Protein Engineering**

An alternative approach, which has also been broadly employed to weaken PPIs of mAbs at high protein concentrations, is protein engineering by essential point mutations. This is a more direct method which purposely mutates particular amino acid residue(s) on the RSA regions (or RSA interfaces), especially charged, aromatic, or hydrophobic ones. Unfortunately, mAbs may undergo dramatic property changes (conformational or colloidal or biological) with such “key” amino acid replacement(s). Different protein engineering studies regarding a series of mAbs with varying RSA mechanisms have been performed to examine the alteration of protein RSA propensity as well as solution properties.<sup>88,99,108,109</sup> These studies demonstrate that an optimally engineered mAbs possessed the properties of reduced self-association propensity, decreased protein size and solution viscosity, and enhanced solubility, while with

minimum loss of antigen-binding affinity. Albeit there are many successful cases, there are also some limitations by using this protein engineering approach. Normally, preceding knowledge of interaction sites, particular amino acids, or even PPIs mechanism is required, which must be obtained by other approaches, such as computational or analytical methods such as HDX-MS, providing information on selecting specific amino acids for mutation analysis. Also, potential conformational alterations could happen with one or more amino acids substitution, which may further induce a set of adverse effects, such as loss of binding activity, partial denaturation, irreversible aggregation, and reduced thermal stability. For example, since RSA sites are often at mAb CDR regions, which are the critical sequences of antibody (paratope) for antigen binding, mutation of amino acid residues especially the charged or aromatic ones could tremendously influence antibody-antigen binding affinity. Therefore, a number of mutations with different amino acids are usually needed to comprehensively determine and examine protein RSA propensity, physical stability, solution properties, and antigen binding affinity.<sup>88,109</sup>

#### **1.4.3.3. Lyophilization**

In addition to aqueous liquid solution formulations, mAbs have also been prepared and developed in lyophilized formulations to improve stability and minimize aggregation and chemical degradation pathways. Physical stability can be greatly enhanced during long term storage due to restricting mobility by employing a lyophilized formulation with suitable excipients and lyoprotectants, for example, carbohydrates such as trehalose and sucrose.<sup>110-112</sup> Freeze drying can also minimize other potential hydrolytic reactions by removal of water.<sup>110</sup> Several commercial mAbs are formulated as lyophilized dosage forms such as canakinumab, omalizumab, efalizumab, palivizumab, trastuzumab,

infliximab, etc.<sup>113</sup> Some of these have a concentration above 100 mg/mL after reconstitution, indicating a potential possibility to formulate high-concentration protein solutions for SC administration.<sup>113</sup> However, many drawbacks also exist using a lyophilization strategy to formulate high-concentration mAbs prone to RSA. One critical and unique challenge is the long reconstitution time for a lyophilized high protein concentration drug product, which can dramatically limit practical usage as well as commercial marketability.<sup>114</sup> It has been reported previously that reconstitution time of high concentration (>100 mg/mL) lyophilized protein containing cakes can be as long as 30 mins or more.<sup>114</sup> In addition, lyophilization is a stress condition for mAbs, in which aggregation or partial structural unfolding might take place during freezing or sublimation steps of the lyophilization process. Therefore, proper selection of excipients (lyoprotectants), including appropriate type and amount, and an optimized lyophilization cycle are usually required to keep mAbs in their native state both during freeze drying, long term storage in the solid state, and upon reconstitution.

#### **1.4.3.4. Use of Recombinant Human Hyaluronidase Enzyme**

The extracellular matrix (ECM) contains a network of collagenous fibrils which are embedded within glycosaminoglycan- and proteoglycan-rich viscoelastic gel-like substances, a fundamental barrier to the effective subcutaneous delivery of antibody drugs and thus limiting injection volume to less than 2 mL.<sup>115</sup> Due to such fibril networks in ECM, it can take up to several days for mAbs to reach maximal levels in plasma after SC injection.<sup>115</sup> However, the use of recombinant human hyaluronidase enzyme (rHuPH20) can potentially overcome this significant barrier by depolymerization of the viscoelastic component of the interstitial matrix. The dispersion of locally injected mAbs

could be substantially enhanced by using rHuPH20 without tissue distortion. Therefore, this effect will allow for notable increases in injection volumes, and thus it could be possible to decrease protein concentrations (avoid antibody self-association) as well as reduce as frequently the number of dosing required via SC administration. Furthermore, rHuPH20 could essentially alter pharmacokinetic profiles and dramatically augment the absolute bioavailability of mAb therapeutics.<sup>116</sup> More importantly, the interstitial viscoelastic barriers are usually restored within 24 hours of SC injection without histologic alteration or other potential signs of inflammation.<sup>116</sup>

There are now several commercialized mAb drugs with rHuPH20 co-formulated and usually co-administered by SC injections/infusions with the active therapeutic mAbs, such as trastuzumab and rituximab, for the treatment of breast and lymphoma cancer, respectively.<sup>82,117</sup> It has been shown that the use of rHuPH20 is safe for SC injections and results in similar drug plasma concentrations in comparison to intravenous injections, but markedly shortens the infusion times.<sup>82,118</sup>

### **1.5. Formulation Development Challenges and Opportunities for sIgA as Therapeutic mAb Candidate**

As the most dominant antibody in the mucosal compartments, sIgAs play a critical role binding and protecting against pathogenic substances, such as bacteria as well as viruses, which enlightens the possibilities of sIgA as therapeutic mAb candidates for the treatment of bacteria/virus-induced diseases or infections on mucosal membranes.<sup>119,120</sup> However, due to the complex nature of sIgAs, combined with need to provide protection in the harsh conditions in gastrointestinal (GI) tract, a variety of formulation challenges

will be encountered upon the development of sIgA as an orally delivered therapeutic drug candidate.<sup>121,122</sup>

### **1.5.1. High Molecular Weight Species of sIgA**

Unlike IgG, sIgA is present in the external secretions in polymeric forms, predominantly in a tail-to-tail dimer structure linked with J chain and SC chain by disulfide bonds. In addition, however, higher order oligomers such as trimers and tetramers are also observed for sIgA.<sup>123,124</sup> Possessing eight cysteine residues, the J chain substantially increases the chances to form polymeric sIgAs by potential disulfide bonds.<sup>125,126</sup> Moreover, based on immunochemical studies, polymeric sIgA often has multiple J chains, which further enhances the possibility to form higher-order structures for sIgA molecule.<sup>12,127</sup> However, it has also been found that some polymeric IgAs exist in serum without J chain. These IgAs cannot be transported to mucosal membranes, indicating that J chain might not be obligatory for IgA to form polymeric structure, but necessary for sIgA formation and epithelial transportation.<sup>11,128,129</sup> In terms of biological functions, polymeric sIgA maintains or even possesses better activities than monomeric IgA, acting as a digestion-resistant, high potent molecule against pathogens.<sup>130</sup> It has been reported that the polymeric forms of sIgA can potentially inhibit intracellular virus production, and have functions on neutralizing particular toxins or pathogenic bacteria, such as neutralizing proinflammatory antigens.<sup>67,131</sup>

### **1.5.2. Challenges Associated with Oral Protein Delivery**

Oral delivery of small molecules as therapeutic drugs has been consistently widely used, given that it provides benefits in terms of less manufacturing costs, ease of

administration, and thus increased patient compliance. For large molecules, like proteins or specifically monoclonal antibodies, several significant challenges for oral delivery include the instability of proteins in the GI tract, and unpredictable absorption across the intestinal epithelial membrane to the systemic circulation in lymphatic or blood vessels, which probably acts as the major barriers regarding efficient oral protein drug delivery for systemic distribution in the body.<sup>121,132,133</sup> As discussed below, the oral delivery of sIgA is potentially more promising since it not being used for systemic delivery but rather is being considered for local oral delivery to bind and neutralize enteric disease causing microorganisms found in the GI tract.

#### **1.5.2.1. Gastric pH**

In the human stomach, gastric fluid is an acidic in nature for digestion purposes, composed of hydrochloric acid (HCl), potassium chloride (KCl) and sodium chloride (NaCl). The pH of gastric acid is about 1.5-3.5 in the human adult stomach lumen, which plays a key role in digestion of ingested proteins by denaturing and unfolding them.<sup>134</sup> Degradation of proteins in the highly acidic condition of the stomach is believed to be through destabilization of the three-dimensional structural folding due to alterations of ionic and hydrogen bonding.<sup>135</sup> Such low pH environment is always maintained in human stomach through the proton pump  $H^+/K^+$  ATPase. Therefore, therapeutic proteins, such as mAbs, will be at least partially denatured, and thus lose some of their characteristic folded structures, and at the same time, some of the peptide bonds between amino acid residues in the polypeptide chains will be exposed at low pH to be eventually broken down by digestive enzymes (see Section 1.5.2.2.)

### **1.5.2.2. Proteases**

Another significant challenge associated with protein oral delivery is the presence of a variety of proteases in GI tract. Pepsin is one of the main digestive enzymes predominantly found in the human stomach. It belongs to endopeptidase class of enzymes which can break down proteins rather non-specifically (in terms of amino acid sequences) into small peptides. As the most efficient digestive enzyme, pepsin cleaves peptide bonds between amino acid residues in the polypeptide backbone of proteins between hydrophobic and especially aromatic amino acids.<sup>136</sup> The most active state of pepsin is usually at low pH ranges (particularly at pH =2) and between 37 °C and 42 °C.<sup>137</sup> Furthermore, intestinally secreted enzymes, such as trypsin and chymotrypsin, also have notable functions on protein digestion. Trypsin is a serine protease formed in the small intestine, cleaving bonds in the polypeptide chains primarily at the carboxyl side of two amino acids, arginine and lysine, except under the condition that the following amino acid is proline. The optimal operating temperature for trypsin is about 37 °C and the optimum pH is at about 8.<sup>138</sup> As for chymotrypsin, it is a digestive enzyme acting in the duodenum as the important component of pancreatic juice. Chymotrypsin is usually activated in the presence of trypsin and preferentially cleaves peptide bonds in proteins at the sites of aromatic amino acids, such as phenylalanine, tyrosine, and tryptophan. The optimum pH and temperature for chymotrypsin are approximately pH 8 and 40 °C, respectively.<sup>139</sup> Other enzymes in the intestine, such as elastase and brush-border membrane-bound enzymes carboxypeptidases A and B, can also induce hydrolysis of particular sites within proteins, causing protein degradation.<sup>121</sup>

### **1.5.2.3. Absorption**

Protein therapeutics, including mAbs, are mostly hydrophilic with a  $\log P$  value below zero.<sup>140</sup> Therefore, unlike some smaller, hydrophobic substances, therapeutic mAbs normally cannot follow the transcellular route of absorption via passive diffusion.<sup>140</sup> In terms of paracellular pathway, the dimension of such space lies a range of 10 to 50 Å, which can probably only fit for small hydrophilic molecules, rather than macromolecules, such as mAbs (diameter of 9-12 nm).<sup>141,142</sup> However, some studies have demonstrated that smaller proteins, such as insulin, can be internalized after being absorbed on the apical membrane by particular types of endocytosis.<sup>143</sup> As for other potentially orally delivered proteins, after binding to specific receptors on the surface of epithelial cells in the small intestine, they could be actively transported across the epithelial lining through certain types of membrane-bound vesicles.<sup>144</sup> However, most of the proteins would degrade and/or be structurally altered causing them to lose their biological functions by such active transportation pathway during the process of release at the basolateral membrane or secretion into the interstitial space. Therefore, it turns out that successful transportation across epithelial cells in human small intestine is a big hurdle for oral delivery of large macromolecules such as proteins (including mAbs). Since the three dimensional structure of mAbs is closely related to their biological activities, it is of high importance to keep them in their folded, intact forms through absorption process. Although many strategies have been studied to obtain efficient and proper strategy for intestinal absorption for protein-based therapeutics, such as use of permeation enhancement agents, employment of protease inhibitors, or modulating tight-junction permeability, some concerns or issues still exist in terms of widespread acceptance or



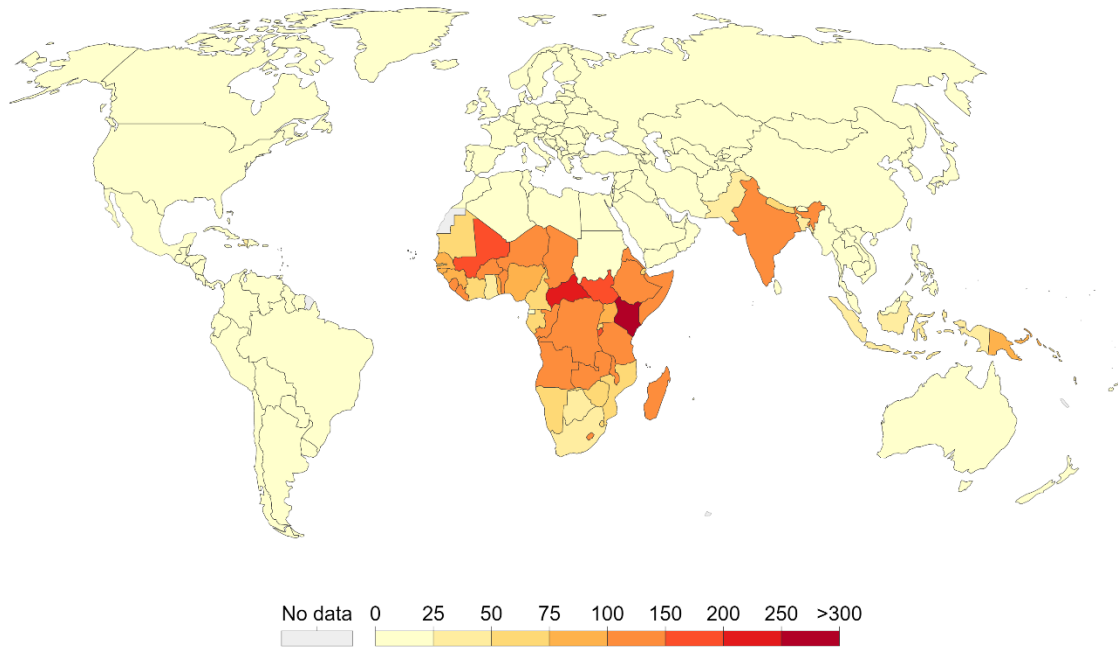
potential safety considerations for use of these approaches with protein drug candidates.<sup>145-147</sup>

### **1.5.3. Mucosa Compartment as an “Ideal” Place for sIgA-based Treatments**

As the “first line” of immune defense, sIgA plays a key role in immunoprotection within the mucosal membranes. It is the sIgA form (especially sIgA2) that is the predominantly present immunoglobulin in the GI tract, especially in the intestinal phase, and performs critical effects on neutralizing pathogenic bacteria, viruses, and toxins. In addition, the multi-chain composition and polymeric property of sIgA makes it more protease-resistant and more stable in the harsh-environment (low pH in the gastric phase) as compared to less tolerant molecules such as IgG. Therefore, sIgAs could potentially be developed as an orally delivered drug candidate for passive immunization in the mucosal compartment, for treatments of diseases or infections in the GI tract.

#### **1.5.3.1. Diarrheal Diseases**

Diarrheal diseases continue to be the leading causes of death for children under 5-years old, especially in the low- and mid-income countries (Figure 5). Although the mortality rate decreased to a large extent from 2005 to 2015, due to vaccination and improved sanitation, still about half million children (under five) die worldwide each year due to such enteric diseases.<sup>148</sup> Some of the causes of diarrheal diseases in under-developed or developing countries include poor quality life of children coupled with lack of basic sanitation, bad climatic or environmental conditions, and unavailability of medical treatments and health-care facilities.<sup>149-151</sup>



Source: IHME, Global Burden of Disease (GBD)

CC BY-SA

**Figure 5.** Diarrheal disease death rates (per 100,000), 2016<sup>152</sup> (Figure reprinted)

Previously, severe dehydration and significant fluid loss were the two major reasons that led to diarrhoea induced deaths. Currently, other potential causes, such as septic bacterial infections, are gradually becoming the dominant reason for diarrhoea-associated deaths. Diarrhoea is normally a symptom of potential infections in human intestinal tract, which can usually be caused by various infectious agents including bacteria, viruses, and parasitic organisms. Rotavirus, enterotoxigenic *Escherichia coli* (ETEC), *vibrio cholerae*, *Shigella*, *entamoeba histolytica*, and *giardia lamblia* are important infection sources of diarrheal diseases in developing countries.<sup>153-156</sup> Among them, rotavirus and ETEC are the two most common etiological agents of moderate-to-severe diarrheal diseases in these countries.<sup>157,158</sup> Although there are vaccines available for rotavirus-induced diarrhoea, their availability and efficacy is limited in the developing world. There is currently no vaccines approved for human use for diseases caused by

ETEC.<sup>158</sup> Since these pathogens are found mainly in the intestinal tract, including adhesions on epithelial cells and excretions of different toxins, passive immunization using potential mAbs, especially sIgA, could potentially greatly enhance and contribute to immune responses in local regions, such as small intestine. Therefore, diarrhoea are the first disease targets that orally delivered sIgA can be utilized as potential drug candidate for corresponding binding key antigens found on the microorganisms, treatments. Other bacterial/virus-induced diseases or infections of the GI tract can also be potentially targets for sIgA treatments in the future.

#### **1.5.4. Possible Formulation Approaches for Oral Delivery of sIgA**

Although sIgA has a relatively high stability particularly under the conditions present in the GI tract, low pH conditions in stomach and the presence of a variety of digestive enzymes would eventually “destroy” the conformational structural integrity of sIgA in the gut lumen, decreasing or eliminating its biological activities. As a result, proper buffers or excipients as well as certain oral delivery approaches are particularly desired to formulate sIgA for fulfilling successful oral delivery purposes. Since the goal is to use this treatment approach in the developing world, low-cost approaches are also a critical factor in the design of sIgA formulations. And eventually, the well-formulated, stable, low cost sIgA candidates could be developed as a potential orally delivered drug products to treat different diseases or infections in human GI tract.

##### **1.5.4.1. Protease Inhibitors**

To alter activities of different enzymes in the GI tract, protease inhibitors could potentially be employed to protect therapeutic sIgA mAbs from digestion during oral

delivery. Several potential enzyme inhibitors have been studied previously, including soybean trypsin inhibitor, aprotinin, chromastatin, and camostat mesilate.<sup>159-161</sup> However, it is also shown that long-term administration of these inhibitors would result in deficiency of such enzymes in humans.<sup>159</sup> Therefore, selection of proper type and amount of enzyme inhibitors would be necessary when co-formulated along with the active sIgA antibody therapeutics, and the proteolytic enzymes commonly follow dose-dependent inhibitory effects.<sup>161</sup> Furthermore, other potential enzyme inhibitors, such as duck and chicken ovomucoids, and polymer inhibitor conjugates (carboxymethyl cellulose-Elastinal), also showed efficient protection for insulin against trypsin or chymotrypsin, which might be good protease inhibitor candidates for oral mAbs delivery.<sup>143,162,163</sup> Several major inhibition mechanisms have been determined and reported previously.<sup>164</sup> The vast majority of enzyme inhibitors can, acting as a competitive inhibitors, preferentially bind to a critical portion of the protease in a substrate-like manner, which presumably blocks the binding between digestive enzymes and target substances. Besides, plenty of enzyme inhibitors have secondary binding sites outside the active site, increasing the surface area of protein interactions to obtain greater affinity, and improving the binding specificity of particular inhibitors. Last but not least, some protease inhibitors, known as suicide substrates, can covalently bind to proteolytic enzymes, such as Serpin (Serine protease inhibitor), and thus interrupts conformational structures via chemical modifications, thereby irreversibly inhibiting enzymatic activities.<sup>165,166</sup>

#### **1.5.4.2. Buffers or Reagents for Gastric pH Neutralization**

In terms of the relative low pH environment in human stomach, protein therapeutics are prone to undergo conformational alterations and loss of their biological activities.

Therefore, appropriate strategies are desired to mitigate acidic pH effects (by primarily neutralizing gastric fluid pH) on protein structures. Previously, it has been demonstrated that the use of bicarbonate buffers (as well as other buffering agents) protects orally delivered rotavirus vaccines from acidic denaturation by pH neutralization.<sup>167</sup> Other studies also have shown that a versatile pH-responsive hydrogel, which exhibited pH-responsive activity, and could be applied as a platform for delivery of gastric-sensitive protein therapeutics to the intestinal tract.<sup>168</sup> As a result, appropriate design and use of pH neutralizing buffers or reagents could substantially improve mAbs stability in the GI tract during oral delivery. However, it is also critical to consider mAbs storage stability in such solution conditions. Strong basic solutions, large amount of salts, and protein-reagent reactions might also alter protein structural integrity and stability.

#### **1.5.4.3. Novel Mucoadhesive Encapsulation Carrier Systems**

To enhance the stability and absorption of therapeutic proteins during oral delivery, encapsulation and delivery by novel carrier system could also be potentially employed. A variety of mucoadhesive polymers, such as poly lactic-co-glycolic acid (PLGA), chitosan, and thiolated polymer, have been extensively used for these purposes in laboratory and animal studies.<sup>169-171</sup> These formulations could be prepared in nanoparticles or microspheres and encapsulate therapeutic proteins inside, providing a microenvironment that is less accessible to proteases or acidic pH. Encapsulation potentially then could effectively protect protein drug candidates from enzyme degradation during oral delivery. These polymers can adhere to the mucosal membranes and thus affect the concentration gradient of proteins, increasing bioavailability for a prolonged time.<sup>160,172</sup> However, based on previous studies, the protein-containing nanoparticles or microspheres have technical

challenges and problems including broad size distribution with poor reproducibility.<sup>173</sup> Furthermore, during the preparation and storage, it is also a big challenge to keep protein drug candidate itself intact and stable, without losing biological activities.<sup>173</sup> In addition, manufacturing of such novel carrier system for protein oral delivery will be at a comparatively high cost, substantially increasing burdens for patients. Therefore, although the application of novel mucoadhesive encapsulation carrier systems is very attractive approach, additional studies will be needed to produce more reliable and affordable orally delivered drug products with these types of formulations.

#### **1.5.4.4. “Decoy” Protein Protection**

A decoy substance (or pseudo-substance) typically refers to a particular protein additive that possesses similar structure to compete as a substrate of the proteolytic enzymes. This simple approach would allow the decoy protein to competitively bind to the proteolytic enzyme and leave the actual drug candidate intact. Such a strategy could also be employed for the oral delivery of therapeutic proteins such as sIgAs. A variety of proteins can potentially be the “decoy” substances, such as casein, other milk proteins, soy proteins, albumin, etc. Although some of them probably don’t have highly similar structures as a sIgA protein therapeutics, they are more susceptible to be digested in the presence of proteases, and could be added in large excess, and thus would be digested instead of the active proteins drug candidate. As a result, the “decoy” protein strategy, especially in combination with infant milk, could presumably be a suitable, low-cost stabilization approach for oral delivery of sIgA drug candidates to infants.

## 1.6. References

1. Rajpal A, Strop P, Yeung YA, Chaparro-Riggers J, Pons J 2014. Introduction: Antibody structure and function. *Therapeutic Fc-Fusion Proteins*:1-44.
2. Nezlin R. 1998. *The immunoglobulins: structure and function*. ed.: Academic Press.
3. ThermoFisherScientific. *Immunoglobulin Structure and Classes*. ed.
4. Hadley G 2007. Basic Histology. *Journal of Anatomy* 211(3):412-413.
5. Cattaneo A, Neuberger MS 1987. Polymeric immunoglobulin M is secreted by transfectants of non-lymphoid cells in the absence of immunoglobulin J chain. *The EMBO journal* 6(9):2753-2758.
6. Fazel S, Wiersma EJ, Shulman MJ 1997. Interplay of J chain and disulfide bonding in assembly of polymeric IgM. *International immunology* 9(8):1149-1158.
7. Collins C, Tsui FW, Shulman MJ 2002. Differential activation of human and guinea pig complement by pentameric and hexameric IgM. *European journal of immunology* 32(6):1802-1810.
8. Davis A, Collins C, Yoshimura M, D'agostaro G, Shulman M 1989. Mutations of the mouse mu H chain which prevent polymer assembly. *The Journal of Immunology* 143(4):1352-1357.
9. Chapuis RM, Koshland ME 1974. Mechanism of IgM polymerization. *Proceedings of the National Academy of Sciences* 71(3):657-661.
10. Mihaesco C, Mihaesco E, Metzger H 1973. Variable J-chain content in human IgM. *FEBS Lett* 37(2):303-306.
11. Brandtzaeg P 1976. Complex formation between secretory component and human immunoglobulins related to their content of J chain. *Scandinavian journal of immunology* 5(4):411-419.
12. Grubb AO 1978. Quantitation of J chain in human biological fluids by a simple immunochemical procedure. *Acta Medica Scandinavica* 204(1-6):453-465.
13. Rogentine G, Rowe D, Bradley J, Waldmann T, Fahey J 1966. Metabolism of human immunoglobulin D (IgD). *The Journal of Clinical Investigation* 45(9):1467-1478.
14. Übelhart R, Hug E, Bach MP, Wossning T, Dühren-von Minden M, Horn AH, Tsiantoulas D, Kometani K, Kurosaki T, Binder CJ 2015. Responsiveness of B cells is regulated by the hinge region of IgD. *Nature immunology* 16(5):534.
15. Chen K, Xu W, Wilson M, He B, Miller NW, Bengten E, Edholm E-S, Santini PA, Rath P, Chiu A 2009. Immunoglobulin D enhances immune surveillance by activating antimicrobial, proinflammatory and B cell-stimulating programs in basophils. *Nature immunology* 10(8):889.
16. Capron M, Jouault T, Prin L, Joseph M, Ameisen JC, Butterworth AE, Papin JP, Kusnierz JP, Capron A 1986. Functional study of a monoclonal antibody to IgE Fc receptor (Fc epsilon R2) of eosinophils, platelets, and macrophages. *The Journal of experimental medicine* 164(1):72-89.
17. Pritchard D, Quinnell R, Walsh E 1995. Immunity in humans to *Necator americanus*-. IgE, parasite weight and fecundity. *Parasite immunology* 17(2):71-75.
18. Turner JD, Faulkner H, Kamgno J, Kennedy MW, Behnke J, Boussinesq M, Bradley JE 2005. Allergen-specific IgE and IgG4 are markers of resistance and susceptibility in a human intestinal nematode infection. *Microbes and Infection* 7(7-8):990-996.
19. Permin H, Wiik A 1978. The prevalence of IgE antinuclear antibodies in rheumatoid arthritis and systemic lupus erythematosus. *Acta Pathologica Microbiologica Scandinavica Section C Immunology* 86(1-6):245-249.
20. Elkayam O, Tamir R, Pick A, Wysenbeek A 1995. Serum IgE concentrations, disease activity, and atopic disorders in systemic lupus erythematosus. *Allergy* 50(1):94-96.
21. Cox L, Williams B, Sicherer S, Oppenheimer J, Sher L, Hamilton R, Golden D 2008. Pearls and pitfalls of allergy diagnostic testing: report from the American college of allergy, asthma and

immunology/American academy of allergy, asthma and immunology specific IgE test task force. *Annals of Allergy, Asthma & Immunology* 101(6):580-592.

22. Janeway Jr CA, Travers P, Walport M, Shlomchik MJ 2001. The structure of a typical antibody molecule.
23. Janeway CA, Travers P, Walport M, Shlomchik MJ 2005. *Immunobiology: the immune system in health and disease*.
24. Reichert JM 2012. Marketed therapeutic antibodies compendium. *mAbs* 4(3):413-415.
25. Schroeder HW, Jr., Cavacini L 2010. Structure and function of immunoglobulins. *J Allergy Clin Immunol* 125(2 Suppl 2):S41-52.
26. Arnold JN, Wormald MR, Sim RB, Rudd PM, Dwek RA 2007. The impact of glycosylation on the biological function and structure of human immunoglobulins. *Annu Rev Immunol* 25:21-50.
27. Butler M, Quelhas D, Critchley AJ, Carchon H, Hebestreit HF, Hibbert RG, Vilarinho L, Teles E, Matthijs G, Schollen E 2003. Detailed glycan analysis of serum glycoproteins of patients with congenital disorders of glycosylation indicates the specific defective glycan processing step and provides an insight into pathogenesis. *Glycobiology* 13(9):601-622.
28. Abès R, Teillaud J-L 2010. Impact of glycosylation on effector functions of therapeutic IgG. *Pharmaceuticals* 3(1):146-157.
29. Sutton B, Phillips D. 1983. The three-dimensional structure of the carbohydrate within the Fc fragment of immunoglobulin G. ed.: Portland Press Limited.
30. Subedi GP, Barb AW 2015. The Structural Role of Antibody N-Glycosylation in Receptor Interactions. *Structure (London, England : 1993)* 23(9):1573-1583.
31. Liu H, Bulseco G-G, Sun J 2006. Effect of posttranslational modifications on the thermal stability of a recombinant monoclonal antibody. *Immunology letters* 106(2):144-153.
32. Higel F, Seidl A, Sörgel F, Friess W 2016. N-glycosylation heterogeneity and the influence on structure, function and pharmacokinetics of monoclonal antibodies and Fc fusion proteins. *European Journal of Pharmaceutics and Biopharmaceutics* 100:94-100.
33. Liu L 2017. Pharmacokinetics of monoclonal antibodies and Fc-fusion proteins. *Protein & cell*:1-18.
34. More AS. 2017. ELUCIDATION OF THE IMPACT OF N-GLYCAN STRUCTURE ON PHYSICAL STABILITY AND LOCAL FLEXIBILITY OF WELL-DEFINED IgG1-Fc GLYCOFORMS FROM A PHARMACEUTICAL DEVELOPMENT PERSPECTIVE. ed.: University of Kansas.
35. Gonzalez-Quintela A, Alende R, Gude F, Campos J, Rey J, Meijide L, Fernandez-Merino C, Vidal C 2008. Serum levels of immunoglobulins (IgG, IgA, IgM) in a general adult population and their relationship with alcohol consumption, smoking and common metabolic abnormalities. *Clinical & Experimental Immunology* 151(1):42-50.
36. Stapleton NM, Andersen JT, Stemerding AM, Bjarnarson SP, Verheul RC, Gerritsen J, Zhao Y, Kleijer M, Sandlie I, De Haas M 2011. Competition for FcRn-mediated transport gives rise to short half-life of human IgG3 and offers therapeutic potential. *Nature communications* 2:599.
37. Vidarsson G, Dekkers G, Rispens T 2014. IgG Subclasses and Allotypes: From Structure to Effector Functions. *Frontiers in Immunology* 5:520.
38. Davies AM, Sutton BJ 2015. Human IgG4: a structural perspective. *Immunological reviews* 268(1):139-159.
39. Woof J, Russell M 2011. Structure and function relationships in IgA. *Mucosal immunology* 4(6):590.
40. Bonner A, Perrier C, Corthésy B, Perkins SJ 2007. Solution structure of human secretory component: implications for biological function. *Journal of Biological Chemistry*.
41. Kerr M 1990. The structure and function of human IgA. *Biochemical journal* 271(2):285.



42. Crottet P, Corthésy B 1998. Secretory component delays the conversion of secretory IgA into antigen-binding competent F (ab')<sub>2</sub>: a possible implication for mucosal defense. *The Journal of Immunology* 161(10):5445-5453.
43. Woof JM, Kerr MA 2006. The function of immunoglobulin A in immunity. *The Journal of Pathology: A Journal of the Pathological Society of Great Britain and Ireland* 208(2):270-282.
44. Novak J, Julian BA, Tomana M, Mestecky J 2008. IgA glycosylation and IgA immune complexes in the pathogenesis of IgA nephropathy. *Seminars in nephrology* 28(1):78-87.
45. Royle L, Roos A, Harvey DJ, Wormald MR, Van Gijlswijk-Janssen D, Redwan E-RM, Wilson IA, Daha MR, Dwek RA, Rudd PM 2003. Secretory IgA N- and O-glycans provide a link between the innate and adaptive immune systems. *Journal of Biological Chemistry* 278(22):20140-20153.
46. Field M, Amatayakul-Chantler S, Rademacher T, Rudd P, Dwek R 1994. Structural analysis of the N-glycans from human immunoglobulin A1: comparison of normal human serum immunoglobulin A1 with that isolated from patients with rheumatoid arthritis. *Biochemical Journal* 299(1):261-275.
47. Mattu TS, Pleass RJ, Willis AC, Kilian M, Wormald MR, Lellouch AC, Rudd PM, Woof JM, Dwek RA 1998. The glycosylation and structure of human serum IgA1, Fab, and Fc regions and the role of N-glycosylation on Fc $\alpha$  receptor interactions. *Journal of Biological Chemistry* 273(4):2260-2272.
48. Basset C, Devauchelle V, Durand V, Jamin C, Pennec Y, Youinou P, Dueymes M 1999. Glycosylation of immunoglobulin A influences its receptor binding. *Scandinavian journal of immunology* 50(6):572-579.
49. Stockert RJ 1995. The asialoglycoprotein receptor: relationships between structure, function, and expression. *Physiological reviews* 75(3):591-609.
50. Reinholdt J, Tomana M, Mortensen S, Kilian M 1990. Molecular aspects of immunoglobulin A1 degradation by oral streptococci. *Infection and immunity* 58(5):1186-1194.
51. Falk P, Roth KA, Boren T, Westblom TU, Gordon JI, Normark S 1993. An in vitro adherence assay reveals that *Helicobacter pylori* exhibits cell lineage-specific tropism in the human gastric epithelium. *Proceedings of the National Academy of Sciences* 90(5):2035-2039.
52. Boren T, Falk P, Roth KA, Larson G, Normark S 1993. Attachment of *Helicobacter pylori* to human gastric epithelium mediated by blood group antigens. *Science* 262(5141):1892-1895.
53. Tarelli E, Smith AC, Hendry BM, Challacombe SJ, Pouria S 2004. Human serum IgA1 is substituted with up to six O-glycans as shown by matrix assisted laser desorption ionisation time-of-flight mass spectrometry. *Carbohydrate research* 339(13):2329-2335.
54. Plaut AG 1983. The IgA1 proteases of pathogenic bacteria. *Annual Reviews in Microbiology* 37(1):603-622.
55. Chintalacheruvu KR, Li JY, Bhola N, Kobayashi K, Fernandez CZ, Morrison SL 2002. Cysteine residues required for the attachment of the light chain in human IgA2. *The Journal of Immunology* 169(9):5072-5077.
56. Loomes LM, Stewart WW, Mazengera RL, Senior BW, Kerr MA 1991. Purification and characterisation of human immunoglobulin IgA1 and IgA2 isotypes from serum. *Journal of immunological methods* 141(2):209-218.
57. Gleeson M, Hall ST, McDonald WA, Flanagan AJ, Clancy RL 1999. Salivary IgA subclasses and infection risk in elite swimmers. *Immunology and cell biology* 77(4):351-355.
58. Brandtzaeg P 1992. Humoral immune response patterns of human mucosae: induction and relation to bacterial respiratory tract infections. *Journal of Infectious Diseases* 165(Supplement\_1):S167-S176.
59. Mazanec MB, Nedrud JG, Kaetzel CS, Lamm ME 1993. A three-tiered view of the role of IgA in mucosal defense. *Immunology today* 14(9):430-435.
60. Mantis NJ, Rol N, Corthésy B 2011. Secretory IgA's complex roles in immunity and mucosal homeostasis in the gut. *Mucosal immunology* 4(6):603-611.

61. Borrok MJ, Luheshi NM, Beyaz N, Davies GC, Legg JW, Wu H, Dall'Acqua WF, Tsui P 2015. Enhancement of antibody-dependent cell-mediated cytotoxicity by endowing IgG with FcαRI (CD89) binding. *mAbs* 7(4):743-751.
62. Shibuya A, Honda S-i. Springer seminars in immunopathology, 2006, pp 377.
63. Kikuno K, Kang DW, Tahara K, Torii I, Kubagawa HM, Ho KJ, Baudino L, Nishizaki N, Shibuya A, Kubagawa H 2007. Unusual biochemical features and follicular dendritic cell expression of human Fcα/μ receptor. *European journal of immunology* 37(12):3540-3550.
64. Wang R, Fu Y, Zhao Q, Pan L, Zhang W 2009. Human Fcα/μR and pIgR distribute differently in intestinal tissues. *Biochemical and biophysical research communications* 381(2):148-152.
65. Woof JM, Kerr MA 2006. The function of immunoglobulin A in immunity. *J Pathol* 208(2):270-282.
66. Mazanec MB, Coudret CL, Fletcher DR 1995. Intracellular neutralization of influenza virus by immunoglobulin A anti-hemagglutinin monoclonal antibodies. *Journal of virology* 69(2):1339-1343.
67. Fujioaka H, Emancipator SN, Aikawa M, Huang DS, Blatnik F, Karban T, DeFife K, Mazanec MB 1998. Immunocytochemical colocalization of specific immunoglobulin A with sendai virus protein in infected polarized epithelium. *Journal of Experimental Medicine* 188(7):1223-1229.
68. Bomsel M, Heyman M, Hocini H, Lagaye S, Belec L, Dupont C, Desgranges C 1998. Intracellular neutralization of HIV transcytosis across tight epithelial barriers by anti-HIV envelope protein dIgA or IgM. *Immunity* 9(2):277-287.
69. Russell MW, Reinholdt J, Kilian M 1989. Anti-inflammatory activity of human IgA antibodies and their Fabα fragments: inhibition of IgG-mediated complement activation. *European journal of immunology* 19(12):2243-2249.
70. Griffiss JM, Goroff D 1983. IgA blocks IgM and IgG-initiated immune lysis by separate molecular mechanisms. *The Journal of Immunology* 130(6):2882-2885.
71. Vidarsson G, van der Pol W-L, van den Elsen JM, Vilé H, Jansen M, Duijs J, Morton HC, Boel E, Daha MR, Corthésy B 2001. Activity of human IgG and IgA subclasses in immune defense against *Neisseria meningitidis* serogroup B. *The Journal of Immunology* 166(10):6250-6256.
72. Kaplon H, Reichert JM 2018. Antibodies to watch in 2019. *mAbs*:1-20.
73. Kaplon H, Reichert JM 2018. Antibodies to watch in 2019. *MABs*.
74. creative-biolabs. 2018. New Monoclonal Antibody Drug Approvals Hit Record Levels in 2017. ed.
75. Elgundi Z, Reslan M, Cruz E, Sifniotis V, Kayser V 2017. The state-of-play and future of antibody therapeutics. *Advanced drug delivery reviews* 122:2-19.
76. Skoda-Smith S, Torgerson TR, Ochs HD 2010. Subcutaneous immunoglobulin replacement therapy in the treatment of patients with primary immunodeficiency disease. *Therapeutics and clinical risk management* 6:1.
77. Schweizer D, Serno T, Goepferich A 2014. Controlled release of therapeutic antibody formats. *European Journal of Pharmaceutics and Biopharmaceutics* 88(2):291-309.
78. Esfandiary R, Hayes DB, Parupudi A, Casas-finet J, Bai S, Samra HS, Shah AU, Sathish HA 2013. A Systematic Multitechnique Approach for Detection and Characterization of Reversible Self-Association during Formulation Development of Therapeutic Antibodies. *Journal of Pharmaceutical Sciences* 102(1):62-72.
79. Shire SJ, Shahrokh Z, Liu J 2004. Challenges in the development of high protein concentration formulations. *Journal of pharmaceutical sciences* 93(6):1390-1402.
80. Sukumar M, Doyle BL, Combs JL, Pekar AH 2004. Opalescent appearance of an IgG1 antibody at high concentrations and its relationship to noncovalent association. *Pharmaceutical research* 21(7):1087-1093.
81. Kanai S, Liu J, Patapoff TW, Shire SJ 2008. Reversible Self-Association of a Concentrated Monoclonal Antibody Solution Mediated by Fab–Fab Interaction That Impacts Solution Viscosity. *Journal of Pharmaceutical Sciences* 97(10):4219-4227.

82. Hamizi S, Freyer G, Bakrin N, Henin E, Mohtaram A, Le Saux O, Falandry C 2013. Subcutaneous trastuzumab: development of a new formulation for treatment of HER2-positive early breast cancer. *OncoTargets and therapy* 6:89.
83. Saito S, Hasegawa J, Kobayashi N, Kishi N, Uchiyama S, Fukui K 2012. Behavior of monoclonal antibodies: relation between the second virial coefficient ( $B_2$ ) at low concentrations and aggregation propensity and viscosity at high concentrations. *Pharmaceutical research* 29(2):397-410.
84. Yadav S, Liu J, Shire SJ, Kalonia DS 2010. Specific interactions in high concentration antibody solutions resulting in high viscosity. *Journal of pharmaceutical sciences* 99(3):1152-1168.
85. Yadav S, Sreedhara A, Kanai S, Liu J, Lien S, Lowman H, Kalonia DS, Shire SJ 2011. Establishing a link between amino acid sequences and self-associating and viscoelastic behavior of two closely related monoclonal antibodies. *Pharmaceutical research* 28(7):1750-1764.
86. Liu J, Nguyen MDH, Andya JD, Shire SJ 2005. Reversible Self-Association Increases the Viscosity of a Concentrated Monoclonal Antibody in Aqueous Solution. *Journal of Pharmaceutical Sciences* 94(9):1928-1940.
87. Arora J, Hu Y, Esfandiary R, Sathish HA, Bishop SM, Joshi SB, Middaugh CR, Volkin DB, Weis DD 2016. Charge-mediated Fab-Fc interactions in an IgG1 antibody induce reversible self-association, cluster formation, and elevated viscosity. *MAbs* 8(8):1561-1574.
88. Geoghegan JC, Fleming R, Damschroder M, Bishop SM, Sathish HA, Esfandiary R 2016. Mitigation of reversible self-association and viscosity in a human IgG1 monoclonal antibody by rational, structure-guided Fv engineering. *MAbs* 8(5):941-950.
89. Whitaker N, Xiong J, Pace SE, Kumar V, Middaugh CR, Joshi SB, Volkin DB 2017. A formulation development approach to identify and select stable ultra-high-concentration monoclonal antibody formulations with reduced viscosities. *Journal of pharmaceutical sciences* 106(11):3230-3241.
90. Salinas BA, Sathish HA, Bishop SM, Harn N, Carpenter JF, Randolph TW 2010. Understanding and Modulating Opalescence and Viscosity in a Monoclonal Antibody Formulation. *Journal of Pharmaceutical Sciences* 99(1):82-93.
91. Esfandiary R, Parupudi A, Casas-Finet J, Gadre D, Sathish H 2015. Mechanism of reversible self-association of a monoclonal antibody: role of electrostatic and hydrophobic interactions. *J Pharm Sci* 104(2):577-586.
92. Harris RJ, Shire SJ, Winter C 2004. Commercial manufacturing scale formulation and analytical characterization of therapeutic recombinant antibodies. *Drug development research* 61(3):137-154.
93. Woods JM, Nesta D 2010. Formulation effects on opalescence of a high-concentration MAb. *BioProcess Int* 8(9):48-59.
94. Goswami S, Wang W, Arakawa T, Ohtake S 2013. Developments and challenges for mAb-based therapeutics. *Antibodies* 2(3):452-500.
95. Mason BD, Zhang L, Remmele RL, Zhang J 2011. Opalescence of an IgG2 monoclonal antibody solution as it relates to liquid-liquid phase separation. *Journal of pharmaceutical sciences* 100(11):4587-4596.
96. Roberts CJ 2014. Therapeutic protein aggregation: mechanisms, design, and control. *Trends in Biotechnology* 32(7):372-380.
97. Li L, Kumar S, Buck PM, Burns C, Lavoie J, Singh SK, Warne NW, Nichols P, Luksha N, Boardman D 2014. Concentration dependent viscosity of monoclonal antibody solutions: explaining experimental behavior in terms of molecular properties. *Pharmaceutical research* 31(11):3161-3178.
98. Clodfelter DK, Pekar AH, Rebhun DM, Destrampe KA, Havel HA, Myers SR, Brader ML 1998. Effects of non-covalent self-association on the subcutaneous absorption of a therapeutic peptide. *Pharmaceutical research* 15(2):254-262.
99. Chow C-K, Allan BW, Chai Q, Atwell S, Lu J 2016. Therapeutic antibody engineering to improve viscosity and phase separation guided by crystal structure. *Molecular pharmaceuticals* 13(3):915-923.

100. Nishi H, Miyajima M, Nakagami H, Noda M, Uchiyama S, Fukui K 2010. Phase separation of an IgG1 antibody solution under a low ionic strength condition. *Pharmaceutical research* 27(7):1348-1360.
101. Lewus RA, Darcy PA, Lenhoff AM, Sandler SI 2011. Interactions and phase behavior of a monoclonal antibody. *Biotechnology progress* 27(1):280-289.
102. Raut AS, Kalonia DS 2015. Liquid–Liquid Phase Separation in a Dual Variable Domain Immunoglobulin Protein Solution: Effect of Formulation Factors and Protein–Protein Interactions. *Molecular pharmaceutics* 12(9):3261-3271.
103. Raut AS, Kalonia DS 2016. Pharmaceutical perspective on opalescence and liquid–liquid phase separation in protein solutions. *Molecular pharmaceutics* 13(5):1431-1444.
104. Luo H, Lee N, Wang X, Li Y, Schmelzer A, Hunter AK, Pabst T, Wang WK 2017. Liquid-liquid phase separation causes high turbidity and pressure during low pH elution process in Protein A chromatography. *Journal of Chromatography A* 1488:57-67.
105. Pindrus M, Shire SJ, Kelley RF, Demeule B, Wong R, Xu Y, Yadav S 2015. Solubility Challenges in High Concentration Monoclonal Antibody Formulations: Relationship with Amino Acid Sequence and Intermolecular Interactions. *Molecular Pharmaceutics* 12(11):3896-3907.
106. Melander W, Horváth C 1977. Salt effects on hydrophobic interactions in precipitation and chromatography of proteins: An interpretation of the lyotropic series. *Archives of Biochemistry and Biophysics* 183(1):200-215.
107. Arora J, Hickey JM, Majumdar R, Esfandiary R, Bishop SM, Samra HS, Middaugh CR, Weis DD, Volkin DB. *MAbs*, 2015, pp 525-539.
108. Wu S-J, Luo J, O'neil KT, Kang J, Lacy ER, Canziani G, Baker A, Huang M, Tang QM, Raju TS 2010. Structure-based engineering of a monoclonal antibody for improved solubility. *Protein Engineering, Design & Selection* 23(8):643-651.
109. Shan L, Mody N, Sormani P, Rosenthal KL, Damschroder MM, Esfandiary R 2018. Developability assessment of engineered monoclonal antibody variants with a complex self-association behavior using complementary analytical and in silico tools. *Molecular pharmaceutics* 15(12):5697-5710.
110. Carpenter JF, Chang BS, Garzon-Rodriguez W, Randolph TW. 2002. Rational design of stable lyophilized protein formulations: theory and practice. *Rational design of stable protein formulations*, ed.: Springer. p 109-133.
111. Bhambhani A, Blue J 2010. Lyophilization strategies for development of a high-concentration monoclonal antibody formulation: benefits and pitfalls. *Am Pharm Rev* 13(1):31-38.
112. Garidel P, Presser I. 2019. Lyophilization of High-Concentration Protein Formulations. *Lyophilization of Pharmaceuticals and Biologicals*, ed.: Springer. p 291-325.
113. Warne NW 2011. Development of high concentration protein biopharmaceuticals: the use of platform approaches in formulation development. *European journal of pharmaceutics and biopharmaceutics* 78(2):208-212.
114. Cao W, Krishnan S, Ricci MS, Shih L-Y, Liu D, Gu JH, Jameel F 2013. Rational design of lyophilized high concentration protein formulations-mitigating the challenge of slow reconstitution with multidisciplinary strategies. *European Journal of Pharmaceutics and Biopharmaceutics* 85(2):287-293.
115. Frost GI 2007. Recombinant human hyaluronidase (rHuPH20): an enabling platform for subcutaneous drug and fluid administration. *Expert opinion on drug delivery* 4(4):427-440.
116. Bookbinder L, Hofer A, Haller M, Zepeda M, Keller G-A, Lim J, Edgington T, Shepard H, Patton J, Frost G 2006. A recombinant human enzyme for enhanced interstitial transport of therapeutics. *Journal of Controlled Release* 114(2):230-241.
117. Wasserman RL, Melamed I, Stein MR, Gupta S, Puck J, Engl W, Leibl H, McCoy B, Empson VG, Belmont D 2012. Recombinant human hyaluronidase-facilitated subcutaneous infusion of human immunoglobulins for primary immunodeficiency. *Journal of Allergy and Clinical Immunology* 130(4):951-957. e911.

118. Shpilberg O, Jackisch C 2013. Subcutaneous administration of rituximab (MabThera) and trastuzumab (Herceptin) using hyaluronidase. *British journal of cancer* 109(6):1556.
119. Renegar KB, Small P 1991. Passive transfer of local immunity to influenza virus infection by IgA antibody. *The Journal of Immunology* 146(6):1972-1978.
120. Dickinson EC, Gorga JC, Garrett M, Tuncer R, Boyle P, Watkins SC, Alber SM, Parizhskaya M, Trucco M, Rowe MI 1998. Immunoglobulin A supplementation abrogates bacterial translocation and preserves the architecture of the intestinal epithelium. *Surgery* 124(2):284-290.
121. Wang J, Yadav V, Smart AL, Tajiri S, Basit AW 2015. Toward oral delivery of biopharmaceuticals: an assessment of the gastrointestinal stability of 17 peptide drugs. *Molecular pharmaceutics* 12(3):966-973.
122. Yadav V, Varum F, Bravo R, Furrer E, Basit AW 2016. Gastrointestinal stability of therapeutic anti-TNF  $\alpha$  IgG1 monoclonal antibodies. *International journal of pharmaceutics* 502(1-2):181-187.
123. Johansen F-E, Braathen R, Brandtzaeg P 2001. The J chain is essential for polymeric Ig receptor-mediated epithelial transport of IgA. *The Journal of Immunology* 167(9):5185-5192.
124. Vaerman J-P, Langendries A, Maelen CV 1995. Homogenous IgA monomers, dimers, trimers and tetramers from the same IgA myeloma serum. *Immunological investigations* 24(4):631-641.
125. Johansen F, Braathen R, Brandtzaeg P 2000. Role of J chain in secretory immunoglobulin formation. *Scandinavian journal of immunology* 52(3):240-248.
126. Bastian A, Kratzin H, Fallgren-Gebauer E, Eckart K, Hilschmann N. 1995. Intra- and inter-chain disulfide bridges of J chain in human S-IgA. *Advances in Mucosal Immunology*, ed.: Springer. p 581-583.
127. Brandtzaeg P 1975. Immunochemical studies on free and bound J chain of human IgA and IgM. *Scandinavian journal of immunology* 4(5):439-450.
128. Brandtzaeg P, Prydz H 1984. Direct evidence for an integrated function of J chain and secretory component in epithelial transport of immunoglobulins. *Nature* 311(5981):71.
129. Hendrickson BA, Rindisbacher L, Corthesy B, Kendall D, Waltz DA, Neutra MR, Seidman J 1996. Lack of association of secretory component with IgA in J chain-deficient mice. *The Journal of Immunology* 157(2):750-754.
130. Longet S, Miled S, Lötscher M, Miescher SM, Zuercher AW, Corthésy B 2013. Human plasma-derived polymeric IgA and IgM antibodies associate with secretory component to yield biologically active secretory-like antibodies. *Journal of Biological Chemistry* 288(6):4085-4094.
131. Stubbe H, Berdoz J, Kraehenbuhl J-P, Corthésy B 2000. Polymeric IgA is superior to monomeric IgA and IgG carrying the same variable domain in preventing *Clostridium difficile* toxin A damaging of T84 monolayers. *The Journal of Immunology* 164(4):1952-1960.
132. Smart AL, Gaisford S, Basit AW 2014. Oral peptide and protein delivery: intestinal obstacles and commercial prospects. *Expert opinion on drug delivery* 11(8):1323-1335.
133. Varum F, Hatton G, Basit A 2013. Food, physiology and drug delivery. *International journal of pharmaceutics* 457(2):446-460.
134. Marieb EN, Hoehn K. 2007. *Human anatomy & physiology*. ed.: Pearson Education.
135. Mahato RI, Narang AS, Thoma L, Miller DD 2003. Emerging trends in oral delivery of peptide and protein drugs. *Critical Reviews™ in Therapeutic Drug Carrier Systems* 20(2&3).
136. Dunn BM 2001. Overview of pepsin-like aspartic peptidases. *Current protocols in protein science* 25(1):21.23. 21-21.23. 26.
137. Johnston N, Dettmar PW, Bishwokarma B, Lively MO, Koufman JA 2007. Activity/stability of human pepsin: implications for reflux attributed laryngeal disease. *The Laryngoscope* 117(6):1036-1039.
138. Hustoft HK, Malerod H, Wilson SR, Reubsæet L, Lundanes E, Greibrokk T. 2012. A critical review of trypsin digestion for LC-MS based proteomics. *Integrative Proteomics*, ed.: InTech.
139. EnzymeEducationInstitute. <https://enzymeeducationinstitute.com/enzymes/chymotrypsin/>. ed.

140. Camenisch G, Alsenz J, van de Waterbeemd H, Folkers G 1998. Estimation of permeability by passive diffusion through Caco-2 cell monolayers using the drugs' lipophilicity and molecular weight. *European journal of pharmaceutical sciences* 6(4):313-319.
141. Morishita M, Peppas NA 2006. Is the oral route possible for peptide and protein drug delivery? *Drug Discov Today* 11(19-20):905-910.
142. Rubas W, Cromwell M, Shahrokh Z, Villagran J, Nguyen TN, Wellton M, Nguyen TH, Mrsny R 1996. Flux measurements across Caco-2 monolayers may predict transport in human large intestinal tissue. *Journal of pharmaceutical sciences* 85(2):165-169.
143. Agarwal V, Khan MA 2001. Current status of the oral delivery of insulin. *Pharm Technol* 10:76-90.
144. Bastian S, Walton P, Ballard F, Belford D 1999. Transport of IGF-I across epithelial cell monolayers. *Journal of endocrinology* 162(3):361-369.
145. Ward PD, Tippin TK, Thakker DR 2000. Enhancing paracellular permeability by modulating epithelial tight junctions. *Pharmaceutical science & technology today* 3(10):346-358.
146. Salamat-Miller N, Johnston TP 2005. Current strategies used to enhance the paracellular transport of therapeutic polypeptides across the intestinal epithelium. *International journal of pharmaceutics* 294(1-2):201-216.
147. Salama NN, Eddington ND, Fasano A. 2006. Tight junction modulation and its relationship to drug delivery. *Tight junctions*, ed.: Springer. p 206-219.
148. Troeger C, Forouzanfar M, Rao PC, Khalil I, Brown A, Reiner Jr RC, Fullman N, Thompson RL, Abajobir A, Ahmed M 2017. Estimates of global, regional, and national morbidity, mortality, and aetiologies of diarrhoeal diseases: a systematic analysis for the Global Burden of Disease Study 2015. *The Lancet Infectious Diseases* 17(9):909-948.
149. Leyk S, Norlund PU, Nuckols JR 2012. Robust assessment of spatial non-stationarity in model associations related to pediatric mortality due to diarrheal disease in Brazil. *Spatial and spatio-temporal epidemiology* 3(2):95-105.
150. Oliveira AFd, Leite IdC, Valente JG 2015. Global burden of diarrheal disease attributable to the water supply and sanitation system in the State of Minas Gerais, Brazil: 2005. *Ciencia & saude coletiva* 20:1027-1036.
151. Fontoura VM, Graepp-Fontoura I, Santos FS, Neto MS, de Almeida Tavares HS, Bezerra MOL, de Oliveira Feitosa M, Neves AF, de Moraes JCM, Nascimento LFC 2018. Socio-environmental factors and diarrheal diseases in under five-year old children in the state of Tocantins, Brazil. *PloS one* 13(5):e0196702.
152. Ritchie H, Roser M. 2018. Causes of Death. Published online at OurWorldInData.org. Retrieved from: '<https://ourworldindata.org/causes-of-death>'. [Online Resource]. ed.
153. Iijima Y, Oundo JO, Hibino T, Saidi SM, Hinenoya A, Osawa K, Shirakawa T, Osawa R, Yamasaki S 2017. High prevalence of diarrheagenic *Escherichia coli* among children with diarrhea in Kenya. *Japanese journal of infectious diseases* 70(1):80-83.
154. Tickell KD, Brander RL, Atlas HE, Pernica JM, Walson JL, Pavlinac PB 2017. Identification and management of *Shigella* infection in children with diarrhoea: a systematic review and meta-analysis. *The Lancet Global Health* 5(12):e1235-e1248.
155. Tubatsi G, Bonyongo M, Gondwe M 2015. Water use practices, water quality, and households' diarrheal encounters in communities along the Boro-Thamalakane-Boteti river system, Northern Botswana. *Journal of Health, Population and Nutrition* 33(1):21.
156. Bener A, Ehlayel MS, Abdulrahman HM 2011. Exclusive breast feeding and prevention of diarrheal diseases: A study in Qatar. *Revista Brasileira de Saúde Materno Infantil* 11(1):83-87.
157. Paulo RLP, Rodrigues ABD, Machado BM, Gilio AE 2016. The impact of rotavirus vaccination on emergency department visits and hospital admissions for acute diarrhea in children under 5 years. *Revista da Associação Médica Brasileira* 62(6):506-512.

158. Rollenhagen JE, Jones F, Hall E, Maves R, Nunez G, Espinosa N, O'Dowd A, Prouty MG, Savarino SJ 2018. Establishment, validation and application of a New World Primate model of ETEC disease for vaccine development. *Infection and immunity:IAI*. 00634-00618.
159. Yamamoto A, Taniguchi T, Rikyuu K, Tsuji T, Fujita T, Murakami M, Muranishi S 1994. Effects of various protease inhibitors on the intestinal absorption and degradation of insulin in rats. *Pharmaceutical research* 11(10):1496-1500.
160. Muheem A, Shakeel F, Jahangir MA, Anwar M, Mallick N, Jain GK, Warsi MH, Ahmad FJ 2016. A review on the strategies for oral delivery of proteins and peptides and their clinical perspectives. *Saudi Pharmaceutical Journal* 24(4):413-428.
161. TOZAKI H, EMI Y, Horisaka E, FUJITA T, YAMAMOTO A, MURANISHI S 1997. Degradation of insulin and calcitonin and their protection by various protease inhibitors in rat caecal contents: implications in peptide delivery to the colon. *Journal of pharmacy and pharmacology* 49(2):164-168.
162. Park K, Kwon IC, Park K 2011. Oral protein delivery: Current status and future prospect. *Reactive and Functional Polymers* 71(3):280-287.
163. Marschütz MK, Bernkop-Schnürch A 2000. Oral peptide drug delivery: polymer-inhibitor conjugates protecting insulin from enzymatic degradation in vitro. *Biomaterials* 21(14):1499-1507.
164. Farady CJ, Craik CS 2010. Mechanisms of macromolecular protease inhibitors. *Chembiochem* 11(17):2341-2346.
165. Gettins PG 2002. Serpin structure, mechanism, and function. *Chemical reviews* 102(12):4751-4804.
166. Egelund R, Rodenburg KW, Andreasen PA, Rasmussen MS, Guldberg RE, Petersen TE 1998. An ester bond linking a fragment of a serine proteinase to its serpin inhibitor. *Biochemistry* 37(18):6375-6379.
167. Vadrevu KM, Prasad SD. 2015. Rotavirus vaccine compositions and process for preparing the same. ed.: Google Patents.
168. Hibbins AR, Kumar P, Choonara YE, Kondiah PP, Marimuthu T, du Toit LC, Pillay V 2017. Design of a versatile pH-responsive hydrogel for potential oral delivery of gastric-sensitive bioactives. *Polymers* 9(10):474.
169. Damgé C, Michel C, Aprahamian M, Couvreur P 1988. New approach for oral administration of insulin with polyalkylcyanoacrylate nanocapsules as drug carrier. *Diabetes* 37(2):246-251.
170. Mathiowitz E, Jacob JS, Jong YS, Carino GP, Chickering DE, Chaturvedi P, Santos CA, Vijayaraghavan K, Montgomery S, Bassett M 1997. Biologically erodable microspheres as potential oral drug delivery systems. *Nature* 386(6623):410.
171. TAKKA FA, S 1999. Calcium alginate microparticles for oral administration: II effect of formulation factors on drug release and drug entrapment efficiency. *Journal of microencapsulation* 16(3):291-301.
172. Carvalho FC, Bruschi ML, Evangelista RC, Gremião MPD 2010. Mucoadhesive drug delivery systems. *Brazilian journal of pharmaceutical sciences* 46(1):1-17.
173. Ma G 2014. Microencapsulation of protein drugs for drug delivery: strategy, preparation, and applications. *Journal of controlled release* 193:324-340.

## **Chapter 2**

Characterization of Excipient Effects on Reversible Self-association, Backbone Flexibility, and Solution Properties of an IgG1 Monoclonal Antibody at High Concentrations: Part 1



## 2.1. Introduction

Over the past two decades, monoclonal antibodies (mAbs) have become a key class of therapeutic drugs used for treating a variety of diseases including cancer, autoimmune disease, inflammatory disease, and transplant rejection.<sup>1,2,3</sup> To date, approximately 70 therapeutic mAbs have been authorized for use by the FDA in the United States. Among the best-selling drugs in the last several years, therapeutic mAbs occupy a large proportion.<sup>4-6</sup> In antibody therapy, relatively high dosing (~1-10 mgs/kg) via the two major routes of parenteral administration, subcutaneous (SC) and intravenous (IV), is used. For many chronic diseases such as asthma, autoimmune disease, and certain allergic conditions, frequent administration is usually required. Therefore, self-administration or home-based treatments are preferred.<sup>7,8</sup> SC injections using prefilled syringes (with or without auto-injectors) typically require limited injection volumes (less than 2 mL) to optimize injection time and reduce injection pain.<sup>8,9</sup> As a result, formulation of high-concentration mAb solutions is required both to reach therapeutic windows and to meet patient needs for SC administration.

When formulating high-concentration mAbs, many pharmaceutical challenges are encountered including high solution viscosity, opalescence, decreased colloidal stability and high aggregation propensity.<sup>8,10-12</sup> These effects are due to protein-protein interactions (PPIs) at high mAb concentrations, leading to reversible self-association (RSA), formation of oligomeric species within their native states by intermolecular non-

covalent interactions.<sup>13,14</sup> Such interactions between protein molecules can form a network of higher-ordered protein complexes, which greatly increase solution viscosity, resulting in high pressure during protein filtration (during manufacturing) and protein administration (e.g., syringeability). In addition, pain on injection with highly viscous solutions can occur in patients.<sup>13,15-17</sup> Finally, mAb RSA might promote formation of structurally altered aggregation precursors (nuclei) to initiate the formation of irreversible aggregates, potentially leading to decreased protein bioavailability, poor pharmacokinetic properties and unwanted anti-drug immune responses.<sup>18,19</sup>

Another challenge often encountered with high-concentration mAb solutions is liquid-liquid phase separation, a phenomenon in which two distinct liquid layers are formed.<sup>20-23</sup> When phase separation occurs, most of the protein remains in the high density phase induced by formation of intermolecular interactions, leaving only a small quantity of protein in the low density phase. The actual protein concentrations in the two phases depends largely on the surface of the protein molecule itself, pH, secondary solutes and temperature.<sup>23</sup> Uncommonly high viscosity and opalescence have been identified for certain phase separated mAb solutions.<sup>11,12,21,24</sup> Also, substantially decreased physical stability has sometimes been reported when mAbs undergo phase separation.<sup>20,25,26</sup>

Excipients are added to mAb formulations for particular purposes such as increasing stability and solubility, reducing viscosity, and potentially enhancing efficacy.<sup>27-</sup>

<sup>31</sup> Some excipients enhance the stability of mAbs by direct interaction mechanisms (including hydrophobic, electrostatic, and dipole-dipole forces), while others by indirect interactions (such as protein preferential exclusion).<sup>28,29</sup> A variety of excipients have been shown to have different effects on stabilizing mAbs in therapeutic mAb formulations such as sugars, salts, polymers, surfactants, polyols and amino acids.<sup>28-36</sup> Hydrogen exchange-mass spectrometry (HX-MS) is a well-established high-resolution technique for exploring protein dynamics and conformational flexibility including the effect of excipients on aggregation propensity and reversible self-association in low and high concentration mAb formulations, respectively.<sup>13,32-36</sup> Under certain circumstances, such as RSA or interaction with excipients, the exchange rate can be altered in specific regions, indicating local alterations of backbone dynamics.<sup>13</sup> HX-MS has been used to elucidate molecular effects of excipients<sup>32-37</sup> and chemical changes (e.g., asparagine deamidation,<sup>38</sup> deglycosylation,<sup>35</sup> post-translational modifications,<sup>39</sup> and engineered point mutations<sup>40</sup>) on mAb conformational dynamics. We recently demonstrated that a particular IgG1 (mAb-J) undergoes extensive RSA at high protein concentrations via electrostatic attractive interactions between segments of the Fab and Fc domains as determined by HX-MS analysis.<sup>41</sup> In addition, we demonstrated the ability of both arginine and sodium chloride to disrupt mAb-J RSA in a concentration dependent manner.

In this study, we expand those observations by examining a series of charged excipients possessing different abilities to disrupt specific protein-protein interactions

(PPI) sites for mAb-J, the same IgG1 antibody previously measured by HX-MS. We then correlate these results with their effects on mAb-J physical stability and solution properties. Specifically, the effect(s) of four charged amino acids (Arg, Lys, Asp, Glu) and sodium chloride on both solution properties (e.g., turbidity, viscosity) and mAb-J's physical properties (hydrodynamic diameter, relative solubility, phase separation) were examined in a series of mAb-J protein concentrations (from 5 to 60 mg/mL). HX-MS analysis was then performed to obtain local information on backbone dynamics of mAb-J (5 mg/mL and 60 mg/mL) in the presence of the selected excipients. The HX-MS information is then used to help better understand the mechanisms by which these excipients partially or more extensively disrupt RSA within specific regions of mAb-J at high protein concentrations.

## **2.2. Materials and Methods**

### **2.2.1. Sample Preparation**

A highly purified IgG1 monoclonal antibody, mAb-J, was obtained from MedImmune LLC, Gaithersburg, MD, at a concentration of 150 mg/mL. The mAb-J stock solution was buffer-exchanged to a base buffer "BB" (20 mM citrate phosphate buffer containing 30 mM NaCl) with or without excipient (from 30 to 100 mM) by dialysis at 4°C and pH 6.0 for 24 hours using 3.5 kDa molecular weight cutoff membranes (Slide-A-Lyzer, Thermo Scientific, Rockford, IL). Excipients such as sodium chloride (NaCl), L-arginine

hydrochloride (Arg), L-lysine hydrochloride (Lys), L-glutamic acid monosodium salt (Glu), and L-aspartic acid sodium salt (Asp) were obtained from Sigma-Aldrich (St. Louis, MO). After dialysis into the BB buffer with excipients, 5-60 mg/mL mAb-J samples were prepared by diluting the dialyzed sample with corresponding dialysis buffer.

### **2.2.2. Solution Appearance Study**

Dialyzed mAb-J samples were diluted with corresponding base buffers (BB with or without selected excipients, and at excipient concentrations ranging from 30 to 100 mM at pH 6.0) to prepare a series of mAb-J solutions at various concentrations ranging from 5 to 60 mg/mL. Base buffer contained 20 mM citrate phosphate buffer with 30 mM NaCl at pH 6.0. Each diluted sample was filled into a 2 mL FIOLEX® clear Type 1 glass vial (Schott North America, Elmsford, NY) with a fill volume of 1 mL. This series of vials was visually assessed and photographed.

### **2.2.3. Ultraviolet Absorption Spectroscopy**

A Nanodrop 2000 spectrophotometer (Thermo Scientific, Rockford, IL) was used to measure absorbance of mAb-J samples by ultraviolet absorption spectroscopy ( $A_{280\text{nm}}$ ). An extinction coefficient value of  $1.58 \text{ mL}\cdot\text{mg}^{-1}\cdot\text{cm}^{-1}$  was calculated based on mAb-J primary sequence to determine protein concentrations.<sup>42</sup>

### **2.2.4. Turbidity Measurements**

A series of mAb-J standard solutions was prepared in BB at various protein concentrations, showing different solution opalescence (turbidity). Each standard solution

was measured in (1) a volume of 3 mL by a HACH 2100 AN turbidimeter (HACH, Loveland, CO; 90-degree nephelometric detector with a wavelength of 455 nm) to obtain turbidity values (NTU), and (2) a volume of 160  $\mu$ L SpectraMax® M5 Multi-Mode Microplate Reader (Molecular Devices, Inc., Sunnyvale, CA) at 500 nm to obtain O.D.<sub>500nm</sub> values (see Supplemental Figure S1). The two sets of data were correlated and plotted to make a linear standard curve between turbidity and O.D.<sub>500nm</sub>. Corning black 96-well plates with clear bottoms (Corning Incorporated, Corning, NY) were then used to measure the O.D.<sub>500nm</sub> of all mAb-J samples (at different protein concentrations in BB with or without excipients) using SoftMax Pro Software (Corning Incorporated, Corning, NY).

### **2.2.5. Dynamic Light Scattering**

Samples of mAb-J were prepared in a concentration of 10 mg/mL in the absence or presence of 100 mM excipients. A Wyatt DynaPro Plate Reader II dynamic light scattering instrument (Wyatt Technology, Santa Barbara, CA) equipped with an 830 nm laser was used to measure the hydrodynamic diameter of mAb-J in different buffer conditions using the Stokes-Einstein equation per instrument software. All mAb-J samples were measured by fifteen 5 second acquisitions (after centrifugation of samples at 2000 rpm for 2 mins). The solution viscosity of each sample was measured separately using an m-VROC viscometer (Rheosence, San Ramon, CA) at 25°C, and viscosity

correction was implemented in instrument software for calculation of corrected hydrodynamic diameters.

### **2.2.6. Viscosity Measurements**

Dialyzed mAb-J samples were diluted with base buffer to make various excipient solutions at different protein concentrations from 10 to 60 mg/mL. The viscosity of mAb-J samples in the presence of 30-100 mM excipients was measured at 25°C by an m-VROC viscometer (RheoSense, San Ramon, CA). This was performed by injecting samples at a rate of 100  $\mu$ L/min and at a shear rate of 1420 1/s using a 1 mL glass syringes (Hamilton Co, Reno, NV).

### **2.2.7. Composition-Gradient Multi-Angle Light Scattering (CG-MALS)**

Samples of mAb-J at 2 and 20 mg/mL (containing 10% w/v trehalose in BB) with or without 100 mM excipients were prepared and filtered through a 0.22-micron size Millex-GV syringe filter unit (EMD Millipore, Billerica, MA) before injecting into the system. A CG-MALS instrument with dual syringe-pump Calypso sample preparation and delivery unit (Wyatt Technology, Santa Barbara, CA) was used to perform static light scattering analysis at room temperature. A series of association models were examined to fit light scattering data as a function of concentration by employing the Calypso software (Wyatt Technology, Santa Barbara, CA). Light scattering was measured at 90° with a series of mAb-J solutions (~0.2 mg/mL to 20 mg/mL) diluted by a dual syringe-pump Calypso sample preparation and delivery unit. Excess Rayleigh ratio ( $R_{\theta}$ ) was then obtained and

plotted depending on mAb-J concentration, getting the osmotic second virial coefficient ( $B_{22}$ ), a measurement of non-ideal solution behavior resulting from two-body interactions. Chi<sup>2</sup> testing was used to determine the best association model for mAb-J with or without excipients. The experimental details of this method have been described in detail elsewhere.<sup>41</sup>

### **2.2.8. PEG-Induced Precipitation Study**

Stock solutions of PEG-10,000 (20% w/v PEG) were used to prepare a series of PEG solutions (from 0% to 20% w/v PEG) using BB with or without 100 mM excipients at pH 6.0. Sample-containing 96-well plates were incubated overnight at room temperature. After centrifugation of incubated samples at 1233 xg for 15 min, 200  $\mu$ L filtrate of each well was transferred to another clear 96-well collection plate (Greiner Bio-One North America Inc., Monroe, NC) for  $A_{280\text{nm}}$  absorbance measurement. A spectraMax<sup>®</sup> M5 Multi-Mode Microplate Reader (Molecular Devices, Inc., Sunnyvale, CA) was used to determine the final mAb-J concentration. The %PEG<sub>midpt</sub> was determined by mathematical fitting as described previously<sup>43</sup> using Python (x, y) version 2.7.9.0, which is a python-language-based open-source software. Furthermore, the relative apparent solubility values (or the apparent thermodynamic activity) were obtained by plotting the transition-area data points of the same sigmoidal curve on a log scale and extrapolating to 0% PEG as described previously.<sup>44</sup>

### **2.2.9. Lyophilization of mAb-J Samples**



Samples of mAb-J at 5 mg/mL and 60 mg/mL were prepared by dialysis against BB (containing 10% w/v trehalose). For each vial, a 2-leg, 13 mm siliconized rubber stopper (Wheaton Industries Inc., Millville, NJ) was used to partially stopper the vials, and a LyoStar II lyophilizer (SP Scientific, Warminster, PA) was then used to lyophilize all mAb-J samples using a freeze drying cycle previously described.<sup>13,41</sup> Lyophilized samples were assessed visually and photographed to display the cake appearance. The concentration of post-reconstitution mAb-J samples was obtained using ultraviolet absorption spectroscopy ( $A_{280\text{nm}}$ ) after a 0.22-micron membrane filtration, and the slopes of optical density values from 310 nm to 395 nm was examined to evaluate the formation of soluble protein aggregates.

#### **2.2.10. Size Exclusion Chromatography (SEC)**

Analysis of mAb-J samples was performed using a SEC-HPLC system with an inline UV detector at 214 nm. Freeze-dried samples (5 mg/mL and 60 mg/mL) were diluted to 0.5 mg/mL using D<sub>2</sub>O, and then centrifuged at 14,000 g for 5 min prior to SEC analysis to eliminate any insoluble aggregates. A Shimadzu HPLC system equipped with a photodiode array detector was used to measure SEC eluates. Two columns, a 7.8 mm × 30 cm Tosoh TSK-Gel BioAssist G3SWxL and a 6.0 mm x 4 cm guard column (TOSOH Biosciences, King of Prussia, PA), were used for species separation. mAb-J samples were eluted in a mobile phase of 200 mM phosphate buffer (pH 6.8) at a flow rate of 0.7 mL/min. mAb-J monomer, fragment, and soluble aggregates (e.g., dimer) of post-

lyophilization samples were calculated and then compared to non-lyophilized samples based on chromatography peak areas. The experimental details of this method have been described in detail elsewhere.<sup>41</sup>

#### **2.2.11. Karl-Fischer Titration**

Coulometric Karl-Fischer (KF) determination of water moisture for lyophilized mAb-J samples was conducted using a C20 Compact Karl Fischer Coulometer (Mettler-Toledo LLC., Columbus, OH). AQUASTAR® CombiCoulomat (EMD Chemicals Inc., Gibbstown, NJ) was used as the reaction reagent for this purpose. Lyophilized mAb-J cakes were weighed and transferred to a reaction beaker, and final water content was obtained with units of ppm (part per million) using methodology described in the instrument manual.

#### **2.2.12. Deuteration of Excipients (Amino Acids)**

Excipients were dissolved in D<sub>2</sub>O to remove exchangeable hydrogen and dried in a Vacufuge vacuum concentrator (Eppendorf, Hauppauge, NY) at 30°C until only powder was remaining. This process was repeated three times and then the powder was reconstituted in D<sub>2</sub>O-based 5 mM citrate-phosphate buffer to prepare 100 mM excipients solutions, which were adjusted with deuterium chloride and deuterium oxide to obtain final pH of 6.0, without correction for the deuterium isotope effect.

#### **2.2.13. Hydrogen Exchange-Mass Spectrometry (HX-MS)**

The HX-MS method has been described in extensive detail previously.<sup>13,41</sup> The lyophilized mAb-J samples (5 mg/mL and 60 mg/mL) and 100 mM excipient-containing

(excluding NaCl) deuterium buffer were equilibrated at 25°C on an EchoTherm chilling/heating plate (Torrey Pines Scientific, Inc., Carlsbad, CA). To start deuterium labelling in mAb-J, 930 µL of excipient-containing D<sub>2</sub>O-based 5 mM citrate-phosphate buffer (uncorrected pH = 6.0) was transferred to the lyophilized mAb-J sample to reconstitute the freeze-dried protein cake. Air bubbles and insoluble aggregates were removed by centrifugation. The reconstituted mAb-J samples were incubated and labelled for 2760 seconds and then quenched by mixing 20 µL of the exchanged mAb-J sample with 180 µL of quench buffer (0.5 M tris(2-carboxyethyl) phosphine hydrochloride (TCEP), 4 M guanidine hydrochloride, and 0.2 M sodium phosphate at pH 2.5 pre-equilibrated at 1°C). 60 µL of the quenched mAb-J samples were loaded into a 100 µL sample loop by a LEAP H/DX PAL robot (LEAP Technologies, Carrboro, NC) into an Agilent 1260 infinity series LC (Agilent Technologies, Santa Clara, CA). Three columns (an immobilized pepsin column, a peptide desalting trap, and a C18 column) were used to digest mAb-J samples, desalt and concentrate the digested peptides, and finally separate them by gradient elution, as described previously.<sup>13,41</sup> Peptide carryover in the immobilized pepsin column was minimized by washing the pepsin column with two wash solutions following a cleaning procedure after each injection as described previously.<sup>45</sup> The refrigerated column compartment was kept at 1°C to minimize back exchange, and mobile phases composed of water and 90% acetonitrile/10% water, both containing 0.1% (v/v) formic acid, were used to separate and elute peptides into an Agilent 6530 quadrupole-time of

flight mass spectrometer (Agilent Technologies, Santa Clara, CA), equipped with a standard electrospray ionization source operated in positive mode for measuring the deuterium level of each peptide.

#### **2.2.14. HX-MS Data Processing and Analysis**

All the identified peptides were confirmed by using accurate mass ( $\pm 10$  ppm) and tandem MS with collision induced dissociation on the quadrupole-time of flight mass spectrometer (Agilent 6530 QTOF MS). Three replicate sets of HX-MS data were analyzed using HDExaminer software (Sierra Analytics, California), including re-analysis of previously obtained raw data for mAb-J in BB,<sup>1</sup> and data were also manually reviewed for chromatographic peak integration adjustments. A confidence interval was estimated by propagation of random error using the 99<sup>th</sup> percentile of the standard deviations from triplicate technical replicates, giving a value of  $\pm 0.43$  Da for the significant differences in our dataset. HX-MS results were processed to compare mAb-J dynamics with and without excipients at both low and high protein concentrations, demonstrate excipient efficacy at disrupting RSA and also the intrinsic effects on mAb-J, especially at high protein concentrations. HX-MS results are displayed on a homology model of mAb-J created previously, based on crystal structures of an isolated Fc and an in-silico generated KOL/Padlan structure of an Fab. The results of the mAb-J homology models were displayed by Pymol software version 1.4.1 (Schrödinger LLC, Portland, OR).

## 2.3. Results

### 2.3.1. Solution Properties of mAb-J in the Absence/Presence of Excipients

As a first step to evaluate the effect of various additives on the solution properties of low to high concentrations of mAb-J, we visually examined the solutions. In Figure 1a, a series of mAb-J solutions show the effects of protein concentration on solution appearance. The clarity of mAb-J solution at 5 mg/mL was similar to protein-free buffer (result not shown). However, as the concentration of mAb-J increased from 10 to 60 mg/mL, opalescence increased. When the concentration of mAb-J was close to 60 mg/mL, an obvious phase separation phenomenon was observed with ~5 mg/mL protein in the low density phase and ~300 mg/mL protein in the high density phase. The five excipients showed varying ability to prevent mAb-J opalescence at high protein concentrations, as illustrated in Figure 1a-e. The addition of Arg and Lys (Figure 1b and c) inhibited turbidity, and even at a high protein concentration of 60 mg/mL, mAb-J solutions with 100 mM Arg or Lys were almost transparent and similar in appearance to the solution of base buffer (BB) alone. Furthermore, 30 mM Arg prevented turbidity of 60 mg/mL mAb-J better than 30 mM Lys. Finally, Figure 1 panels a, d and e show the effect of NaCl, Glu, and Asp. Although NaCl, Glu, and Asp prevented mAb-J from undergoing phase separation, high-concentration protein solutions still exhibited opalescence, especially with NaCl.

To better quantify the opalescence, the turbidity value of each of the mAb-J solutions was then measured to determine the concentration-dependent effects of protein and excipient. As shown in Supplemental Figure S1, solution turbidity (NTU, as measured by a turbidimeter requiring 3 mL sample) correlated very well ( $R^2$  value of 0.99) with O.D.<sub>500nm</sub> values measured with a UV transparent cuvette (using only 160  $\mu$ L sample) for each measurement.<sup>41</sup> Using this standard curve, Figure 2a illustrates the measured O.D.<sub>500nm</sub> values (and corresponding turbidity values) for different concentrations of mAb-J with and without varying concentrations of NaCl. There was one condition (60 mg/mL mAb-J with extra 30 mM NaCl in solution) in which mAb-J showed extremely high turbidity that exceeded the range of the standard curve, so no value could be obtained. For other conditions, however, as NaCl concentration increased and protein concentration decreased, the solution turbidity was reduced to a large extent. As shown in Figure 2b and c, mAb-J solutions in the presence of Arg or Lys not only showed no phase separation (see above), but also showed much lower turbidity values (below 50 NTU) for each of the examined protein concentrations. In contrast, Glu and Asp showed intermediate effects in terms of lowering turbidity values (better than NaCl, but not as effective as Arg and Lys), and yet, these negatively-charged amino acids did prevent phase separation under these conditions (Figure 2d and e).

Solution viscosity was then evaluated to characterize the effect of these five excipients on the solution properties of high-concentration mAb-J solutions. Figure 3

shows solution viscosity as a function of both mAb-J and excipient concentrations. In BB alone with no added charged excipients, the viscosity of mAb-J solutions increased exponentially as the protein concentration increased up to 60 mg/mL (Figure 3a). However, in the presence of excipients, solution viscosity was lower and could be titrated. Solution viscosity of 60 mg/mL mAb-J solution decreased from ~18 to ~2-4 mPa•s in the presence of 100 mM excipient, as shown in Figure 3a-e. Positively-charged amino acids (Arg and Lys) had greater ability to reduce solution viscosity than the negatively-charged amino acids (Glu and Asp) or NaCl.

### **2.3.2. Physical Properties of mAb-J in the Absence/Presence of Excipients**

The next stage of the work focused on developing a better understanding of the molecular nature of mAb-J interactions leading to the solution properties described in the preceding sections (solution turbidity, phase separation and elevated viscosity), both in the presence and absence of the five charged excipients. To this end, the hydrodynamic diameter, percentage of associated oligomers, and apparent relative solubility values of mAb-J in these various solutions were determined.<sup>46-50</sup>

Table 1 summarizes the effect of these excipients on the average hydrodynamic diameter of mAb-J at 10 mg/mL determined by dynamic light scattering. The expected average hydrodynamic diameter value for an IgG1 molecule, consistent with values reported previously, is in the range of 9 to 12 nm.<sup>51,52</sup> The average hydrodynamic diameter of mAb-J in BB, however, was 20.4 nm, larger than expected for monomeric mAb-J. With

excipients added to the solution, mAb-J displayed notably lowered hydrodynamic diameters. Furthermore, polydispersity index (PDI) values of these measurements displayed a trend of higher PDI values (indicating broader size distributions) for the mAb-J samples with greater sizes.

Concentration gradient, multi-angle light scattering (CG-MALS) was then used to better characterize different mAb-J oligomers and their mole percentage as a function of protein concentration in the absence and presence of excipients. Large negative  $B_{22}$  values, indicating net attractive forces between proteins,<sup>53,54</sup> have been determined previously for mAb-J.<sup>41</sup> Consistent with these previous results, as shown in Figure 4a, the mole percentage of mAb-J monomer in base buffer decreased notably as the protein concentration increased, remaining only about 50% monomeric at a protein concentration of 20 mg/mL with a concomitant increase in oligomer species, primarily monomer-dimer-tetramer equilibrium (based on the best model). When excipients were added (Figure 4b-f), decreased levels of oligomer formation were observed. MAb-J remained monomeric in the presence of Arg up to the highest concentration examined (~23 mg/mL), suggesting complete disruption of attractive PPIs between mAb-J monomers. In contrast, the mole percentage of mAb-J oligomers still increased to varying extents at the higher protein concentrations (10-23 mg/mL) in the presence of the other excipients, suggesting differential ability to disrupt oligomer formation. A similar protective trend was observed in terms of formation of oligomers. For example, as shown in Figure 4e, with addition of



Glu, the mole percentage of oligomers displayed a similar increasing profile like that of the control (mAb-J in BB). The mAb-J dimer, however, was dominant in Glu-containing solution, while tetramer was the major species in BB.

Finally, the relative apparent solubility (thermodynamic activity) of mAb-J was also affected by addition of excipients. PEG-induced precipitation, a widely used method for measuring relative protein solubility,<sup>43,55-57</sup> was employed to determine the effects of excipients on altering mAb-J apparent solubility. Figure 5a illustrates the concentration of mAb-J as a function of %PEG (w/v) in BB with and without additives, showing sigmoidal curves under different buffer conditions. To compare the effect of different excipients on mAb-J, the relative solubility, the amount of PEG required to precipitate 50% of protein (%PEG<sub>midpt</sub>), was determined (Figure 5b). While 3.5% of PEG was needed to precipitate half of all mAb-J in BB, the %PEG<sub>midpt</sub> values increased in the presence of the additives. To estimate apparent solubility (thermodynamic activity), data points in the transition region of the sigmoidal curves were replotted on a logarithmic scale so that the apparent solubility values of mAb-J at zero PEG concentration could be obtained by extrapolation (Figure 5c). Apparent solubility of ~10 mg/mL was observed for mAb-J in BB. In comparison, higher apparent solubility values (30-50 mg/mL) were determined for mAb-J in presence of negatively charged amino acids (Glu and Asp) and NaCl, while much larger values (~670 mg/mL and ~170 mg/mL) were found for mAb-J in the presence of positively-charged amino acids (Arg and Lys).

To better summarize and compare the results obtained from these diverse biophysical methods, radar chart arrays<sup>58</sup> were generated to visualize and better describe the effects of excipients on solution properties of mAb-J, as shown in Figure 6. In this figure, each corner of the individual radar chart refers to solution conditions (BB buffer either with or without excipients) and their effect on mAb-J solutions at the specific concentration tested by each technique. It can be seen in Figure 6, at the top position of each radar chart, mAb-J in BB buffer alone, undergoes extensive RSA displaying high turbidity, larger hydrodynamic diameter, elevated viscosity, notably high mole percentage of oligomers, and lower relative apparent solubility. When excipients are added to the solution, mAb-J has less extensive RSA along with improved solution properties (e.g., lower turbidity, viscosity, improved relative solubility) with a consistent trend in the relative ability of the amino acid excipients to affect the physical properties of mAb-J solutions as follows: Arg > Lys > Asp > Glu. For NaCl, it is consistently less effective than the positively-charged amino acids for disrupting RSA, but it demonstrates sometimes more beneficial effects on mAb-J than the negatively-charged amino acids, depending on the solution property.

### **2.3.3. HX-MS Reveals the Effects of Excipients on RSA Disruption and Changes of Local Dynamics for mAb-J**

To obtain localized structural information on how the backbone dynamics of mAb-J is affected by these excipients, HX-MS was performed as described previously (for

mAb-J).<sup>41</sup> As a first step to provide a D<sub>2</sub>O environment for mAb-J at high protein concentrations (preceding hydrogen exchange), we generated a lyophilized sample of mAb-J with each excipient as described previously.<sup>41</sup> mAb-J was lyophilized at two concentrations (5 mg/mL and 60 mg/mL) in BB containing 10% (w/v) trehalose (as a lyoprotectant). The lyophilized mAb-J cakes are shown in Supplemental Figure S2a, indicating good cake appearance with minimal cracks at the edge. Karl Fischer titration was used to determine the moisture content of the lyophilized cakes, which is often an important parameter for quality assessment.<sup>59</sup> Supplemental Figure S2b shows the lyophilized samples had moisture content within a range of 1.5% to 2.5%, with an average moisture of about 2% for both mAb-J concentrations, which is more than acceptable for HX-MS analysis. The effect of lyophilization on the mAb-J protein itself was evaluated using UV-Visible spectroscopy and SEC by reconstituting the lyophilized cakes with D<sub>2</sub>O (see Supplemental Table S1). Overall, a similar slope of OD<sub>320-350nm</sub> was obtained after lyophilization and reconstitution, indicating no significant aggregation happened during lyophilization. Also, the protein was found to be 98.4-99.7% monomeric based on SEC (with ~99% protein recovery), with small amounts of aggregates (~1%) that could be removed by centrifugation, and was therefore suitable for use in HX-MS experiments.

To evaluate the effects of the charged amino acids on mAb-J at the molecular level, HX-MS was performed to investigate changes in backbone dynamics and flexibility

at both low and high protein concentrations. In this study, re-analysis of the data acquired in our earlier work using an updated peptide list (see Supplemental Table S2) was performed to define mAb-J RSA interfaces (Figure 7a).<sup>41</sup> Here, we focus on the effects of the charged excipients on disruption and alterations of RSA interfaces. Lyophilized mAb-J samples (5 mg/mL and 60 mg/mL) were reconstituted in excipient-containing (100 mM) D<sub>2</sub>O-buffer to trigger protein amide-hydrogen labeling. Following a 2760s interval of hydrogen exchange, the reaction was quenched, the mAb was then digested with immobilized pepsin and the uptake of deuterium in each peptide was determined by LC-MS as described in Supporting Information. A total of 182 peptides were confirmed (see Supplemental Table S2) leading to 94% percent sequence coverage in both the heavy chain and light chain. Each of the confirmed peptides was analyzed to determine mass difference between two different protein concentration conditions in each of the buffer/excipient conditions. The negative and positive values of mass difference showed protected and de-protected regions in mAb-J at 60 mg/mL, and a significance criterion ( $\pm 0.43$  Da) was applied for determining the degree of excipient effects at different mAb-J regions.

The HX-MS results for each of the peptides, with and without excipients, at both low and high protein concentrations were evaluated. To this end, we compared deuterium-uptake profiles of mAb-J peptides at low (5 mg/mL) vs high protein

concentration (60 mg/mL) with and without excipients, indicating RSA interfaces and effects of excipients on RSA. Figure 7 shows the difference plots, i.e., HX Difference = HX (60 mg/mL) – HX (5 mg/mL), of the deuterium uptake results, in the absence of additives (panel a) and in the presence of four selected excipients (Arg, Lys, Glu, and Asp; panels b-e, respectively). As shown in Figure 7a, three protected regions were identified in mAb-J at 60 mg/mL at the RSA interfaces, which are located in the variable heavy chain ( $V_H$ ), variable light chain ( $V_L$ ), and constant domain of the heavy chain ( $C_{H3}$ ) of the antibody, defining the RSA interface as being heavy chain (HC) 92-116 (CDR H3), light chain (LC) 39-76 (CDR L2), and HC 381-408 ( $C_{H3}$ ), respectively, consistent with our earlier work.<sup>41</sup>

When 100 mM Arg was present in solution at a mAb-J protein concentration of 5 and 60 mg/mL (Figure 7b), two of the three high concentration protected regions in mAb-J due to RSA were eliminated, with only weaker protection at the CDR L2 region still remaining. There was, however, one region (CDR L2) showing slower hydrogen exchange at 60 vs 5 mg/mL, possibly because 100 mM Arg could not fully disrupt the mAb-J PPIs at the protein concentration of 60 mg/mL, especially the CDR L2 regions. Similar effects were observed with Lys (Figure 7c). More details on interpreting HX-MS protection on CDR L2 region are discussed below.

For the negatively-charged amino acids (Glu and Asp), different effects on different regions of mAb-J were observed including less efficiency in disrupting mAb-J RSA interfaces (Figure 7d and e). For the addition of Glu, similar to the effects of Arg and Lys, there is no increased HX protection at 60 mg/mL in the CDR H3 and C<sub>H3</sub> regions indicating that the addition of Glu disrupted the same two RSA interfaces in CDR H3 and C<sub>H3</sub> regions. Moreover, it seems that the RSA interface on CDR L2 was also disrupted by Glu, which in fact was not the case, as indicated by biophysical analysis (see Discussion section). Furthermore, other regions in mAb-J were also affected by the addition of Glu, displaying increased flexibility in primarily four regions of HC, containing V<sub>H</sub> HC 124-138 (TKGPSVFPLAPSSKS), C<sub>H1</sub> HC 208-218 (HKPSNTKVDKK), C<sub>H2</sub> HC 340-352 (ISKAKGQPREPQV), and C<sub>H3</sub> HC 430-450 (SVMHEALHNHYTQKSLSLSPG). Multiple positively-charged amino acids, based on our mAb-J homology model, are exposed on each of the Glu responsive regions, giving +2, +4, +2, and +3 net charges on the increased-flexibility regions of V<sub>H</sub>, C<sub>H1</sub>, C<sub>H2</sub>, C<sub>H3</sub>, respectively. Therefore, it is possible that, at high protein concentrations, Glu interacted with the positively-charged amino acids in these regions, and thus affected local dynamics of mAb-J, thereby increasing HX at 60 mg/mL. For the addition of Asp, this additive also had a comparatively poorer ability to disrupt RSA interfaces for mAb-J in comparison to Arg and Lys, and showed similar results to Glu. In addition to the peptide segments in the HC showing increased flexibility at 60 mg/mL (probably also due to charge interactions between Asp

and local regions of mAb-J), protein segments in CDR L2 showed slowed HX at 60 mg/mL, which is similar to the observations with Arg or Lys, suggesting incomplete disruption of this RSA interface with Asp addition (see Discussion section).

To visualize these effects, homology models of mAb-J were utilized and regions of mAb-J that are affected in terms of changes in local flexibility at high vs low protein concentrations are shown in Figure 8a. The effects of mAb-J concentration in the presence of different excipients are highlighted in color (Figure 8b-e) where regions of mAb-J which showed significant increase or decrease in hydrogen exchange in the presence of excipients. Collectively, the HX-MS observations suggest that significant interactions involving both the Fab and Fc are the major driving force for mAb-J to undergo RSA at high protein concentrations, mainly through electrostatic attractive interactions (net positive charges on the interfaces of the CDR H3 and CDR L2 regions and net negative charges on the interface in C<sub>H3</sub> region). Interaction with charged amino acids weakens mAb-J PPIs and thus disrupts RSA at high protein concentrations. However, weak interactions through CDR L2 region appear to still exist at high protein concentration to varying extents in the presence of different excipients.

## **2.4. Discussion**

Formulating monoclonal antibodies at high protein concentrations is usually required for SC administration to both reach the therapeutic window and increase patient

compliance.<sup>7,8</sup> However, high concentrations of some antibodies can lead to solution opalescence, high viscosity, and even phase separation through intermolecular reversible self-association.<sup>15-17</sup> Many strategies have already been tested to reduce mAb RSA, such as engineering antibodies by mutating specific amino acids,<sup>60</sup> or optimizing antibody formulations by adding excipients, altering pH and ionic strength.<sup>61-63</sup> Herein, we have studied different excipients to identify their ability to disrupt RSA of a specific human immunoglobulin G1 (mAb-J) at both the solution and the molecular levels, to elucidate an improved understanding of how the excipients affect the RSA of this particular mAb.

In this work, the effects of two positively-charged amino acids (Arg and Lys), two negatively-charged amino acids (Glu and Asp), and NaCl on disrupting known sites of PPIs for mAb-J were evaluated. These effects were then correlated with solution properties of mAb-J as a function of increasing protein concentration as well its physical properties. Each of the five charged excipients showed RSA-disrupting effects of mAb-J, albeit to different extents, consistent with electrostatic interactions as probably the dominating driving force for reversible self-association of mAb-J molecules (as reported previously from HX-MS analysis of mAb-J<sup>41</sup>). In that previous work we found that, mAb-J at pH 6.0 (pI ~7.3) contains a region of net +2 charge in each of the two Fab-CDR regions: CDR L2 (LC 39-76, YQQLPGTAPKLLIYDNFNRPSGVPDRFSGSKSGTSASL) and CDR H3 (HC 92-116, AVYYCATVMGKWKIKGGYDYWGRGTL). Another charged region



involved in the RSA interfaces of mAb-J at the same pH is located in the Fc domain, containing net -4 charge peptide segment (HC 381-408, IAVEWESNGQPENNYKTTTPVLDSDGSF). Because electrostatic attractive interactions are likely the dominant force for mAb-J to form high-order oligomers due to RSA, it was of interest to assess how different charged excipients might modulate and improve the physical properties of mAb-J as well as associated solution properties at high protein concentrations.

#### **2.4.1. Effect of Five Excipients on Solution Properties of mAb-J**

For mAb-J in the base buffer (BB) at pH 6.0, increasing the protein concentration led to formation of increasing amounts of mAb-J oligomers in solution as demonstrated by both dynamic light scattering and CG-MALS analysis.<sup>41</sup> This RSA increased turbidity, elevated viscosity and decreased relative apparent solubility as summarized in the radar chart in Figure 6. In addition, as shown in Figure 1, mAb-J in BB not only showed a greater propensity to form more turbid solutions, but to eventually undergo phase separation at higher protein concentrations. The addition of these five charged excipients, however, did improve the mAb-J solution properties, again to varying extents, that overall correlated well with the remaining RSA between mAb-J molecules (as measured by DLS and CG-MALS) and specific Fab-Fc contact sites between mAb-J molecules (at 60 vs 5 mg/mL as measured by HX-MS).

In general, the addition of the five additives clarified the mAb-J solutions based both on their visual appearance and decreased turbidity at high protein concentrations. Our results suggest that, albeit to different extents, all charged excipients we used in this study can disrupt the RSA interface sites of mAb-J by a charge shielding effect, which can be explained by DLVO (Derjaguin-Landau-Verwey-Overbeek) theory.<sup>64</sup> For example, a trend of decreasing the effective charge of mAb-J by increasing the solution ionic strength results in a shorter Debye screening length caused by electrostatic charge screening, and thus electrostatic attractive interactions can be mitigated or even eliminated by the less effective surface charge on mAb-J.<sup>65,66</sup> This charge shielding effect, as observed by the concentration-dependent excipient efficiency of disrupting RSA of mAb-J, was observed to affect solution properties. As increasing levels of the excipients were added to BB (from 30 mM to 100 mM), not only the opalescence of mAb-J solutions dramatically decreased, but phase separation at high protein concentrations was inhibited (Figure 1). Similar results were also seen in by more quantitative measurements including turbidity and viscosity values, where the excipients exhibited concentration-dependent profiles for the reduction of solution turbidity and viscosity. In this work, we examined excipient effects in the concentration range from 30 mM to 100 mM (a range over which Debye–Hückel charge shielding is dominant), because higher excipient concentrations (e.g., 0.2-2 M range) could complicate data interpretation due to competing physical effects on the mAb-J molecules (e.g., salting out effects).

#### 2.4.2. HX-MS Analysis of Effect of Five Excipients on Sites of RSA in mAb-J

For HX-MS analysis, interpretation of HX differences in the presence of various excipients requires correction for the effects on the chemical exchange rate.<sup>67</sup> In our current work, we were unable to incorporate a reporter peptide to compensate for potential chemical exchange effects. Thus, we focused only on differences in hydrogen exchange between high and low protein concentrations in the presence of each individual additive. Three RSA interfaces (CDR L2, CDR H3, and C<sub>H3</sub>) were identified in BB between 60 mg/mL and 5 mg/mL based on slowed HX. More highly oligomerized mAb-J with interacting networks probably formed at 60 mg/mL and thus multiple regions on mAb-J are involved in RSA in BB condition. Based on CG-MALS analysis, which showed a small fraction of lower-order oligomers in solution, PPIs were still present for mAb-J in BB at 5 mg/mL. But due to the relatively higher oligomerized state of mAb-J at higher protein concentration, HX protection could be observed between 60 and 5 mg/mL samples.

The addition of 100 mM of any of these five excipients was sufficient to eliminate the high concentration HX protections particularly in the CDR H3 and C<sub>H3</sub> regions, suggesting that the RSA association in these regions is a signature of the highly oligomerized form. The presence of Arg or Lys in solution mitigated mAb-J RSA to a larger extent, but probably not completely, dissociating high-order mAb-J oligomer to perhaps a dimeric form as probed by CG-MALS. Therefore in HX analysis, there was still a

protection at the CDR L2 region. These results suggest that mAb-J at 60 mg/mL in the presence of Arg or Lys is more dimeric than that at 5 mg/mL. Such HX protection in CDR L2 is probably a signature of the difference between the monomeric and dimeric mAb-J forms. The negatively-charged Glu and Asp were not as effective as Arg or Lys in terms of RSA disruption for mAb-J according to biophysical analysis, but could still eliminate HX protections in CDR H3 and C<sub>H</sub>3 regions. However, the protection of the CDR L2 region was only observed for Asp, and not for Glu, which is probably due to their different RSA disruption efficiency, especially in the CDR L2 region. The absence of HX protection for Glu probably indicates a similar extent of dimerization at both high and low protein concentrations. Greater RSA inhibition effects on the CDR L2 region was observed by Asp addition, resulting in a detectable HX difference between the two protein concentrations.

Therefore, PPIs on potentially mAb-J dimer formation were still detected in the CDR L2 region (LC 39-76, YQQLPGTAPKLLIYDNFNRPSPGVDRFSGSKSGTSASL) even in the presence of excipients. In addition to the net +2 charges in this region, there are also two negatively-charged and three aromatic amino acids, which might induce further Fab-Fab interactions based on the CDR L2 region (possibly electrostatic or hydrophobic interactions).<sup>68</sup> It is also possible that these Fab-Fab interactions were present even in the absence of excipients, forming low-order oligomers, such as dimers.

More extensive associations, involving multiple regions on mAb-J as discussed above, occurred by Fab-Fc electrostatic attractions to form high-order oligomers, transient networks, or even phase separation.<sup>41</sup> As reported in a recent paper<sup>69</sup>, Arg and Lys could increase the surface aromatic hydrophobicity, and Arg was reported more effective than Lys, which might improve the Fab-Fab hydrophobic attractions. Also, as the positively-charged side chains of Arg and Lys are relatively more chaotropic<sup>69</sup>, the surface tension of water decreases, and thus the conformational structure of mAb-J might become altered, exposing some buried amino acid residues. Therefore, Fab-Fab interactions of mAb-J with hydrophobic forces might replace the original Fab-Fc interactions in the presence of Arg or Lys at high protein concentrations. In terms of electrostatic interactions, albeit there is a net +2 charge on CDR L2 interface, it does have two negatively-charged amino acids in this region, which might also be responsible for weak Fab-Fab interactions by charge attraction (even in the presence of excipients at high protein concentrations).

#### **2.4.3. Effect of Five Excipients on Properties of mAb-J**

The addition of NaCl also had the ability to decrease PPIs of mAb-J solutions, but the extent of its effectiveness (in the concentration range examined) was less than the charged amino acids. As shown in Figures 1 and 2, at high mAb-J concentrations, the solutions with NaCl still appeared opalescent and had higher turbidity even in the

presence of relatively high concentration of NaCl. Beyond being charged, the amino acids also possess a positively-charged primary amine group and a negatively-charged carboxylate group, leading to zwitterionic properties. Furthermore, amino acids have larger surface area (due to their non-polar side chains) than the sodium ion, which likely enhances their ability to interact more sites on proteins via other non-covalent mechanisms.<sup>70</sup> Also, NaCl at low concentrations does not have an ability to modify hydrophobic interactions<sup>71,72</sup>. In summary, there are more possible non-covalent interactions between the mAb-J and charged amino acids than between mAb-J and NaCl, and thus charged amino acids more effectively disrupted RSA at high protein concentrations.

As for Glu and Asp, they probably have additional effects on the mAb-J including interaction via other non-covalent mechanisms (e.g., hydrogen bonding or specific interactions) as well as potentially weak preferential exclusion effects.<sup>73,74</sup> Additional interactions with mAb-J were confirmed in HX-MS results (Figures 7 and 8) where it was demonstrated that there were regions of both increased and decreased backbone flexibility in mAb-J in the presence of Glu and Asp at high protein concentrations. These include Fab interaction sites in CDR L2 as described above. Moreover, a combination of different interactions and effects on mAb-J are present for Glu and Asp, which is consistent with their lower ability to improve solution properties due to competing

interactions vs solely interacting at the RSA interfaces of mAb-J molecules. This might include forming hydrogen bonds with the protein, resulting in changes in protein structure, local pH microenvironments and backbone flexibility.<sup>28,75</sup> The increase of backbone flexibility on mAb-J in the presence of Glu or Asp at high concentration was again not necessarily involved with mAb-J RSA.

In this work, Arg-containing mAb-J solutions consistently displayed the best solution properties and the largest fraction of protein monomers, even compared to another positively-charged amino acid, Lys. As discussed above, although electrostatic attractions are the dominant force for formation of mAb-J RSA networks, additional contributions by other non-covalent interactions are also important. For example, Arg can favorably interact with aromatic residues in proteins, by forming cation- $\pi$  interactions.<sup>76-</sup>  
<sup>78</sup> Furthermore, although Arg has a guanidinium group, the carboxylate group in Arg has been shown to limit the interaction of the guanidinium group, weakening Arg's interaction with proteins so that it can no longer extensively alter structure.<sup>78</sup> Also, Arg has a relatively larger surface area than Lys, which contributes more steric repulsion, leading to fewer surface-exposed attraction sites on mAb-J and thus might reduce the chance for protein interactions.<sup>71</sup> Other studies also indicate Arg can increase protein solubility, increase second osmotic virial coefficient ( $B_{22}$ , with increasing positive values indicating repulsive effects), and suppress formation of protein dimers, which are consistent with our results

(Figure 4 and 5).<sup>79-81</sup> Moreover for the HX-MS results, mAb-J still demonstrated weak protection in the CDR L2 region even with Arg or Lys in solution. Therefore, it is possible that positively-charged amino acids localize and act primarily on C<sub>H</sub>3 domain RSA interfaces rather than CDR L2 and that other potential interactions may occur with the CDR L2 region when the original electrostatic interactions involving Fab and Fc sites are broken at high protein concentrations.<sup>68</sup> So it is likely that disruption of a combination of different non-covalent forces which induce the apparent RSA interfaces in the mAb-J molecule, and Arg is most able to outcompete for all of these non-covalent sites of interactions. Similar observations have been reported that Arg has a higher ability than sodium to disrupt PPIs, decrease viscosity, and increase solubility by not only a charge shielding effect, but also cation- $\pi$  interaction.<sup>69,82,83</sup> Although high concentrations of Arg promoted protein aggregation in some reported cases, low concentrations induce significant effects by decreasing dynamic viscosity and increasing colloidal stability, without strongly influencing protein conformational stability and aggregation propensity.<sup>82</sup> In our work, as shown in Figure 1b, Arg also effectively prevented phase separation by disrupting PPIs even at low excipient concentrations.

#### **2.4.4. Comparative Results in Companion Paper with Different IgG1 mAb**

This work is part one of two studies examining the inter-relationships of pharmaceutical excipients, solution properties and molecular interactions in high



concentration mAb solutions. In the companion paper (Part II), we performed a similar series of studies with a second IgG1 mAb (mAb-C) which has been previously shown to undergo a different predominant mechanism of RSA at high protein concentrations. For mAb-c, hydrophobic attractions mediated by Fab-Fab interactions in the CDR regions have been shown to be the dominant driving force in intermolecular associations.<sup>13</sup> Therefore, a different set of excipients were employed with varying ability to affect hydrophobic interactions in mAb-C. Taken together, using two different mAbs (mAb-J and mAb-C) that display RSA by different mechanisms, these studies demonstrate the rational design of high concentration mAb formulations with specific additives by (1) elucidating the ability of additives to disrupt specific intermolecular interactions leading to RSA a mAb by HX-MS, and then (2) correlating these findings with their effects in a concentration-dependent manner on both the solution properties (opalescence, phase separation and viscosity) and molecular physical properties (average size and relative solubility) of the mAb at high protein concentrations.

## 2.5. References

1. Nelson AL, Dhimolea E, Reichert JM 2010. Development trends for human monoclonal antibody therapeutics. *Nat Rev Drug Discov* 9(10):767-774.
2. Chames P, Van Regenmortel M, Weiss E, Baty D 2009. Therapeutic antibodies: successes, limitations and hopes for the future. *British Journal of Pharmacology* 157(2):220-233.
3. Wang W, Singh S, Zeng DL, King K, Nema S 2007. Antibody structure, instability, and formulation. *Journal of pharmaceutical sciences* 96(1):1-26.
4. [Internet] A-S. Cited 2016 June 10. Therapeutic monoclonal antibodies approved or in review in the European Union or the United States, available at <http://www.antibodysociety.org/news/approved-antibodies/>. ed.
5. [Internet] BTC. Cited 2016 June 10. Woburn (MA): Bioprocess Technology Consultants, Inc. bioTRAK database, available from: <http://www.bptc.com/pipeline-databases.php>. ed.
6. [Internet] DF. Cited 2016 June 10. Silver Spring (MD): U.S. Food and Drug Administration, Center for Drug Evaluation and Research, available at <http://www.accessdata.fda.gov/scripts/cder/drugsatfda/index.cfm>. ed.
7. Armstrong NJ, Bowen MN, Maa Y-F. 2013. High-concentration monoclonal antibody formulations. ed.: Google Patents.
8. Shire SJ, Shahrokh Z, Liu J 2004. Challenges in the development of high protein concentration formulations. *Journal of pharmaceutical sciences* 93(6):1390-1402.
9. Stockwin L, Holmes S 2003. Antibodies as therapeutic agents: vive la renaissance! Expert opinion on biological therapy 3(7):1133-1152.
10. Alford JR, Kendrick BS, Carpenter JF, Randolph TW 2008. High concentration formulations of recombinant human interleukin - 1 receptor antagonist: II. aggregation kinetics. *Journal of pharmaceutical sciences* 97(8):3005-3021.
11. Sukumar M, Doyle BL, Combs JL, Pekar AH 2004. Opalescent appearance of an IgG1 antibody at high concentrations and its relationship to noncovalent association. *Pharmaceutical research* 21(7):1087-1093.
12. Salinas BA, Sathish HA, Bishop SM, Harn N, Carpenter JF, Randolph TW 2010. Understanding and modulating opalescence and viscosity in a monoclonal antibody formulation. *Journal of pharmaceutical sciences* 99(1):82-93.
13. Arora J, Hickey JM, Majumdar R, Esfandiary R, Bishop SM, Samra HS, Middaugh CR, Weis DD, Volkin DB 2015. Hydrogen exchange mass spectrometry reveals protein interfaces and distant dynamic coupling effects during the reversible self-association of an IgG1 monoclonal antibody. *mAbs* 7(3):525-539.
14. Esfandiary R, Parupudi A, Casas - Finet J, Gadre D, Sathish H 2015. Mechanism of Reversible Self - Association of a Monoclonal Antibody: Role of Electrostatic and Hydrophobic Interactions. *Journal of pharmaceutical sciences* 104(2):577-586.

15. Connolly Brian D, Petry C, Yadav S, Demeule B, Ciaccio N, Moore Jamie M, Shire Steven J, Gokarn Yatin R 2012. Weak Interactions Govern the Viscosity of Concentrated Antibody Solutions: High-Throughput Analysis Using the Diffusion Interaction Parameter. *Biophysical Journal* 103(1):69-78.
16. Kanai S, Liu J, Patapoff TW, Shire SJ 2008. Reversible self - association of a concentrated monoclonal antibody solution mediated by Fab–Fab interaction that impacts solution viscosity. *Journal of pharmaceutical sciences* 97(10):4219-4227.
17. Liu J, Nguyen MD, Andya JD, Shire SJ 2005. Reversible self - association increases the viscosity of a concentrated monoclonal antibody in aqueous solution. *Journal of pharmaceutical sciences* 94(9):1928-1940.
18. Brems DN, Alter LA, Beckage MJ, Chance RE, DiMarchi RD, Green LK, Long HB, Pekar AH, Shields JE, Frank BH 1992. Altering the association properties of insulin by amino acid replacement. *Protein Engineering* 5(6):527-533.
19. Clodfelter DK, Pekar AH, Rebhun DM, Destrampe KA, Havel HA, Myers SR, Brader ML 1998. Effects of non-covalent self-association on the subcutaneous absorption of a therapeutic peptide. *Pharmaceutical research* 15(2):254-262.
20. Nishi H, Miyajima M, Nakagami H, Noda M, Uchiyama S, Fukui K 2010. Phase separation of an IgG1 antibody solution under a low ionic strength condition. *Pharmaceutical research* 27(7):1348-1360.
21. Mason BD, Zhang L, Remmele RL, Zhang J 2011. Opalescence of an IgG2 monoclonal antibody solution as it relates to liquid–liquid phase separation. *Journal of pharmaceutical sciences* 100(11):4587-4596.
22. Raut AS, Kalonia DS 2016. Effect of Excipients on Liquid–Liquid Phase Separation and Aggregation in Dual Variable Domain Immunoglobulin Protein Solutions. *Molecular Pharmaceutics* 13(3):774-783.
23. Chow C-K, Allan BW, Chai Q, Atwell S, Lu J 2016. Therapeutic Antibody Engineering To Improve Viscosity and Phase Separation Guided by Crystal Structure. *Molecular Pharmaceutics* 13(3):915-923.
24. Raut AS, Kalonia DS 2015. Opalescence in Monoclonal Antibody Solutions and Its Correlation with Intermolecular Interactions in Dilute and Concentrated Solutions. *Journal of Pharmaceutical Sciences* 104(4):1263-1274.
25. Demeule B, Lawrence MJ, Drake AF, Gurny R, Arvinte T 2007. Characterization of protein aggregation: The case of a therapeutic immunoglobulin. *Biochimica et Biophysica Acta (BBA) - Proteins and Proteomics* 1774(1):146-153.
26. Bye JW, Platts L, Falconer RJ 2014. Biopharmaceutical liquid formulation: a review of the science of protein stability and solubility in aqueous environments. *Biotechnology Letters* 36(5):869-875.
27. Akers MJ 2002. Excipient–drug interactions in parenteral formulations. *Journal of pharmaceutical sciences* 91(11):2283-2300.
28. Kamerzell TJ, Esfandiary R, Joshi SB, Middaugh CR, Volkin DB 2011. Protein–excipient interactions: Mechanisms and biophysical characterization applied to protein formulation development. *Advanced drug delivery reviews* 63(13):1118-1159.
29. Ohtake S, Kita Y, Arakawa T 2011. Interactions of formulation excipients with proteins in solution and in the dried state. *Advanced drug delivery reviews* 63(13):1053-1073.

30. Baek Y, Zydney AL 2018. Intermolecular interactions in highly concentrated formulations of recombinant therapeutic proteins. *Curr Opin Biotechnol* 53:59-64.
31. Oki S, Nishinami S, Shiraki K 2018. Arginine suppresses opalescence and liquid-liquid phase separation in IgG solutions. *Int J Biol Macromol* 118(Pt B):1708-1712.
32. Manikwar P, Majumdar R, Hickey JM, Thakkar SV, Samra HS, Sathish HA, Bishop SM, Middaugh CR, Weis DD, Volkin DB 2013. Correlating excipient effects on conformational and storage stability of an IgG1 monoclonal antibody with local dynamics as measured by hydrogen/deuterium - exchange mass spectrometry. *Journal of pharmaceutical sciences* 102(7):2136-2151.
33. Jensen PF, Rand KD 2016. Hydrogen Exchange: A Sensitive Analytical Window into Protein Conformation and Dynamics. *Hydrogen Exchange Mass Spectrometry of Proteins: Fundamentals, Methods, and Applications*:1.
34. Wei H, Mo J, Tao L, Russell RJ, Tymiak AA, Chen G, Iacob RE, Engen JR 2014. Hydrogen/deuterium exchange mass spectrometry for probing higher order structure of protein therapeutics: methodology and applications. *Drug discovery today* 19(1):95-102.
35. Houde D, Arndt J, Domeier W, Berkowitz S, Engen JR 2009. Characterization of IgG1 Conformation and Conformational Dynamics by Hydrogen/Deuterium Exchange Mass Spectrometry. *Analytical Chemistry* 81(7):2644-2651.
36. Chen G, Warrack BM, Goodenough AK, Wei H, Wang-Iverson DB, Tymiak AA 2011. Characterization of protein therapeutics by mass spectrometry: recent developments and future directions. *Drug Discovery Today* 16(1-2):58-64.
37. Majumdar R, Manikwar P, Hickey JM, Samra HS, Sathish HA, Bishop SM, Middaugh CR, Volkin DB, Weis DD 2013. Effects of Salts from the Hofmeister Series on the Conformational Stability, Aggregation Propensity, and Local Flexibility of an IgG1 Monoclonal Antibody. *Biochemistry* 52(19):3376-3389.
38. Tang L, Sundaram S, Zhang J, Carlson P, Matathia A, Parekh B, Zhou Q, Hsieh M-C 2013. Conformational characterization of the charge variants of a human IgG1 monoclonal antibody using H/D exchange mass spectrometry. *mAbs* 5(1):114-125.
39. Houde D, Peng Y, Berkowitz SA, Engen JR 2010. Post-translational Modifications Differentially Affect IgG1 Conformation and Receptor Binding. *Molecular & Cellular Proteomics : MCP* 9(8):1716-1728.
40. Majumdar R, Esfandiary R, Bishop SM, Samra HS, Middaugh CR, Volkin DB, Weis DD 2015. Correlations between changes in conformational dynamics and physical stability in a mutant IgG1 mAb engineered for extended serum half-life. *mAbs* 7(1):84-95.
41. Arora J, Hu Y, Esfandiary R, Sathish HA, Bishop SM, Joshi SB, Middaugh CR, Volkin DB, Weis DD 2016. Charge-mediated Fab-Fc interactions in an IgG1 antibody induce reversible self-association, cluster formation, and elevated viscosity. *MAbs* 8(8):1561-1574.
42. Gill SC, Von Hippel PH 1989. Calculation of protein extinction coefficients from amino acid sequence data. *Analytical biochemistry* 182(2):319-326.
43. Gibson TJ, McCarty K, McFadyen IJ, Cash E, Dalmonte P, Hinds KD, Dinerman AA, Alvarez JC, Volkin DB 2011. Application of a High-Throughput Screening Procedure with PEG-Induced Precipitation to

Compare Relative Protein Solubility During Formulation Development with IgG1 Monoclonal Antibodies. *Journal of Pharmaceutical Sciences* 100(3):1009-1021.

44. Toprani VM, Joshi SB, Kuelzo LA, Schwartz RM, Middaugh CR, Volkin DB 2016. A Micro-Polyethylene Glycol Precipitation Assay as a Relative Solubility Screening Tool for Monoclonal Antibody Design and Formulation Development. *J Pharm Sci* 105(8):2319-2327.

45. Majumdar R, Manikwar P, Hickey JM, Arora J, Middaugh CR, Volkin DB, Weis DD 2012. Minimizing Carry-Over in an Online Pepsin Digestion System used for the H/D Exchange Mass Spectrometric Analysis of an IgG1 Monoclonal Antibody. *Journal of The American Society for Mass Spectrometry* 23(12):2140-2148.

46. Kanai S, Liu J, Patapoff TW, Shire SJ 2008. Reversible Self-Association of a Concentrated Monoclonal Antibody Solution Mediated by Fab–Fab Interaction That Impacts Solution Viscosity. *Journal of Pharmaceutical Sciences* 97(10):4219-4227.

47. Liu J, Nguyen MDH, Andya JD, Shire SJ 2005. Reversible Self-Association Increases the Viscosity of a Concentrated Monoclonal Antibody in Aqueous Solution. *Journal of Pharmaceutical Sciences* 94(9):1928-1940.

48. Saluja A, Kalonia DS 2008. Nature and consequences of protein–protein interactions in high protein concentration solutions. *International Journal of Pharmaceutics* 358(1–2):1-15.

49. Lilyestrom WG, Yadav S, Shire SJ, Scherer TM 2013. Monoclonal Antibody Self-Association, Cluster Formation, and Rheology at High Concentrations. *The Journal of Physical Chemistry B* 117(21):6373-6384.

50. Bethea D, Wu S-J, Luo J, Hyun L, Lacy ER, Teplyakov A, Jacobs SA, O'Neil KT, Gilliland GL, Feng Y 2012. Mechanisms of self-association of a human monoclonal antibody CNTO607. *Protein Engineering Design and Selection*.

51. Esfandiary R, Hayes DB, Parupudi A, Casas - finet J, Bai S, Samra HS, Shah AU, Sathish HA 2013. A Systematic Multitechnique Approach for Detection and Characterization of Reversible Self-Association during Formulation Development of Therapeutic Antibodies. *Journal of Pharmaceutical Sciences* 102(1):62-72.

52. Armstrong JK, Wenby RB, Meiselman HJ, Fisher TC 2004. The Hydrodynamic Radii of Macromolecules and Their Effect on Red Blood Cell Aggregation. *Biophysical Journal* 87(6):4259-4270.

53. Alford JR, Kendrick BS, Carpenter JF, Randolph TW 2008. Measurement of the Second Osmotic Virial Coefficient for Protein Solutions Exhibiting Monomer-Dimer Equilibrium. *Analytical biochemistry* 377(2):128-133.

54. George A, Wilson WW 1994. Predicting protein crystallization from a dilute solution property. *Acta Crystallographica Section D: Biological Crystallography* 50(4):361-365.

55. Middaugh CR, Tisel WA, Haire RN, Rosenberg A 1979. Determination of the apparent thermodynamic activities of saturated protein solutions. *Journal of Biological Chemistry* 254(2):367-370.

56. Kumar V, Sharma VK, Kalonia DS 2009. Effect of polyols on polyethylene glycol (PEG)-induced precipitation of proteins: Impact on solubility, stability and conformation. *International Journal of Pharmaceutics* 366(1–2):38-43.

57. More AS, Toprani VM, Okbazghi SZ, Kim JH, Joshi SB, Middaugh CR, Tolbert TJ, Volkin DB 2016. Correlating the impact of well-defined oligosaccharide structures on physical stability profiles of IgG1-Fc glycoforms. *Journal of pharmaceutical sciences* 105(2):588-601.
58. Kalonia C, Kumru OS, Kim JH, Middaugh CR, Volkin DB 2013. Radar chart array analysis to visualize effects of formulation variables on IgG1 particle formation as measured by multiple analytical techniques. *Journal of pharmaceutical sciences* 102(12):4256-4267.
59. Scholz E. 2012. Karl Fischer titration: determination of water. ed.: Springer Science & Business Media.
60. Geoghegan JC, Fleming R, Damschroder M, Bishop SM, Sathish HA, Esfandiary R. *mAbs*, 2016, pp 1-10.
61. Rosenbaum D, Zukoski C 1996. Protein interactions and crystallization. *Journal of crystal growth* 169(4):752-758.
62. Velez O, Kaler E, Lenhoff A 1998. Protein interactions in solution characterized by light and neutron scattering: comparison of lysozyme and chymotrypsinogen. *Biophysical journal* 75(6):2682-2697.
63. Sahin E, Grillo AO, Perkins MD, Roberts CJ 2010. Comparative effects of pH and ionic strength on protein-protein interactions, unfolding, and aggregation for IgG1 antibodies. *Journal of pharmaceutical sciences* 99(12):4830-4848.
64. Derjaguin BV, Churaev NV, Muller VM. 1987. The Derjaguin—Landau—Verwey—Overbeek (DLVO) Theory of Stability of Lyophobic Colloids. *Surface Forces*, ed., Boston, MA: Springer US. p 293-310.
65. De Young LR, Fink AL, Dill KA 1993. Aggregation of globular proteins. *Accounts of chemical research* 26(12):614-620.
66. Zhang J. 2012. Protein-protein interactions in salt solutions. ed.: INTECH Open Access Publisher.
67. Toth RTt, Mills BJ, Joshi SB, Esfandiary R, Bishop SM, Middaugh CR, Volkin DB, Weis DD 2017. Empirical Correction for Differences in Chemical Exchange Rates in Hydrogen Exchange-Mass Spectrometry Measurements. *Anal Chem* 89(17):8931-8941.
68. Shan L, Mody N, Sormanni P, Rosenthal K, Damschroder M, Esfandiary R 2018. Developability assessment of engineered monoclonal antibody variants with a complex self-association behavior using complementary analytical and in silico tools. *Molecular pharmaceutics*.
69. Troeger C, Colombara DV, Rao PC, Khalil IA, Brown A, Brewer TG, Guerrant RL, Houpt ER, Kotloff KL, Misra K, Petri WA, Platts-Mills J, Riddle MS, Swartz SJ, Forouzanfar MH, Reiner RC, Hay SI, Mokdad AH 2018. Global disability-adjusted life-year estimates of long-term health burden and undernutrition attributable to diarrhoeal diseases in children younger than 5 years. *The Lancet Global Health* 6(3):e255-e269.
70. Zhang Y, Cremer PS 2010. Chemistry of Hofmeister anions and osmolytes. *Annual review of physical chemistry* 61:63-83.
71. Hung JJ, Dear BJ, Dinin AK, Borwankar AU, Mehta SK, Truskett TT, Johnston KP 2018. Improving Viscosity and Stability of a Highly Concentrated Monoclonal Antibody Solution with Concentrated Proline. *Pharm Res* 35(7):133.

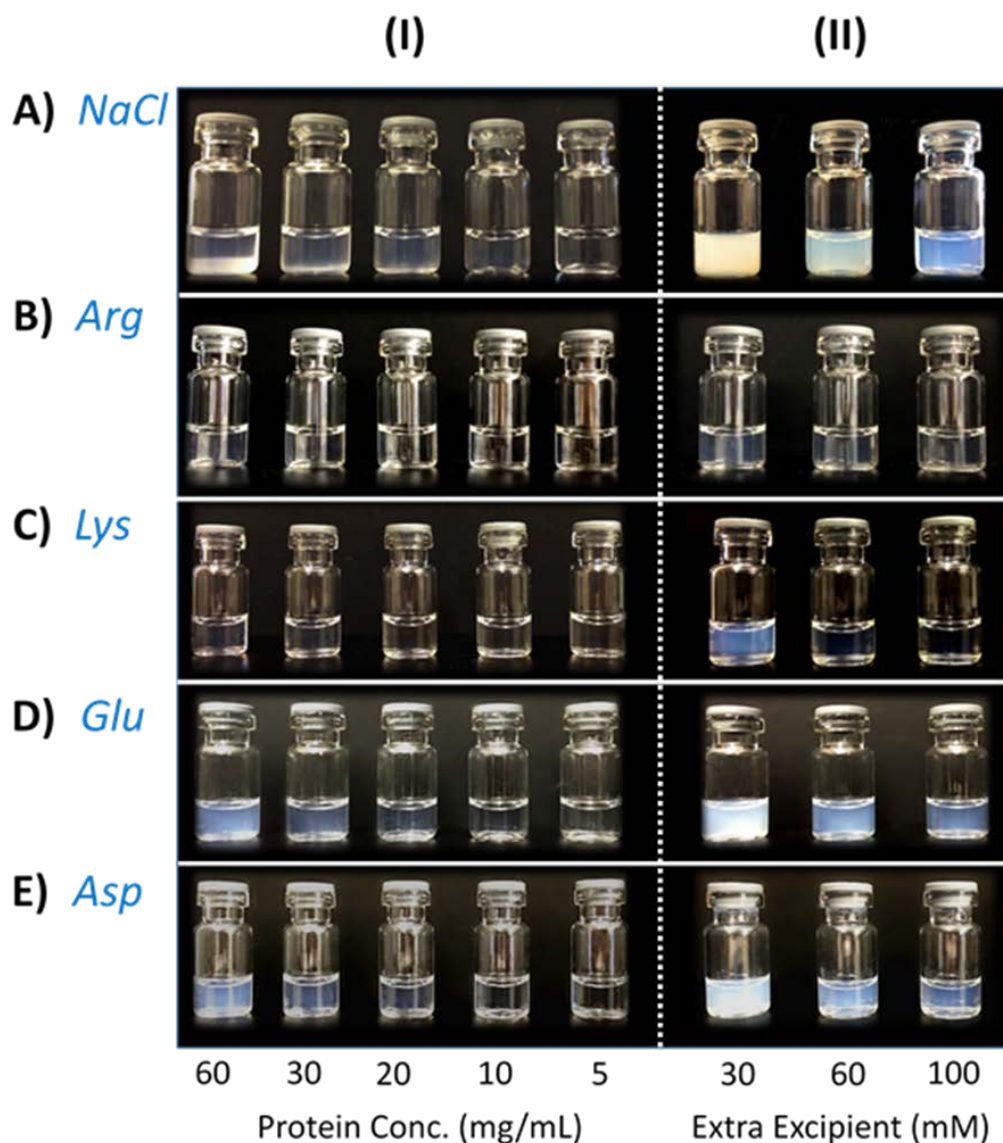
72. Inoue N, Takai E, Arakawa T, Shiraki K 2014. Specific decrease in solution viscosity of antibodies by arginine for therapeutic formulations. *Mol Pharm* 11(6):1889-1896.
73. Arakawa T, Timasheff SN 1984. Mechanism of protein salting in and salting out by divalent cation salts: balance between hydration and salt binding. *Biochemistry* 23(25):5912-5923.
74. Arakawa T, Tsumoto K, Kita Y, Chang B, Ejima D 2007. Biotechnology applications of amino acids in protein purification and formulations. *Amino acids* 33(4):587-605.
75. Yang Z 2009. Hofmeister effects: an explanation for the impact of ionic liquids on biocatalysis. *Journal of biotechnology* 144(1):12-22.
76. Arakawa T, Ejima D, Tsumoto K, Obeyama N, Tanaka Y, Kita Y, Timasheff SN 2007. Suppression of protein interactions by arginine: a proposed mechanism of the arginine effects. *Biophysical chemistry* 127(1):1-8.
77. Gallivan JP, Dougherty DA 1999. Cation- $\pi$  interactions in structural biology. *Proceedings of the National Academy of Sciences* 96(17):9459-9464.
78. Shukla D, Trout BL 2010. Interaction of arginine with proteins and the mechanism by which it inhibits aggregation. *The Journal of Physical Chemistry B* 114(42):13426-13438.
79. Arakawa T, Tsumoto K 2003. The effects of arginine on refolding of aggregated proteins: not facilitate refolding, but suppress aggregation. *Biochemical and biophysical research communications* 304(1):148-152.
80. Ho JG, Middelberg AP, Ramage P, Kocher HP 2003. The likelihood of aggregation during protein renaturation can be assessed using the second virial coefficient. *Protein science* 12(4):708-716.
81. Blasig I, Winkler L, Lassowski B, Mueller S, Zuleger N, Krause E, Krause G, Gast K, Kolbe M, Piontek J 2006. On the self-association potential of transmembrane tight junction proteins. *Cellular and Molecular Life Sciences CMLS* 63(4):505-514.
82. Bauer KC, Suhm S, Woll AK, Hubbuch J 2017. Impact of additives on the formation of protein aggregates and viscosity in concentrated protein solutions. *Int J Pharm* 516(1-2):82-90.
83. Whitaker N, Xiong J, Pace SE, Kumar V, Middaugh CR, Joshi SB, Volkin DB 2017. A Formulation Development Approach to Identify and Select Stable Ultra-High-Concentration Monoclonal Antibody Formulations With Reduced Viscosities. *J Pharm Sci* 106(11):3230-3241.

## 2.6. Figures and Tables

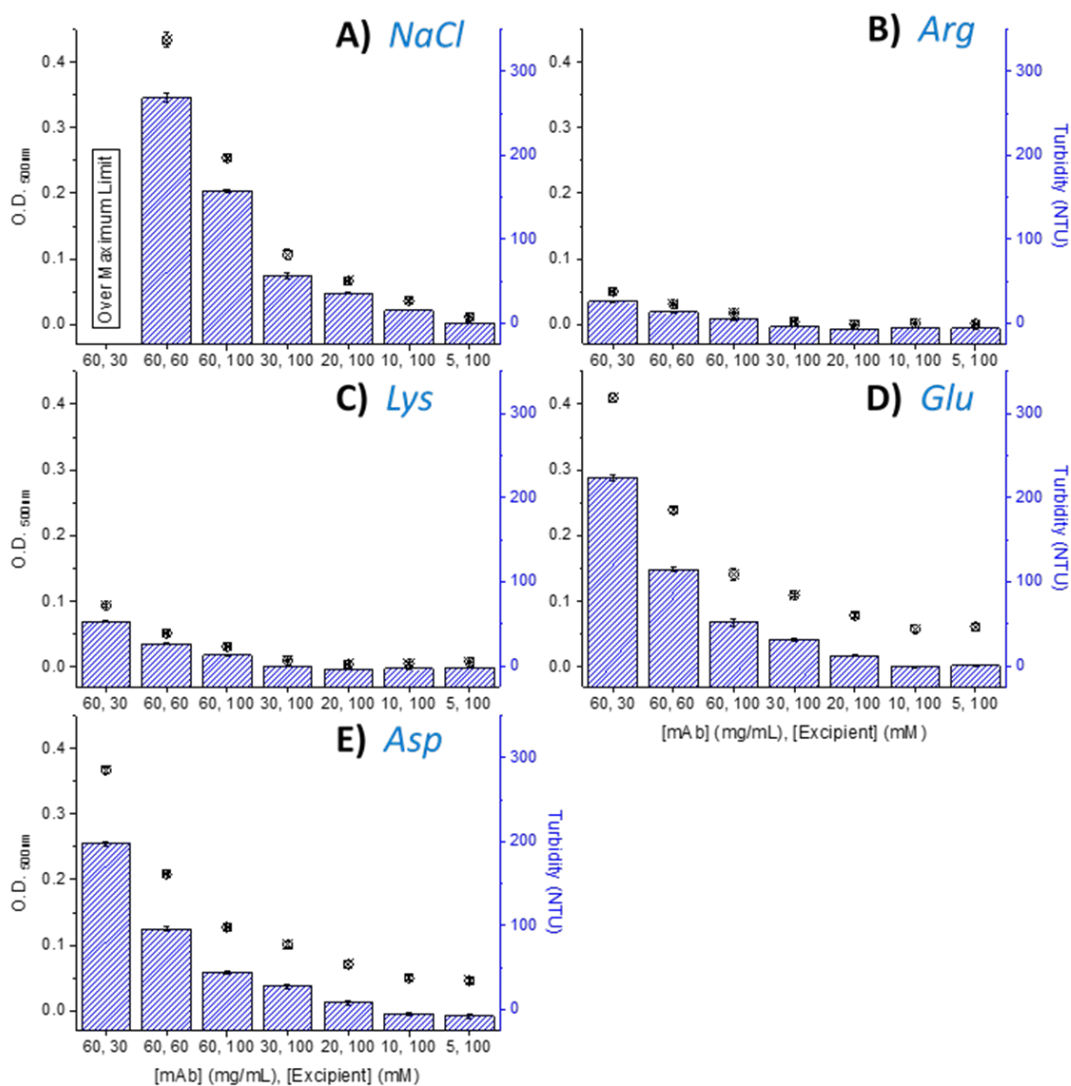
**Table 2.1.** Excipient effects on the hydrodynamic diameter of mAb-J as measured by dynamic light scattering. All measurements were taken at 25°C with a protein concentration of 10 mg/mL at pH 6.0. All excipients have a concentration of 100 mM in solution in base buffer (BB). Triplicate measurements were performed for this study. SD denotes the sample standard deviation.

Condition	Hydrodynamic Diameter (nm)		Polydispersity Index	
	<i>Mean</i>	<i>SD</i>	<i>Mean</i>	<i>SD</i>
BB	20.4	0.8	0.125	0.019
NaCl	14.3	0.1	0.107	0.013
Arg	12.15	0.02	0.057	0.018
Lys	12.7	0.1	0.075	0.018
Glu	15.22	0.03	0.103	0.014
Asp	14.9	0.1	0.104	0.025

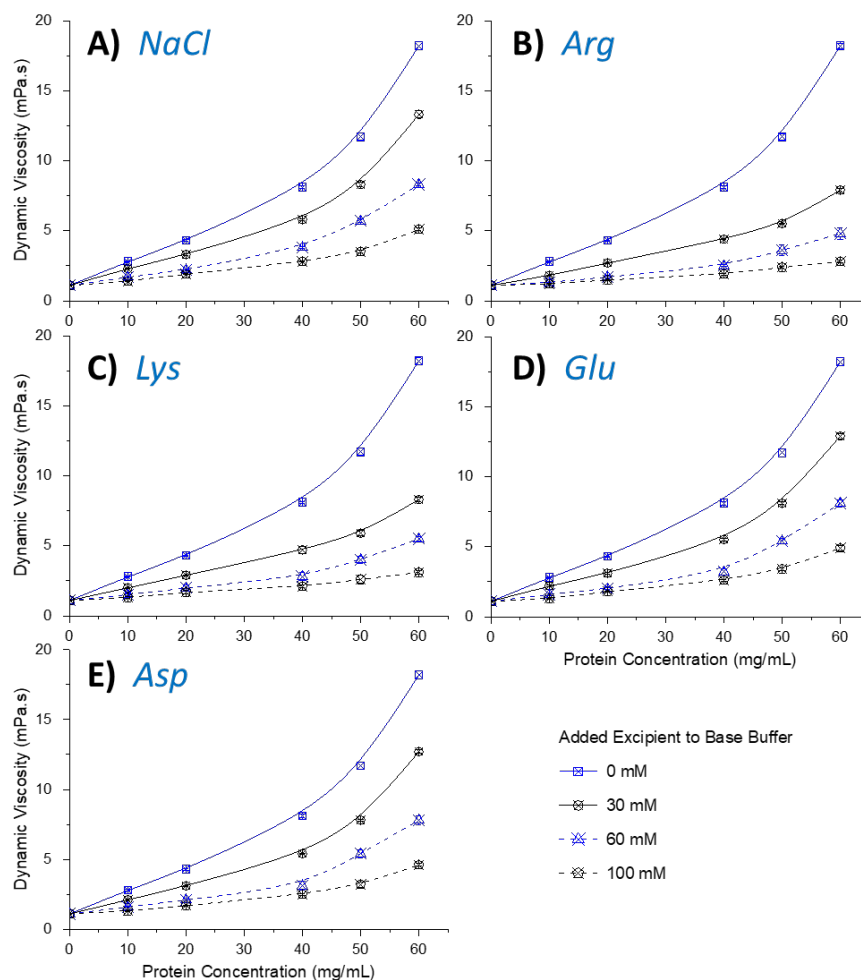




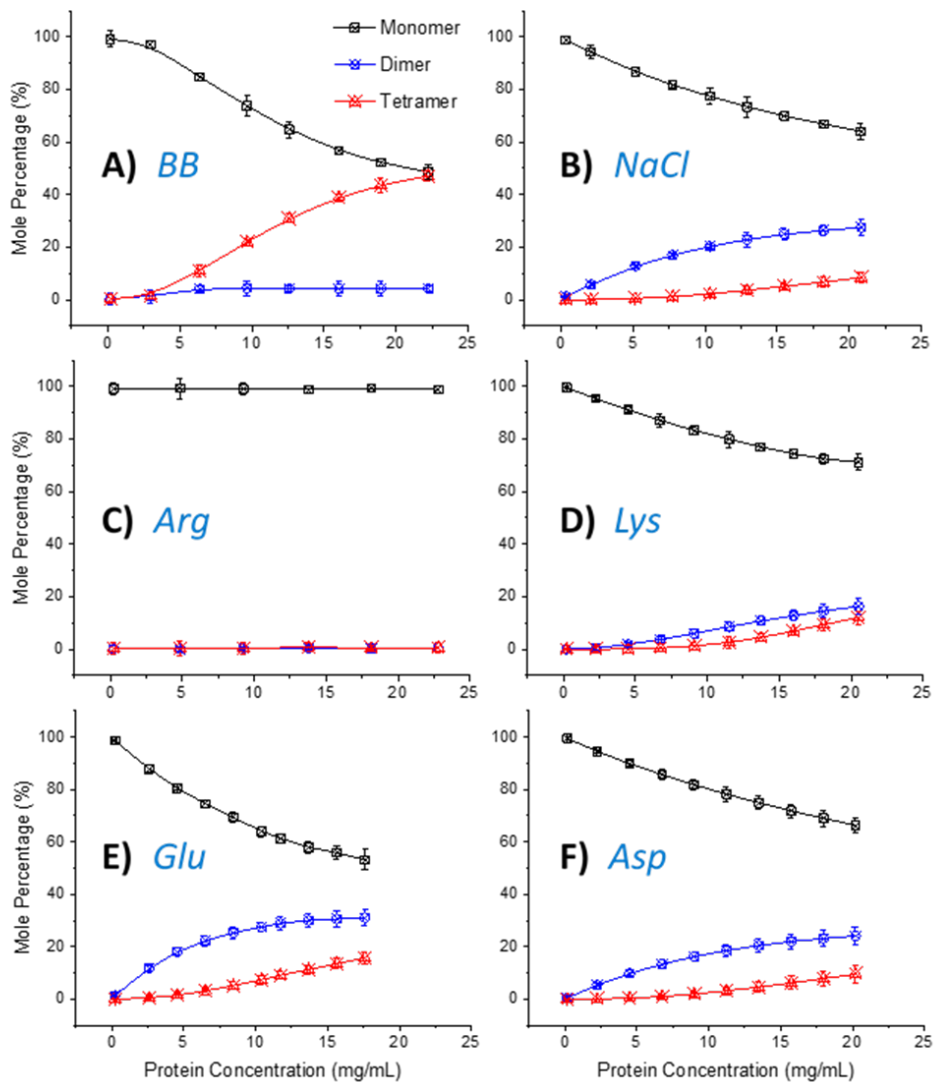
**Figure 2.1.** Excipient effects on mAb-J solution opalescence and phase separation based on solution appearance. Excipients are (A) NaCl, (B) Arg, (C) Lys, (D) Glu, and (E) Asp. Column I represents mAb-J was in BB + 100 mM excipients (except (A) row, which in BB only), but as the protein concentration varied from 5 to 60 mg/mL. Column II shows mAb-J was at 60 mg/mL. In addition to BB, extra amount of excipient was in solution. Representative samples shown were photographed at room temperature.



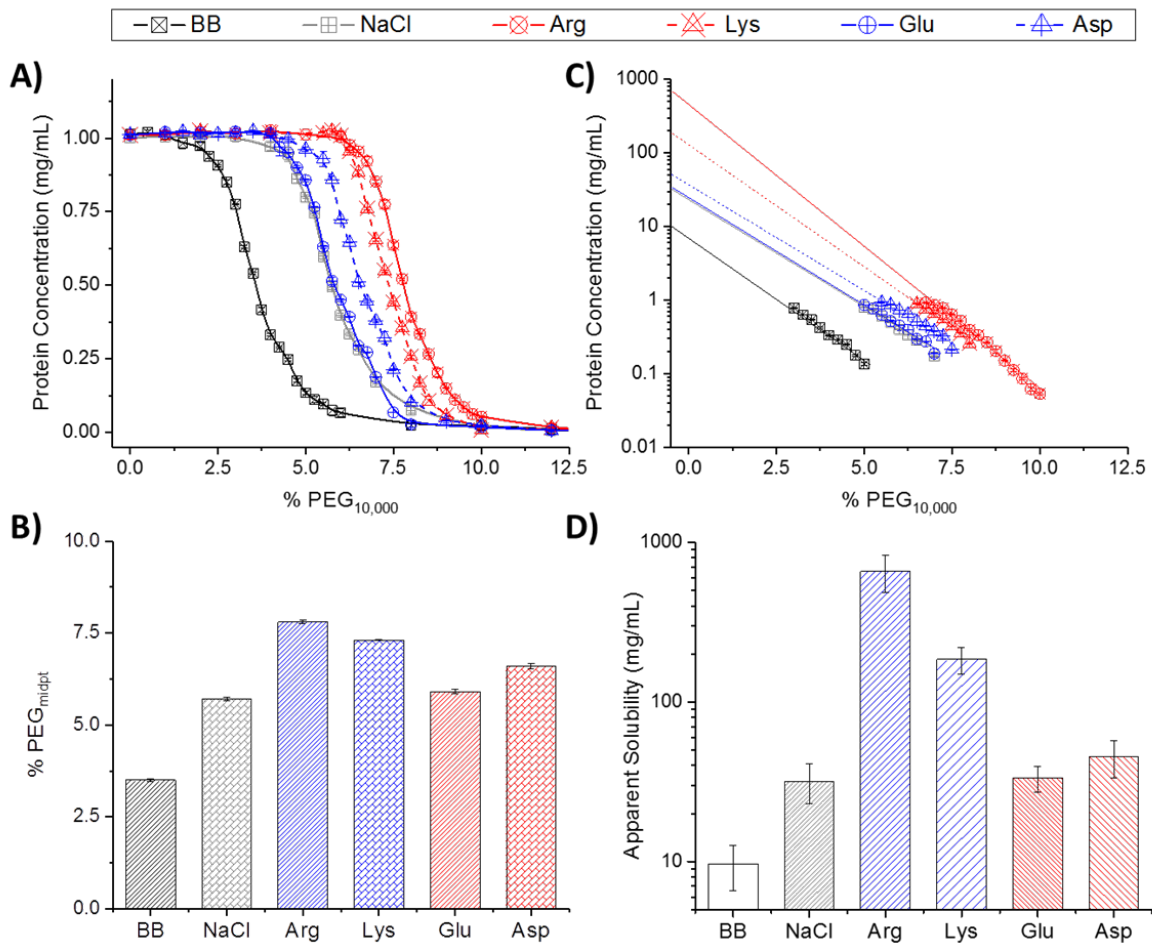
**Figure 2.2.** Turbidity values of mAb-J solutions as a function of both protein and excipient concentrations. Turbidity was calculated from a linear standard curve in Supplemental Figure S1 based on the relationship between O.D.<sub>500nm</sub> and turbidity. Blue bars indicate the turbidity of mAb-J solution in the presence of (A) NaCl, (B) Arg, (C) Lys, (D) Glu, and (E) Asp, while the original measured O.D.<sub>500nm</sub> values are shown in black circle symbol. All data are presented as mean  $\pm$  standard deviation; n = 3.



**Figure 2.3.** Excipient effects on solution viscosity profile of mAb-J vs. protein concentration at 25°C in the presence (A) NaCl,<sup>1</sup> (B) Arg,<sup>1</sup> (C) Lys, (D) Glu, and (E) Asp. Dynamic viscosity was measured in a range of protein concentrations (from 0 to 60 mg/mL) at indicated excipient concentrations in BB containing 20 mM citrate phosphate with 30 mM NaCl at pH 6.0. The viscosity curves for mAb-J alone and in the presence of NaCl and Arg have been published previously and are shown again here comparison to the other additives.<sup>1</sup> All data are presented as mean  $\pm$  standard deviation;  $n = 3$ .

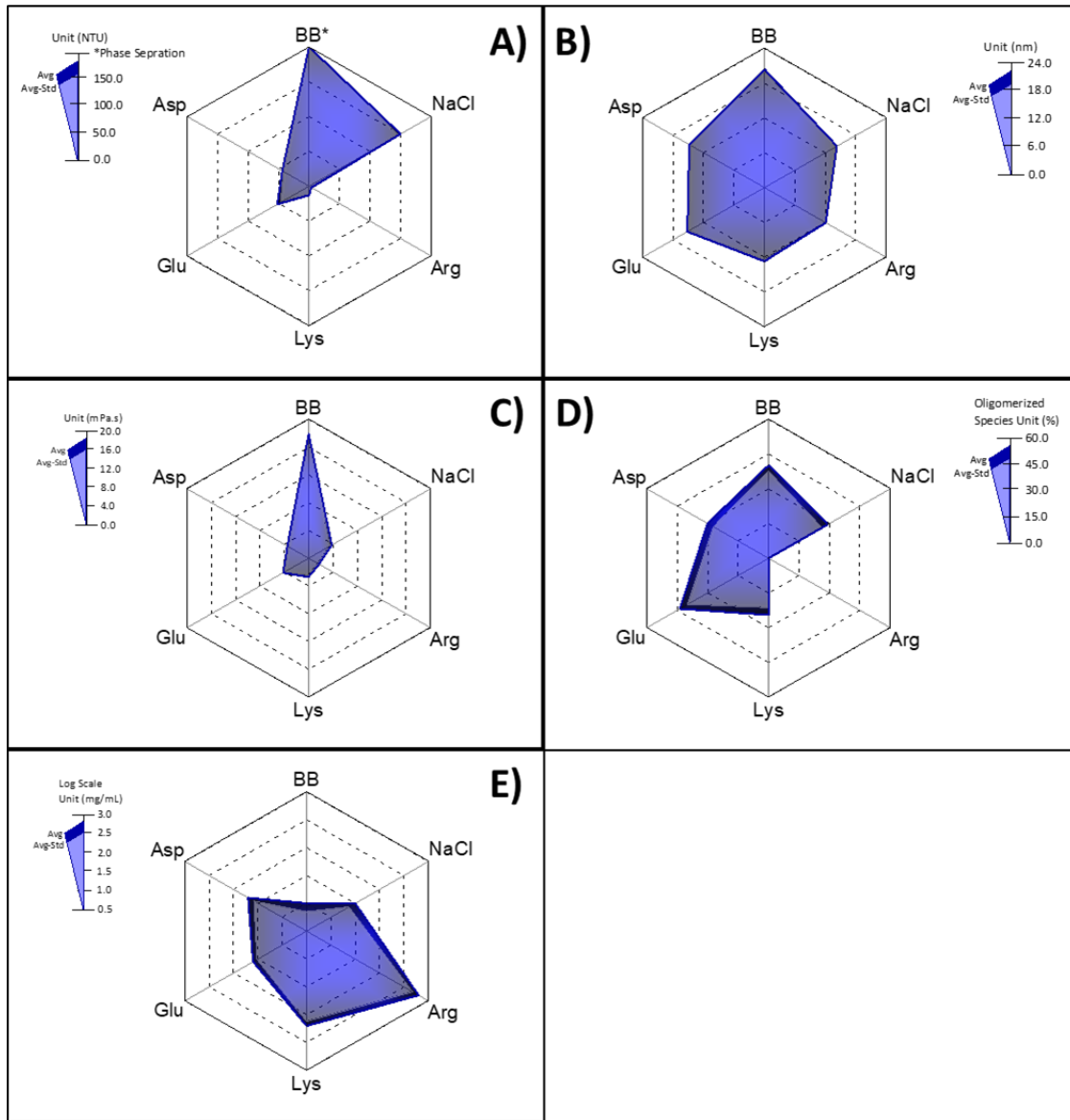


**Figure 2.4.** Excipient effects on self-association of mAb-J as measured and analyzed by static light scattering, showing mole percentage of three mAb-J species (monomer, dimer, and tetramer) in (A) BB,<sup>1</sup> (B) NaCl,<sup>1</sup> (C) Arg,<sup>1</sup> (D) Lys, (E) Glu, and (F) Asp. A concentration of 100 mM was applied for all excipients. Samples of mAb-J were measured by CG-MALS instrument at room temperature. All data are presented as mean  $\pm$  standard deviation;  $n = 3$ .



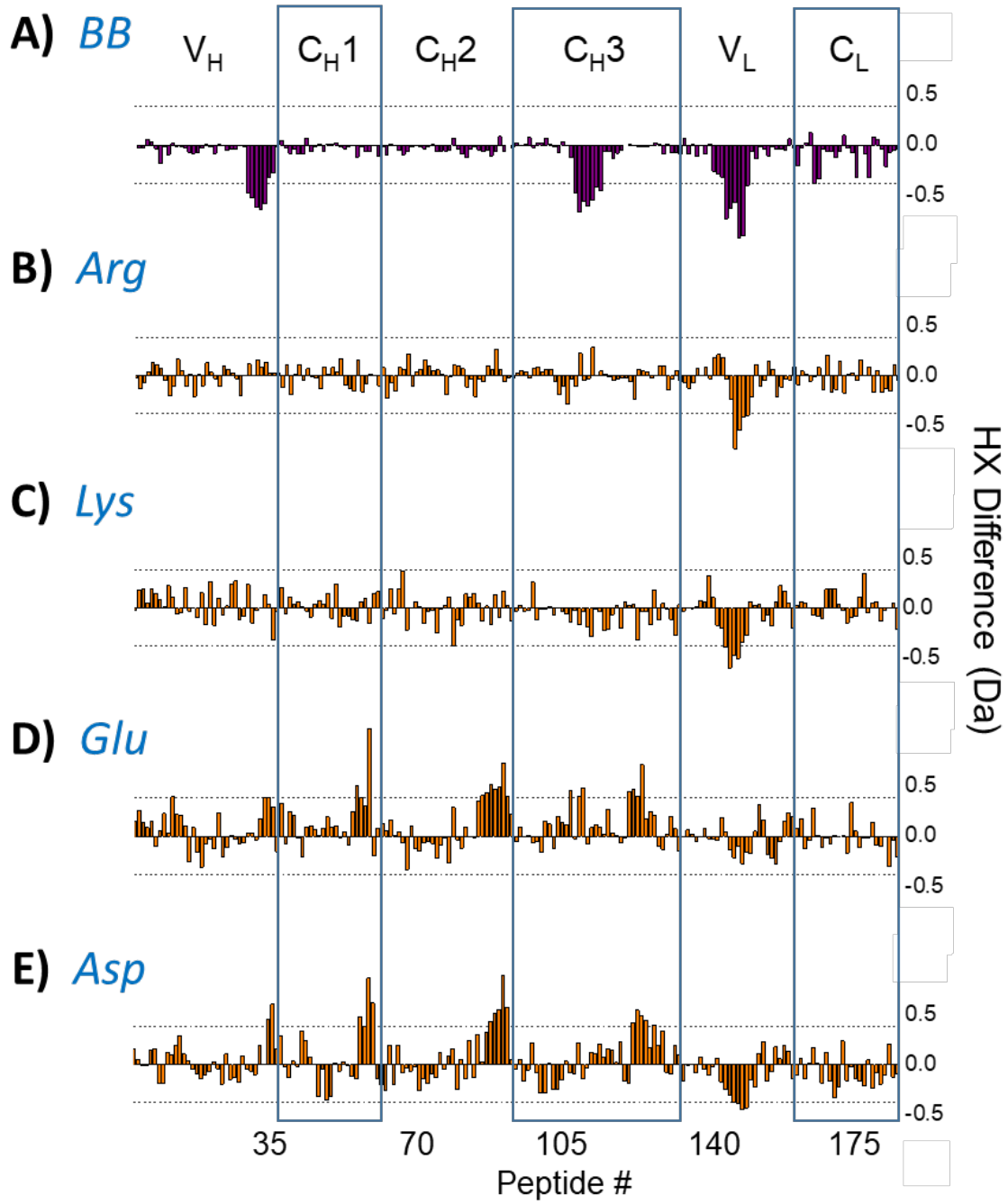
**Figure 2.5.** Relative apparent solubility (thermodynamic activity) of mAb-J as measured by %PEG<sub>10,000</sub> precipitation assay. (A) Change of mAb-J concentration as a function of %PEG<sub>10,000</sub> with and without excipients. (B) %PEG<sub>midpt</sub> values indicate the amount of PEG<sub>10,000</sub> that precipitated half of the total protein out of solution. (C) Apparent solubility values of mAb-J were obtained from Y-axis extrapolation of transition-area data points in each sigmoidal curve of (A). (D) Comparison of mAb-J apparent solubility values in both absence and presence of various excipients. All data are presented as mean  $\pm$  standard deviation; n = 3.

Figure 2.6.



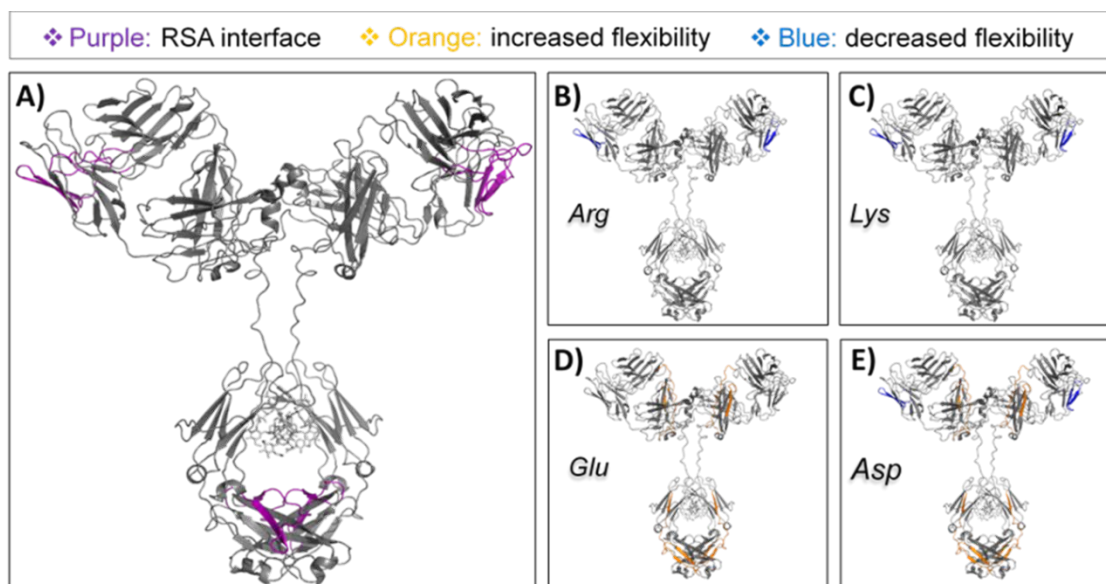
**Figure 2.6.** Radar chart array analysis to evaluate effects of excipient on mAb-J RSA and solution properties summarizing results from Figures 2-5 and from Table 1. Excipients in BB have a concentration of 100 mM. The radar charts indices indicate (A) turbidity at the concentration of 60 mg/mL (The asterisk on BB condition indicates unmeasurable turbidity value due to phase separation), (B) hydrodynamic diameter at 10 mg/mL, (C) viscosity solution at 60 mg/mL, (D) oligomerized mAb-J (%) at 15 mg/mL, and (E) apparent solubility values. The perimeter of the outermost polygon displays the mean morphology parameter; the perimeter of the polygon-labeled “mean - standard deviation” displays the value of mean minus one standard deviation; and the distance between the perimeters of the two polygons (along an axis) is one standard deviation. Triplicate measurements were performed.

Figure 2.7.

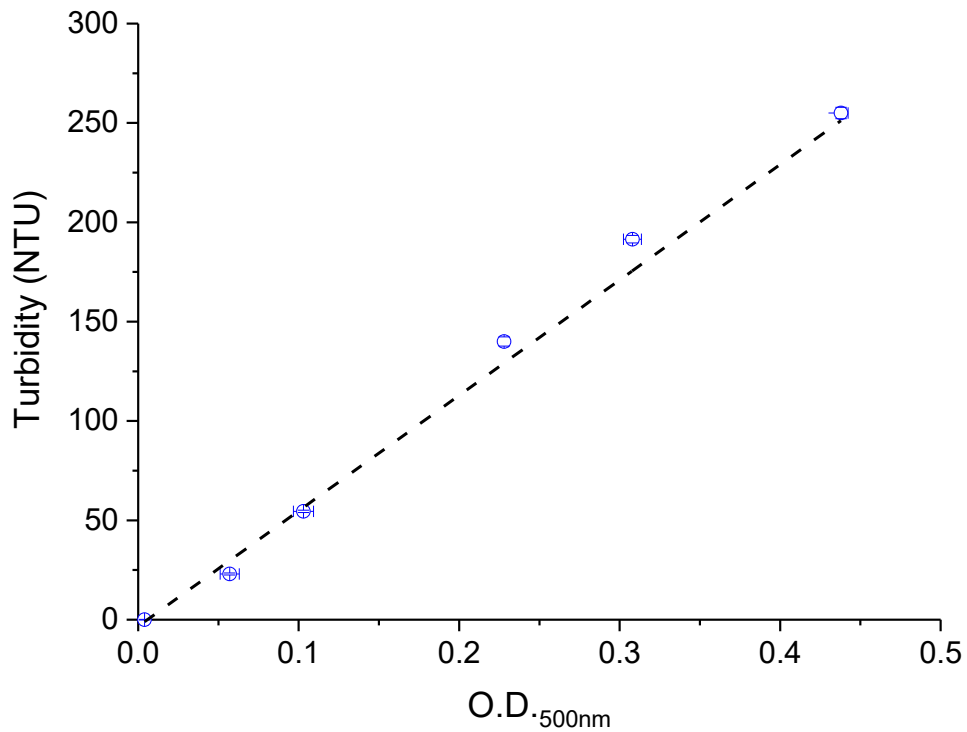




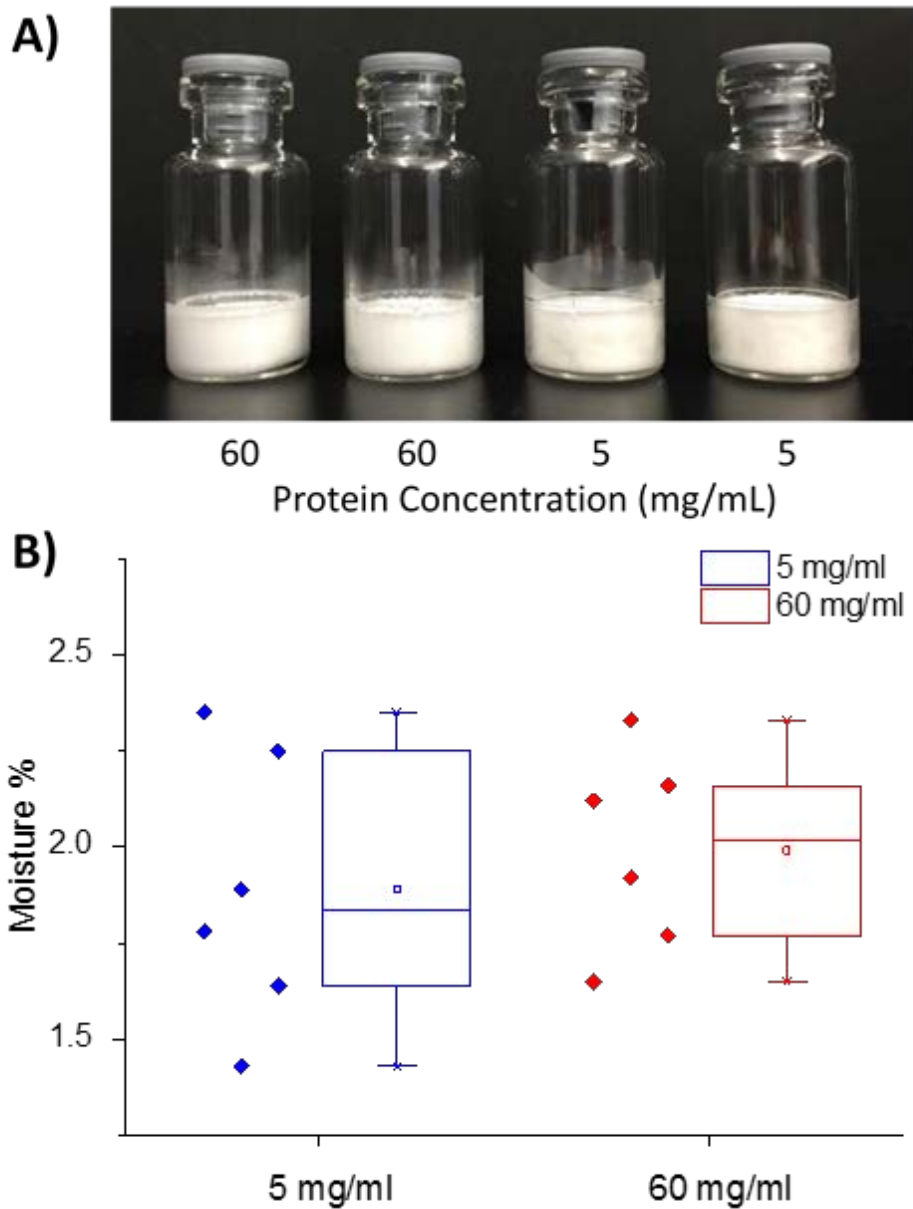
**Figure 2.7.** HX difference plot to show effect of excipients on local region flexibility of mAb-J as measured by HX-MS. (A) shows the mass difference of each peptide between 60 mg/mL and 5 mg/mL of mAb-J concentrations in the absence of excipients, which was obtained by re-analysis of data acquired earlier in our lab using an updated peptide list (see Supplemental Table S2) for comparisons of the excipient disruption effects on the RSA interfaces of mAb-J.<sup>1</sup> Other panels also represent the mass difference between two protein concentrations, but in the presence of 100 mM excipients, including (B) Arg, (C) Lys, (D) Glu, and (E) Asp. Peptides are indexed in order from the N-to-C termini of the heavy chain followed by the light chain of mAb-J (see Supplemental Table S2 for the locations and sequences of the peptides). HX difference in Da is shown along with vertical axis between different solution situations. Positive and negative values imply increased or decreased HX by mAb-J, respectively at 60 mg/mL. The mAb domain boundaries are approximate because several peptides span two domains. The dashed horizontal lines denote the limit for significant HX differences as detailed in the Supplemental Information. Three independent HX measurements was performed.



**Figure 2.8.** Excipient effects on local flexibility of mAb-J as measured by HX-MS plotted on mAb-J homology models. (A) mAb-J RSA interfaces in purple color, which was also published in a previous article.<sup>1</sup> Excipient effect on mAb-J RSA is demonstrated in the following panels, including (B) Arg, (C) Lys, (D) Glu, and (E) Asp. Flexibility change of specific region in the presence of excipients is shown in orange and blue, representing increased and decreased flexibility, respectively. Changes in flexibility of particular peptide segments were derived from the differential exchange data in Figure 7.



**Supplemental Figure 2.1.** Standard curve between nephelometric turbidity (NTU) and O.D.<sub>500nm</sub> values for various high concentration mAb-J solutions (see Figures 1 and 2 of manuscript). Linear regression was performed to fit equation  $y = a + b \cdot x$ , where “a” is equal to -3.4 and “b” is equal to 581.2, with the R-Square value of 0.99. All data are presented as mean  $\pm$  SD; n = 3.



**Supplemental Figure 2.2.** Description of lyophilized cakes of mAb-J. (A) Appearance and (B) moisture determination of lyophilized mAb-J samples at both low and high protein concentrations. Formulation contains 20 mM citrate phosphate with 30 mM NaCl and 10% w/v trehalose at pH 6.0. Moisture data are presented as mean  $\pm$  SD; n = 6.

**Supplemental Table 2.1.** Characterization of pre-lyophilization and post-lyophilization (and reconstitution) samples of mAb-J at low and high protein concentrations using UV-visible spectroscopy and size exclusion chromatography. All data are presented as mean  $\pm$  sample standard deviation; n = 3.

mAb-J	Ultraviolet-Visible Spectroscopy			Size Exclusion Chromatography			
	Protein Conc. (mg/mL)	% Protein Recovery	Slope of O.D. <sub>320-350</sub> nm	% Monomer	% Soluble Aggregates	% Fragments	% Insoluble Aggregates
Pre-Lyo (5 mg/mL)	5.1 $\pm$ 0.0	99.1 $\pm$ 1.0	-1.0E-4 $\pm$ 3.6E-5	99.8 $\pm$ 0.1	0.2 $\pm$ 0.1	0.0 $\pm$ 0.1	0.0 $\pm$ 0.1
Post-Lyo (5 mg/mL)	5.1 $\pm$ 0.1		-6.7E-5 $\pm$ 2.3E-5	98.8 $\pm$ 0.7	0.2 $\pm$ 0.1	0.0 $\pm$ 0.1	1.0 $\pm$ 0.7
Pre-Lyo (60 mg/mL)	59.2 $\pm$ 0.1	98.8 $\pm$ 0.6	-5.8E-5 $\pm$ 2.8E-5	99.7 $\pm$ 0.1	0.3 $\pm$ 0.1	0.0 $\pm$ 0.1	0.0 $\pm$ 0.1
Post-Lyo (60 mg/mL)	58.5 $\pm$ 0.4		-4.0E-5 $\pm$ 3.1E-5	98.4 $\pm$ 0.6	0.3 $\pm$ 0.1	0.0 $\pm$ 0.1	1.3 $\pm$ 0.6

**Supplemental Table 2.2.** Peptide list of mAb-J from pepsin digestion during HX-MS

analysis with their corresponding peptide locations.

Peptide Number	Location	Peptide Number	Location	Peptide Number	Location
1	Heavy 1-10 (VH)	36	Heavy 117-121 (CH1)	71	Heavy 246-255 (CH2)
2	Heavy 1-17 (VH)	37	Heavy 150-159 (CH1)	72	Heavy 246-256 (CH2)
3	Heavy 2-10 (VH)	38	Heavy 160-167 (CH1)	73	Heavy 257-264 (CH2)
4	Heavy 4-10 (VH)	39	Heavy 163-178 (CH1)	74	Heavy 257-265 (CH2)
5	Heavy 11-22 (VH)	40	Heavy 167-178 (CH1)	75	Heavy 266-281 (CH2)
6	Heavy 17-32 (VH)	41	Heavy 168-178 (CH1)	76	Heavy 267-281 (CH2)
7	Heavy 29-35 (VH)	42	Heavy 172-178 (CH1)	77	Heavy 270-281 (CH2)
8	Heavy 30-35 (VH)	43	Heavy 179-183 (CH1)	78	Heavy 282-290 (CH2)
9	Heavy 33-49 (VH)	44	Heavy 184-188 (CH1)	79	Heavy 304-310 (CH2)
10	Heavy 34-49 (VH)	45	Heavy 184-189 (CH1)	80	Heavy 305-309 (CH2)
11	Heavy 35-49 (VH)	46	Heavy 184-197 (CH1)	81	Heavy 305-310 (CH2)
12	Heavy 36-44 (VH)	47	Heavy 184-201 (CH1)	82	Heavy 310-317 (CH2)
13	Heavy 36-49 (VH)	48	Heavy 185-194 (CH1)	83	Heavy 313-323 (CH2)
14	Heavy 37-50 (VH)	49	Heavy 187-201 (CH1)	84	Heavy 317-329 (CH2)
15	Heavy 45-49 (VH)	50	Heavy 188-201 (CH1)	85	Heavy 320-324 (CH2)
16	Heavy 47-50 (VH)	51	Heavy 189-197 (CH1)	86	Heavy 328-338 (CH2)
17	Heavy 48-50 (VH)	52	Heavy 189-201 (CH1)	87	Heavy 329-335 (CH2)
18	Heavy 50-58 (VH)	53	Heavy 189-203 (CH1)	88	Heavy 338-352 (CH2)
19	Heavy 50-60 (VH)	54	Heavy 190-201 (CH1)	89	Heavy 340-352 (CH2)
20	Heavy 51-59 (VH)	55	Heavy 190-202 (CH1)	90	Heavy 353-362 (CH2)
21	Heavy 60-66 (VH)	56	Heavy 201-212 (CH1)	91	Heavy 353-368 (CH2)
22	Heavy 71-79 (VH)	57	Heavy 202-213 (CH1)	92	Heavy 353-369 (CH2)
23	Heavy 71-80 (VH)	58	Heavy 203-217 (CH1)	93	Heavy 361-369 (CH2)
24	Heavy 81-86 (VH)	59	Heavy 203-219 (CH1)	94	Heavy 363-369 (CH2)
25	Heavy 82-86 (VH)	60	Heavy 204-210 (CH1)	95	Heavy 363-370 (CH2)
26	Heavy 84-91 (VH)	61	Heavy 208-216 (CH2)	96	Heavy 370-372 (CH2)
27	Heavy 84-92 (VH)	62	Heavy 229-245 (CH2)	97	Heavy 370-384 (CH2)
28	Heavy 87-93 (VH)	63	Heavy 231-240 (CH2)	98	Heavy 372-380 (CH3)
29	Heavy 92-108 (VH)	64	Heavy 231-242 (CH2)	99	Heavy 373-380 (CH3)
30	Heavy 97-111 (VH)	65	Heavy 235-238 (CH2)	100	Heavy 373-382 (CH3)
31	Heavy 101-116 (VH)	66	Heavy 239-244 (CH2)	101	Heavy 373-384 (CH3)
32	Heavy 104-116 (VH)	67	Heavy 239-246 (CH2)	102	Heavy 381-383 (CH3)
33	Heavy 109-116 (VH)	68	Heavy 239-245 (CH2)	103	Heavy 381-384 (CH3)
34	Heavy 110-116 (VH)	69	Heavy 245-255 (CH2)	104	Heavy 381-394 (CH3)
35	Heavy 111-116 (VH)	70	Heavy 245-256 (CH2)	105	Heavy 381-402 (CH3)

106	Heavy 383-402 (CH3)	132	Heavy 489-499 (CH3)	158	Light 580-588 (CL)
107	Heavy 384-402 (CH3)	133	Heavy 489-500 (CH3)	159	Light 580-590 (CL)
108	Heavy 385-394 (CH3)	134	Heavy 489-501 (CH3)	160	Light 581-588 (CL)
109	Heavy 385-402 (CH3)	135	Light 489-505 (VL)	161	Light 582-588 (CL)
110	Heavy 385-408 (CH3)	136	Light 500-505 (VL)	162	Light 584-590 (CL)
111	Heavy 395-402 (CH3)	137	Light 500-526 (VL)	163	Light 589-591 (CL)
112	Heavy 396-402 (CH3)	138	Light 502-526 (VL)	164	Light 589-601 (CL)
113	Heavy 403-408 (CH3)	139	Light 516-526 (VL)	165	Light 592-595 (CL)
114	Heavy 408-410 (CH3)	140	Light 526-531 (VL)	166	Light 592-601 (CL)
115	Heavy 409-414 (CH3)	141	Light 526-533 (VL)	167	Light 592-603 (CL)
116	Heavy 410-413 (CH3)	142	Light 527-531 (VL)	168	Light 594-601 (CL)
117	Heavy 410-414 (CH3)	143	Light 527-532 (VL)	169	Light 595-601 (CL)
118	Heavy 411-414 (CH3)	144	Light 527-533 (VL)	170	Light 614-633 (CL)
119	Heavy 415-426 (CH3)	145	Light 527-534 (VL)	171	Light 617-633 (CL)
120	Heavy 415-427 (CH3)	146	Light 527-535 (VL)	172	Light 634-640 (CL)
121	Heavy 428-450 (CH3)	147	Light 527-538 (VL)	173	Light 634-641 (CL)
122	Heavy 430-450 (CH3)	148	Light 527-539 (VL)	174	Light 634-650 (CL)
123	Heavy 433-451 (CH3)	149	Light 534-539 (VL)	175	Light 635-640 (CL)
124	Heavy 437-450 (CH3)	150	Light 539-543 (VL)	176	Light 641-650 (CL)
125	Heavy 445-450 (CH3)	151	Light 544-559 (VL)	177	Light 650-659 (CL)
126	Heavy 456-484 (CH3)	152	Light 550-559 (VL)	178	Light 658-666 (CL)
127	Heavy 474-488 (CH3)	153	Light 560-572 (VL)	179	Light 658-667 (CL)
128	Heavy 484-488 (CH3)	154	Light 560-573 (VL)	180	Light 658-668 (CL)
129	Heavy 484-499 (CH3)	155	Light 560-579 (VL)	181	Light 660-666 (CL)
130	Heavy 485-488 (CH3)	156	Light 560-581 (VL)	182	Light 660-668 (CL)
131	Heavy 485-501 (CH3)	157	Light 579-581 (VL)		

1. Arora J, Hu Y, Esfandiary R, Sathish HA, Bishop SM, Joshi SB, Middaugh CR, Volkin DB, Weis DD 2016. Charge-mediated Fab-Fc interactions in an IgG1 antibody induce reversible self-association, cluster formation, and elevated viscosity. *MAbs* 8(8):1561-1574.

## **Chapter 3**

Characterization of Excipient Effects on Reversible Self-association, Backbone Flexibility, and Solution Properties of an IgG1 Monoclonal Antibody at High Concentrations: Part 2



### 3.1. Introduction

Monoclonal antibodies (mAbs) are parenterally administered to patients as biotherapeutic drugs primarily by intravenous (IV) or subcutaneous (SC) injection.<sup>1</sup> The latter route offers the potential of reducing costs, saving time, and increasing patient compliance by having patients self-administer.<sup>1,2,25</sup> As outlined in detail in the Part 1 companion paper,<sup>3</sup> successful formulation of mAbs as high concentration protein dosage forms is a challenge in terms of both protein instability (e.g., aggregation and reversible self-association) and pharmaceutical solution properties (e.g., high viscosity).

One of the challenges of formulating mAbs at high concentrations is caused by reversible self-association (RSA), a phenomenon in which native proteins undergo specific, non-covalent, concentration- and temperature- dependent, reversible protein-protein interactions (PPIs).<sup>1,4-11</sup> Formation of intermolecular protein complexes by RSA can dramatically increase solution viscosity, resulting in pharmaceutical development challenges including high pressure during processing (e.g., sterile filtration) and clinical administration (injection via syringe).<sup>12</sup> In addition, aggregation nuclei might form, potentially leading to the creation of aggregates of varying size (i.e., small soluble aggregates, subvisible particles and larger visible particulates). Such aggregates might not only reduce antibody therapeutic potency, but could also potentially generate unwanted immune responses.<sup>13,14</sup> Moreover, high opalescence and even phase separation can occur in high concentration mAb solutions.<sup>5,6</sup> For patients, injection of

highly viscous or turbid mAb solutions should be avoided due to potential pain on injection and an inability to view the solution for the presence of particulates.<sup>2</sup> Based on these considerations, various strategies to mitigate RSA in high concentration mAb solutions are often required.

The two major approaches taken to reduce RSA in mAb candidates during their development are point mutations through protein engineering<sup>15-17</sup> and formulation development including the addition of excipients.<sup>18,19</sup> Both strategies are mAb-specific and require systematic work for each individual mAb. For example, protein engineering approaches require site-specific information in the regions that initiate mAb-mAb interactions. Although point mutations can work well to reduce RSA, the binding affinity between the mAb and its antigen can potentially also be altered (i.e., increased or decreased), and the physicochemical stability profile of the mAb can also be affected. In addition, it is usually too late for a mAb molecule to be re-engineered once it enters clinical development since it will likely be considered a new molecular entity. Alternatively, formulation approaches focus on optimizing the environment around mAb molecules, rather than altering the mAb molecule itself. Although additives can be identified that reduce RSA, their effect(s) on mAb stability (i.e., conformational, colloidal and chemical degradation pathways) and relative solubility in solution must be evaluated.

The companion paper in this issue describes an IgG1 mAb referred to as mAb-J, which finds electrostatic interactions to be the dominant force that drives RSA. This work

(part two) examines the effect of a series of additives on the RSA of a different human monoclonal IgG1 (mAb-C) that has been previously shown to undergo RSA by an apolar mechanism. As reported previously, high solution viscosity was observed for mAb-C at relatively high protein concentrations, and potential PPI sites on mAb-C as well as potential dominant interaction forces were identified,<sup>20,21</sup> as being increasingly driven by specific hydrophobic interactions as the solution pH increased from 6 to 8 (approaching the mAb-C isoelectric point (pI) range of 9.1–9.4).<sup>22</sup> Using HX-MS differential analysis of high vs. low concentrations of mAb-C at pH 7.0, it was demonstrated that Fab-Fab interactions, including specific CDR regions, rich in hydrophobic and aromatic amino acid residues, plays a crucial role in the RSA of mAb-C.<sup>22</sup>

It has also been demonstrated that point mutation of specific hydrophobic amino acid residues in the mAb-C RSA regions manifested improved solution properties (reduced extent of PPIs).<sup>15</sup> Concomitantly, however, antigen binding affinity of mAb-C decreased significantly (by ~200-400 fold).<sup>15</sup> Therefore, modulating mAb-C RSA by employing different additives (i.e., evaluating and better understanding the effect of these additives) at high protein concentrations was the major goal of this work. We therefore evaluated both solution and molecular behavior as well as backbone flexibility alterations of mAb-C at various protein concentrations in the absence/ presence of five additives known to affect protein hydrophobic interactions to varying extents.

Based on previous work showing that certain regions within specific CDRs in mAb-C (containing many hydrophobic and aromatic amino acid residues) were the dominant sites of interaction for mAb-C RSA,<sup>20</sup> we selected a series of additives to compare their RSA-disrupting properties including a chaotropic salt (guanidine hydrochloride, GdnHCl), a hydrophobic salt (trimethylphenylammonium iodide, TMPAI), an aromatic amino acid derivative (tryptophan amide hydrochloride, TrpNH<sub>2</sub>HCl), a kosmotropic salt (sodium sulfate, Na<sub>2</sub>SO<sub>4</sub>), and a less polar solvent (ethanol). A variety of biophysical techniques were employed to examine mAb-C solution properties as well as protein molecular behavior in the presence of the excipients. Hydrogen exchange-mass spectrometry (HX-MS) was also used to better understand the effect of these additives on particular regions of mAb-C known to be involved in the RSA of mAb-C.

## **3.2. Materials and Methods**

### **3.2.1. Materials**

MedImmune LLC (Gaithersburg, MD) provided a highly purified IgG1 antibody (mAb-C) in a stock solution at 10 mg/mL. A base buffer (BB) solution, selected as the baseline condition to examine mAb-C reversible self-association (RSA), contained 40 mM potassium phosphate at pH 7.5. The stock solution of mAb-C was first concentrated to 70 mg/mL and then buffer exchanged into the desired BB solution (with and without various additives). Dialysis was performed using 3.5 kDa molecular weight cutoff membranes

(Slide-A-Lyzer, Thermo Scientific, Rockford, IL) at 4 °C overnight against BB or BB with various additives (including 0.5 M guanidine hydrochloride (GdnHCl); 150 mM sodium sulfate (Na<sub>2</sub>SO<sub>4</sub>); 150 mM trimethylphenylammonium iodide (TMPAI); 150 mM tryptophan amide hydrochloride (TrpNH<sub>2</sub>HCl), 150 mM phenylalanine amide hydrochloride (PheNH<sub>2</sub>HCl), and 15% ethanol). Different excipient concentrations were used based on their relative hydrophobicity. For example, TMPAI, TrpNH<sub>2</sub>HCl, PheNH<sub>2</sub>HCl and Na<sub>2</sub>SO<sub>4</sub> were examined at a concentration of 150 mM due to these molecules possessing aromatic groups and/or displaying salting-out effects at higher concentrations. Because of lack of these properties, elevated amounts of GdnHCl were used (0.5 M). Finally, as a co-solvent, 15% v/v ethanol was used, and even at this concentration, protein precipitation was noted in some experiments (see Results section). These additives were obtained from Sigma-Aldrich (St. Louis, MO) or Chem-Impex International (“CII”) (Wood Dale, IL).

### 3.2.2. Ultraviolet Absorption Spectroscopy

Protein concentration was measured by ultraviolet absorption spectroscopy ( $A_{280\text{nm}}$ ) obtained by a Nanodrop 2000 spectrophotometer (Thermo Scientific, Rockford, IL) based on the  $E_{1\text{cm}}^{0.1\%}$  value of  $1.54 \text{ mL} \cdot \text{mg}^{-1} \cdot \text{cm}^{-1}$  which was calculated by the following equations.<sup>23</sup>

$$\epsilon (\text{M}^{-1} \cdot \text{cm}^{-1}) = (5500n_W) + (1490n_Y) + (125n_C) \text{ (Eq.1)}$$

$$\varepsilon (\text{mL} \cdot \text{mg}^{-1} \cdot \text{cm}^{-1}) = \frac{\varepsilon (\text{M}^{-1} \cdot \text{cm}^{-1})}{\text{MW} (\text{g} \cdot \text{mol}^{-1})} \text{ (Eq.2)}$$

in which,  $\varepsilon$  is the absorbance extinction coefficient, MW is the molecular weight,  $n_W$ ,  $n_Y$ , and  $n_C$  are the total numbers of tryptophan, tyrosine, and cysteine residues in mAb-C, respectively.

### 3.2.3. Viscosity Measurements

Dynamic viscosity of dialyzed mAb-C sample was measured with and without additives at different protein concentrations, from 5 mg/mL up to 60 mg/mL. An m-VROC viscometer (Rheosence, San Ramon, CA) along with a temperature control system was used for determining mAb-C viscosity at both 4°C and 25°C. The mAb-C sample was injected at a constant flow rate through a sensor chip channel, in which four pressure sensors monitored the pressure drop from the inlet to the outlet.

### 3.2.4. Hydrodynamic Diameter Measurements by Dynamic Light Scattering (DLS)

To measure mAb-C hydrodynamic diameter, a concentration of 10 mg/mL was used with and without additives. A Wyatt DynaPro Plate Reader II dynamic light scattering instrument (Wyatt Technology, Santa Barbara, CA) equipped with a 830 nm laser was utilized to determine the size of mAb-C in different buffer conditions, based on the Stokes-Einstein equation:

$$D_H = \frac{k \cdot T}{3 \cdot \pi \cdot \eta \cdot D_m} \text{ (Eq.3)}$$

in which,  $D_H$  is hydrodynamic diameter,  $k$  is the Boltzmann constant,  $T$  is absolute temperature,  $D_m$  is mutual-diffusion coefficient,  $\pi$  is a mathematical constant, and  $\eta$  is the solution viscosity. A 20  $\mu$ L mAb-C sample was pipetted into the well of a 384-well plate, and triplicate measurements were performed. Viscosity values were obtained separately from a m-VROC viscometer (Rheosence, San Ramon, CA) at 25°C, and automatic viscosity correction was implemented in the operating software for calculating the corrected hydrodynamic diameter.

### 3.2.5. Protein Interaction Parameter ( $k_{D2}$ ) by Dynamic Light Scattering (DLS)

The  $k_{D2}$  parameter was obtained to determine RSA propensity of mAb-C in solution using DLS.<sup>24-28</sup> For solutions containing proteins with high-interaction propensity, the mutual-diffusion coefficient ( $D_m$ ) is concentration-dependent, and proportional to self-diffusion coefficient ( $D_s$ ), as shown in equation 4 below.

$$D_m = D_s(1 + k_D \cdot c) \text{ (Eq.4)}$$

where  $k_D$  is the overall protein interaction parameter, and  $c$  is the protein concentration.

The  $k_D$  expansion equation contains more specific parameters as shown below.

$$k_D = k_{D2} + k_{D3} \cdot c + k_{D4} \cdot c^2 \dots \dots \text{ (Eq.5)}$$

The second, third, fourth... interaction sub-parameters will appear more notable as the protein concentration goes higher and higher. Usually within a certain protein

concentration range, one specific interaction sub-parameter will be dominant, reflecting the major interaction force from PPIs. In this study, a protein concentration range of 1-10 mg/mL mAb was used to determine protein interaction parameter for mAb-C, and according to the experimental results,  $k_{D2}$  was the major factor influencing mAb-C PPIs, so other sub-parameters will be much smaller than  $k_{D2}$ , and didn't contribute significantly to  $k_D$ . Based on the Taylor expansion (Eq.6) and expanded DLS equation (Eq.7), a final equation to determine the  $k_{D2}$  parameter was obtained (Eq.8) as shown below.

$$1 + x + x^2 + x^3 + \dots = \frac{1}{1+x} \text{ (Eq.6)}$$

$$D_m = D_s(1 + k_{D2} \cdot c + k_{D3} \cdot c^2 + k_{D4} \cdot c^3 \dots \dots) \text{ (Eq.7)}$$

$$\frac{1}{D_m} = \frac{1}{D_s} - c \cdot \frac{k_{D2}}{D_s} \text{ (Eq.8)}$$

Therefore, there is a linear relationship between  $1/D_m$  and  $c$ , with  $1/D_s$  as the intercept, and  $k_{D2}/D_s$  as the slope. A negative value of  $k_{D2}$  means attractive interactions between mAb molecules, and a positive value of  $k_{D2}$  shows repulsive interactions. In addition, the larger the absolute value, the stronger protein interactions present in solution.<sup>29-32</sup> The  $k_{D2}$  and  $D_s$  values were obtained in the units of L/kg and  $m^2/s$ , respectively.

### 3.2.6. Composition-Gradient Multi-Angle Light Scattering (CG-MALS)



To identify and quantify various oligomeric mAb-C species in solution, CG-MALS was used, where CG (a dual syringe-pump Calypso sample preparation and delivery unit from Wyatt Technology, Santa Barbara, CA) is a solution pump used to prepare a series of mAb-C solutions at different concentrations, and MALS is a system for detecting static light scattering signals and analysis (at room temperature). For each solution condition with or without additives, samples of two mAb-C (2 and 20 mg/mL) were prepared in a volume of about 5 mL and filtered through a 0.22-micron Millex-GV syringe filter unit (EMD Millipore, Billerica, MA) before loading onto the CG pump system. Different concentrations of mAb-C in a range of 0.2-20 mg/mL were sequentially prepared for analysis. To correlate the scattering signal induced by the protein to its molecular properties, the excess scattering intensity was normalized per unit volume as well as solid angle depending on the incident intensity. Finally, a series of association models were evaluated by fitting light scattering data points at different mAb concentrations by using the Calypso software (Wyatt Technology, Santa Barbara, CA).<sup>33</sup> A data fitting model with Chi<sup>2</sup> ( $\chi^2$ ) testing was used to determine the best association/dissociation model for mAb-C with or without various additives.<sup>33</sup> Data were plotted as each oligomer fraction as a function of mAb-C concentration.

### **3.2.7. PEG-Induced Precipitation Assay**

The relative apparent solubility (thermodynamic activity) values of mAbs can be an important property to monitor, especially when high-protein-concentration mAb solutions need to be manufactured.<sup>34</sup> Samples of mAb-C prepared in base buffer (BB, 40 mM potassium phosphate buffer at pH 7.5) with or without additives were prepared with a stock solution of PEG<sub>10,000</sub> (20% w/v PEG) to obtain a series of PEG solutions (from 0% to 20% w/v PEG). Protein solutions with varying concentrations of %PEG were transferred to a UV-transparent 96-well plate (Greiner Bio-One North America Inc., Monroe, NC) for concentration measurement by  $A_{280\text{nm}}$  values using a spectraMax® M5 Multi-Mode Microplate Reader (Molecular Devices, Inc., Sunnyvale, CA). However,  $A_{280\text{nm}}$  could not be obtained for all solutions including the ones containing TMPAI, TrpNH<sub>2</sub>HCl, or PheNH<sub>2</sub>HCl. For these mAb solutions, alternative methods were utilized for mAb-C concentration determination including a BCA assay kit (Thermo Fisher Scientific, Waltham, MA) or size exclusion chromatography (SEC) (as described below). Standard curves were established for these two methods, shown in Supplemental Figure S1. Determination of mAb-C concentration in the PEG precipitation assay was obtained using the same procedure and calculated via standard curve.

A standard 4-parameter, modified Hill-slope sigmoidal curve equation<sup>35</sup> was used to fit PEG assay data using Origin software.

$$y = b + \frac{t-b}{1+e^{s(\text{mid}-x)}} \text{ (Eq.9)}$$

in which, mid is x-axis midpoint, t is the top plateau, b is the bottom plateau, and s is the slope. Furthermore, by the replotting of the transition-region data points (from fitted sigmoidal curve) into Y axis log scale, the relative apparent solubility can be determined at 0% PEG solution by performing an extrapolation based on the following equation.<sup>36</sup>

$$\text{LogS} = \text{LogS}_0 - \beta \cdot [\text{PEG}] \text{ (Eq.10)}$$

where  $S_0$  is the apparent solubility of mAb-C in PEG-free buffer, S is the observed apparent solubility of mAb-C in PEG-containing buffers, and [PEG] is the concentration of PEG<sub>10,000</sub>.

### **3.2.8. Lyophilization of mAb-C Samples**

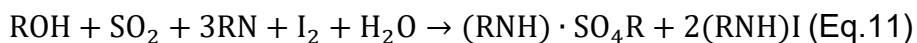
Both 5 mg/mL and 60 mg/mL of mAb-C in 20 mM potassium phosphate buffer at pH 7.5 were prepared with 10% w/v trehalose for lyophilization. FIOLAX<sup>®</sup> clear 1 mL glass vials (Schott North America, Elmsford, NY) were used to hold the mAb-C samples (0.5 mL), and were partially stoppered by 2-leg, 13 mm siliconized rubber stoppers (Wheaton Industries Inc., Millville, NJ). Lyophilization was performed using a LyoStar II lyophilizer (SP Scientific, Warminster, PA) employing a conservative freeze drying cycle over ~3 days as described previously.<sup>20</sup> Cake appearance was determined visually and recorded in photos of the post-lyophilization samples. After filtration with 0.22-micron membrane, reconstituted mAb-C samples were measured to determine their protein concentration using  $A_{280\text{nm}}$  values as described above.

### 3.2.9. Size Exclusion Chromatography (SEC)

A SEC-HPLC system with an inline UV absorbance detector at 214 nm was used to measure species for post-lyophilization mAb-C samples as described in detail elsewhere.<sup>33</sup> Two analytical columns (a 7.8 mm × 30 cm Tosoh TSK-Gel BioAssist G3SWxL and a 6.0 mm x 4 cm guard column [TOSOH Biosciences, King of Prussia, PA]) were utilized to separate varying species. A mobile phase of 200 mM phosphate buffer (pH 6.8) at a flow rate of 0.7 mL/min was used to elute mAb-C samples. Monomer, fragment, and soluble aggregates (e.g., dimer) of post-lyophilization mAb-C samples were determined and then compared to non-lyophilized samples based on peak areas at 5 and 60 mg/mL protein concentrations. The amount of insoluble aggregates were calculated by the difference between the total areas of the SEC chromatograms of the lyophilized and non-lyophilized mAb-C samples.

### 3.2.10. Karl-Fischer Titration

The moisture content of lyophilized mAb-C samples was measured by Coulometric Karl-Fischer (KF) titration following vendor instructions and as described in detail elsewhere.<sup>37</sup> Water content of lyophilized mAb-C freeze-dried cakes was obtained with units of ppm (parts per million). The following is the standard reaction equation (Eq. 11) for the KF reaction to determine water content of samples.



### **3.2.11. Circular Dichroism (CD)**

In order to confirm the native structure of mAb-C after lyophilization, a Chirascan Plus Circular Dichroism Spectrometer (Applied Photophysics Ltd., Leatherhead, UK) was used to determine any secondary structure alterations before and after lyophilization as described in detail elsewhere.<sup>20</sup> Far-ultraviolet (UV) CD spectra of lyophilized and non-lyophilized mAb-C samples (0.2 mg/mL) were collected from 200 nm to 260 nm using 0.1 cm path length quartz cuvettes.

### **3.2.12. Excipients Deuteration**

To provide a low H environment and minimize their effects on hydrogen exchange, each of the additives used in this study were put into pure D<sub>2</sub>O to remove all exchangeable H and replaced by D, except ethanol, which was directly purchased in deuterated form as ethanol-d<sub>6</sub> (Sigma-Aldrich, Inc., St. Louis, MO). Additive-containing D<sub>2</sub>O was dried in a Vacufuge™ vacuum concentrator (Eppendorf, Hauppauge, NY) at 30°C overnight until only excipient crystals remained. After repeating this procedure 3 times, exchangeable H in excipients should be essentially fully replaced by D. Then the excipient crystals were reconstituted in a D<sub>2</sub>O-based 20 mM potassium phosphate buffer at pH 7.5. Finally, D<sub>2</sub>O buffers were re-adjusted with deuterium oxide and/or deuterium chloride to obtain a final solution pH of 7.5, without further correction for the deuterium isotope effect.

### 3.2.13. Hydrogen Exchange-Mass Spectrometry (HX-MS)

Labeling was initiated for both 5 and 60 mg/mL lyophilized mAb-C samples when they were reconstituted with D<sub>2</sub>O-based buffers (containing deuterated excipients). The reconstituted mAb-C samples were centrifuged to remove air bubbles and any potential insoluble aggregates, and then equilibrated at 25°C on an Echotherm chilling/heating plate (Torrey Pines Scientific, Inc., Carlsbad, CA). The labeling reaction was for 3600 sec which was then quenched by a volume ratio of 1 to 9 mixing with a quench buffer (0.5 M tris (2-carboxyethyl) phosphine hydrochloride (TCEP), 4 M guanidine hydrochloride, and 0.2 M sodium phosphate at pH 2.5 pre-equilibrated at 1°C). A LEAP H/DX PAL (LEAP Technologies, Carrboro, NC), with a refrigerated column compartment (containing an immobilized pepsin column, desalting trap column, and C18 column)<sup>20,33</sup>, and an Agilent 1260 infinity series LC (Agilent Technologies, Santa Clara, CA) were used for sample injection, online protein digestion, desalting, peptide concentration and separation. The pepsin column was cleaned by two washes after each injection to minimize peptide carryover,<sup>38</sup> and double gradients with mobile phases composed of water or 90% acetonitrile, both containing 0.1% (v/v) formic acid, were performed to firstly separate peptides and secondly clean the system. From quenching, samples were kept at 1°C to minimize back exchange until introduced into an Agilent 6530 quadrupole-time of flight mass spectrometer (Q-TOF Agilent Technologies, Santa Clara, CA). Peptide ionization

was produced by a standard electrospray ionization source operated in positive mode, and different m/z signals of each peptide were distinguished by a TOF analyzer. More details concerning this hydrogen exchange methodology have been published previously.<sup>33</sup>

#### **3.2.14. HX-MS Data Processing and Analysis**

Pepsin digested peptides were identified by peptide mapping with a mass accuracy range of  $\pm 10$  ppm. Tandem MS with collision induced dissociation on the quadrupole-time of flight mass spectrometer (Agilent 6530 QTOF MS) was applied to confirm identified peptides. HDEaminer software (Sierra Analytics, California) was employed to analyze three replicate sets of HX data. Manual inspection was also performed to minimize bias from the automatic analysis by HDEaminer. Deuterium uptake plots with average deuterium uptake values as well as standard deviations were obtained based on three replicates. The 99<sup>th</sup> percentile of the standard deviations based on triplicate measurements was obtained ( $\pm 0.67$  Da) as the critical criteria in our dataset,<sup>20</sup> indicating a threshold for the significant differences.

#### **3.2.15. Homology Modeling and Protein-Additive Docking**

A mAb-C homology model, built previously to demonstrate potential RSA regions at high protein concentrations,<sup>39</sup> was based on the mAb-C primary sequence, and crystal structures of an isolated Fc and an in-silico generated KOL/Padlan structure of an

Fab.<sup>40,41</sup> The homology model was then prepared, charged, and minimized via a Molecular Operating Environment (MOE 2016 of Chemical Computing Group ULC).<sup>42</sup> The complementarity determining regions (CDRs) of mAb-C were identified by MOE software based on sequence analysis of the variable regions. Hydrophobic patches of 170 Å<sup>2</sup> of solvent-accessible surface area were also identified in MOE. Simple local rigid body docking between mAb-C RSA interfaces and selected excipients were modelled using MOE software based on a combination of energetics and shape complementarity. Docking to model the excipients-mAb interface used 100 runs for each compound and a triangle marcher technique for placement stage, affinity dG for rescoring and forcefield method for refining. Potential docking locations and lowest-energy poses (less than -7 kcal/mol) were demonstrated using a mAb-C homology model.

### **3.3. Results**

#### **3.3.1. Additive Effects on Solution Properties of mAb-C**

The viscosity of mAb-C solutions of increasing protein concentration was measured in base buffer (BB) alone and in the presence of five additives at two temperatures, 4°C and 25°C. As shown in Figure 1, the dynamic viscosity values increased exponentially as a function of protein concentration. For example, values of 12.8 and 3.5 centipoise (Cp) are seen at a protein concentration of 60 mg/mL in BB alone at 4°C and 25°C, respectively. The addition of the different additives to mAb-C solutions



perturbed the solution dynamic viscosity at all temperatures. GdnHCl had the largest effect on reducing the viscosity of mAb-C solutions, showing values of 4.7 and 2.1 Cp at a protein concentration of 60 mg/mL at 4°C and 25°C, respectively. Similarly, both TMPAI and TrpNH<sub>2</sub>HCl also decreased the solution viscosity of mAb-C with TMPAI showing comparatively greater effect. Since solution viscosity is related to PPIs, especially at high mAb-C concentrations, the ability of these three excipients to reduce viscosity is probably due to their RSA-disrupting properties.<sup>2,7,19</sup> Interestingly, Na<sub>2</sub>SO<sub>4</sub> had the opposite effect, resulting in increased mAb-C solution viscosity. For example, at a protein concentration of 60 mg/mL, a viscosity value of 16.5 Cp was observed at 4°C in BB containing Na<sub>2</sub>SO<sub>4</sub> compared to 12.8 Cp in BB alone. Due to varying amounts of precipitation observed with some of the mAb-C solutions at 4°C, dynamic viscosity measurements for mAb-C were not performed in 15% (v/v) ethanol.

### **3.3.2. Additive Effects on Molecular Behavior of mAb-C**

The relative apparent solubility (thermodynamic activity) as determined by PEG<sub>10,000</sub> induced precipitation assay is not only an indicator of PPIs,<sup>43</sup> but also provides a practical rank ordering of excipient effects on relative protein solubility. Sigmoidal curves of mAb-C protein concentration as a function of the amount of %PEG<sub>10,000</sub> were obtained in the absence and presence of additives as shown in Figure 2A. The %PEG<sub>midpt</sub> values (the amount of PEG<sub>10,000</sub> needed to precipitate half of the total protein in solution)

obtained for mAb-C in the presence of each additive are shown in Figure 2b. In BB alone, a %PEG<sub>midpt</sub> value of 4.0% was obtained, while in the presence of the additives, this value changed in different directions and varying magnitudes. For example, GdnHCl, TMPAI, and TrpNH<sub>2</sub>HCl showed increased %PEG<sub>midpt</sub> values of 7.4, 5.8, 5.3% respectively, indicating higher relative solubility of mAb-C in comparison to that in BB. With ethanol, however, the relative solubility of mAb-C decreased showing a %PEG<sub>midpt</sub> value of 2.0%. Moreover, in the presence of Na<sub>2</sub>SO<sub>4</sub>, mAb-C showed higher relative solubility (%PEG<sub>midpt</sub> value of 5.0%) at an excipient concentration of 150 mM, but lower relative solubility (%PEG<sub>midpt</sub> value of 2.5%) in 0.5 M Na<sub>2</sub>SO<sub>4</sub>. Finally, the apparent solubility values in the absence of PEG<sub>10,000</sub> in solution were estimated by extrapolation of the linear portion of data in Figure 2a as plotted in Figure 2c and displayed in Figure 2d. The results are overall consistent with the trend of excipient effects on the relative solubility of mAb-C as reflected by the %PEG<sub>midpt</sub> values.

The effect of these five additives on the average size of mAb-C complexes in solution were determined by dynamic light scattering (DLS) as shown in Figures 3. In general, the hydrodynamic diameter of an antibody molecule is around 9-12 nm.<sup>44</sup> In contrast, DLS measurements showed a hydrodynamic diameter of 22 nm for mAb-C in the base buffer at 10 mg/mL indicating mAb-C molecules are prone to form larger-size complexes. In the presence of GdnHCl, mAb-C showed a diameter value of 12 nm

(consistent with monomer) indicating a disruption of the complexes. Similarly, TMPAI, TrpNH<sub>2</sub>HCl, and ethanol also possessed some ability to reduce mAb-C hydrodynamic diameter by disrupting PPIs, displaying values of approximately 13 nm, 15 nm, and 18 nm, respectively. The addition of Na<sub>2</sub>SO<sub>4</sub> resulted in the opposite effect, increasing the hydrodynamic diameter of mAb-C to 31 nm, a result consistent with Na<sub>2</sub>SO<sub>4</sub> effects on mAb-C solution viscosity (indicating an ability to promote intermolecular interactions among mAb-C molecules). Polydispersity index values between ~10-20% were observed for all samples.

The protein interaction parameter,  $k_{D2}$ , for mAb-C was also measured by DLS in the presence and absence of the five additives. Positive and negative values for  $k_{D2}$  indicate repulsive and attractive interactions between mAb-C molecules, respectively. As shown in Figure 3b, a  $k_{D2}$  value of -81 mL/g was measured for mAb-C in BB, indicating extensive attractive interactions between mAb-C molecules. Values of  $k_{D2}$  of -11, -35, -44, or -50 mL/g in the presence of GdnHCl, TMPAI, TrpNH<sub>2</sub>HCl, or ethanol, respectively, were observed indicating their ability to weaken mAb-C PPIs. Na<sub>2</sub>SO<sub>4</sub> resulted in a  $k_{D2}$  value of -161 mL/g consistent with stronger attractive interactions for mAb-C. In summary, the values of both hydrodynamic diameter and protein interaction parameter ( $k_{D2}$ ) as measured by DLS showed similar trends of excipient effects on RSA of mAb-C.

The size and nature of mAb-C complexes in solution were further examined by static light scattering using CG-MALS as shown in Figure 4. The fraction of each species was calculated based on curve-fitted the scattering signal as a function of protein concentration. For example, as displayed in Figure 4a, the monomeric fraction of mAb-C in the base buffer decreased as protein concentration increased. Concomitantly, multimers of mAb-C including dimer, trimer and hexamer increased. In the presence of 0.5 M GdnHCl, the distribution of species vs protein concentration was dramatically altered. As shown in Figure 4b, >95% of mAb-C remained monomeric across the concentration range examined. In Figure 4c and d, it can be seen that the addition of 0.15M TMPAI and TrpNH<sub>2</sub>HCl reduced the extent of complex formation for mAb-C, but to a lesser extent than GdnHCl, protecting monomeric mAb-C from becoming oligomeric species. In contrast, mAb-C in a 15% ethanol-containing solution showed a similar speciation profile, but comparatively different multimer pattern, compared to BB alone (Figure 4e). Finally, as shown in Figure 4f, a rapid decrease of monomeric mAb-C along with a rapid increase of hexamers were observed in mAb-C solution in the presence of 0.15M Na<sub>2</sub>SO<sub>4</sub> as the mAb-C concentration was increased.

To better compare and visualize these additive effects on mAb-C solution and molecular properties, the preceding results can be displayed as radar charts (Figure 5). Comparative results for dynamic viscosity values (at a protein concentration of 60 mg/mL

at 4°C), apparent solubility values, fraction of monomeric mAb-C from CG-MALS (at 20 mg/mL), and protein interaction  $k_{D2}$  values are displayed in Figure 5a-d, respectively. Each corner of the individual radar chart represents a solution condition (BB, BB with GdnHCl, TMPAI, TrpNH<sub>2</sub>HCl, ethanol, and Na<sub>2</sub>SO<sub>4</sub> clockwise from the top corner). By summarizing the data together, differential effects of the five different additives on mAb-C can be more easily assessed. Three additives show consistent RSA-disruption effects with a ranking order of GdnHCl > TMPAI > TrpNH<sub>2</sub>HCl. In contrast, although ethanol demonstrates an ability to disrupt PPIs of mAb-C, it had detrimental effects on relative solubility. Finally, Na<sub>2</sub>SO<sub>4</sub> consistently shows RSA-promotion effects on mAb-C across the different measurements at high concentrations.

### **3.3.3. Alteration of mAb-C RSA Propensity by Excipients as Measured by HX-MS**

To better understand backbone flexibility alterations of mAb-C in the presence of these five additives at high vs. low protein concentrations, hydrogen exchange-mass spectrometry (HX-MS) was employed. The deuterium environment of mAb-C was provided by a lyophilization-reconstitution method at 5 and 60 mg/mL, as described previously.<sup>20</sup> Briefly, mAb-C was first lyophilized and then reconstituted with excipient-containing D<sub>2</sub>O. To confirm the integrity of lyophilized mAb-C samples, analytical characterization of reconstituted mAb-C was performed, as shown in Supplemental Figure S2 and Supplemental Table S1. As shown by a combination of visual inspection

(acceptable cake integrity), moisture content (0.5-2.0% water by Karl Fischer titration), overall secondary structure (similar CD spectra), and absence of aggregation (~99% protein recovery with 98-99% monomer as determined by UV spectroscopy and SEC analysis, respectively), lyophilized mAb-C samples retained their integrity after lyophilization and reconstitution. Thus these samples are suitable for use in HX-MS analysis.

After reconstitution with D<sub>2</sub>O buffer to trigger mAb-C amide-hydrogen labeling in the presence or absence of the five additives, a 3600 seconds incubation was performed before quenching the HX reaction. Peptides were obtained by immobilized pepsin digestion and analyzed by LC-MS as described in the Supporting Information. A total of 200 peptides were confirmed (see Supplemental Table S2), with 98% and 100% sequence coverage of the heavy chain and light chain, respectively. The mass difference for each peptide was obtained based on 5 and 60 mg/mL protein concentrations, both with and without excipients. A value of 0.67 Da, representing a 99% confidence interval significance criteria for peptide mass differences was used to identify significantly different HX between 60 and 5 mg/mL. As shown in Figure 6, HX differences for each peptide are plotted in the absence and presence of excipients. For panel a,  $\Delta\text{HX} = \text{HX}(\text{BB}, 60 \text{ mg/mL}) - \text{HX}(\text{BB}, 5 \text{ mg/mL})$ ; and for panels b-f:  $\Delta\text{HX} = \text{HX}(\text{BB} + \text{excipient}, 60 \text{ mg/mL}) - \text{HX}(\text{BB} + \text{excipient}, 5 \text{ mg/mL})$ .

Although RSA sites were determined previously for mAb-C at 60 mg/mL at pH 7.0,<sup>20</sup> additional regions of mAb-C might be involved in PPIs at pH 7.5, used here to deliberately increase mAb-C RSA propensity. Five significant protection regions of mAb-C at pH 7.5 were observed, as shown in Figure 6a. As reported previously, the CDR L2 region was the primary RSA site for mAb-C at pH 7.0, where it showed strong protection at high protein concentration.<sup>20</sup> The CDR H2 was also observed to have increased protection at high protein concentrations, especially at shorter labeling times.<sup>20</sup> In this study (Figure 6a), consistent with these previous results, significant protection was observed in the CDR L2 region (sequence Y<sub>504</sub>VASSLQS<sub>511</sub>, peptide 156-161), however HX differences in the CDR H2 region did not exceed the significance limit at the single HX time point examined. Additional regions of mAb-C showed protection at pH 7.5 covering CDR H1 (sequence G<sub>11</sub>YTFTGYMHV<sub>22</sub>, peptide 3-11), the beginning region of C<sub>H1</sub> (sequence V<sub>123</sub>SSASTKGPSVFPLAPSSKSTSGGTAALGCLVKDYFPEPV<sub>163</sub>, peptide 61-69), and the end region of C<sub>H3</sub> (sequence A<sub>439</sub>LHNHYTQKSLSLSPG<sub>454</sub>, peptide 140-145), and CDR L3 (sequence F<sub>538</sub>ATYYCQQANSFPWT<sub>552</sub>, peptide 171-176), indicating extensive, multi-region intermolecular interactions.

Different additives were examined for their ability to either promote or disrupt regions of RSA within mAb-C. Consistent with the biophysical results, the most efficient solute in terms of disrupting RSA interaction sites within mAb-C was GdnHCl (Figure 6b)

where essentially all of the RSA sites were diminished except for the one located in the C<sub>H3</sub> region. As shown in Figure 6c and d, TMPAI and TrpNH<sub>2</sub>HCl also had the ability to disrupt RSA between mAb-C molecules, especially in the CDR H1, CDR H2, CDR L2, and CDR L3 regions, although some weak protection still exists. For other regions of RSA, however, these two additives did not affect mAb-C RSA-induced protection. As for ethanol effects (Figure 6e), only the RSA regions on the light chain variable regions of mAb-C were disrupted, and little effect was seen on the other RSA sites. In contrast, as shown in Figure 6f, Na<sub>2</sub>SO<sub>4</sub> promoted protection during deuterium exchange of mAb-C, especially within the RSA regions.

To better visualize these specific RSA regions on mAb-C at pH 7.5, the HX-defined RSA interface is shown mapped onto a mAb-C homology model shown in Figure 7. Molecular modeling using MOE software (see Methods section) was utilized to examine additive binding as shown in Figure 8. The colored structures highlight the CDR regions while the remaining regions of the mAb are shown in white. The RSA interaction sites, based on HX-MS results, are highlighted in the space-filling representation as shown on the left-side panel in Figure 7. This shows that the variable regions of both the heavy and light chains are primarily responsible for mAb-C RSA, with a small hydrophobic site at the end of C<sub>H3</sub> domain also contributing to RSA. As an additional analysis, hydrophobic patches, shown in green areas on the right-side panel homology model in Figure 7 were



identified in the homology model. Interestingly, some of the top-ranked hydrophobic patches (greater than 200 Å<sup>2</sup> solvent-accessible surface area) overlap with the RSA sites. Modeling based on local rigid docking was then performed at the major RSA sites in the CDR regions of both heavy and light chains of mAb-C with three of the additives, GdnH<sup>+</sup>, TMPA<sup>+</sup>, and TrpNH<sub>2</sub>H<sup>+</sup>. Interactions stronger than -7 kcal/mol are shown on the Fab homology model of mAb-C in Figure 8. Five locations were found for GdnH<sup>+</sup> to interact with these mAb-C CDR regions, while only three locations were detected for TMPA<sup>+</sup> and TrpNH<sub>2</sub>H<sup>+</sup>.

### **3.4. Discussion**

Although protein engineering approaches have been shown in some cases to mitigate mAb intermolecular protein-protein interactions (and thus optimizing solution properties at high mAb concentrations),<sup>15,16,45,46</sup> a more straight-forward strategy (that does alter the molecule itself) is excipient addition to improve the solution properties of mAbs at high concentrations. This can be pursued by either an excipient screening approach to semi-empirically identify stabilizers,<sup>47</sup> or by a more rational additive selection process based on a mechanistic understanding of RSA interactions for a particular mAb (as outlined in the companion paper in this issue with mAb-J). In this work, we continue to examine the latter, more targeted approach to excipient selection by using HX-MS to

identify regions of mAb-C (and associated molecular mechanisms) resulting in a more rational selection of additives to disrupt specific RSA interactions within a mAb.

As reported previously, a major RSA site on mAb-C was CDR L2 at pH 7.0. This involved regions containing hydrophobic and aromatic amino acid residues that appeared to result in protein-protein interactions among mAb-C molecules.<sup>20</sup> In this work, as we increased solution pH from 7.0 to 7.5, not only the CDR L2 region, but additional regions within mAb-C showed protection from deuterium exchange when comparing high vs. low protein concentrations by HX-MS (Figure 6). This indicates more PPI sites mediated in RSA of mAb-C under these conditions. Since mAb-C has an isoelectric point (pI) ranging from 9.1-9.4 (data not shown), the protein will have less net positive charge, and thus weaker charge repulsion, presumably allowing mAb-C molecules to more easily self-associate at pH 7.5 (vs. pH 7.0). Computational mapping of hydrophobic patches on mAb-C, as shown in Figure 7, is in general agreement with the protected surfaces identified by HX-MS, consistent with apolar interactions being a major force that drives mAb-C RSA. It is quite possible, however, that additional cross-interactions (e.g., Fab-Fab, Fab-Fc) sites between mAb-C molecules under these conditions (base buffer at pH 7.5) form leading to additional interaction networks.<sup>18,20,33,48,49</sup> Hydrophobic interactions between mAb-C molecules at high protein concentrations are probably not the only source that induce PPIs. Other weak intermolecular forces, such as dipole-dipole coupling, hydrogen

bonding, or even electrostatic interactions, could also contribute to mAb-C RSA to some extent.<sup>20</sup>

Similar to the HX-MS analysis described in the companion paper with mAb-J, potential chemical exchange rate differences in mAb-C formulated with the various additives prevent direct comparisons between HX kinetics in the different formulations.<sup>50</sup> Thus, we focused on HX difference between high and low protein concentrations of mAb-C in the presence of each additive separately. PPIs of mAb-C in base buffer were not only observed at the high concentration (60 mg/mL), but also detected, albeit to a much lower extent, at the low protein concentration (5 mg/mL). For example, this was seen by CG-MALS analysis examining the size distribution of mAb-C at ~1-20 mg/mL. HX-MS analysis was primarily based on the difference of RSA extent between high and low protein concentrations. Thus, we are comparing conditions with more vs less RSA rather than complete vs no RSA. Such HX-MS analysis shows that several specific regions of mAb-C undergo PPI resulting in protection of these regions from hydrogen exchange (Figure 6a).

#### **3.4.1. Effects of Hydrophobic (TMPAI and TrpNH<sub>2</sub>HCl) and Chaotropic (GdnHCl) Salts on RSA of mAb-C**

In the presence of the additives either with hydrophobic apolar character, including TMPAI (I<sup>-</sup> is also a stronger chaotrope than Cl<sup>-</sup>) and TrpNH<sub>2</sub>HCl (both at 0.15M), or with

properties attributed to chaotropes, including GdnHCl (at 0.5M), HX-MS analysis shows several RSA regions within mAb-C had diminished protection from hydrogen exchange, especially at CDR H1, CDR H2, CDR L2, and CDR L3 (Figure 6b-d). Beyond the CDRs, there were a few additional regions of mAb-C that show protection at high concentration. For example, the end of C<sub>H</sub>3 region in the presence of GdnHCl, and both the beginning of C<sub>H</sub>1 and the end of C<sub>H</sub>3 in the presence of TMPAI and TrpNH<sub>2</sub>HCl manifest protection. Such phenomena probably indicates that these three excipients could dissociate higher-order oligomeric mAb-C complexes to smaller dimeric or trimeric forms (consistent with CG-MALS studies). Thus, the remaining interactions at C<sub>H</sub>1 and/or C<sub>H</sub>3 regions are possibly a signature of difference between dimeric/trimeric complexes of mAb-C.

Combining these HX-MS results with the biophysical and solution measurements, it can be seen that GdnHCl, TMPAI, and TrpNH<sub>2</sub>HCl all displayed an ability to disrupt RSA interactions within mAb-C with a rank ordering of effectiveness of GdnHCl > TMPAI > TrpNH<sub>2</sub>HCl. Presumably, the major effects of these additives are mediated by the cations: GdnH<sup>+</sup>, TMPA<sup>+</sup>, and TrpNH<sub>3</sub><sup>+</sup>. Several types of protein-excipient interactions (hydrogen bonding, preferential hydration, electrostatic interactions, dispersive interactions, cation- $\pi$  interactions) could each effectively disrupt the PPIs within proteins.<sup>51,52</sup> Although TMPAI and TrpNH<sub>2</sub>HCl have the potential for  $\pi$ - $\pi$  interactions (via their aromatic rings interacting with aromatic rings in amino acid residues in mAb-C), GdnHCl, as a chaotropic

salt,<sup>53</sup> was more effective in terms of diminishing PPIs for mAb-C.<sup>54</sup> Preferential interactions of GdnHCl with mAb-C might more effectively compete PPIs.<sup>52</sup> However, comparisons are complicated because I<sup>-</sup> from TMPAI is a stronger chaotrope than Cl<sup>-</sup>.<sup>55</sup> Therefore, albeit similar properties exist between cations of TMPAI and TrpNH<sub>2</sub>HCl, the anions of these two additives, including I<sup>-</sup> and Cl<sup>-</sup>, may play roles that differentiate their RSA-disrupting efficiency.<sup>56,57</sup> Furthermore, the size of the cations may also be a determining factor since their rank order by size is GdnH<sup>+</sup><TMPA<sup>+</sup><TrpNH<sub>2</sub>H<sup>+</sup> which reverses the rank order of their effectiveness in disrupting RSA. Therefore, steric hindrance might decrease the tendency for larger excipients to interact with the surface of mAb-C; it may be easier for smaller excipients to access shallow pockets on the mAb-C surface. Consistent with this hypothesis, we found in protein-excipient docking analysis that there were more potential interaction sites for GdnH<sup>+</sup> than for the other two excipients (Figure 7). Although GdnHCl showed greater ability to disrupt PPIs compared to the other two hydrophobic salts, the concentration used in this study was higher, and guanidine decreased the conformational stability of mAb-C, as indicated by lower thermal melting temperature values (data not shown).

### **3.4.2. Effects of Ethanol on RSA of mAb-C**

In the case of the HX-MS results for mAb-C in the presence of 15% ethanol, several unique trends were observed. For example, many of the RSA regions within mAb-

C were retained, except for the CDR L2 and CDR L3 regions, thus resulting in either a diminished RSA of mAb-C at 60 mg/mL or promotion of RSA at 5 mg/ml, but to a lesser extent than observed in the presence of either GdnHCl, TPAI, and TrpNH<sub>2</sub>HCl, or Na<sub>2</sub>SO<sub>4</sub>, respectively. In comparison to mAb-C in BB alone, there was also one region (middle of C<sub>L1</sub>) that shows increased protection at high protein concentration in the presence of ethanol (Figure 6e).

Ethanol, as a less polar solvent, was used to determine its effects on mAb-C PPIs. As shown in Figures 2, 3, 4 and 6, the results of relative solubility, DLS, CG-MALS and HX-MS demonstrated a contradictory trend on the extent of RSA for mAb-C in the presence of ethanol. Moreover, the conformation of mAb-C was also easily perturbed as a function of temperature with ethanol in solution (data not shown). It has been broadly reported that ethanol could alter both intramolecular and intermolecular interactions by preferentially interacting with hydrophobic residues,<sup>58-60</sup> but it also, depending on the temperature, decreases protein solubility to different extents.<sup>60-63</sup> In fact, due to lower protein solubility in ethanol,<sup>64,65</sup> the addition of ethanol led to the precipitation of mAb-C in high concentration solutions during viscosity measurements especially at lower temperatures. Finally, addition of ethanol could alter original solution hydrogen bonding networks, surface tension, and density, which may further perturb the molecular behavior of mAb-C.<sup>66,67</sup> As a result, multiple effects of ethanol on mAb-C created diverse

observations based on different biophysical or HX techniques, requiring more systemic studies to better understand its complicated effects on mAb-C.

### **3.4.3. Effects of Na<sub>2</sub>SO<sub>4</sub> on RSA of mAb-C**

In the presence of 0.15M Na<sub>2</sub>SO<sub>4</sub>, elevated levels of PPIs within mAb-C were detected by HX-MS, showing overall an even more extensive extent of protection within the mAb-C RSA regions (Figure 6f). Na<sub>2</sub>SO<sub>4</sub> was the only additive examined in this work that promoted mAb-C RSA, as observed in all biophysical and HX analysis. This resulted in relatively higher solution dynamic viscosity as well as a larger hydrodynamic size (and a larger protein interaction parameter) of mAb-C complexes as measured by DLS. As a kosmotropic salt, Na<sub>2</sub>SO<sub>4</sub> is excluded from surfaces of mAb-C molecules, and at the same time increases surface tension of bulk water, which likely contributes to mAb-C molecules forming relatively larger higher-order oligomeric species (as shown in CG-MALS studies in Figure 4).<sup>68,69</sup> In comparison to mAb-C in BB alone, 150 mM of Na<sub>2</sub>SO<sub>4</sub> added to BB shows increased relative solubility of mAb-C, while 0.5 M of Na<sub>2</sub>SO<sub>4</sub> reduced its solubility. At relatively low concentrations (150 mM) of Na<sub>2</sub>SO<sub>4</sub>, salting-in (charge-shielding) effects are probably the dominant factor that increases mAb-C solubility as described by Debye-Huckel theory.<sup>70</sup> Essentially, mAb-C molecules are surrounded by salt counterions, screening their charges, which will decrease the electrostatic free energy of mAb-C molecules and increase solvent activity, and finally

lead to higher relative solubility.<sup>70</sup> At higher salt concentrations (0.5 M), however, salting-out effects begin to dominant as the major influence. Here water molecules are attracted by salt ions, and a decreased number of water molecules interacting with mAb-C, leading to protein dehydration, and thus stronger PPIs among mAb-C molecules and ultimately protein precipitation.<sup>71</sup>

### **3.5. Conclusions**

In this work (Part II) with mAb-C, along with a companion paper (Part I) in this issue with mAb-J, we examined the role of additives and excipients in disrupting and enhancing specific protein-protein interactions that lead to the RSA of two different IgG1 mAbs at high protein concentrations. In this work, the solution properties, molecular features and backbone flexibility (at specific sites known to facilitate RSA) were evaluated for a human monoclonal IgG1 antibody (mAb-C), previously demonstrated to undergo RSA via Fab-Fab interactions (at specific peptide segments within the CDR regions of mAb-C rich in hydrophobic amino acids). These parameters were evaluated in the presence a chaotropic salt (GdnHCl), hydrophobic salt (TMPAI), aromatic amino acid derivative (TrpNH<sub>2</sub>HCl), kosmotropic salt (Na<sub>2</sub>SO<sub>4</sub>), and a less polar solvent (ethanol). The ability of these additives to disrupt RSA and improve the solution properties of mAb-C at high protein concentrations was demonstrated and ranked ordered (GdnHCl > TMPAI > TrpNH<sub>2</sub>HCl). Contradictory results were observed for ethanol probably due to



coexistence of multiple effects of the less polar solvent on mAb-C. Na<sub>2</sub>SO<sub>4</sub>, on the other hand, showed the opposite effect and promoted the RSA of mAb-C and resulted in less desirable solution properties.

In a companion paper (Part I), similar experiments were performed with a different human IgG1 mAb (mAb-J) that displays RSA at high protein concentration primarily through a different molecular mechanism (charge interactions between Fab-FC regions of the antibody).<sup>13</sup> A series of charged excipients were then employed in the companion paper to determine their effects on the solution properties, molecular attributes and backbone flexibility. By examining two different human IgG1 mAbs (mAb-J and mAb-C) that undergo RSA by different molecular mechanisms, these two studies demonstrate a rational approach to the development of high concentration mAb formulations by (1) determining the molecular mechanism of RSA by HX-MS analysis, (2) selecting specific additives expected to disrupt these known intermolecular interactions and rank-order their ability to do so by HX-MS, and then (3) evaluating the effects of these specific additives on the solution properties (e.g., viscosity) and molecular attributes (e.g., size and relative solubility) of the mAb at high protein concentrations.

### 3.6. References

1. Armstrong NJ, Bowen MN, Maa Y-F. 2013. High-concentration monoclonal antibody formulations. ed.: Google Patents.
2. Shire SJ, Shahrokh Z, Liu J 2004. Challenges in the development of high protein concentration formulations. *Journal of pharmaceutical sciences* 93(6):1390-1402.
3. Hu Y, Arora J, Joshi SB, Esfandiary R, Middaugh CR, Weis DD, Volkin DB 2019. Characterization of excipient effects on reversible self-association, flexibility, and solution properties of an IgG1 monoclonal antibody at high concentrations: Part 1 (Companion Manuscript).
4. Liu J, Nguyen MDH, Andya JD, Shire SJ 2005. Reversible Self-Association Increases the Viscosity of a Concentrated Monoclonal Antibody in Aqueous Solution. *Journal of Pharmaceutical Sciences* 94(9):1928-1940.
5. Nishi H, Miyajima M, Nakagami H, Noda M, Uchiyama S, Fukui K 2010. Phase separation of an IgG1 antibody solution under a low ionic strength condition. *Pharmaceutical research* 27(7):1348-1360.
6. Mason BD, Zhang L, Remmele RL, Zhang J 2011. Opalescence of an IgG2 monoclonal antibody solution as it relates to liquid-liquid phase separation. *Journal of pharmaceutical sciences* 100(11):4587-4596.
7. Connolly Brian D, Petry C, Yadav S, Demeule B, Ciaccio N, Moore Jamie M, Shire Steven J, Gokarn Yatin R 2012. Weak Interactions Govern the Viscosity of Concentrated Antibody Solutions: High-Throughput Analysis Using the Diffusion Interaction Parameter. *Biophysical Journal* 103(1):69-78.
8. Lilyestrom WG, Yadav S, Shire SJ, Scherer TM 2013. Monoclonal Antibody Self-Association, Cluster Formation, and Rheology at High Concentrations. *The Journal of Physical Chemistry B* 117(21):6373-6384.
9. Raut AS, Kalonia DS 2015. Liquid-Liquid Phase Separation in a Dual Variable Domain Immunoglobulin Protein Solution: Effect of Formulation Factors and Protein-Protein Interactions. *Molecular pharmaceutics* 12(9):3261-3271.
10. Raut AS, Kalonia DS 2015. Opalescence in Monoclonal Antibody Solutions and Its Correlation with Intermolecular Interactions in Dilute and Concentrated Solutions. *Journal of Pharmaceutical Sciences* 104(4):1263-1274.
11. Baek Y, Zydney ALJCoib 2018. Intermolecular interactions in highly concentrated formulations of recombinant therapeutic proteins. 53:59-64.
12. Saluja A, Badkar AV, Zeng DL, Nema S, Kalonia DS 2006. Application of high-frequency rheology measurements for analyzing protein-protein interactions in high protein concentration solutions using a model monoclonal antibody (IgG2). *J Pharm Sci* 95(9):1967-1983.
13. Roberts CJ 2014. Therapeutic protein aggregation: mechanisms, design, and control. *Trends in Biotechnology* 32(7):372-380.

14. Barnett GV, Drenski M, Razinkov V, Reed WF, Roberts CJ 2016. Identifying protein aggregation mechanisms and quantifying aggregation rates from combined monomer depletion and continuous scattering. *Anal Biochem* 511:80-91.
15. Geoghegan JC, Fleming R, Damschroder M, Bishop SM, Sathish HA, Esfandiary R 2016. Mitigation of reversible self-association and viscosity in a human IgG1 monoclonal antibody by rational, structure-guided Fv engineering. *MAbs* 8(5):941-950.
16. Bethea D, Wu SJ, Luo J, Hyun L, Lacy ER, Teplyakov A, Jacobs SA, O'Neil KT, Gilliland GL, Feng Y 2012. Mechanisms of self-association of a human monoclonal antibody CNTO607. *Protein Eng Des Sel* 25(10):531-537.
17. Teplyakov A, Obmolova G, Wu SJ, Luo J, Kang J, O'Neil K, Gilliland GL 2009. Epitope mapping of anti-interleukin-13 neutralizing antibody CNTO607. *J Mol Biol* 389(1):115-123.
18. Nishi H, Miyajima M, Wakiyama N, Kubota K, Hasegawa J, Uchiyama S, Fukui K 2011. Fc domain mediated self-association of an IgG1 monoclonal antibody under a low ionic strength condition. *J Biosci Bioeng* 112(4):326-332.
19. Yadav S, Laue TM, Kalonia DS, Singh SN, Shire SJ 2012. The influence of charge distribution on self-association and viscosity behavior of monoclonal antibody solutions. *Mol Pharm* 9(4):791-802.
20. Arora J, Hickey JM, Majumdar R, Esfandiary R, Bishop SM, Samra HS, Middaugh CR, Weis DD, Volkin DB 2015. Hydrogen exchange mass spectrometry reveals protein interfaces and distant dynamic coupling effects during the reversible self-association of an IgG1 monoclonal antibody. *mAbs* 7(3):525-539.
21. Esfandiary R, Parupudi A, Casas-Finet J, Gadre D, Sathish H 2015. Mechanism of reversible self-association of a monoclonal antibody: role of electrostatic and hydrophobic interactions. *J Pharm Sci* 104(2):577-586.
22. Arora J, Hickey JM, Majumdar R, Esfandiary R, Bishop SM, Samra HS, Middaugh CR, Weis DD, Volkin DB 2015. Hydrogen exchange mass spectrometry reveals protein interfaces and distant dynamic coupling effects during the reversible self-association of an IgG1 monoclonal antibody. *MAbs* 7(3):525-539.
23. Gill SC, Von Hippel PH 1989. Calculation of protein extinction coefficients from amino acid sequence data. *Analytical biochemistry* 182(2):319-326.
24. Muschol M, Rosenberger F 1995. Interactions in undersaturated and supersaturated lysozyme solutions: Static and dynamic light scattering results. *The Journal of Chemical Physics* 103(24):10424-10432.
25. Liu W, Cellmer T, Keerl D, Prausnitz JM, Blanch HW 2005. Interactions of lysozyme in guanidinium chloride solutions from static and dynamic light-scattering measurements. *Biotechnol Bioeng* 90(4):482-490.
26. Saluja A, Badkar AV, Zeng DL, Nema S, Kalonia DS 2007. Ultrasonic storage modulus as a novel parameter for analyzing protein-protein interactions in high protein concentration solutions: correlation with static and dynamic light scattering measurements. *Biophys J* 92(1):234-244.

27. Yadav S, Liu J, Shire SJ, Kalonia DS 2010. Specific interactions in high concentration antibody solutions resulting in high viscosity. *J Pharm Sci* 99(3):1152-1168.
28. Lehermayr C, Mahler HC, Mader K, Fischer S 2011. Assessment of net charge and protein-protein interactions of different monoclonal antibodies. *J Pharm Sci* 100(7):2551-2562.
29. Wolfram Eberstein YG, Wolfram Saenger 1994. Molecular interactions in crystallizing lysozyme solutions studied by photon correlation spectroscopy. *Journal of Crystal Growth* 143:71—78.
30. Blanco MA, Perevozchikova T, Martorana V, Manno M, Roberts CJ 2014. Protein-protein interactions in dilute to concentrated solutions: alpha-chymotrypsinogen in acidic conditions. *J Phys Chem B* 118(22):5817-5831.
31. Neergaard MS, Kalonia DS, Parshad H, Nielsen AD, Moller EH, van de Weert M 2013. Viscosity of high concentration protein formulations of monoclonal antibodies of the IgG1 and IgG4 subclass - prediction of viscosity through protein-protein interaction measurements. *Eur J Pharm Sci* 49(3):400-410.
32. Shaoxin Li DX, and Junfeng Li 2004. Dynamic Light Scattering Application to Study Protein Interactions in Electrolyte Solutions. *J Biol Phys* 30(4):313–324.
33. Arora J, Hu Y, Esfandiary R, Sathish HA, Bishop SM, Joshi SB, Middaugh CR, Volkin DB, Weis DD 2016. Charge-mediated Fab-Fc interactions in an IgG1 antibody induce reversible self-association, cluster formation, and elevated viscosity. *MAbs* 8(8):1561-1574.
34. Toprani VM, Joshi SB, Kuelz LA, Schwartz RM, Middaugh CR, Volkin DB 2016. A Micro-Polyethylene Glycol Precipitation Assay as a Relative Solubility Screening Tool for Monoclonal Antibody Design and Formulation Development. *J Pharm Sci* 105(8):2319-2327.
35. Gibson TJ, McCarty K, McFadyen IJ, Cash E, Dalmonte P, Hinds KD, Dinerman AA, Alvarez JC, Volkin DB 2011. Application of a High-Throughput Screening Procedure with PEG-Induced Precipitation to Compare Relative Protein Solubility During Formulation Development with IgG1 Monoclonal Antibodies. *Journal of Pharmaceutical Sciences* 100(3):1009-1021.
36. C R Middaugh WAT, R N Haire and A Rosenberg 1979. Determination of the apparent thermodynamic activities of saturated protein solutions. *Journal of pharmaceutical sciences* 254:367-370.
37. Scholz E. 2012. Karl Fischer titration: determination of water. ed.: Springer Science & Business Media.
38. Majumdar R, Manikwar P, Hickey JM, Arora J, Middaugh CR, Volkin DB, Weis DD 2012. Minimizing Carry-Over in an Online Pepsin Digestion System used for the H/D Exchange Mass Spectrometric Analysis of an IgG1 Monoclonal Antibody. *Journal of The American Society for Mass Spectrometry* 23(12):2140-2148.
39. Arora J, Hu Y, Esfandiary R, Sathish H, Bishop S, Joshi SB, Middaugh CR, Volkin DB, Weis DD 2016. Charge-mediated Fab-Fc interactions in an IgG1 antibody induce reversible self-association, cluster formation, and elevated viscosity. Manuscript submitted. *mAbs*.
40. Padlan EA 1994. Anatomy of the antibody molecule. *Molecular Immunology* 31(3):169-217.
41. Matsumiya S, Yamaguchi Y, Saito J-i, Nagano M, Sasakawa H, Otaki S, Satoh M, Shitara K, Kato K 2007. Structural Comparison of Fucosylated and Nonfucosylated Fc Fragments of Human Immunoglobulin G1. *Journal of Molecular Biology* 368(3):767-779.

42. Molecular Operating Environment (MOE), 2013.08; Chemical Computing Group ULC, 1010 Sherbooke St. West, Suite #910, Montreal, QC, Canada, H3A 2R7, 2018. .
43. Kalonia C, Toprani V, Toth R, Wahome N, Gabel I, Middaugh CR, Volkin DB 2016. Effects of Protein Conformation, Apparent Solubility, and Protein–Protein Interactions on the Rates and Mechanisms of Aggregation for an IgG1 Monoclonal Antibody. *The Journal of Physical Chemistry B* 120(29):7062-7075.
44. Reth M 2013. Matching cellular dimensions with molecular sizes. *Nat Immunol* 14(8):765-767.
45. Chow C-K, Allan BW, Chai Q, Atwell S, Lu J 2016. Therapeutic Antibody Engineering To Improve Viscosity and Phase Separation Guided by Crystal Structure. *Molecular Pharmaceutics* 13(3):915-923.
46. Wu SJ, Luo J, O'Neil KT, Kang J, Lacy ER, Canziani G, Baker A, Huang M, Tang QM, Raju TS, Jacobs SA, Teplyakov A, Gilliland GL, Feng Y 2010. Structure-based engineering of a monoclonal antibody for improved solubility. *Protein Eng Des Sel* 23(8):643-651.
47. Whitaker N, Xiong J, Pace SE, Kumar V, Middaugh CR, Joshi SB, Volkin DB 2017. A formulation development approach to identify and select stable ultra–high-concentration monoclonal antibody formulations with reduced viscosities. *Journal of pharmaceutical sciences* 106(11):3230-3241.
48. Easterbrook-Smith SB, Vandenberg RJ, Alden JR 1988. The role of Fc: Fc interactions in insoluble immune complex formation and complement activation. *Molecular immunology* 25(12):1331-1337.
49. Carpenter JF, Crowe JH 1988. The mechanism of cryoprotection of proteins by solutes. *Cryobiology* 25(3):244-255.
50. Toth RT, Mills BJ, Joshi SB, Esfandiary R, Bishop SM, Middaugh CR, Volkin DB, Weis DD 2017. Empirical Correction for Differences in Chemical Exchange Rates in Hydrogen Exchange-Mass Spectrometry Measurements. *Anal Chem* 89(17):8931-8941.
51. Kamerzell TJ, Esfandiary R, Joshi SB, Middaugh CR, Volkin DB 2011. Protein–excipient interactions: Mechanisms and biophysical characterization applied to protein formulation development. *Advanced drug delivery reviews* 63(13):1118-1159.
52. Hong T, Iwashita K, Shiraki K 2018. Viscosity Control of Protein Solution by Small Solutes: A Review. *Current Protein and Peptide Science* 19(8):746-758.
53. Zangi R 2009. Can salting-in/salting-out ions be classified as chaotropes/kosmotropes? *The Journal of Physical Chemistry B* 114(1):643-650.
54. Oki S, Nishinami S, Shiraki K 2018. Arginine suppresses opalescence and liquid–liquid phase separation in IgG solutions. 118:1708-1712.
55. Zhang Y, Cremer PS 2006. Interactions between macromolecules and ions: the Hofmeister series. *Current opinion in chemical biology* 10(6):658-663.
56. Ahmed M, Namboodiri V, Singh AK, Mondal JA 2014. On the intermolecular vibrational coupling, hydrogen bonding, and librational freedom of water in the hydration shell of mono- and bivalent anions. *The Journal of chemical physics* 141(16):164708.
57. Dougherty RC 2001. Density of salt solutions: effect of ions on the apparent density of water. *The Journal of Physical Chemistry B* 105(19):4514-4519.

58. Brandts JF, Hunt L 1967. Thermodynamics of protein denaturation. III. Denaturation of ribonuclease in water and in aqueous urea and aqueous ethanol mixtures. *Journal of the American Chemical Society* 89(19):4826-4838.
59. Brandts JF 1964. The thermodynamics of protein denaturation. I. The denaturation of chymotrypsinogen. *Journal of the American Chemical Society* 86(20):4291-4301.
60. Yoshizawa S, Arakawa T, Shiraki K 2014. Dependence of ethanol effects on protein charges. *International journal of biological macromolecules* 68:169-172.
61. Pace CN, Trevino S, Prabhakaran E, Scholtz JM 2004. Protein structure, stability and solubility in water and other solvents. *Philosophical Transactions of the Royal Society of London B: Biological Sciences* 359(1448):1225-1235.
62. Yoshikawa H, Hirano A, Arakawa T, Shiraki K 2012. Effects of alcohol on the solubility and structure of native and disulfide-modified bovine serum albumin. *International Journal of Biological Macromolecules* 50(5):1286-1291.
63. Yoshikawa H, Hirano A, Arakawa T, Shiraki K 2012. Mechanistic insights into protein precipitation by alcohol. *International Journal of Biological Macromolecules* 50(3):865-871.
64. Chin JT, Wheeler SL, Klibanov AM 1994. On protein solubility in organic solvent. *Biotechnology and Bioengineering* 44(1):140-145.
65. Tscheliessnig A, Satzer P, Hammerschmidt N, Schulz H, Helk B, Jungbauer A 2014. Ethanol precipitation for purification of recombinant antibodies. *J Biotechnol* 188:17-28.
66. Ghoufi A, Artzner F, Malfreyt P 2016. Physical properties and hydrogen-bonding network of water-ethanol mixtures from molecular dynamics simulations. *The Journal of Physical Chemistry B* 120(4):793-802.
67. Li F, Men Z, Li S, Wang S, Li Z, Sun C 2018. Study of hydrogen bonding in ethanol-water binary solutions by Raman spectroscopy. *Spectrochimica Acta Part A: Molecular and Biomolecular Spectroscopy* 189:621-624.
68. R. A. Curtis JMP, H. W. Blanch 1998. Protein-protein and protein-salt interactions in aqueous protein solutions containing concentrated electrolytes. *Biotechnology and Bioengineering* 57(1):11-21.
69. Wayne Melander CH 1977. Salt effects on hydrophobic interactions in precipitation and chromatography of proteins: An interpretation of the lyotropic series. *Archives of Biochemistry and Biophysics* 183(1):200-215.
70. Long FA, McDevit WF 1952. Activity Coefficients of Nonelectrolyte Solutes in Aqueous Salt Solutions. *Chemical Reviews* 51(1):119-169.
71. Duong-Ly KC, Gabelli SB 2014. Salting out of proteins using ammonium sulfate precipitation. *Methods Enzymol* 541:85-94.

### 3.7. Figures and Tables

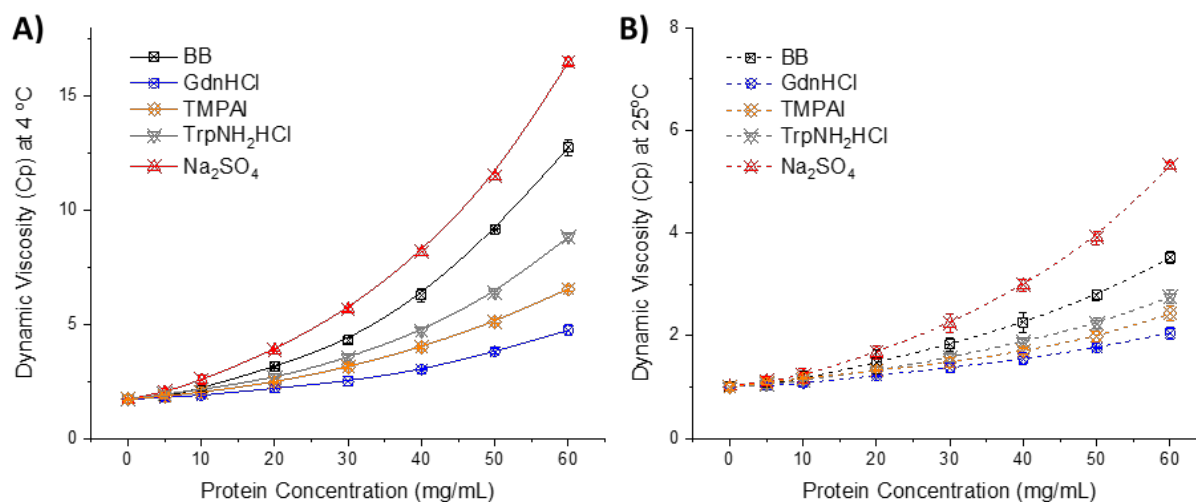


**Figure 3.1.** Effect of additives on dynamic viscosity of mAb-C solutions at varying protein concentrations at (A) 4°C and (B) 25°C. Excipients were at 150 mM, except GdnHCl (0.5 M) and ethanol (15% v/v) in base buffer (BB). Data are presented as mean  $\pm$  standard deviation;  $n = 3$ .

**Figure 3.2.**

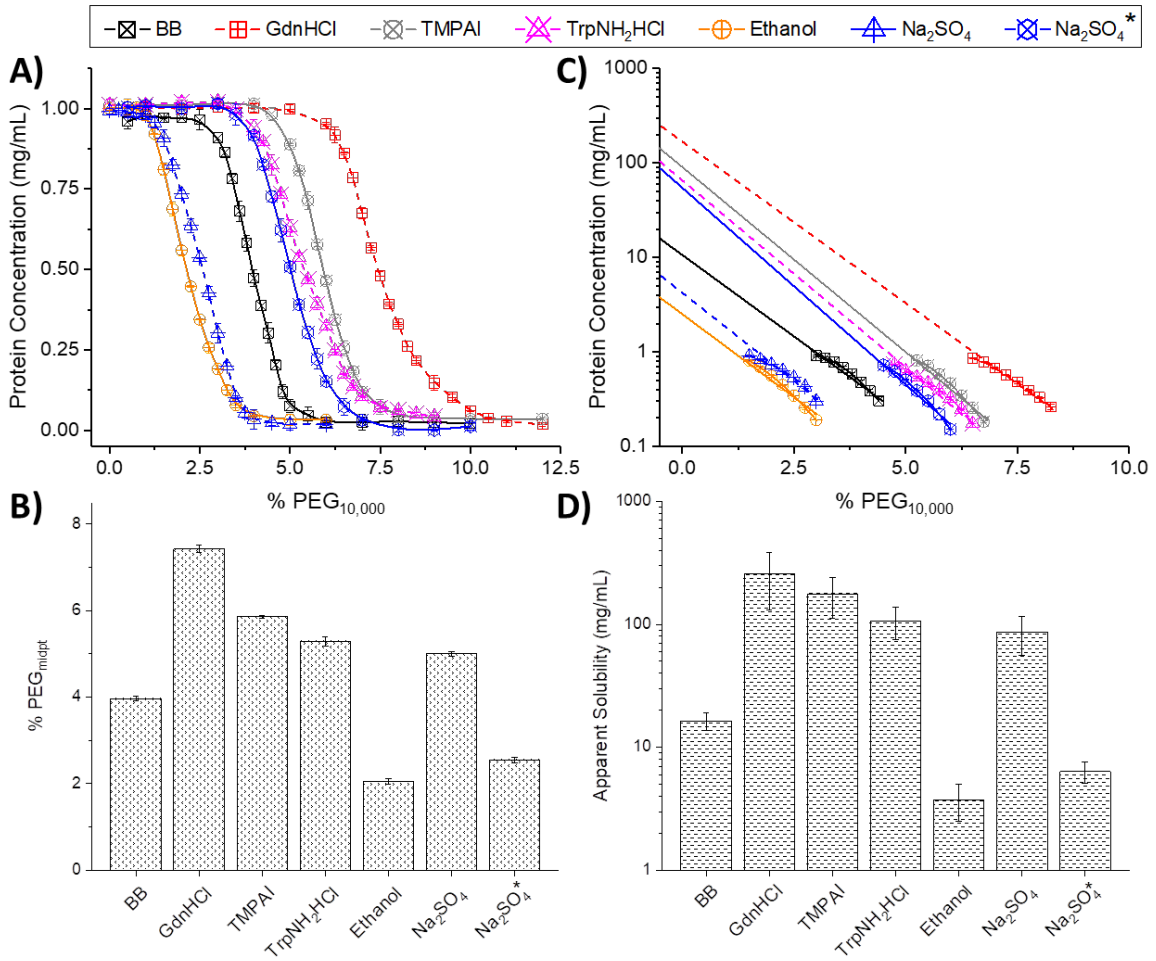




**Figure 3.2.** Relative apparent solubility (thermodynamic activity) of mAb-C as measured by PEG<sub>10,000</sub> induced precipitation assay. **(A)** Change of mAb-C concentration as a function of %PEG<sub>10,000</sub> added to solution (data fit by sigmoidal curves). **(B)** %PEG<sub>midpt</sub> values are shown in a bar chart, indicating the amount of PEG<sub>10,000</sub> that was needed to precipitate half of total protein out of solution. **(C)** Apparent solubility values were obtained from Y-axis extrapolation of data points in the transition range shown in panel A. **(D)** Comparison of the apparent solubility values obtained for mAb-C in the absence/presence of various additives. Two concentrations of sodium sulfate (150 mM for “Na<sub>2</sub>SO<sub>4</sub>” and 0.5 M for “Na<sub>2</sub>SO<sub>4</sub>\*”) were used for this study. Other excipient solutions had a concentration of 150 mM, except GdnHCl (0.5 M) and ethanol (15% v/v) in BB. Multiple methods were employed to determine protein concentration, including UV<sub>280nm</sub> for mAb-C in BB, and BB in the presence of GdnHCl, ethanol, and Na<sub>2</sub>SO<sub>4</sub>; BCA assay for mAb-C solution in the presence of TMPAI (Supplemental Figure S1a), and SEC method for mAb-C solution in the presence of TrpNH<sub>2</sub>HCl (Supplemental Figure S1b). Data are presented as mean ± standard deviation; n = 3.

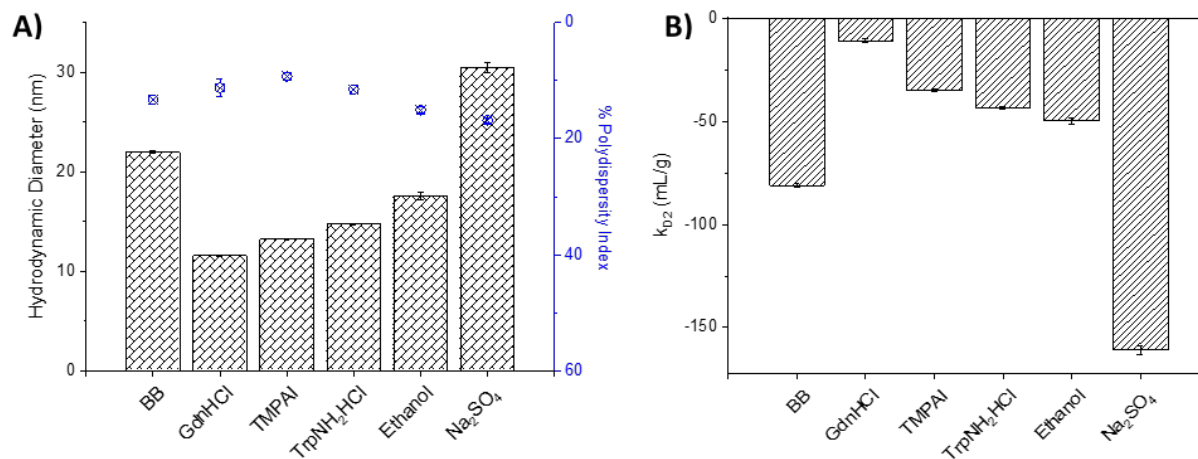


**Figure 3.3.** Effect of additives on mAb-C hydrodynamic diameter and protein interaction parameter ( $k_{D2}$ ) as determined by dynamic light scattering. (A) Hydrodynamic diameter (bars, left axis) and polydispersity values (squares, right axis) were determined at a protein concentration of 10 mg/mL, and (B)  $k_{D2}$  values were calculated from a series of mAb-C hydrodynamic diameter measurements from 1-10 mg/mL protein concentrations at 25°C. Additives concentration was 150 mM, except GdnHCl (0.5 M) and ethanol (15% v/v) in BB. DLS cumulative data was weighted by intensity. Data are presented as mean  $\pm$  standard deviation;  $n = 3$ .

Figure 3.4.

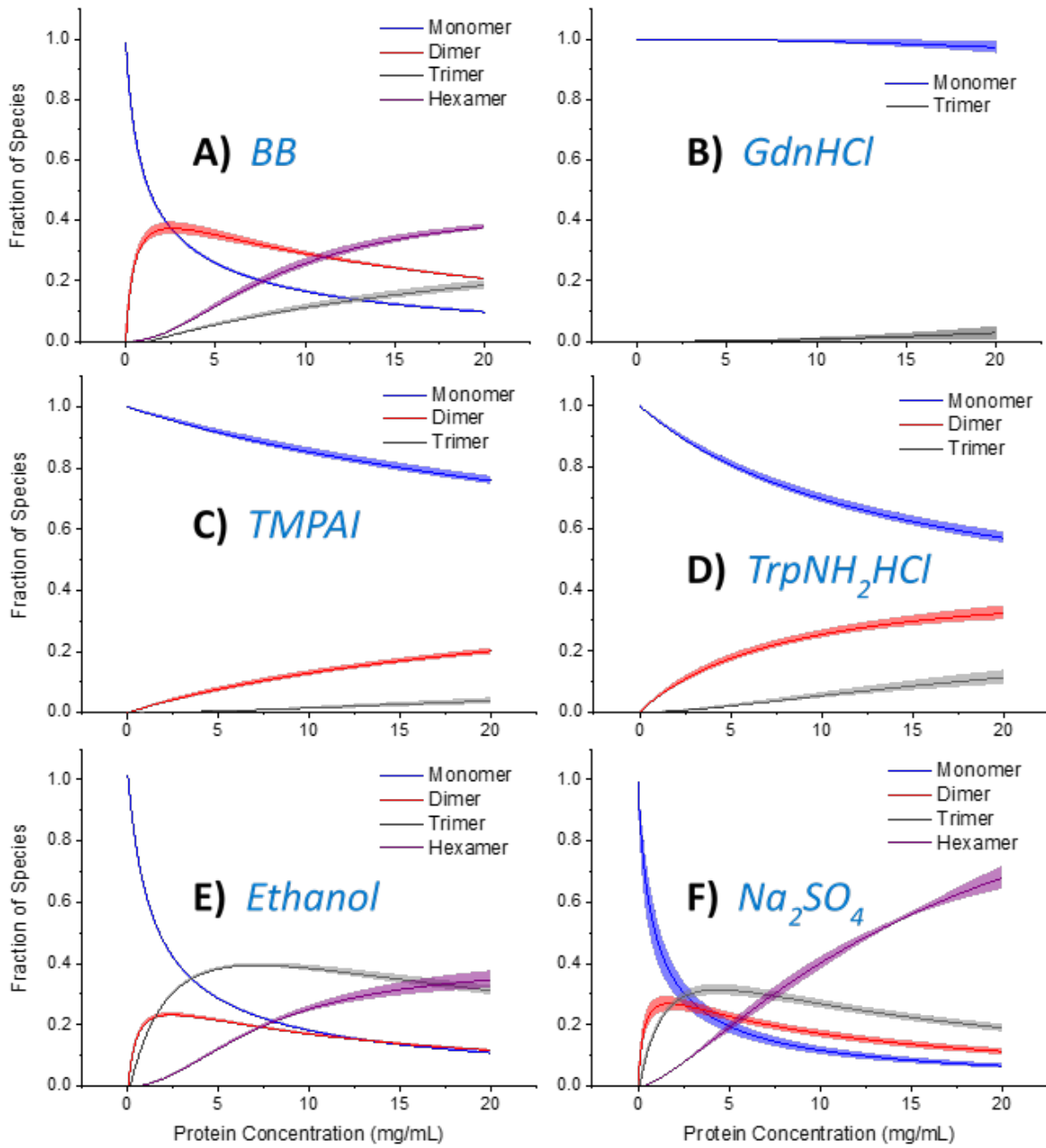


**Figure 3.4.** Effect of additives on the self-association induced complexes of mAb-C as determined by static light scattering from CG-MALS analysis. Fraction of various species was determined as a function of protein concentration in the absence/presence of different additives in base buffer (BB) containing **(A)** BB alone, or BB with **(B)** GdnHCl, **(C)** TMPAI, **(D)** TrpNH<sub>2</sub>HCl, **(E)** ethanol, and **(F)** Na<sub>2</sub>SO<sub>4</sub>. Concentration of excipients was 150 mM, except GdnHCl (0.5 M) and ethanol (15% v/v). Measurements were performed at room temperature. All data are presented as mean ± standard deviation; n = 3.

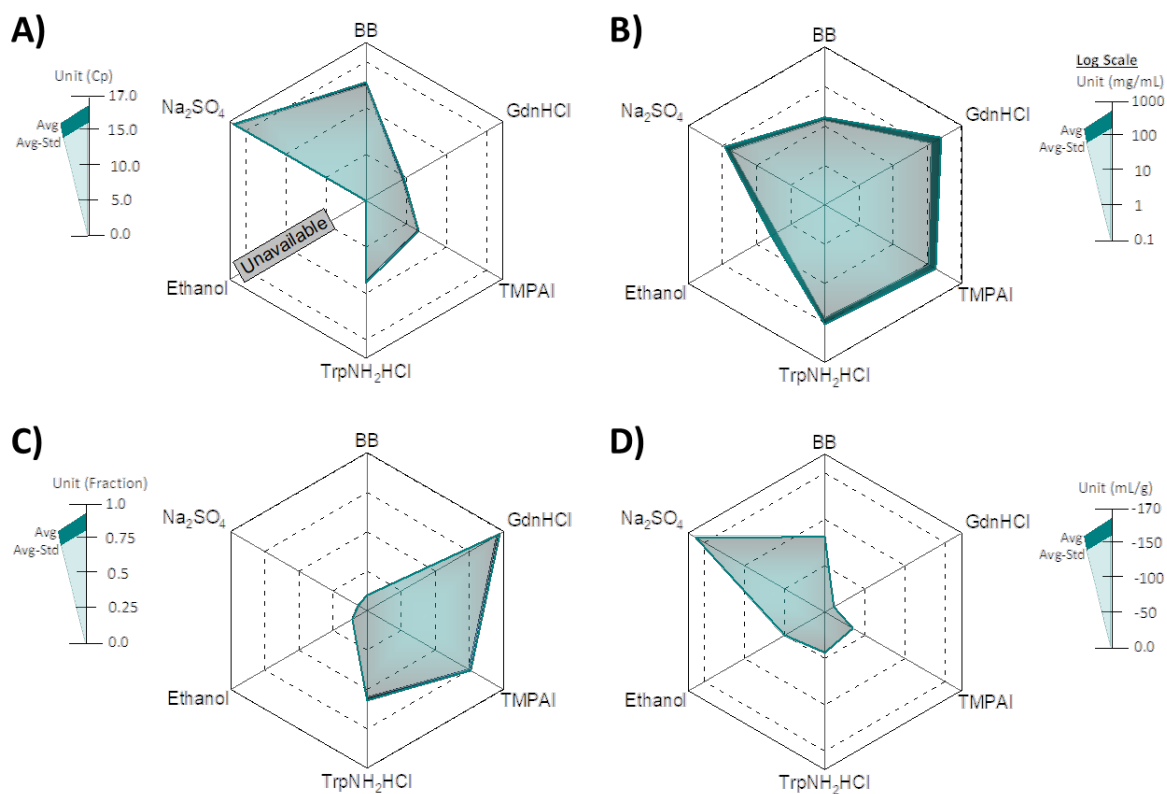


**Figure 3.5.** Radar chart array analysis to better visualize excipient effects on mAb-C solution and molecular properties. Except for GdnHCl (0.5 M) and ethanol (15% v/v), all other additive solutions have a concentration of 150 mM. Specifically, **(A)** dynamic viscosity values at protein concentration of 60 mg/mL, **(B)** mAb-C apparent solubility values in log scale, **(C)** the fraction of mAb-C monomer at the concentration of 20 mg/mL as measured by CG-MALS, and **(D)** the values of protein interaction parameter ( $k_{D2}$ ). The

distance between the perimeters of the two polygons (along an axis) is one standard deviation. Triplicate measurements were performed.

Figure 3.6.

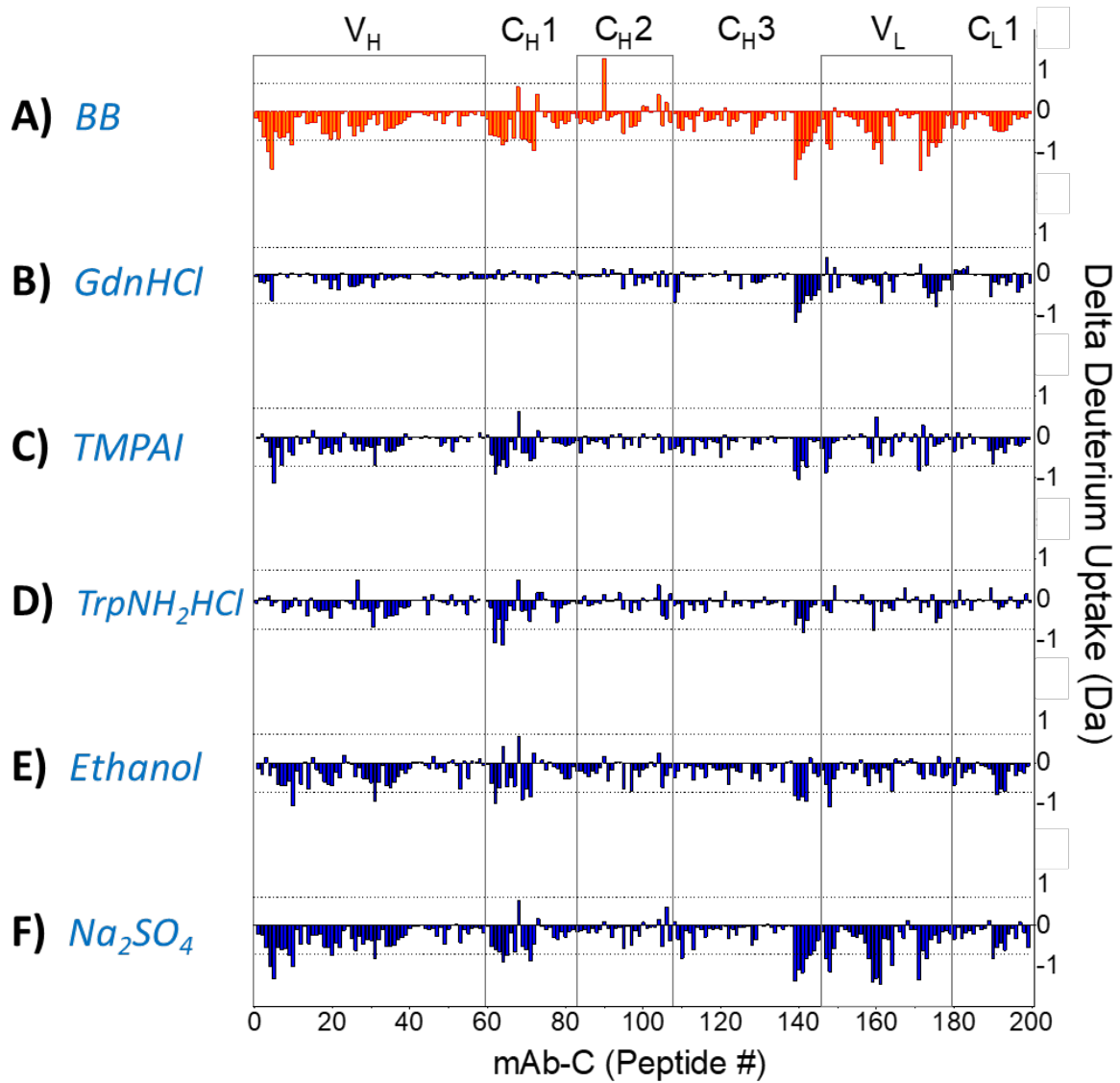


**Figure 3.6.** Effect of additives on mAb-C RSA and backbone flexibility by mass difference plot from HX-MS. **(A)** Mass difference of each peptide between 60 mg/mL and 5 mg/mL of mAb-C in BB. Panels **(B)** GdnHCl (0.5 M), **(C)** TMPAI (150 mM), **(D)** TrpNH<sub>2</sub>HCl (150 mM), **(E)** ethanol (15% v/v), and **(F)** Na<sub>2</sub>SO<sub>4</sub> (150 mM) shows effects of different excipients on alteration of protein interactions as well as local peptide flexibility. Alternate backgrounds indicate antibody domain boundaries. The number of peptides is ordered from the N-to-C termini of the heavy chain followed by the light chain of mAb-C. Positive values imply increased backbone flexibility, while negative values mean the opposite. The dashed horizontal lines are the 99% confidence criteria. Three independent HX measurements was performed.

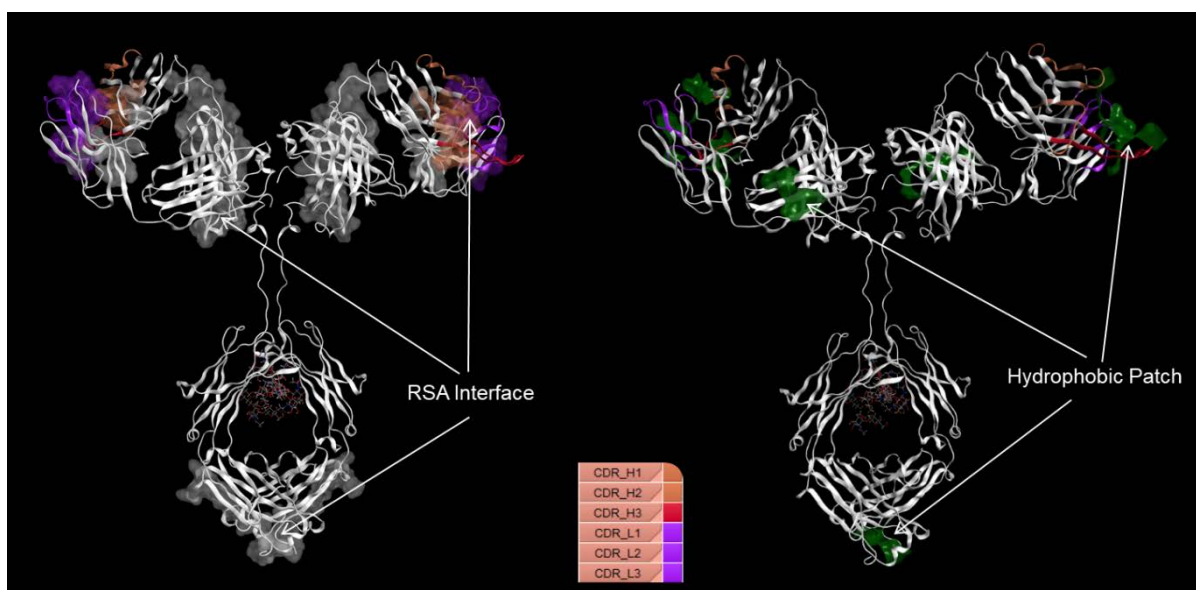


**Figure 3.7.** RSA interfaces defined and hydrophobic patches visualized on mAb-C. RSA interfaces of mAb-C, as defined by HX protection, are shown on the left in space-filling representation. Brown, red, and purple colors denote CDR H1, H2, H3, and CDR L1, L2, and L3, respectively. Hydrophobic patches ( $> 200 \text{ \AA}^2$ , and are displayed in green) predicted by homology modeling using Molecular Operating Environment (MOE) are shown on the right side.



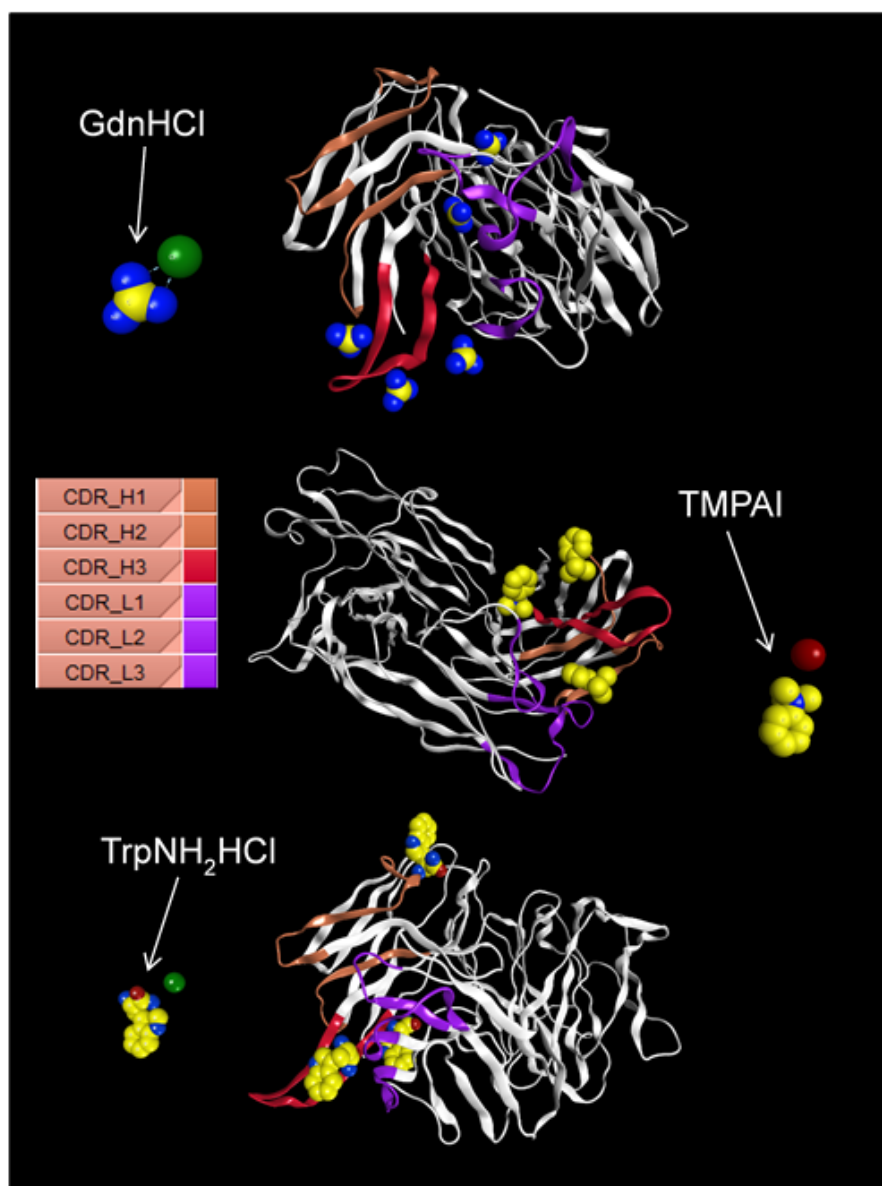
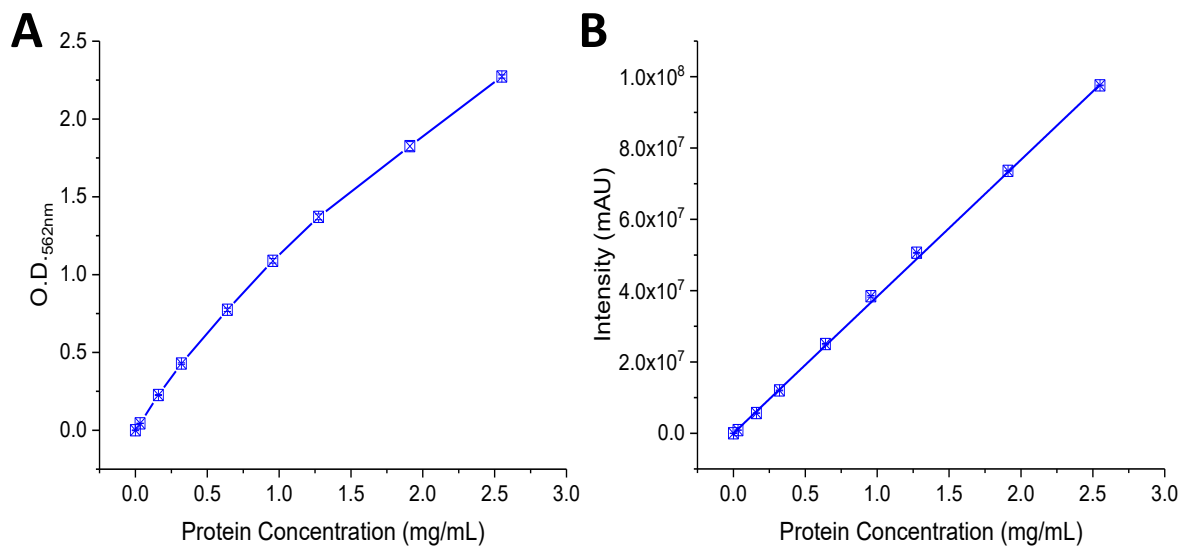
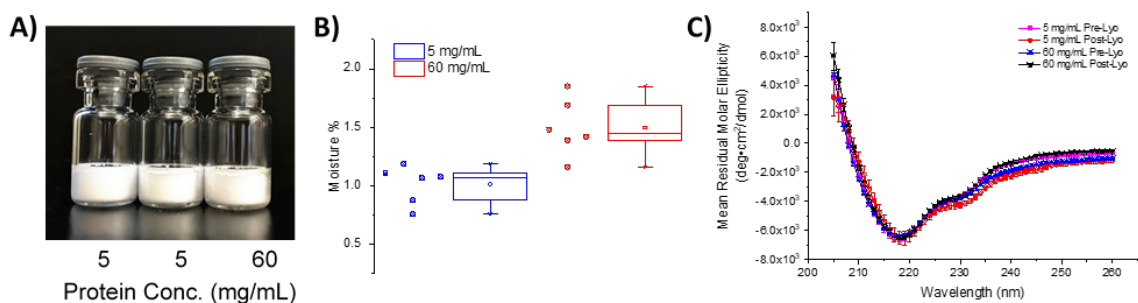


**Figure 3.8.** Local rigid docking of excipients to identify favorable locations for binding on the Fab RSA sites of mAb-C at pH 7.5 calculated using MOE. Top-ranking candidates (below -7 kcal/mol) are shown on the Fab domain of the mAb-C homology model. For additive molecules, blue, yellow, red, green, and dark red represent nitrogen, carbon, oxygen, chloride, and iodide respectively.



**Supplemental Figure 3.1.** Standard curves of BCA and SEC using known concentrations of mAb-C to determine protein concentration of mAb-C for PEG<sub>10,000</sub> induced precipitation assay (see **Figure 4** of manuscript). **(A)** Fitting of BCA assay results between O.D.<sub>562nm</sub> and protein concentration, which was based on an equation  $y = (a \cdot b + c \cdot x^d)/(b + x^d)$ , where “a”=1.6 × 10<sup>-2</sup>, “b”=3.4 × 10<sup>7</sup>, “c”=2.8 × 10<sup>7</sup>, and “d”=1.2. **(B)** Linear regression between SEC absorbance values at 214 nm and protein concentration, with an equation of  $y = a \cdot x + b$ , in which “a”=3.8 × 10<sup>7</sup>, “b”=1.7 × 10<sup>5</sup>. Data are presented as mean ± standard deviation; n = 3.



**Supplemental Figure 3.2.** Lyophilization of mAb-C solutions. **(A)** Representative vials displaying cake appearance post freeze-drying, **(B)** moisture content of lyophilized cakes determined by Karl Fischer titration, and **(C)** CD spectra of mAb-C pre- and post-lyophilization samples (after reconstitution) at both low and high protein concentrations. Solutions contains 20 mM potassium phosphate with 10% trehalose (w/v) at pH 7.5 with indicated concentration of mAb-C. Data are presented as mean  $\pm$  standard deviation;  $n = 6$  for moisture measurements;  $n = 3$  for CD measurements.

**Supplemental Table 3.1.** Analytical characterization of pre-lyophilization and post-lyophilization (and reconstitution) samples of mAb-C as measured by UV-Vis spectroscopy and SEC. The protein concentration and percent aggregate formation were determined for reconstituted mAb-C samples lyophilized at low and high protein concentrations. Data are presented as mean  $\pm$  standard deviation; n = 3.

mAb-C	Ultraviolet-Visible Spectroscopy			Size Exclusion Chromatography			
	<i>Protein Conc. (mg/mL)</i>	<i>% Protein Recovery</i>	<i>Slope of O.D.<sub>320-350 nm</sub></i>	<i>% Monomer</i>	<i>% Soluble Aggregates</i>	<i>% Fragments</i>	<i>% Insoluble Aggregates</i>
Pre-Lyo (5 mg/mL)	5.6 $\pm$ 0.0	98.9 $\pm$ 0.9	-5.0E-5 $\pm$ 4.2E-5	99.0 $\pm$ 0.1	1.0 $\pm$ 0.1	0.0 $\pm$ 0.1	0.0 $\pm$ 0.1
Post-Lyo (5 mg/mL)	5.5 $\pm$ 0.0		-1.2E-4 $\pm$ 6.3E-5	98.6 $\pm$ 0.1	1.1 $\pm$ 0.1	0.0 $\pm$ 0.1	0.4 $\pm$ 0.1
Pre-Lyo (60 mg/mL)	57.5 $\pm$ 0.3	98.5 $\pm$ 1.0	-6.9E-5 $\pm$ 5.5E-5	98.9 $\pm$ 0.1	1.1 $\pm$ 0.1	0.0 $\pm$ 0.1	0.0 $\pm$ 0.1
Post-Lyo (60 mg/mL)	56.6 $\pm$ 0.5		-8.8E-5 $\pm$ 4.8E-5	97.8 $\pm$ 0.1	1.1 $\pm$ 0.1	0.0 $\pm$ 0.1	1.1 $\pm$ 0.1

**Supplemental Table 3.2.** Peptide list of mAb-C from pepsin digestion during HX-MS analysis with their corresponding peptide locations.

Peptide Number	Location	Peptide Number	Location	Peptide Number	Location
1	Heavy 1-4 (VH)	36	Heavy 67-80 (VH)	71	Heavy 164-187 (CH1)
2	Heavy 1-10 (VH)	37	Heavy 71-78 (VH)	72	Heavy 167-182 (CH1)
3	Heavy 1-17 (VH)	38	Heavy 71-79 (VH)	73	Heavy 171-182 (CH1)
4	Heavy 1-22 (VH)	39	Heavy 71-80 (VH)	74	Heavy 172-182 (CH1)
5	Heavy 1-32 (VH)	40	Heavy 74-79 (VH)	75	Heavy 183-187 (CH1)
6	Heavy 5-17 (VH)	41	Heavy 79-83 (VH)	76	Heavy 188-193 (CH1)
7	Heavy 5-22 (VH)	42	Heavy 80-83 (VH)	77	Heavy 188-201 (CH1)
8	Heavy 5-32 (VH)	43	Heavy 81-86 (VH)	78	Heavy 188-205 (CH1)
9	Heavy 11-22 (VH)	44	Heavy 83-93 (VH)	79	Heavy 193-201 (CH1)
10	Heavy 11-32 (VH)	45	Heavy 84-93 (VH)	80	Heavy 193-205 (CH1)
11	Heavy 18-22 (VH)	46	Heavy 84-94 (VH)	81	Heavy 194-205 (CH1)
12	Heavy 18-32 (VH)	47	Heavy 84-95 (VH)	82	Heavy 206-217 (CH1)
13	Heavy 33-36 (VH)	48	Heavy 87-93 (VH)	83	Heavy 243-248 (CH2)
14	Heavy 33-44 (VH)	49	Heavy 87-94 (VH)	84	Heavy 243-259 (CH2)
15	Heavy 33-45 (VH)	50	Heavy 94-99 (VH)	85	Heavy 243-260 (CH2)
16	Heavy 33-46 (VH)	51	Heavy 94-101 (VH)	86	Heavy 249-259 (CH2)
17	Heavy 33-47 (VH)	52	Heavy 95-99 (VH)	87	Heavy 249-260 (CH2)
18	Heavy 33-48 (VH)	53	Heavy 95-101 (VH)	88	Heavy 250-259 (CH2)
19	Heavy 33-49 (VH)	54	Heavy 96-101 (VH)	89	Heavy 250-260 (CH2)
20	Heavy 33-59 (VH)	55	Heavy 100-112 (VH)	90	Heavy 260-268 (CH2)
21	Heavy 35-48 (VH)	56	Heavy 102-112 (VH)	91	Heavy 260-269 (CH2)
22	Heavy 37-59 (VH)	57	Heavy 107-112 (VH)	92	Heavy 261-268 (CH2)
23	Heavy 45-48 (VH)	58	Heavy 108-112 (VH)	93	Heavy 261-269 (CH2)
24	Heavy 45-49 (VH)	59	Heavy 113-120 (VH)	94	Heavy 261-270 (CH2)
25	Heavy 49-59 (VH)	60	Heavy 113-122 (VH)	95	Heavy 269-285 (CH2)
26	Heavy 50-59 (VH)	61	Heavy 121-150 (CH1)	96	Heavy 270-273 (CH2)
27	Heavy 50-60 (VH)	62	Heavy 121-152 (CH1)	97	Heavy 270-285 (CH2)
28	Heavy 50-70 (VH)	63	Heavy 121-153 (CH1)	98	Heavy 271-285 (CH2)
29	Heavy 60-66 (VH)	64	Heavy 123-150 (CH1)	99	Heavy 274-285 (CH2)
30	Heavy 60-70 (VH)	65	Heavy 123-153 (CH1)	100	Heavy 308-314 (CH2)
31	Heavy 60-79 (VH)	66	Heavy 153-163 (CH1)	101	Heavy 309-313 (CH2)
32	Heavy 61-70 (VH)	67	Heavy 153-182 (CH1)	102	Heavy 309-314 (CH2)
33	Heavy 67-70 (VH)	68	Heavy 154-163 (CH1)	103	Heavy 314-317 (CH2)
34	Heavy 67-78 (VH)	69	Heavy 154-182 (CH1)	104	Heavy 315-326 (CH2)
35	Heavy 67-79 (VH)	70	Heavy 164-182 (CH1)	105	Heavy 315-329 (CH2)

106	Heavy 315-341 (CH2)	137	Heavy 414-418 (CH3)	169	Light 537-540 (VL)
107	Heavy 327-341 (CH2)	138	Heavy 419-454 (CH3)	170	Light 537-546 (VL)
108	Heavy 342-356 (CH2)	139	Heavy 432-454 (CH3)	171	Light 538-569 (VL)
109	Heavy 342-364 (CH3)	140	Heavy 434-454 (CH3)	172	Light 540-552 (VL)
110	Heavy 342-373 (CH3)	141	Heavy 435-454 (CH3)	173	Light 540-570 (VL)
111	Heavy 357-364 (CH3)	142	Heavy 436-454 (CH3)	174	Light 541-569 (VL)
112	Heavy 357-373 (CH3)	143	Heavy 437-454 (CH3)	175	Light 541-570 (VL)
113	Heavy 357-375 (CH3)	144	Heavy 439-454 (CH3)	176	Light 542-570 (VL)
114	Heavy 365-373 (CH3)	145	Heavy 449-454 (CH3)	177	Light 559-569 (VL)
115	Heavy 365-374 (CH3)	146	Light 455-476 (VL)	178	Light 560-569 (VL)
116	Heavy 365-375 (CH3)	147	Light 455-486 (VL)	179	Light 570-579 (CL)
117	Heavy 365-376 (CH3)	148	Light 459-486 (VL)	180	Light 570-586 (CL)
118	Heavy 367-373 (CH3)	149	Light 478-486 (VL)	181	Light 571-579 (CL)
119	Heavy 374-376 (CH3)	150	Light 487-489 (VL)	182	Light 571-586 (CL)
120	Heavy 374-384 (CH3)	151	Light 487-500 (VL)	183	Light 578-586 (CL)
121	Heavy 375-384 (CH3)	152	Light 487-501 (VL)	184	Light 580-588 (CL)
122	Heavy 376-384 (CH3)	153	Light 487-502 (VL)	185	Light 580-597 (CL)
123	Heavy 376-387 (CH3)	154	Light 490-500 (VL)	186	Light 587-589 (CL)
124	Heavy 377-384 (CH3)	155	Light 501-503 (VL)	187	Light 590-597 (CL)
125	Heavy 377-386 (CH3)	156	Light 501-508 (VL)	188	Light 590-602 (CL)
126	Heavy 385-387 (CH3)	157	Light 501-516 (VL)	189	Light 590-608 (CL)
127	Heavy 385-388 (CH3)	158	Light 501-524 (VL)	190	Light 590-615 (CL)
128	Heavy 385-398 (CH3)	159	Light 501-525 (VL)	191	Light 598-615 (CL)
129	Heavy 385-406 (CH3)	160	Light 503-524 (VL)	192	Light 603-615 (CL)
130	Heavy 385-412 (CH3)	161	Light 504-508 (VL)	193	Light 616-626 (CL)
131	Heavy 389-406 (CH3)	162	Light 509-516 (VL)	194	Light 616-632 (CL)
132	Heavy 399-406 (CH3)	163	Light 509-524 (VL)	195	Light 627-632 (CL)
133	Heavy 400-406 (CH3)	164	Light 525-528 (VL)	196	Light 633-646 (CL)
134	Heavy 407-412 (CH3)	165	Light 525-536 (VL)	197	Light 634-649 (CL)
135	Heavy 413-418 (CH3)	166	Light 525-537 (VL)	198	Light 636-649 (CL)
136	Heavy 413-431 (CH3)	167	Light 526-536 (VL)	199	Light 639-649 (CL)
137	Heavy 414-417 (CH3)	168	Light 526-537 (VL)	200	Light 650-668 (CL)

## **Chapter 4**

Structure Characterization and Stability Assessments of Secretory IgA  
Monoclonal Antibodies as Potential Candidates for Passive Immunization by Oral  
Administration

## 4.1. Introduction

Diarrheal diseases are the second leading cause of death in developing countries, especially in Sub-Saharan Africa and South Asia,<sup>1-3</sup> with ~0.6 million children under 5 years of age dying each year due to complications caused by severe diarrhea.<sup>4-6</sup> A major cause of diarrhea is from drinking water contaminated by pathogenic bacteria, viruses, or parasites.<sup>4</sup> Enterotoxigenic *Escherichia coli* (ETEC) is the most common bacterial cause of diarrhea-associated mortality, which leads to approximately one quarter of all diarrheal episodes for infants and children less than 5-years of age.<sup>7-10</sup> To further complicate these problems, enhanced antibiotic resistance has been found in many ETEC strains.<sup>11-13</sup> Thus, the development of an ETEC vaccine is considered the most effective and feasible strategy to prevent diarrheal diseases among children in developing countries,<sup>14,15</sup> and has become a high priority for the World Health Organization.<sup>16</sup> Currently, no ETEC vaccines are commercially available and numerous challenges impede ETEC vaccine development including heterogeneity of potential target antigens (e.g., virulence factors such as enterotoxins and colonization factors),<sup>4</sup> poor mucosal immunogenicity, potential safety issues of such antigens, and cost hurdles to develop, manufacture and commercialize such prophylactic vaccines.<sup>8,17</sup>

Due to these challenges, there is growing interest in the use of passive immunization strategies to treat ETEC-induced diarrheal diseases in targeted populations



by oral delivery of neutralizing immunoglobulins. For example, local delivery of antibodies that bind and neutralize ETEC in the gut could be utilized to prevent infection. Multiple virulence factors from ETEC have been recognized as potential antigens for passive immunity,<sup>11,18</sup> including secretion heat-labile enterotoxin (LT) which directly induces diarrhea by prompting solute retention and loss of water absorption in the intestinal lumen. LT is a heterohexameric A-B subunit toxin comprised of a catalytically active A subunit and five B subunits.<sup>18</sup> Subunit A has ADP-ribosylation activity, which covalently modifies the subunit of the GTP-binding protein (Gs), leading to the constitutive activation of adenylate cyclase and production of 3',5'-cyclic AMP (cAMP).<sup>19</sup> Consequently, continuous release of chloride and water into intestinal lumen causes watery diarrhea while the five B subunits mediate LT binding to glycolipid and glycoprotein receptors on host cells.<sup>19</sup> Thus, antibody-induced neutralization of LT enzymatic activity and inhibition of adhesion could potentially be effective in controlling ETEC infection.

Secretory IgA (sIgA) antibodies are of particular interest for passive immunization during oral administration due to its natural abundance in secretions and mucosal surfaces.<sup>20</sup> As the most abundant isotype of immunoglobulins in mucosal membranes, secretory IgAs (sIgAs) play crucial roles in protecting gut mucosal surfaces from pathogens and toxins.<sup>21-23</sup> Secretory IgAs functions to promote clearance of pathogens, maintenance of intestinal homeostasis, direct neutralization of bacterial virulence factors

(e.g., enterotoxins), and modulation of proinflammatory responses.<sup>21-24</sup> sIgA antibodies consist of dimeric IgG-like molecules, linked by a joining chain (J-chain), and complexed with a secretory component (SC) chain<sup>25</sup> (see results section). The SC protein is acquired as the polymeric immunoglobulin receptor cleaves upon transport across epithelial cells into mucosal surfaces and secretions. sIgA antibodies are inherently more resistant to proteolysis by digestive enzymes when compared to IgG in the gastrointestinal tract.<sup>26,27</sup>

In this work, three anti-LT isotype variants of the same mAb (sIgA1, sIgA2 and IgG1) were expressed and purified from CHO cells in quantities of 5-10 mg. A series of physicochemical methods were developed (to accommodate limited availability of material) and utilized to characterize the anti-LT sIgA1, sIgA2, and IgG1 mAbs in terms of primary structure, post-translational modifications (i.e., N-linked glycosylation), molecular weight and size heterogeneity, physicochemical stability, aggregation propensity, and relative solubility. In addition, we examined the stability of the three mAbs under conditions that mimic the gastric phase of oral delivery using simulated gastric fluids in a modified *in vitro* gastric digestive model. The results are evaluated in terms of relative rank-ordering of the pharmaceutical stability of these molecules from the point of view of future formulation development work to optimize storage stability as well as stability during oral delivery.

## **4.2. Materials and Methods**

#### **4.2.1. Sample Preparation**

The three anti-heat labile toxin (LT) immunoglobulins (slgA1, slgA2, and IgG1) were expressed in CHO cells and purified by MassBiologics (University of Massachusetts Medical School, Boston, MA). The antibodies were prepared in 10 mM sodium phosphate, 150 mM NaCl, pH 7.2 (phosphate-buffered saline, PBS) and stored at 2-8°C. Protein concentration was determined by ELISA using known concentrations of slgA1, slgA2 or IgG1 as standards. The protein concentration was confirmed by HPLC. When protein concentration was determined by UV-visible spectroscopy, extinction coefficients were calculated based on the primary sequences<sup>28</sup> as 1.49, 1.49, 1.64 mL·mg<sup>-1</sup>·cm<sup>-1</sup> for slgA1, slgA2 and IgG1, respectively.

#### **4.2.2. Sodium Dodecyl Sulfate Polyacrylamide Gel Electrophoresis (SDS-PAGE)**

Twenty µL of each 0.2 mg/mL Ig sample was mixed with or without 1 µL of PNGase F (New England BioLabs, Ipswich, MA) and incubated overnight at 37°C. Both deglycosylated and glycosylated Ig samples were reduced with 50 mM dithiothreitol (DTT, Invitrogen, Carlsbad, CA) at 70°C for 30 min. Reduced and non-reduced samples were then mixed with 4X LDS loading dye (Life Technologies, Grand Island, NY) containing 100 mM iodoacetamide (IAM, Life Technologies), and incubated at 100°C for 5 min. Samples were cooled to room temperature (RT) and separated by SDS-PAGE using NuPAGE 10% Bis-tris gels (Life Technologies) and MOPS running buffer (Life

Technologies) at 150 V for 75 min. Gels were stained with Coomassie Blue R-250 (Teknova, Hollister, CA) and destained with 40% methanol 10% acetic acid. Gels were digitized using an Alphamager (Protein Simple, Santa Clara, CA) gel imaging system.

#### **4.2.3. Size Exclusion Chromatography (SEC)**

A Shimadzu Prominence ultra-fast liquid chromatography HPLC system equipped with a diode array detector (with absorbance detection at 214 nm) was utilized. The system was equilibrated at 0.5 mL/min flow rate in 0.2 M sodium phosphate buffer at pH 6.8 for at least 2 hours. Ten  $\mu\text{L}$  of each Ig (10  $\mu\text{g}$  total protein per injection) was injected and separated by a TOSOH TSKgel G4000SWXL column (8  $\mu\text{m}$  particle size, 7.8 mm ID  $\times$  30 cm) for sIgA or a TOSOH TSK-Gel BioAssist G3SWxl column (5  $\mu\text{m}$  size, 7.8 mm ID  $\times$  30 cm) for IgG1 with a corresponding guard column operated at ambient temperature (Tosoh Biosciences) using a 30-minute run time. Gel filtration molecular weight standards (Bio-Rad, Hercules, CA) were injected before and after the Ig sample sets to ensure integrity of the column and HPLC system. Potential presence of larger aggregates were determined by running Ig samples with and without the SEC column (i.e., protein percentage recovery). Greater than 95% protein recovery was obtained for each of the three mAbs by SE-HPLC, indicating minimal loss of protein (e.g., larger aggregates) by using optimized SE-HPLC conditions for sIgA vs IgG1. Data were analyzed using LC-Solution software (Shimadzu, Kyoto, Japan).

#### **4.2.4. Sedimentation Velocity Analytical Ultracentrifugation (SV-AUC)**

SV-AUC was performed using a Proteome Lab XL-I (Beckman Coulter) analytical ultracentrifuge equipped with a scanning ultraviolet-visible optical system. Samples were diluted to 0.2 mg/mL in PBS pH 7.2 and transferred into Beckman charcoal-epon two sector cells with a 12 mm centerpiece and sapphire windows. All experiments were performed at 20°C after at least 1 hour of equilibration after the rotor reached 20°C. SV-AUC was performed at a rotor speed of 40,000 RPM and with detection at 280 nm. The data were analyzed using Sedfit (Dr. Peter Schuck, NIH). The partial specific volume was calculated using Sednterp (software provided by Professor Thomas Laue, University of New Hampshire and BITC) based on the primary sequence. The buffer density and viscosity used in the analysis were also calculated using Sednterp based on the composition of the buffer. The density and viscosity of PBS were calculated to be 1.0059 g/mL and 0.01021 Poise, respectively. A continuous c(s) distribution model was applied with a range from 0 to 15 svedbergs, with a resolution of 300 points per distribution and a confidence level of 0.95. Baseline, radial independent noise, and time independent noise were fit parameters, while the meniscus and bottom positions were set manually.

#### **4.2.5. LC-MS Peptide Mapping**

Ninety  $\mu$ L of 0.5 mg/mL Ig samples were reduced with 3  $\mu$ L of 0.5 M DTT for 30 min at 80°C and alkylated with 6  $\mu$ L of 0.5 M IAM for 30 min at 37°C in the dark. The samples

were then incubated overnight at 37°C with 12 µg of trypsin or chymotrypsin (~1:25 enzyme:Ig ratio). The following day, the samples were heated to 98°C for 5 min to inactivate the enzyme. After cooling down, samples were treated with PNGase F (New England BioLabs, Ipswich, MA) as described above to remove N-linked oligosaccharides. Before LC-MS injections, 0.05% (v/v) trifluoroacetic acid was added, and samples were centrifuged for 5 min at 14,000 xg. The peptides from the digested protein solution were then separated by reversed phase UHPLC (Thermo Scientific) using a C18 column (1.7µm, 2.1 x 150 mm, Waters Corporation) and a 85 min 0-30% B gradient (A: H<sub>2</sub>O and 0.05% trifluoroacetic acid; B: ACN and 0.05% trifluoroacetic acid; 200 µl/min flow rate). MS was performed using a LTQ-XL ion trap (Thermo Scientific) and Xcalibur v2.0 software (Thermo Scientific). The instrument was tuned using a standard calibration peptide (Angiotensin II, Sigma) for maximal sensitivity prior to running any experiments. The mass spectra were acquired in the LTQ over a mass range of m/z 400-1900 using an ion selection threshold of 40,000 counts and a dynamic exclusion duration of 5 sec. Raw experimental files were processed using PepFinder 2.0 software (Thermo Scientific). The database used for this experiment consisted of the primary sequences of all Ig molecules. Potential Cys carbamidomethylation, Asn deamidation, and Met oxidation were included in the analysis. Peptide assignments of MS/MS spectra were validated using a confidence score of > 95%.

#### **4.2.6. Total Carbohydrate Analysis**

A glycoprotein carbohydrate estimation kit (Thermo-Fisher #23260) was used to determine the total carbohydrate content (both N- and O-linked glycosylation) in Ig samples as a percentage of total protein mass. Prior to experiments, proteins were buffer exchanged into PBS pH 7.2 using 30 kD MWCO filters (EMD Millipore, Billerica, MA) to remove trace of detergent and a final concentration of 0.25 mg/mL Ig was used in each reaction. The recommended procedure by the manufacturer was used. Absorbance at 550 nm was read using a SpectraMax M5 microtiter plate reader (Molecular Devices). Lysozyme, BSA, ovalbumin, Apo-transferrin, fetuin, and  $\alpha$ 1-acid were used as glycoprotein standards to construct a standard curve.

#### **4.2.7. N-Glycan Oligosaccharide Analysis**

A GlycoWorks RapiFluor-MS N-Glycan Kit (Waters Corporation, Milford, MA) was used to identify and quantify all N-linked glycans following the manufacturer instructions. Briefly, Ig samples were centrifuged at 10,000 rpm for 5 mins, 7.5  $\mu$ L of 2 mg/mL Igs were mixed with 15.3  $\mu$ L ultrapure water and 6  $\mu$ L Rapi-surfactant and heated at 90°C for 3 min. After cooling to ambient temperature, 1.2  $\mu$ L of Rapi-PNGase F was added and samples were incubated at 50°C for 5 min to release N-linked glycans. Labeling was performed by combining oligosaccharide samples with 12  $\mu$ L RapiFluor-MS reagent for 5 min. The reaction was diluted in 358  $\mu$ L of acetonitrile and the reaction products purified

using a HILIC  $\mu$ Elution plate. The plate was washed three times in wash buffer (1% formic acid, 90% acetonitrile) and eluted in 90  $\mu$ L of elution buffer. The samples were further diluted in 310  $\mu$ L of diluent buffer. Fluor-MS N-glycan analysis was performed using an Agilent 1260 Infinity II HPLC system equipped with a 1260 FLD detector (Agilent, Santa Clara, CA) and an Agilent 6230 electrospray ionization Time-of-Flight mass spectrometer (Agilent, Santa Clara, CA). A HILIC AdvanceBio Glycan Mapping column (120 Å, 2.1 x 150 mm, 2.7  $\mu$ m), that was operated at 45°C, was used to separate various N-glycans. Fifty  $\mu$ L of prepared samples was injected into LC-MS system, with a flow rate of 0.6 mg/mL and a gradient run time of 55 min. Fluorescence was obtained using excitation and emission wavelengths of 265 and 425 nm, respectively. MS was acquired simultaneously from 400 to 2000 m/z at a constant scan rate of one spectrum per second. N-glycans were assigned based on m/z values using a N-glycan database,<sup>29</sup> and N-glycan quantification was calculated on integration of the fluorescence chromatogram.

#### **4.2.8. Conformational Stability Assessments**

Thermal unfolding experiments were performed with Ig samples diluted in either PBS pH 7.2 or buffer exchanged into a simulated gastric fluid (SGF, 94mM NaCl, 13mM KCl) with 10 mM citrate phosphate (CP) buffer at pH 3.0<sup>30</sup>. Samples were then diluted in the corresponding buffer to a final concentration of 0.2 mg/mL. A fluorescence plate reader equipped with a charge-coupled device (CCD) detector (Fluorescence



Innovations, Minneapolis, MN) was used to obtain intrinsic tryptophan fluorescence spectra. Twenty  $\mu\text{L}$  of each sample were loaded into a 384-well plate (Hard-Shell 384-well PCR plates), and overlaid with 2  $\mu\text{L}$  of silicon oil (ThermoFisher Scientific, Waltham, MA). Samples were excited at 295 nm (>95% tryptophan emission) and the emission spectra were recorded from 300 to 450 nm with an integration time of 100 ms. Temperature ramps were programmed from 10 to 100°C with an increment of 2.5°C per step. The mean center of spectra mass (MSM) peak algorithm was used to analyze the data to determine the shift in fluorescence peak position as a function of temperature.

Denaturant unfolding experiments were performed using 8 M stocks of GdnHCl prepared in either PBS pH 7.2 or SGF containing 10 mM CP buffer at pH 3.0. Ig samples were buffer exchanged and diluted to final Ig concentration of 0.2 mg/mL, with a series of GdnHCl concentrations from 0 to 5.5 M. Ten  $\mu\text{L}$  of each Ig sample was transferred to a 384-well plate (Hard-Shell 384-well PCR plates) and incubated at 4°C overnight before performing fluorescence measurements as above, but without the silicone oil overlay and at a fixed temperature (10°C). Data analysis was performed as described above.

#### **4.2.9. Relative Protein Solubility (Polyethylene Glycol Precipitation Assay)**

Relative solubility of Igs was performed by adapting the method by Gibson et al.<sup>31</sup> and Toprani et al.<sup>32</sup> using smaller volumes. Briefly, 384-well polystyrene filter plates (Corning Life Sciences, Corning, NY) were used. Thirty percent w/v PEG<sub>10,000</sub> stock

solutions were prepared in either PBS pH 7.2 or SGF containing 10 mM CP buffer pH 3.0. Various concentrations of PEG<sub>10,000</sub> solutions ranging from 0 to 25% w/v were prepared with Ig concentration of 0.2 mg/mL in both buffer conditions. Samples were incubated overnight at RT in dark. The next day, plates were centrifuged at 1,233 × g for 15 min and directly eluted into a clean 384-well plate. Relative protein concentration in each well was determined using a SpectraMax M5 plate reader (Molecular Devices) using detection at 214 nm. %PEG<sub>midpt</sub> values were then calculated as described previously.<sup>31</sup>

#### **4.2.10. In vitro Model of Gastric Digestion**

To determine the stability of the proteins under simulated gastric conditions, each Ig was diluted in simulated gastric fluid (SGF), which was composed of 94 mM NaCl, 13 mM KCl, 0.15 mM CaCl<sub>2</sub>, along with 10 mM citrate-phosphate buffer pH 3.5 (added to maintain pH). Proteins were either diluted directly into SGF/CP buffer alone or SGF/CP buffer with added bicarbonate buffer (9:1 ratio of the digestion solution and a bicarbonate neutralization buffer containing 0.03 M trisodium citrate and 0.3 M sodium bicarbonate at pH 8.5<sup>33</sup>) at a final protein concentration of 0.2 mg/mL. The reaction was started when the pepsin (2000 U/mL pepsin, Sigma)<sup>30</sup> was added to the solution and samples were incubated at 37°C for varying amounts of time. The reaction was quenched by the addition of 400 mM NaOH to adjust to neutral pH. Samples were then analyzed by SDS-PAGE and ELISA. For ELISA analysis, samples were diluted in ELISA blocking buffer (0.1%

BSA in PBS) at 40 µg/mL and 1 µg/mL of sIgAs and IgG1 digested samples based on the starting concentration, respectively and stored at -20°C until analysis.

#### **4.2.11. Immobilized Pepsin Digestion**

Ig samples were diluted in SGF/CP buffer (see composition above) at a final concentration of 0.2 mg/mL. Immobilized pepsin-agarose (Thermo-Fisher) was washed three times in SGF by centrifugation at 12,000 x g prior to addition to the diluted Ig mixture to a final pepsin concentration of 2000 U/mL. Samples were incubated at 37°C with end over end rotation to keep the beads in suspension. Beads were removed by centrifugation at 12,000 x g for 1 min upon completion of the desired incubation times, and the supernatant was removed. Samples were then neutralized by addition of 400mM NaOH prior to analysis by SE-HPLC. SE-HPLC was performed as described above, but with an injection volume of 25 µl.

#### **4.2.12. Enzyme-Linked Immunosorbent Assay (ELISA)**

96-well affinity immunoassay plates (Thermal Scientific, Rochester, NY) were coated with 1.0 µg/mL Heat-Labile Enterotoxin, B subunit (LTB) from *E. coli* (Sigma E8656) in PBS pH 7.2 and incubated overnight at 4°C. The following day, after removing coating solution, 96-well plates were filled with 200 µL of ELISA blocking buffer (0.1% BSA in PBS) for 2 hours at room temperature. After flicking out blocking buffer, digested Ig samples were loaded 1:1 with blocking buffer and 1:1 serial dilutions were performed

using blocking buffer as the diluent. Samples were incubated for 30 mins at room temperature. Plates were washed three times with 0.05% Tween-20 in PBS, then 50  $\mu$ L/well of HRP conjugated Goat anti-human Ig protein (Fisher, Southern Biotechnology Associates) diluted in blocking buffer (1:15,000 was added and incubated for 30 mins at room temperature. Plates were washed as before, and 100  $\mu$ L/well TMB substrate solution (3,3',5,5'-Tetramethylbenzidine (TMB)) was added and incubated for 5 min at room temperature in the dark. The reaction was quenched with 100  $\mu$ L/well 1 M phosphoric acid. Optical density (OD) was recorded using a SpectraMax M5 microtiter plate reader (Molecular Devices) at 450 nm.

### **4.3. Results**

#### **4.3.1. Characterization of Purity, Primary Structure and Post-translational Modifications of sIgA vs. IgG mAbs**

As shown schematically in Figure 1A, sIgA antibodies are composed of two IgG-like molecules which are disulfide linked by a ~16 kDa joining chain (termed the J-chain), and also a ~70 kDa secretory component (SC) chain that is complexed via the heavy chains in the Fc domains.<sup>25</sup> The combined molecular weight of sIgA polypeptide chains is ~400 kDa which increases to ~460-480 kDa due to 15-20% N-linked and O-linked glycosylation depending upon the sIgA subclass (see below). In comparison to sIgAs, IgG

antibodies are less structurally complex and smaller (~150 kDa with 1-2% N-linked glycosylation). There are two main subclasses of sIgAs (sIgA1 and sIgA2) which structurally differ primarily in their hinge regions (e.g., length of hinge region, disulfide-bonding pattern, and the type and number of attached glycosylation sites)<sup>34</sup> as depicted schematically in Figure 1A. Two and three conserved N-linked glycans are found on each Fc domain of sIgA1 and sIgA2, respectively, while sIgA2 also possesses one or two additional N-linked glycans on the C<sub>H</sub>1 domain. Another key structural difference is sIgA1 contains multiple O-glycans on its elongated hinge region, while sIgA2 possesses a shorter hinge region that lacks such glycosylation.<sup>35</sup> Both subclasses contain several N-linked glycosylation sites on the J-chain and SC.<sup>36</sup>

SDS-PAGE analysis was performed under non-reducing and reducing conditions, both with and without PNGase F treatment to remove N-glycans, as shown in Figure 1B. Under non-reduced conditions, both sIgA1 and sIgA2 mAbs displayed smear bands with a composition of monomer, dimer, and higher molecular weight (MW) species (i.e., migrating near the top of gel) when compared to IgG1 (~150 kDa), which is consistent with the composition of sIgA antibodies (Figure 1A). The sIgA1 and sIgA2 samples had multiple high molecular weight bands that are primarily covalently cross-linked disulfide bonded species upon comparison to the reduced samples (and consistent with previous reports).<sup>37-39</sup> Conversely, IgG1 showed relatively higher purity in the non-reduced sample

with primarily a single band. Under reducing conditions, three major components were identified for the sIgA mAb samples: the SC (~70 kDa), heavy chain (~50 kDa), and light chain (~25 kDa). Note, the J-chain (~16 kDa) was not observed by SDS-PAGE (consistent with literature results; see discussion). Specifically for sIgA2, we also observed two bands at relatively lower molecular weights (~17 kDa and ~40 kDa), which could represent sIgA2 fragments rather than J chain (for the former) due to their disappearance after reduction. The heavy and light chains of the PNGase F-treated, reduced sIgAs migrated at slightly lower MW on the gel, indicating deglycosylation of these molecules. As expected, no migration differences were observed for the light chain bands independent of PNGase F treatment. In contrast, in the reduced IgG1 sample, both heavy (~50 kDa) and light (~25 kDa) chains were observed, and small amount of fragments (~17 kDa) were also seen. Since the IgG1 heavy chain is N-glycosylated (see below), it also displayed lower MW migration after PNGase F treatment.

To confirm the primary sequence and identify potential post-translational modifications (PTMs), LC-MS peptide mapping was performed on the three mAbs. Due to the PNGase F treatment required for successful chromatographic resolution (data not shown), contributions of the N-glycans were not detected, and this PTM was examined separately (see below). Due to the sequence similarity (>97%) of sIgA1 and sIgA2, including both the variable and constant regions, many peptides were similar in terms of

elution profile (Figure 2A). At the same time, some differences in peptide elution profiles were also observed thus demonstrating a unique profile for each sIgA. For IgG1, the base peak chromatogram was significantly different when compared to the sIgAs, indicating a distinct digestion profile. Therefore, “fingerprint” chromatograms were obtained for each of the three mAbs. The sequence coverage obtained for each of the polypeptide chains is shown in Figure 2B. Overall, >85% coverage was obtained for each polypeptide chain for each mAbs. The light chain displayed the best coverage (97-100%), the heavy chain coverage was from 83% to 97%, and SC and J chain displayed 86-87% and 83-96% sequence coverage, respectively. In terms of PTMs, no notable chemical modifications on sIgA1 and sIgA2 mAbs were observed. For IgG1, N-terminal pyroglutamic acid formation and C-terminal lysine residual truncation were identified in the heavy chain, which are commonly observed PTMs with IgG1 mAbs.<sup>40,41</sup>

Glycosylation of antibodies plays an important role in functional activity (effector function and potentially antigen binding) as well as physical properties such as solubility and stability.<sup>42-45</sup> A combination of total carbohydrate content as well the identification and quantification of the N-glycan profile was determined for each of the three anti-LT mAbs. As shown in Figure 3A, a substantial difference in the total carbohydrate content between sIgAs mAbs (18.7% and 18.5% for sIgA1 and sIgA2, respectively), and IgG1 (1.2%) was observed. This result is consistent with the known structure and post-translational

modifications of each mAb (Figure 1A). Further analysis was performed to identify specific N-glycan type and relative quantification was performed by removal and derivatization of the N-glycans followed by chromatographic separation with detection by a combination of MS analysis and fluorescence measurements (see methods). Twenty-four and twenty-three different N-glycans for slgA1 (Figure 3B) and slgA2 (Figure 3C) were identified, with G2+NANA and G2F+NANA as the most dominant glycan types, respectively. In contrast, as shown in Figure 3D, the IgG1 mAb displayed a much simpler N-glycan profile, with 5 major N-glycan oligosaccharides, in which glycan G0F was the most dominant type (>80%). Each N-glycan type and corresponding percent composition found in each anti-LT mAb are summarized in Figure 4. It can be seen that the N-linked oligosaccharide composition and distribution greatly differs between the slgA and IgG1 mAbs, as well as between the slgA1 and slgA2 mAbs.

#### **4.3.2. Characterization of Size and Aggregation Profile of slgA vs IgG mAbs**

In addition to size analysis under denaturing conditions by SDS-PAGE (see Figure 1B), size distribution profile under non-denaturing conditions was determined for each of the three mAbs using two orthogonal methods, SV-AUC and SE-HPLC, as shown in Figure 5A and 5B, respectively. Two size categories (monomeric slgA and higher molecular weight (HMW) species) were used to classify the species distribution of each sample. For slgA1 and slgA2 samples, multiple peaks were identified by both SV-AUC



and SE-HPLC, with SV-AUC displaying superior peak resolution, especially for larger MW species. For IgG1, a more homogeneous peak distribution was observed (it should be noted that to optimize separation of different species and percent recovery, different SEC columns were employed for the sIgA vs. IgG1 samples, and thus the IgG1 eluted at an earlier retention time; see methods). Overall, similar species distribution results were achieved in comparing SV-AUC and SE-HPLC results after peak area integration (Figure 5C). Both sIgA1 and sIgA2 samples displayed a relatively high amount of HMW species in solution, representing ~50% and ~80% of total protein, respectively. On the other hand, <10% of total protein was in the form of HMW species in the IgG1 sample. For each of the observed species, the molecular weight values were estimated, based on sedimentation coefficient values and comparison to the gel filtration standards for SV-AUC and SE-HPLC, respectively, as shown in Supplemental Table S1.

#### **4.3.3. Conformational Stability and Relative Solubility Assessment of sIgA vs IgG mAbs**

The sIgA1, sIgA2 and IgG1 mAbs were then compared in terms of their conformational stability and relative solubility profiles under two different pH solution conditions including pH 7.2 (to evaluate stability/relative solubility under storage conditions at neutral pH) and pH 3.0 (to evaluate stability/relative solubility under gastric conditions at acidic pH). First, the conformational stability of the mAbs was examined as

a function of temperature. As shown in Figure 6A, solution pH effects the overall tertiary structure of the mAbs as a function of increasing temperature as determined by intrinsic Trp fluorescence spectroscopy. One major transition was observed to begin at 60-70°C at pH 7.2 for each of the mAbs. When the solution pH was decreased to 3.0, however, multiple transitions were detected across the entire temperature range, and a red shift was observed at 10°C. These results suggest that the overall tertiary structure of each mAb is partially altered under acidic pH solution conditions. Second, the conformational stability of the three mAbs was examined by the addition of increasing amounts of the chemical denaturant guanidine hydrochloride (GdnHCl), by monitoring changes in overall tertiary structure of the mAbs by fluorescence spectroscopy as shown in Figure 6B. The slgA1 and slgA2 mAbs showed one broad transition as the GdnHCl concentration was increased with a midpoint of ~3M at pH 7.2. At pH 3.0, both slgA mAbs showed lower conformational stability. Two distinct transitions were observed for IgG1 at pH 7.2, with midpoints of ~2 and ~4M GdnHCl. Lower conformational stability was also noted at pH 3.0 for the IgG1 mAb.

Interestingly, in terms of relative apparent solubility as measured by PEG-10,000 precipitation assay, a higher concentration of PEG-10,000 was required at pH 3.0 to precipitate each of the three mAbs compared to pH 7.2 in the relative rank order of slgA1 > slgA2 > IgG1 (Figure 6C). In fact, the slgA1 remained soluble and failed to precipitate

despite addition of the highest concentration PEG-10,000 (25%, w/v) when the solution pH was 3.0. Thus, higher relative apparent solubility was observed for each of three mAbs, albeit to various extents, by decreasing the solution pH from 7.2 to 3.0 (see Discussion section).

#### **4.3.4. Examination of sIgA vs IgG Stability in an In Vitro Gastric Digestion Model to Mimic Oral Administration**

To investigate and compare stability profiles of each of the mAbs under conditions that mimic oral delivery, we adapted an *in vitro* digestion model that focused on the gastric phase using simulated adult conditions for food digestion.<sup>33</sup> In this adapted model, we scaled down the volume requirements and determined the most crucial variables on mAb digestion rates including solution pH, digestion time, and pepsin concentration (data not shown). We fixed the solution pH to 3.5 (using a low concentration of citrate phosphate buffer), optimized the pepsin concentration to 2000 U/mL, and monitored digestion in 1 mL solution as a function of time at 37°C (see methods section). Three analytical techniques (ELISA, non-reducing SDS-PAGE, SE-HPLC) were used to assess the antigen binding activity, purity and size of each the mAbs (and/or their degradation products) vs. incubation time, respectively.

First, the LT-antigen binding activity of each mAb was assessed by ELISA as a function of incubation time in the *in vitro* digestion model. The ELISA binding activity correlated well with antibody activities in functional assays (data not shown). At time zero, the sIgA1, sIgA2 and IgG1 mAbs bound the antigen in a concentration dependent manner with a midpoint between 0.01 to 0.1 mg/mL mAb (Figure 7A, 7B and 7C, respectively). During incubation, a decreased signal (indicating decreasing amounts of mAb binding to the LT antigen) was observed for both sIgA1 and sIgA2. Nonetheless, no shift in the midpoint was noted and some antigen binding was still observed even after overnight digestion (Figure 7 A, B). In contrast, IgG1 lost its LT binding ability to a much greater extent (shift in the midpoint values as well as decreased total signal), and much more rapidly, when compared to the sIgAs (Figure 7C). The majority of the binding capacity of IgG1 sample was lost after 5-10 minutes of digestion. To better compare these results across the three anti-LT mAbs, the percent loss of binding signal was calculated and the relative loss rates were then compared (Figure 7D). For IgG1, the loss of mAb binding to LT antigen was rapid versus the significantly slower rates observed for both of the sIgAs. The co-addition of sodium bicarbonate buffer, which neutralizes the acidic pH leading to irreversible inactivation of pepsin,<sup>46,47</sup> resulted in ~100% retention of LT binding even after overnight incubation in the *in vitro* gastric digestion model as shown in Figure 7D.

Second, non-reducing SDS-PAGE was performed on the same sIgA1, sIgA2 and IgG1 samples incubated in the *in vitro* gastric digestion model (Figure 8). The sIgA1 mAb gradually digested, and a series of digestion byproducts were observed including a major species ~100 kDa, which presumably corresponds to the F(ab')<sub>2</sub> fragment (Figure 7A). After 3 hours, sIgA1 degraded mostly to the ~100 kDa species. This result is consistent with known Fc susceptibility to pepsin digestion into smaller MW peptides while the more resistant F(ab')<sub>2</sub> fragment remains intact.<sup>48,49</sup> As expected, the sIgA1 was essentially completely protected with co-addition of a sodium bicarbonate buffer (Figure 8A). Overall similar observations were made with the sIgA2 mAb as shown in Figure 8B, however, one difference was noted: in addition to the major digestion species of F(ab')<sub>2</sub>, another protein species was detected at ~50 kDa which was likely the Fab fragment. Addition of the bicarbonate buffer played a similar role in protecting sIgA2 from digestion by increasing solution pH. In contrast, IgG1 displayed an accelerated digestion profile when compared to the sIgAs (Figure 8C). After the first time point (5 min), almost all of the IgG1 was digested to F(ab')<sub>2</sub> fragments, and these remained after overnight incubation (Figure 8C). The protective effect of bicarbonate buffer addition was also observed for IgG1. To more directly compare digestion profiles of the three mAbs by non-reduced SDS-PAGE, densitometry analysis of the native mAb band was performed (Figure 8D). Although each of the intact mAbs were fully digested after overnight incubation (without addition of

bicarbonate buffer), the rate of digestion of the sIgAs was much slower when compared to IgG1, indicating an increased resistance to acidic pH and pepsin digestion.

Finally, SE-HPLC was also used to determine the size degradation profile of the three anti-LT mAbs (under non-denaturing conditions) by quantifying the decrease of the intact protein species and increase of the corresponding degradation products (Figure 9). In this experiment, immobilized pepsin was utilized to easily remove the pepsin from the solution, since injection of pepsin containing solutions onto the SEC column resulted in co-elution of the protease with the sIgA degradation products (data not shown). Three major peaks were identified in the SEC chromatograms and were assigned as follows: the main species, large fragments, and small fragments (Figure 9A). Presumably, the intact protein is the large species, while the  $F(ab')_2$  /  $F(ab)$  are the large fragments and smaller peptide byproducts represent the small fragments. As shown in Figure 9A, digestion of sIgA1 was observed as a function of time where the main peak area was reduced at each time point, while there was a concurrent increase in the large and small fragments. For sIgA2, similar trends were observed (Figure 9B). For IgG1, three peaks were also observed, however, the digestion occurred more rapidly (when compared to the sIgAs) based on the reduction of the main peak area (Figure 9C). To facilitate comparisons, the percent of intact mAb as a function of digestion time was determined.

Both slgA1 and slgA2 demonstrated greater resistance to pepsin digestion when compared to IgG1, with no notable differences between slgA1 and slgA2 (Figure 9D).

#### **4.3.5. Comparisons of Stability/Solubility Profiles of slgA1, slgA2 and IgG under Various Conditions**

To better summarize and compare the stability results described above as a function of solution pH and molecule type (slgA1, slgA2, IgG1), a “relative stability index” was determined (Figure 10). Briefly, Figure 10 displays the results of the relative stability comparisons between the three anti-LT mAbs in terms of conformational stability at pH 7.2 and 3.0 (vs. temperature and vs. GdnHCl) as shown in Figure 10A, the relative apparent solubility at pH 7.2 and 3.0 as shown in Figure 10B, and finally, the stability profile during incubation in the *in vitro* digestion model (37°C, pH 3.5 with pepsin) as shown in Figure 10C. For each condition, three values (1, 2, and 3) were assigned to each of the three mAbs corresponding to their relative rank ordering in stability (highest, intermediate, and lowest). These values in Figure 10A and B were determined from the replotting of Figure 6 data as shown in Supplemental Figure S1.

As shown in Figure 10A (top panel), the physical properties of the three mAbs at pH 7.2 were ranked ordered as described above, and then the results were combined (bottom panel). It can be seen that slgA1 scored as having the best physical properties

(combination of results from thermal and denaturant unfolding as well as relative solubility), followed by slgA2 with intermediate behavior, and IgG1 as the least desirable properties overall. The same evaluation was carried out at pH 3.0 as shown in Figure 10B, and the same rank ordering of desirable physical properties was calculated at pH 3.0 with slgA1 > slgA2 > IgG1. Results of relative stability index during incubation in the *in vitro* gastric digestion model are shown in Figure 10C based on rank ordering the results from the ELISA, SDS-PAGE and SEC analyses (see Figures 7, 8, 9). The slgA1 and slgA2 mAbs showed an overall similar ranking in terms of relative stability under conditions that mimic oral delivery, with IgG1 displaying the lowest stability overall under these conditions.

#### **4.4. Discussion**

Monoclonal antibodies (mAbs) are now widely used for treating a variety of diseases especially pre-exposure prophylaxis (PreP) for infectious diseases, autoimmune disorders, and cancers.<sup>50</sup> Approximately 70 mAbs are now approved for various therapeutic uses by regulatory agencies, and the vast majority are comprised of the IgG1 antibody subtype and are administered to patients by parenteral injection (intravenous or subcutaneous routes). From a product development point of view, key structural attributes of IgG1 mAbs, which need to be maintained and closely monitored during manufacturing, storage and transport, are now well-established including determination of primary



structure and post-translational modifications (e.g., glycosylation), size and aggregation propensity, higher-order structural integrity and biological activities including antigen binding, and in some cases, effector function.<sup>51-53</sup>

In contrast, we evaluated analytical and formulation challenges with a different class of monoclonal antibodies (secretory IgAs) for administration by a different route (oral delivery) for a different application (passive immunization to protect against enteric diseases in the developing world). Specifically, sIgA1, sIgA2 and IgG1 mAbs targeting heat labile enterotoxin (LT), a major virulence factor of Enterotoxigenic *E. coli* (ETEC), were examined in this work. The potential therapeutic use of sIgAs for passive immunization are of particular interest since they are the predominant immunoglobulin isotype in tears, saliva, breast milk, colostrum, and mucosal surfaces such as the gastrointestinal as well as genitourinary tracts.<sup>26</sup> Regardless of ultimate success of using anti-LT sIgA mAbs for passive immunization against ETEC infections *in vivo* (preclinical animal studies ongoing), generation of milligram quantities of these anti-LT sIgA monoclonal antibodies provided the opportunity to evaluate sIgA mAbs in terms of pharmaceutical development challenges including analytical characterization, stabilization and formulation for oral delivery.

One key challenge to perform extensive analytical and formulation evaluations was the limited amount of purified sIgA material that was available given the early stage of

preclinical development. To this end, with only ~5-10 mg of available material for this work, we first developed a series of analytical tools to assess structural integrity, post-translational modifications, size and aggregation, conformational stability, relative solubility and antigen binding activity. In addition, we aimed to perform many of these assessments under conditions of neutral pH as well as more acidic pH (during incubation in an *in vitro* gastric digestion model). The main objective was to not only better understand the key structural attributes of sIgA mAbs when formulated for oral administration, but also to compare the results to the much more widely studied IgG1 mAb. This was accomplished by examining three anti-LT mAbs produced in CHO cells as described above.

A combination of LC-MS peptide mapping, N-glycan analysis and size comparisons under denaturing (SDS-PAGE) and non-denaturing conditions (SEC and SV-AUC) established the increased structural complexity and heterogeneity of sIgA compared to IgG1 mAbs. For example, the multi-chain composition and higher molecular weight of monomeric sIgA mAbs, along with their more abundant and complex glycosylation patterns, were confirmed. In addition, a higher relative percent of higher molecular weight, multimeric species was demonstrated both the sIgA1 and sIgA2 mAbs vs the IgG1 mAb. Nonetheless, the sIgA mAbs were more physically stable and pepsin-resistant (during incubation at 37°C at pH 3.5) and thus likely more suitable for oral

delivery. This is not unexpected considering sIgA is the most abundant antibody isotype in external secretions and mucosal membranes.<sup>20,54</sup> Based on these results, three key structural attributes for sIgA mAbs were identified in this work including (1) N-glycan profiles, (2) size heterogeneity/aggregation and (3) stability under conditions to mimic oral delivery as discussed in more detail below.

When considering the total amount of carbohydrate and N-linked glycosylation profiles, significant differences were observed between sIgA1 vs. sIgA2 (~18% total carbohydrate with 23-24 different N-glycan oligosaccharides) vs. IgG1 (~1% total carbohydrate with 5 different N-glycan oligosaccharides) expressed in CHO cells. It is expected the glycosylation pattern for sIgA mAbs will be a critical structural attribute to monitor since in nature their heavily glycosylated nature facilitates antibody binding to various pathogens and receptors.<sup>36</sup> For example, the N-glycans on the J chain are usually required for dimer or oligomer formation of sIgAs, and can also bind to polymeric immunoglobulin receptors (pIgR).<sup>55</sup> The secretory components (SC) of sIgAs are also heavily glycosylated, and the wide range of N-glycans on the SC creates diverse glycan epitopes, which can function as targets for lectins and bacterial adhesins.<sup>36,56,57</sup> As a result, glycosylated SC can inhibit bacteria adhesion and prevent the establishment of an infection.<sup>57,58</sup> In addition, the galactose-terminating N-glycans are potential ligands for the asialoglycoprotein receptor (ASGP-R) that could mediate the clearance and half-life of

IgAs.<sup>59,60</sup> Although a relatively simpler N-glycan profile was obtained for IgG1, these glycans are required for maintaining protein stability, increasing solubility, maintaining Fc effector functions, and receptor binding (e.g., Fcγ).<sup>36,61</sup> In terms of future work, identification of the O-glycosylation profile for sIgA mAbs will be important to better understand because of the crucial role it may play in pathogen binding. In addition, batch-to-batch variability of the glycan profiles as well as their effects on sIgA mAb stability (in terms of overall flexibility of the hinge region and protection of the hinge region from protease digestion<sup>36</sup>) will be of interest to further evaluate.

As for size heterogeneity of these three anti-LT mAbs, the IgG1 mAb was relatively more homogeneous containing 91-96% monomeric species with smaller amounts of higher molecular weight (HMW) species (4-9%) as measured by SE-HPLC and SV-AUC. In contrast, both sIgA mAbs not only contained much lower amounts of the monomeric sIgA (50-57% for sIgA1 and 18-22% for sIgA2), but also had much higher levels of HMW species (43-50% for sIgA1 and 78-82% for sIgA2). Since there are several cysteine residues in each J-chain that usually form both inter- and intra-chain disulfide bonds, it is likely that disulfide bond scrambling leading to formation of inter-chain disulfide bonds between the tailpiece and cysteine residues in the heavy chains can occur.<sup>62,63</sup> Thus, the J chain has the potential to be a hotspot for cross-linking oligomers for sIgAs.<sup>62-65</sup> In this work and consistent with published data, the J-chain was not detected by SDS-PAGE

under reducing or non-reducing conditions (although it was readily identified by LC-MS peptide mapping).<sup>66</sup> One possible explanation from previous reports is that the J-chain remains associated with light chain of sIgAs as a complex, and thus co-migrated with the light chain<sup>66,67</sup>, although we did not observe such a complex by SDS-PAGE in terms of MW migration (Figure 1B).

It is expected that presence of aggregates will be a critical structural attribute to monitor with sIgAs. Aggregation is of concern with parenterally administered mAbs due to the loss of potency and the potential for anti-drug immune responses that limit efficacy and potentially affect safety.<sup>68</sup> However, it is not known to what extent this would be a concern during oral delivery of sIgAs. In fact, the polymeric nature of sIgA may not necessarily be a negative attribute in terms of efficacy during oral delivery for passive immunization (as long as mAb drug is not lost due to precipitation and no unwanted immune responses are generated). The biological potency of polymeric sIgAs has been previously reported to be preserved along with some protease resistance.<sup>69</sup> Furthermore, polymeric sIgA may elicit intracellular signaling by binding to pIgRs, and potentially inhibit intracellular virus replication.<sup>70-72</sup> Interestingly, polymeric sIgA can display greater activity, when compared to monomeric sIgA, with regards to neutralizing toxins or whole bacterial cells, such as neutralizing proinflammatory antigens located in the apical recycling endosome.<sup>62,73,74</sup> Since it is likely that both covalent crosslinking as well as non-covalent

interactions between sIgA molecules play a key role in formation of multimers, future work will focus on better understanding the aggregation mechanisms of the sIgA mAbs, not only during production but also during long-term storage over time. The batch-to-batch variability of size distribution and aggregate content of sIgAs will also be of interest to further evaluate.

Finally, another potential critical structural attribute identified in this work is the stability of sIgA1, sIgA2 and IgG1 mAbs under conditions that mimic oral delivery. We adapted a previously reported *in vitro* gastric model for evaluating the fate of various food products and supplements during transit through the digestive tract (see Methods).<sup>30</sup> Due to limited material availability, we focused our experiments on a scaled down version of the gastric phase of digestion, since this is the first major stage that is encountered *in vivo* and contains pepsin that can readily degrade proteins.<sup>75</sup> As a preliminary formulation assessment, we also tested a bicarbonate formulation buffer, which has been successfully used as part of a rotavirus vaccination program during oral vaccination.<sup>33</sup> The stability profile of the mAbs was monitored by ELISA, SDS-PAGE and SEC. Although possessing a trend toward relatively lower binding affinity at time zero, sIgA mAbs showed greatly improved stability of antigen binding properties as measured by ELISA over 24 hr incubation in the *in vitro* gastric digestion conditions (37°C, pH 3.5 in the presence of pepsin). The major digestion product after pepsin digestion was the F(ab')<sub>2</sub> fragment for

each of the three mAbs as determined by SDS-PAGE and SE-HPLC. Nevertheless, the antigen binding values varied over time between the three mAbs. These observations indicate that not all F(ab')<sub>2</sub> fragments retained antigen binding activity to the same extent in comparison to the full length, undigested mAbs. Potential conformational structure changes, allosteric effects, and/or glycosylation may influence these properties.<sup>54,76-79</sup> In terms of future work, sIgA stability profiles under conditions that mimic sequential digestion (including oral, gastric, and intestinal phases) should be evaluated to better understand the stability profile of sIgA candidates under conditions that mimic oral delivery. In addition, these *in vitro* digestion models can be utilized in the future to screen for formulation excipients that may help improve stability and retain potency during oral delivery. The concept was established in this work by demonstrating the protective effect of co-addition of bicarbonate buffer in terms of stabilizing the three anti-LT mAbs during incubation in the *in vitro* gastric digestion model (see Figures 7, 8 and 9).

Smaller molecular weight protein therapeutic drugs (e.g., insulin) have been evaluated for systemic use by oral delivery<sup>80-82</sup>, and face several significant barriers including poor stability (due to acidic pH and digestive enzymes) and very low protein bioavailability. It has been reported that advanced drug delivery systems can be used to improve oral delivery of insulin, e.g. polymeric nanoparticles, micelles, liposomes, microspheres, or pH responsive complexation gels.<sup>80,82-84</sup> In contrast, the goal of this work

is local delivery of the sIgA mAbs to bind and neutralize Enterotoxigenic *E. coli* (ETEC) in the GI tract. Thus, passive immunization with sIgA mAbs may be a more successful approach than systematic delivery by the oral route of administration. However, for passive immunization applications in low-income and developing countries, low cost formulations of sIgA mAbs for treatment of diarrheal diseases is critical, making the use of complex formulations such as advanced delivery technologies less desirable. Thus, longer term, simple liquid formulations (perhaps as an oral supplement) that provide good long-term storage stability of the sIgA mAbs, and also provide protection from acidic pH/proteases degradation during oral delivery would be ideal. In the shorter term, the goal is to facilitate first-in-human clinical studies with sIgA mAbs, not only by further developing the analytical tools utilized in this work to reproducibly prepare and quality control test sIgA mAbs as therapeutic drug candidates, but also to design stabilized formulations for oral administration for use in initial clinical studies.



## 4.5. References

1. Troeger C, Forouzanfar M, Rao PC, Khalil I, Brown A, Reiner RC, Fullman N, Thompson RL, Abajobir A, Ahmed M, Alemayohu MA, Alvis-Guzman N, Amare AT, Antonio CA, Asayesh H, Avokpaho E, Awasthi A, Bacha U, Barac A, Betsue BD, Beyene AS, Boneya DJ, Malta DC, Dandona L, Dandona R, Dubey M, Eshrati B, Fitchett JRA, Gebrehiwot TT, Hailu GB, Horino M, Hotez PJ, Jibat T, Jonas JB, Kasaeian A, Kissoon N, Kotloff K, Koyanagi A, Kumar GA, Rai RK, Lal A, El Razek HMA, Mengistie MA, Moe C, Patton G, Platts-Mills JA, Qorbani M, Ram U, Roba HS, Sanabria J, Sartorius B, Sawhney M, Shigematsu M, Sreeramareddy C, Swaminathan S, Tedla BA, Jagiellonian RT-M, Ukwaja K, Werdecker A, Widdowson M-A, Yonemoto N, El Sayed Zaki M, Lim SS, Naghavi M, Vos T, Hay SI, Murray CJL, Mokdad AH 2017. Estimates of global, regional, and national morbidity, mortality, and aetiologies of diarrhoeal diseases: a systematic analysis for the Global Burden of Disease Study 2015. *The Lancet Infectious Diseases* 17(9):909-948.
2. Troeger C, Colombara DV, Rao PC, Khalil IA, Brown A, Brewer TG, Guerrant RL, Houpt ER, Kotloff KL, Misra K, Petri WA, Platts-Mills J, Riddle MS, Swartz SJ, Forouzanfar MH, Reiner RC, Hay SI, Mokdad AH 2018. Global disability-adjusted life-year estimates of long-term health burden and undernutrition attributable to diarrhoeal diseases in children younger than 5 years. *The Lancet Global Health* 6(3):e255-e269.
3. 2018 WHO. 2016. Global Health Estimates 2016: Deaths by Cause, Age, Sex, by Country and by Region, 2000-2016. Geneva., ed., <http://www.who.int/news-room/fact-sheets/detail/the-top-10-causes-of-death>.
4. Zhang W, Sack DA 2015. Current Progress in Developing Subunit Vaccines against Enterotoxigenic Escherichia coli-Associated Diarrhea. *Clin Vaccine Immunol* 22(9):983-991.
5. Fischer Walker CL, Perin J, Aryee MJ, Boschi-Pinto C, Black RE 2012. Diarrhea incidence in low- and middle-income countries in 1990 and 2010: a systematic review. *BMC Public Health* 12:220.
6. United Nations Children's Fund (UNICEF). 2013. [http://www.unicef.org/publications/files/APR\\_Progress\\_Report\\_2013\\_9\\_Sept\\_2013.pdf](http://www.unicef.org/publications/files/APR_Progress_Report_2013_9_Sept_2013.pdf).
7. Svennerholm A-M, Tobias J 2008. Vaccines against enterotoxigenic Escherichia coli. *Expert Review of Vaccines* 7(6):795-804.
8. Bourgeois AL, Wierzba TF, Walker RI 2016. Status of vaccine research and development for enterotoxigenic Escherichia coli. *Vaccine* 34(26):2880-2886.
9. Kotloff KL, Nataro JP, Blackwelder WC, Nasrin D, Farag TH, Panchalingam S, Wu Y, Sow SO, Sur D, Breiman RF, Faruque ASG, Zaidi AKM, Saha D, Alonso PL, Tamboura B, Sanogo D, Onwuchekwa U, Manna B, Ramamurthy T, Kanungo S, Ochieng JB, Omore R, Oundo JO, Hossain A, Das SK, Ahmed S, Qureshi S, Quadri F, Adegbola RA, Antonio M, Hossain MJ, Akinsola A, Mandomando I, Nhampossa T, Acácio S, Biswas K, O'Reilly CE, Mintz ED, Berkeley LY, Muhsen K, Sommerfelt H, Robins-Browne RM, Levine MM 2013. Burden and aetiology of diarrhoeal disease in infants and young children in developing countries (the Global Enteric Multicenter Study, GEMS): a prospective, case-control study. *The Lancet* 382(9888):209-222.

10. Ahmed T, Bhuiyan TR, Zaman K, Sinclair D, Qadri F 2013. Vaccines for preventing enterotoxigenic *Escherichia coli* (ETEC) diarrhoea. *Cochrane Database Syst Rev* (7):CD009029.
11. Giuntini S, Stoppato M, Sedic M, Ejemel M, Pondish JR, Wisheart D, Schiller ZA, Thomas WD, Barry EM, Cavacini LA 2018. Identification and Characterization of Human Monoclonal Antibodies for Immunoprophylaxis Against Enterotoxigenic *Escherichia coli* Infection. *Infection and immunity:IAI*. 00355-00318.
12. Teresa E-G, Jorge FC, Leova P-G, Raúl FV, Theresa JO, Javier T, Herbert LD 2005. Drug-resistant Diarrheogenic *Escherichia coli*, Mexico *Emerging Infectious Disease Journal* 11(8):1306.
13. Ochoa TJ, Ecker L, Barletta F, Mispireta ML, Gil AI, Contreras C, Molina M, Amemiya I, Verastegui H, Hall ER, Cleary TG, Lanata CF 2009. Age-related susceptibility to infection with diarrheagenic *Escherichia coli* among infants from Periurban areas in Lima, Peru. *Clin Infect Dis* 49(11):1694-1702.
14. Zhang W, Sack DA 2012. Progress and hurdles in the development of vaccines against enterotoxigenic *Escherichia coli* in humans. *Expert review of vaccines* 11(6):677-694.
15. MacLennan CA, Saul A 2014. Vaccines against poverty. *Proceedings of the National Academy of Sciences* 111(34):12307-12312.
16. PATH. 2011 The case for investment in enterotoxigenic *Escherichia coli* vaccines. PATH, Seattle, WA.
17. Sack DA 2012. Progress and hurdles in the development of vaccines against enterotoxigenic *Escherichia coli* in humans AU - Zhang, Weiping. *Expert Review of Vaccines* 11(6):677-694.
18. Rodrigues JF, Mathias-Santos C, Sbrogio-Almeida ME, Amorim JH, Cabrera-Crespo J, Balan A, Ferreira LC 2011. Functional diversity of heat-labile toxins (LT) produced by enterotoxigenic *Escherichia coli*: differential enzymatic and immunological activities of LT1 (hLT) AND LT4 (pLT). *J Biol Chem* 286(7):5222-5233.
19. Johnson AM, Kaushik RS, Francis DH, Fleckenstein JM, Hardwidge PR 2009. Heat-labile enterotoxin promotes *Escherichia coli* adherence to intestinal epithelial cells. *J Bacteriol* 191(1):178-186.
20. Woof JM, Kerr MA 2006. The function of immunoglobulin A in immunity. *The Journal of Pathology: A Journal of the Pathological Society of Great Britain and Ireland* 208(2):270-282.
21. Corthesy B 2013. Multi-faceted functions of secretory IgA at mucosal surfaces. *Front Immunol* 4:185.
22. Mantis NJ, Rol N, Corthesy B 2011. Secretory IgA's complex roles in immunity and mucosal homeostasis in the gut. *Mucosal Immunol* 4(6):603-611.
23. Boullier S, Tanguy M, Kadaoui KA, Caubet C, Sansonetti P, Corthesy B, Phalipon A 2009. Secretory IgA-mediated neutralization of *Shigella flexneri* prevents intestinal tissue destruction by down-regulating inflammatory circuits. *J Immunol* 183(9):5879-5885.
24. Macpherson AJ, McCoy KD, Johansen FE, Brandtzaeg P 2008. The immune geography of IgA induction and function. *Mucosal Immunol* 1(1):11-22.
25. Phalipon A, Cardona A, Kraehenbuhl J-P, Edelman L, Sansonetti PJ, Corthésy B 2002. Secretory component: a new role in secretory IgA-mediated immune exclusion in vivo. *Immunity* 17(1):107-115.

26. Woof JM, Russell MW 2011. Structure and function relationships in IgA. *Mucosal Immunol* 4(6):590-597.
27. Moor K, Diard M, Sellin ME, Felmy B, Wotzka SY, Toska A, Bakkeren E, Arnoldini M, Bansept F, Co AD, Voller T, Minola A, Fernandez-Rodriguez B, Agatic G, Barbieri S, Piccoli L, Casiraghi C, Corti D, Lanzavecchia A, Regoes RR, Loverdo C, Stocker R, Brumley DR, Hardt WD, Slack E 2017. High-avidity IgA protects the intestine by enchainning growing bacteria. *Nature* 544(7651):498-502.
28. Gill SC, von Hippel PH 1989. Calculation of protein extinction coefficients from amino acid sequence data. *Analytical Biochemistry* 182(2):319-326.
29. NIBRT-Waters. Glycan 3+ database, <http://www.glycobase.nibr.ie:8080/glycobase>. ed.
30. Menard O, Bourlieu C, De Oliveira SC, Dellarosa N, Laghi L, Carriere F, Capozzi F, Dupont D, Deglaire A 2018. A first step towards a consensus static in vitro model for simulating full-term infant digestion. *Food Chem* 240:338-345.
31. Gibson TJ, McCarty K, McFadyen IJ, Cash E, Dalmonte P, Hinds KD, Dinerman AA, Alvarez JC, Volkin DB 2011. Application of a high-throughput screening procedure with PEG-induced precipitation to compare relative protein solubility during formulation development with IgG1 monoclonal antibodies. *J Pharm Sci* 100(3):1009-1021.
32. Toprani VM, Joshi SB, Kuelto LA, Schwartz RM, Middaugh CR, Volkin DB 2016. A Micro-Polyethylene Glycol Precipitation Assay as a Relative Solubility Screening Tool for Monoclonal Antibody Design and Formulation Development. *J Pharm Sci* 105(8):2319-2327.
33. Vadrevu KM, Prasad SD. 2015. Rotavirus vaccine compositions and process for preparing the same. ed.: Google Patents.
34. Goritzer K, Maresch D, Altmann F, Obinger C, Strasser R 2017. Exploring Site-Specific N-Glycosylation of HEK293 and Plant-Produced Human IgA Isotypes. *J Proteome Res* 16(7):2560-2570.
35. !!! INVALID CITATION !!! 29.
36. Arnold JN, Wormald MR, Sim RB, Rudd PM, Dwek RA 2007. The impact of glycosylation on the biological function and structure of human immunoglobulins. *Annu Rev Immunol* 25:21-50.
37. Kaartinen M, Imir T, Klockars M, Sandholm M, Makela O 1978. IgA in blood and thoracic duct lymph: concentration and degree of polymerization. *Scandinavian journal of immunology* 7(3):229-230.
38. Rifai A, Chen A, Imai H 1987. Complement activation in experimental IgA nephropathy: An antigen-mediated process. *Kidney international* 32(6):838-844.
39. Todinova S, Krumova S, Gartcheva L, Dimitrova K, Petkova V, Taneva SG 2018. Calorimetric manifestation of IgA monoclonal immunoglobulins in multiple myeloma sera. *Thermochimica Acta* 666:208-211.
40. Hu Z, Zhang H, Haley B, Macchi F, Yang F, Misaghi S, Elich J, Yang R, Tang Y, Joly JC, Snedecor BR, Shen A 2016. Carboxypeptidase D is the only enzyme responsible for antibody C-terminal lysine cleavage in Chinese hamster ovary (CHO) cells. *Biotechnol Bioeng* 113(10):2100-2106.
41. Chelius D, Jing K, Lueras A, Rehder DS, Dillon TM, Vizel A, Rajan RS, Li T, Treuheit MJ, Bondarenko PV 2006. Formation of pyroglutamic acid from N-terminal glutamic acid in immunoglobulin gamma antibodies. *Analytical chemistry* 78(7):2370-2376.

42. Sola RJ, Griebenow K 2009. Effects of glycosylation on the stability of protein pharmaceuticals. *J Pharm Sci* 98(4):1223-1245.
43. Kam RK, Poon TC 2008. The potentials of glycomics in biomarker discovery. *Clinical Proteomics* 4(3):67.
44. Sinclair AM, Elliott S 2005. Glycoengineering: the effect of glycosylation on the properties of therapeutic proteins. *J Pharm Sci* 94(8):1626-1635.
45. Shriver Z, Raguram S, Sasisekharan R 2004. Glycomics: a pathway to a class of new and improved therapeutics. *Nat Rev Drug Discov* 3(10):863-873.
46. Gray VA, Cole E, Toma JMR, Ghidorsi L, Guo J-H, Han J-H, Han F, Hosty CT, Kochling JD, Kraemer J 2014. Use of enzymes in the dissolution testing of gelatin capsules and gelatin-coated tablets--revisions to Dissolution< 711> and Disintegration and Dissolution of Dietary Supplements< 2040. *Dissolution Technologies* 21(4):6-20.
47. Kihara M 2015. Temperature and pH dependency of pepsin activity in the gastric juice of farmed Pacific bluefin tuna *Thunnus orientalis*. *Aquaculture Science* 63(4):459-461.
48. Motyan JA, Toth F, Tozser J 2013. Research applications of proteolytic enzymes in molecular biology. *Biomolecules* 3(4):923-942.
49. Crivianu-Gaita V, Romaschin A, Thompson M 2015. High efficiency reduction capability for the formation of Fab antibody fragments from F(ab)<sub>2</sub> units. *Biochem Biophys Rep* 2:23-28.
50. Chames P, Van Regenmortel M, Weiss E, Baty D 2009. Therapeutic antibodies: successes, limitations and hopes for the future. *British Journal of Pharmacology* 157(2):220-233.
51. Federici M, Lubiniecki A, Manikwar P, Volkin DB 2013. Analytical lessons learned from selected therapeutic protein drug comparability studies. *Biologicals* 41(3):131-147.
52. Lubiniecki A, Volkin DB, Federici M, Bond MD, Nedved ML, Hendricks L, Mehndiratta P, Bruner M, Burman S, DalMonte P 2011. Comparability assessments of process and product changes made during development of two different monoclonal antibodies. *Biologicals* 39(1):9-22.
53. Alsenaidy MA, Jain NK, Kim JH, Middaugh CR, Volkin DB 2014. Protein comparability assessments and potential applicability of high throughput biophysical methods and data visualization tools to compare physical stability profiles. *Frontiers in pharmacology* 5:39.
54. Reilly RM, Domingo R, Sandhu J 1997. Oral delivery of antibodies. *Clinical pharmacokinetics* 32(4):313-323.
55. Johansen F-E, Braathen R, Brandtzaeg P 2001. The J chain is essential for polymeric Ig receptor-mediated epithelial transport of IgA. *The Journal of Immunology* 167(9):5185-5192.
56. Royle L, Roos A, Harvey DJ, Wormald MR, Van Gijlswijk-Janssen D, Redwan E-RM, Wilson IA, Daha MR, Dwek RA, Rudd PM 2003. Secretory IgA N- and O-glycans provide a link between the innate and adaptive immune systems. *Journal of Biological Chemistry* 278(22):20140-20153.
57. Wold AE, Mestecky J, Tomana M, Kobata A, Ohbayashi H, Endo T, Edén CS 1990. Secretory immunoglobulin A carries oligosaccharide receptors for *Escherichia coli* type 1 fimbrial lectin. *Infection and immunity* 58(9):3073-3077.

58. Boren T, Falk P, Roth KA, Larson G, Normark S 1993. Attachment of *Helicobacter pylori* to human gastric epithelium mediated by blood group antigens. *Science* 262(5141):1892-1895.
59. Basset C, Devauchelle V, Durand V, Jamin C, Pennec Y, Youinou P, Dueymes M 1999. Glycosylation of immunoglobulin A influences its receptor binding. *Scandinavian journal of immunology* 50(6):572-579.
60. Stockert RJ 1995. The asialoglycoprotein receptor: relationships between structure, function, and expression. *Physiological reviews* 75(3):591-609.
61. More AS, Toprani VM, Okbazghi SZ, Kim JH, Joshi SB, Middaugh CR, Tolbert TJ, Volkin DB 2016. Correlating the impact of well-defined oligosaccharide structures on physical stability profiles of IgG1-Fc glycoforms. *Journal of pharmaceutical sciences* 105(2):588-601.
62. Schroeder HW, Jr., Cavacini L 2010. Structure and function of immunoglobulins. *J Allergy Clin Immunol* 125(2 Suppl 2):S41-52.
63. Roos A, Bouwman LH, van Gijlswijk-Janssen DJ, Faber-Krol MC, Stahl GL, Daha MR 2001. Human IgA activates the complement system via the mannan-binding lectin pathway. *The Journal of Immunology* 167(5):2861-2868.
64. Delacroix DL, Dive C, Rambaud J, Vaerman J 1982. IgA subclasses in various secretions and in serum. *Immunology* 47(2):383.
65. British Society of Immunology. <https://www.immunology.org/public-information/bitesized-immunology/receptors-and-molecules/immunoglobulin-iga>. ed.
66. Sedykh SE, Buneva VN, Nevinsky GA 2012. Human milk sIgA molecules contain various combinations of different antigen-binding sites resulting in a multiple binding specificity of antibodies and enzymatic activities of abzymes. *PLoS One* 7(11):e48756.
67. Starykovych M, Bilyy R, Semenov D, Richter V, Stoika R, Kit Y Secretory IgA-abzymes hydrolyzing both histone H1 and myelin basic protein are present in colostrum of healthy mothers.
68. Ratanji KD, Derrick JP, Dearman RJ, Kimber I 2014. Immunogenicity of therapeutic proteins: influence of aggregation. *Journal of immunotoxicology* 11(2):99-109.
69. Longet S, Miled S, Lötscher M, Miescher SM, Zuercher AW, Corthésy B 2013. Human plasma-derived polymeric IgA and IgM antibodies associate with secretory component to yield biologically active secretory-like antibodies. *Journal of Biological Chemistry* 288(6):4085-4094.
70. Giffroy D, Courtoy PJ, Vaerman JP 2001. Polymeric IgA binding to the human pIgR elicits intracellular signalling, but fails to stimulate pIgR-transcytosis. *Scandinavian journal of immunology* 53(1):56-64.
71. Corthesy B 2013. Role of secretory IgA in infection and maintenance of homeostasis. *Autoimmunity reviews* 12(6):661-665.
72. Fujioka H, Emancipator SN, Aikawa M, Huang DS, Blatnik F, Karban T, DeFife K, Mazanec MB 1998. Immunocytochemical colocalization of specific immunoglobulin A with sendai virus protein in infected polarized epithelium. *Journal of Experimental Medicine* 188(7):1223-1229.
73. Stubbe H, Berdoz J, Kraehenbuhl J-P, Corthésy B 2000. Polymeric IgA is superior to monomeric IgA and IgG carrying the same variable domain in preventing *Clostridium difficile* toxin A damaging of T84 monolayers. *The Journal of Immunology* 164(4):1952-1960.

74. Fernandez MI, Pedron T, Tournebize R, Olivo-Marin J-C, Sansonetti PJ, Phalipon A 2003. Anti-inflammatory role for intracellular dimeric immunoglobulin a by neutralization of lipopolysaccharide in epithelial cells. *Immunity* 18(6):739-749.
75. Kay RN, Davies AG 1994. Digestive physiology. Colobine monkeys: Their ecology, behaviour and evolution:229-249.
76. Krapp S, Mimura Y, Jefferis R, Huber R, Sondermann P 2003. Structural Analysis of Human IgG-Fc Glycoforms Reveals a Correlation Between Glycosylation and Structural Integrity. *Journal of Molecular Biology* 325(5):979-989.
77. McCoy AJ, Pei XY, Skinner R, Abrahams J-P, Carrell RW 2003. Structure of  $\beta$ -antithrombin and the effect of glycosylation on antithrombin's heparin affinity and activity. *Journal of molecular biology* 326(3):823-833.
78. Wang R, Lai L, Wang S 2002. Further development and validation of empirical scoring functions for structure-based binding affinity prediction. *Journal of computer-aided molecular design* 16(1):11-26.
79. Creighton TE. 1993. *Proteins: structures and molecular properties*. ed.: Macmillan.
80. Lowman A, Morishita M, Kajita M, Nagai T, Peppas N 1999. Oral delivery of insulin using pH-responsive complexation gels. *Journal of pharmaceutical sciences* 88(9):933-937.
81. Damgé C, Maincent P, Ubrich N 2007. Oral delivery of insulin associated to polymeric nanoparticles in diabetic rats. *Journal of controlled release* 117(2):163-170.
82. Alai MS, Lin WJ, Pingale SS 2015. Application of polymeric nanoparticles and micelles in insulin oral delivery. *journal of food and drug analysis* 23(3):351-358.
83. Kisel M, Kulik L, Tsybovsky I, Vlasov A, Vorob'Yov M, Kholodova E, Zabarovskaya Z 2001. Liposomes with phosphatidylethanol as a carrier for oral delivery of insulin: studies in the rat. *International journal of pharmaceutics* 216(1-2):105-114.
84. Zhang Y, Wei W, Lv P, Wang L, Ma G 2011. Preparation and evaluation of alginate–chitosan microspheres for oral delivery of insulin. *European Journal of pharmaceutics and biopharmaceutics* 77(1):11-19.

## 4.6. Figures and Tables

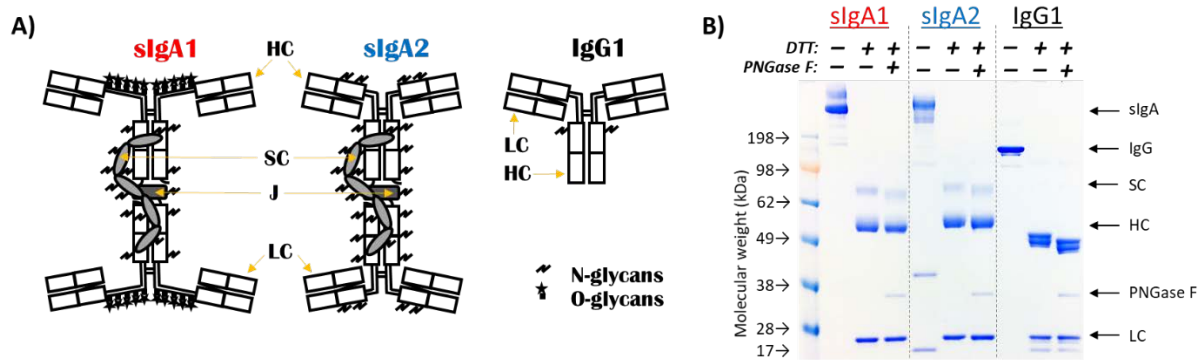


**Figure 4.1.** Structural overview and SDS-PAGE purity analysis of slgA1, slgA2 and IgG1 mAbs used in this study. (A) Schematic representation of immunoglobulin domains within slgA1, slgA2, and IgG1 antibodies. The LC, HC, SC and J polypeptide chains, along with sites of post-translational N- and O-linked glycosylation, are indicated (see text). (B) Representative SDS-PAGE analysis of three anti-LT mAbs under non-reducing and reducing conditions with and without removal of N-glycans by PNGase F treatment. The molecular weight markers are on the far left lane. All bands assignments were based on molecular weight migration only.

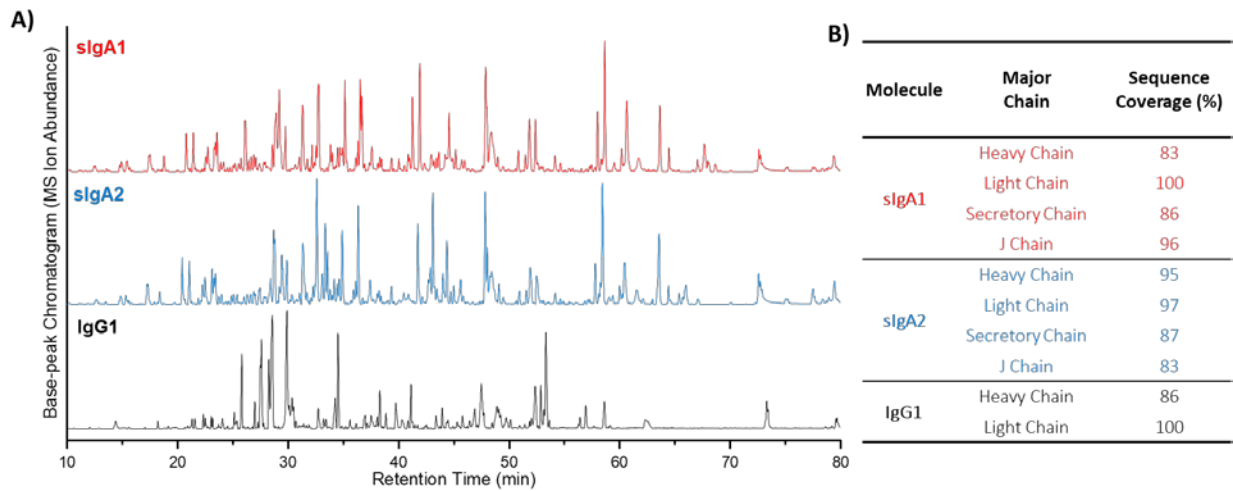


**Figure 4.2.** Representative LC-MS peptide mapping chromatograms of slgA1, slgA2 and IgG1 to confirm the primary sequence of each mAb and to evaluate for chemical post-translational modifications (see text). (A) Representative LC base peak chromatograms of each mAb after trypsin digestion; (B) Percentage primary sequence coverage on each polypeptide chain found in each of the three mAbs.



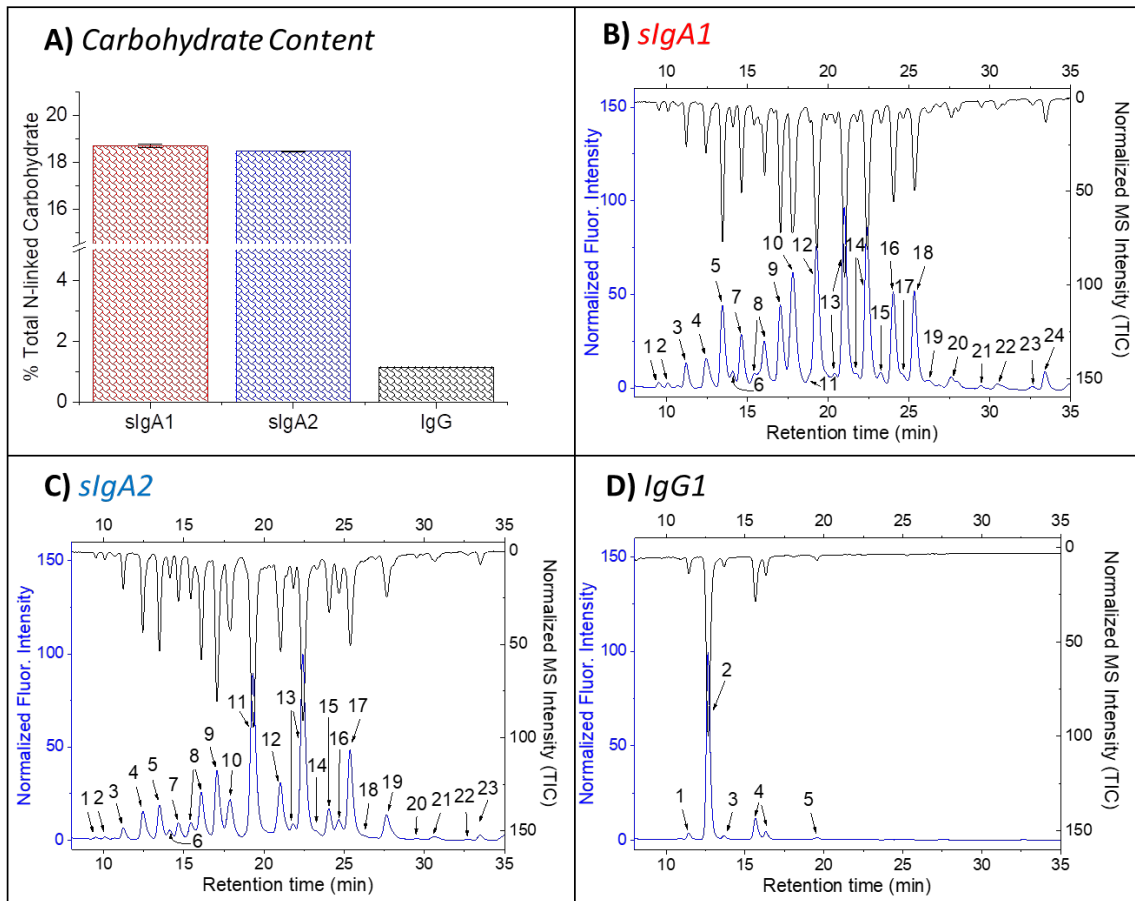


**Figure 4.3.** Glycosylation analysis of sIgA1, sIgA2 and IgG1 mAbs produced in CHO cells. (A) total carbohydrate content. (B, C, D) Representative chromatographic profiles of Fluor-MS N-linked glycans removed from the mAbs are shown for (B) sIgA1, (C) sIgA2, and (D) IgG1. Fluorescence and mass spectrometry results are indicated and peaks are numbered as a series of different N-glycans. See Figure 4 for summary of results. All data are presented as mean  $\pm$  SD; n = 3.

N-glycan	Structure	% Percentage		
		<i>slgA1</i>	<i>slgA2</i>	IgG1
G0-GN		0.3	0.2	-
Man4		0.2	0.1	-
G0		1.8	1.2	2.5
G0F		3.0	3.5	81.4
Man5		6.0	3.1	0.9
G1F-GN		0.3	0.3	-
G1		3.7	1.3	-
G1F		4.6	6.9	14.2
Man6		5.5	6.9	-
G2		10.5	3.7	-
G1F+NANA		0.2	-	-
G2F		12.9	24.4	1.1

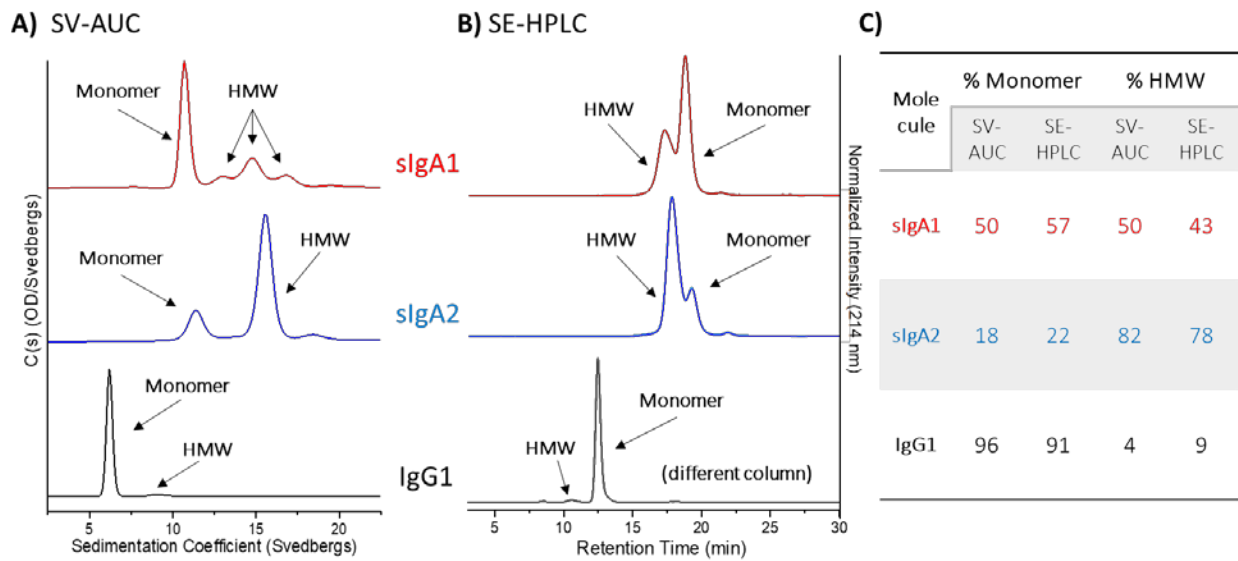
  

N-glycan	Structure	% Percentage		
		<i>slgA1</i>	<i>slgA2</i>	IgG1
G2+NANA		16.5	6.4	-
G2F+NANA		13.5	22.9	-
G2FGal1		0.3	0.3	-
G2+2NANA		7.8	2.4	-
G2F+NGNA		0.3	0.8	-
G2F+2NANA		8.1	10.1	-
G2FGal1+NANA		0.3	0.1	-
Man9		1.5	3.9	-
G3+2NANA		0.2	0.1	-
G3F+2NANA		0.7	0.5	-
G3+3NANA		0.3	0.1	-
G3F+3NANA		1.7	0.6	-

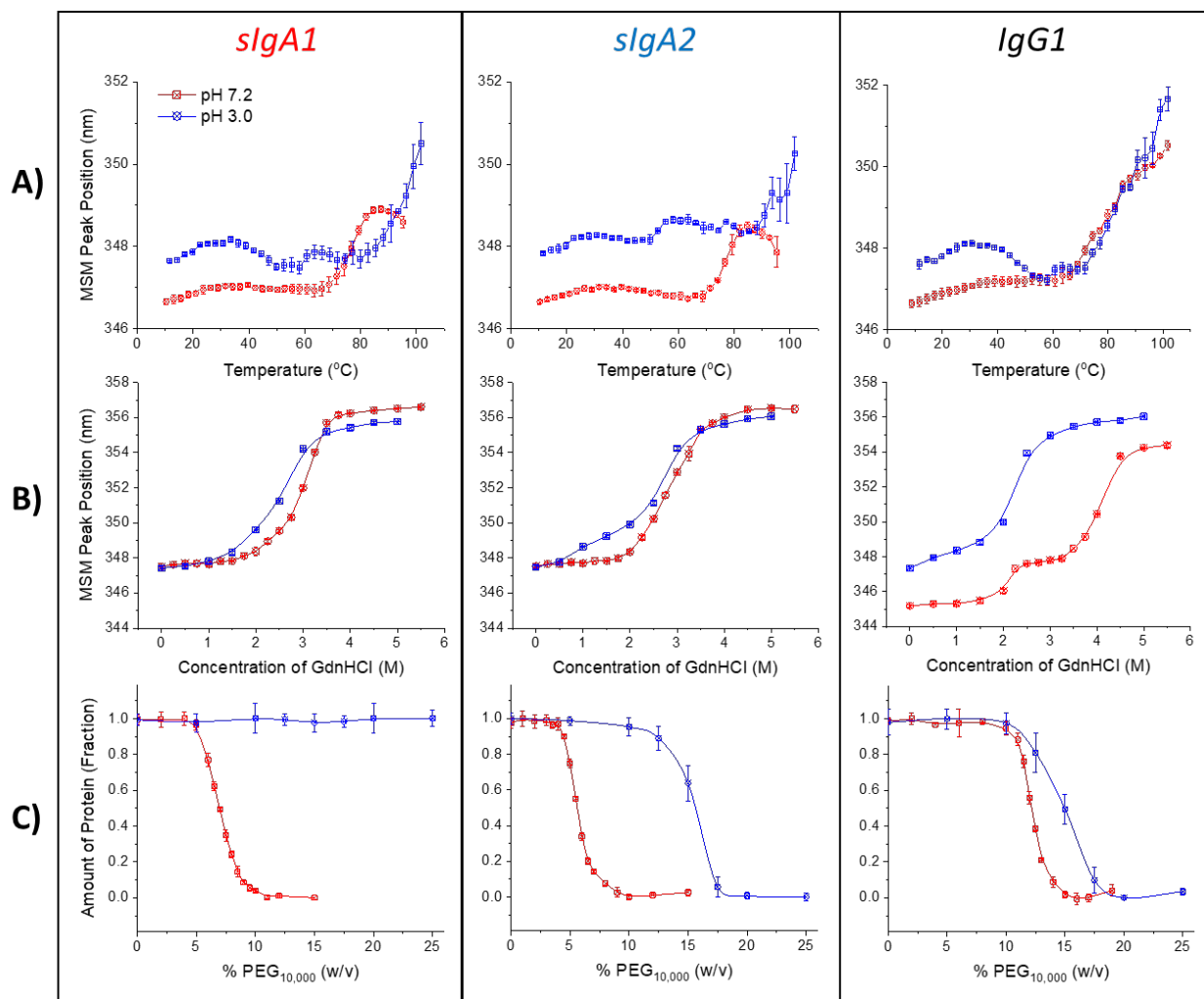
  

N-acetylglucosamine (GlcNAc or GN)	Fucose (Fuc)
Mannose (Man)	Sialic acid (Neu5Ac or NANA)
Galactose (Gal)	N-glycolylneuraminic acid (NGNA)

**Figure 4.4.** Identification and percent composition of each N-glycan type found in *slgA1*, *slgA2* and IgG1 mAbs (produced in CHO cells) as determined by Fluor-MS N-linked glycan analysis. The total number of N-glycans, their respective oxford notations and structures, as well as the relative percentage of the total N-glycans for each mAb is shown. See Figure 3 for representative chromatograms. All data are presented as an average value; n = 3.



**Figure 4.5.** Size analysis of anti-LT sIgA1, sIgA2 and IgG1 mAbs as measured by SV-AUC and SE-HPLC. (A) Representative SV-AUC analysis of the three mAbs. Peaks (monomer or HMW species) were assigned based on sedimentation coefficient values and estimated molecular weight determinations as shown in Supplemental Table S1. (B) Representative SE-HPLC chromatograms of the three mAbs. Peaks (monomer or HMW species) were assigned based retention time values and estimated molecular weight values (based on gel filtration standards) are shown in Supplemental Table S1. Note, a different SEC column was used for IgG1 vs. the two sIgAs mAbs. (C) Relative amount of each species calculated based on the total peak areas for both SV-AUC and SE-HPLC. Representative SV-AUC profiles and SEC chromatograms are shown and percent species are presented as average value; n = 2 for SV-AUC and n = 3 for SE-HPLC, with range and standard deviation values of 0.1 to 4.4% and from 0.1 to 0.6%, respectively.



**Figure 4.6.** Comparison of conformational stability and relative apparent solubility profiles of anti-LT *slgA1*, *slgA2*, and *IgG1* mAbs at pH 7.2 vs. pH 3.0. (A) thermal unfolding as measured by the shift of MSM peak position as a function of temperature, and (B) GdnHCl unfolding as a function of denaturant concentration, both measured by intrinsic Trp fluorescence spectroscopy. (C) relative protein concentration of each mAb as a function of PEG<sub>10,000</sub> concentration (w/v) as measured by UV-visible spectroscopy. All data are presented as mean  $\pm$  SD; n = 3.

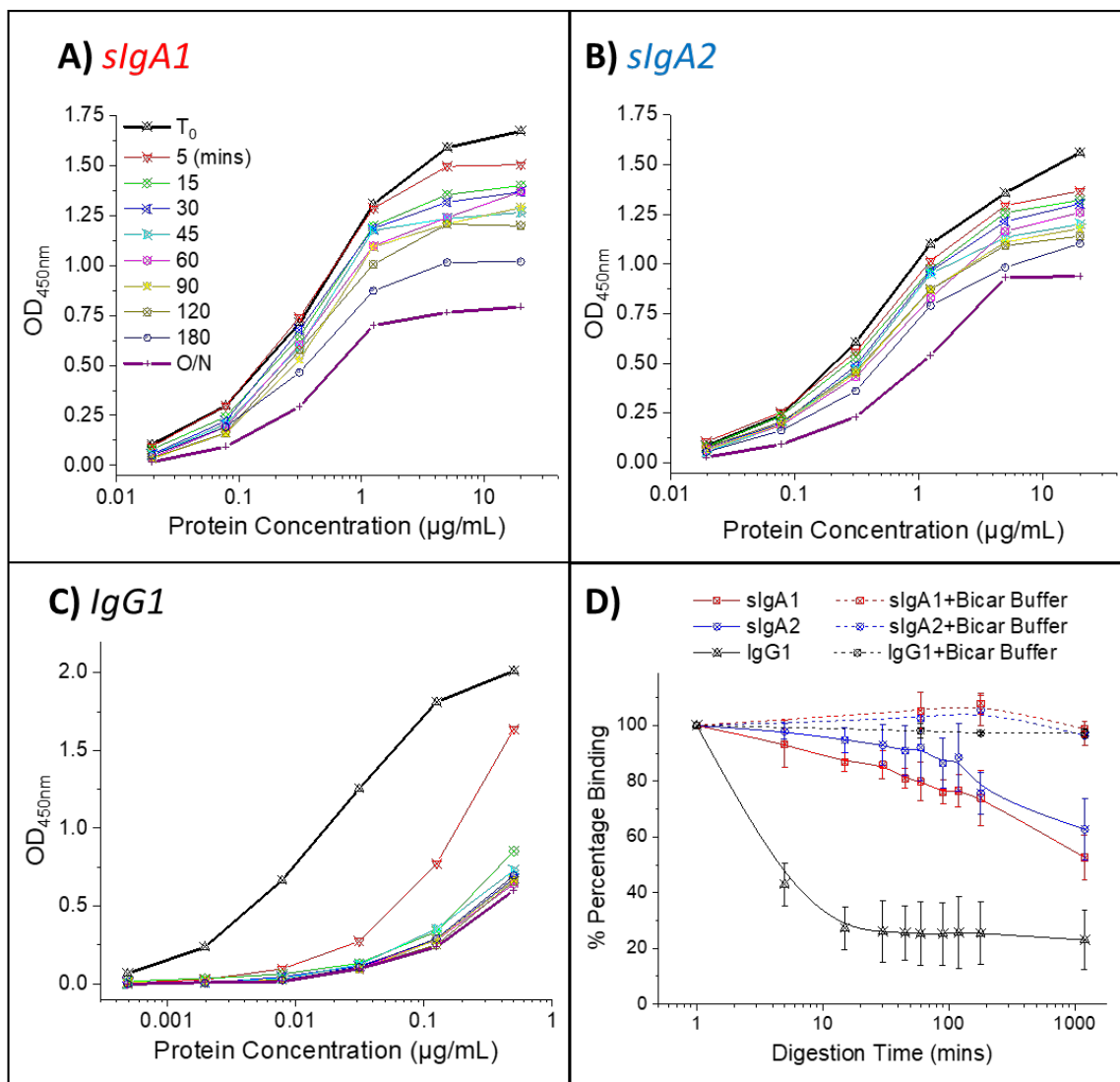


**Figure 4.7.** Comparison of LT-antigen binding curves for the three anti-LT mAbs after incubation in the *in vitro* gastric digestion model as measured by ELISA including (A) *slgA1*, (B) *slgA2*, and (C) *IgG1*. (D) Comparison of the relative percent LT antigen binding remaining for each of the three mAbs based on normalization to the time zero binding curve (with or without bicarbonate buffer) are displayed (mean  $\pm$  SD; n = 3).

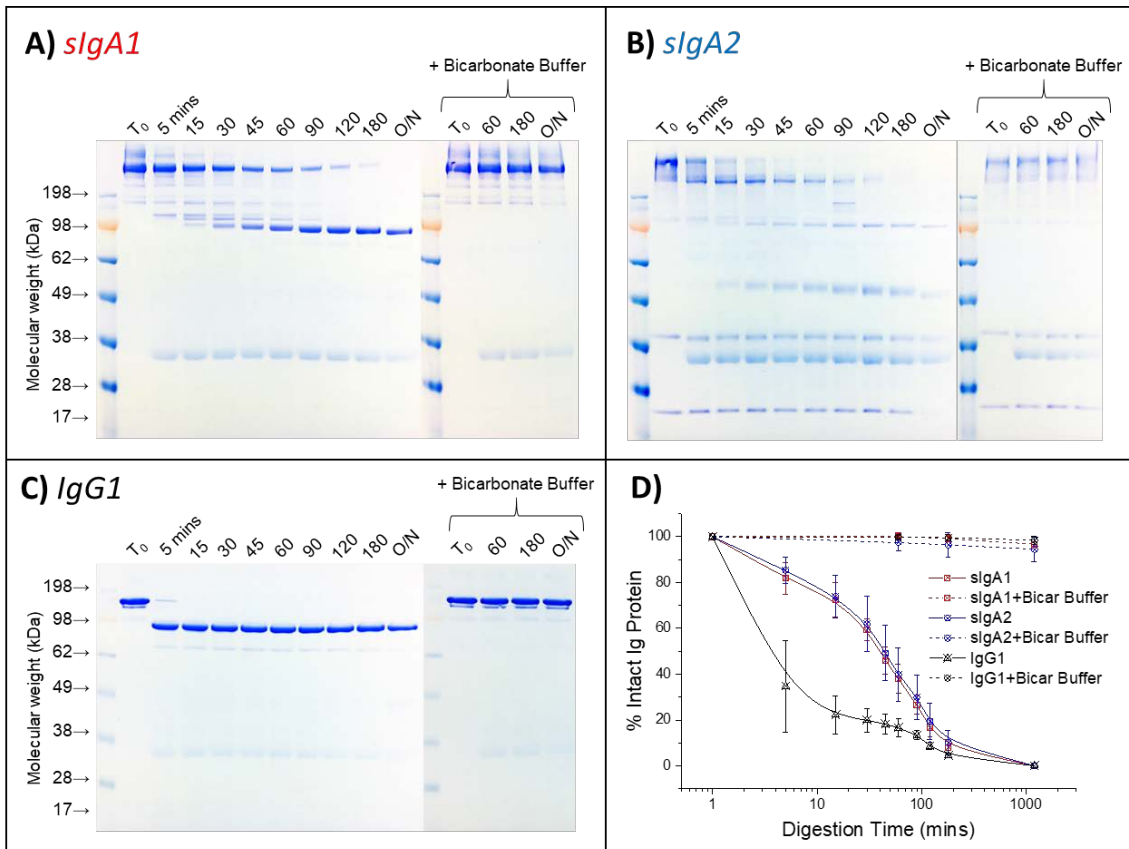


**Figure 4.8.** Comparison of structural integrity of the three anti-LT mAbs after incubation in the *in vitro* gastric digestion model as measured by SDS-PAGE: (A) slgA1, (B) slgA2, and (C) IgG1. Representative SDS-PAGE results of digested mAb samples by time course with or without co-addition of sodium bicarbonate buffer (0.03 M trisodium citrate and 0.3 M sodium bicarbonate at pH 8.5) (D) Comparison of the relative percent main species remaining over time for each of the three mAbs based on densitometry analysis of the main species (intact mAb) normalized to values at time zero (mean  $\pm$  SD; n = 3).

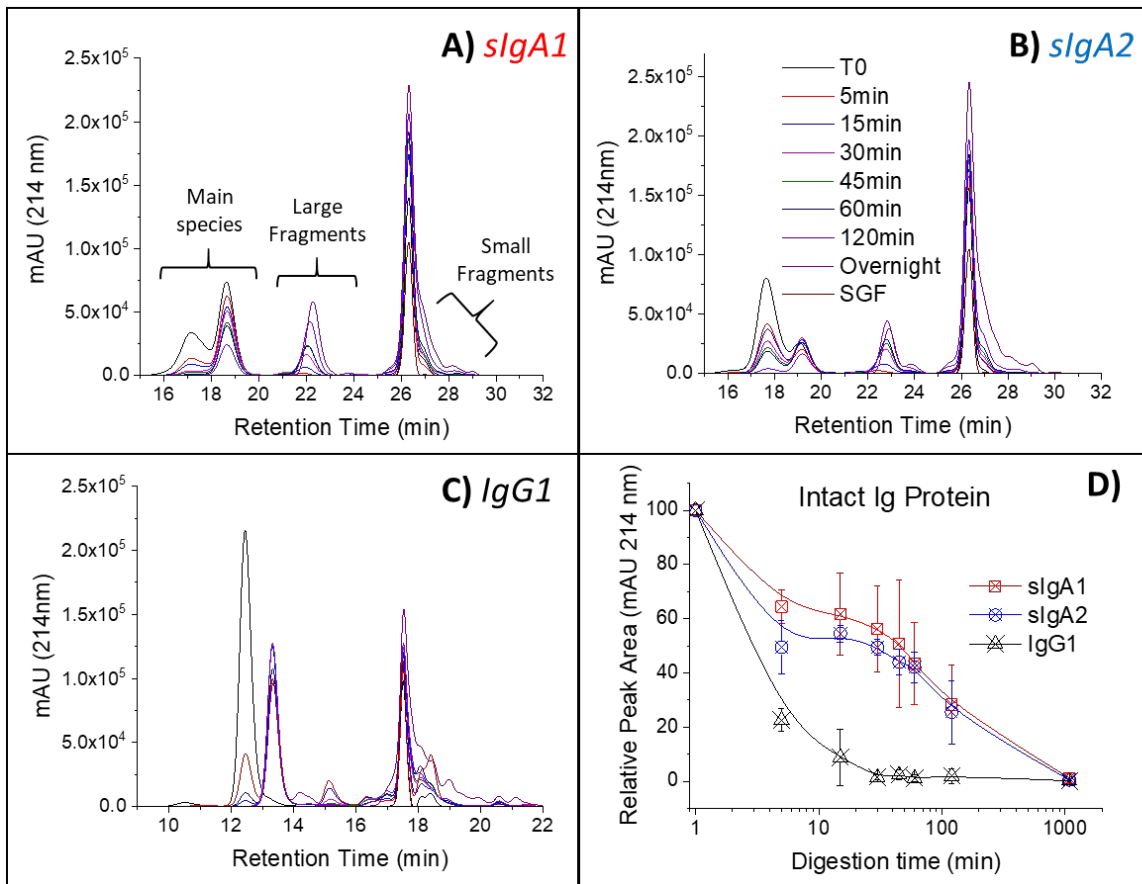


**Figure 4.9.** Comparison of the structural integrity of the three anti-LT mAbs during incubation in the *in vitro* gastric digestion model as measured by SE-HPLC: (A) slgA1, (B) slgA2, and (C) IgG1. Representative SE-HPLC chromatograms with UV 214nm detection are displayed. Samples were incubated in presence of immobilized pepsin as a function of time and analyzed after removal of pepsin-agarose. (D) Comparison of the relative percent main species remaining over time for each of the three mAbs based on main SEC peak integration and normalization to time zero (mean  $\pm$  SD; n = 3).

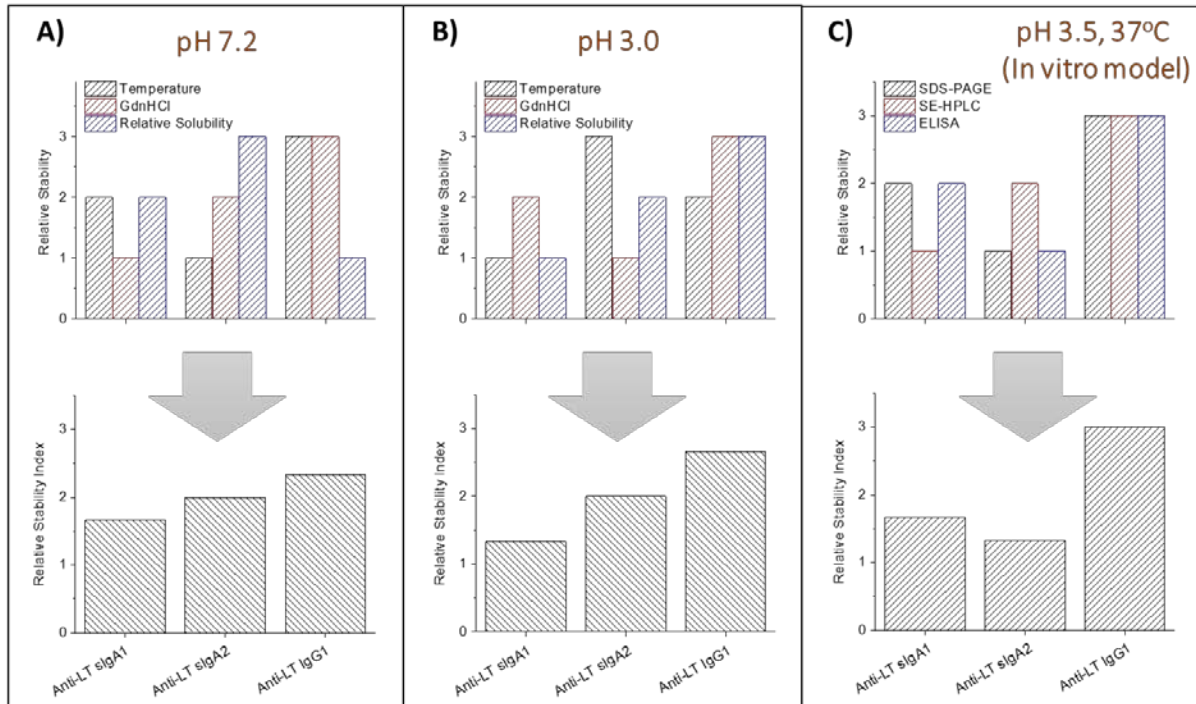
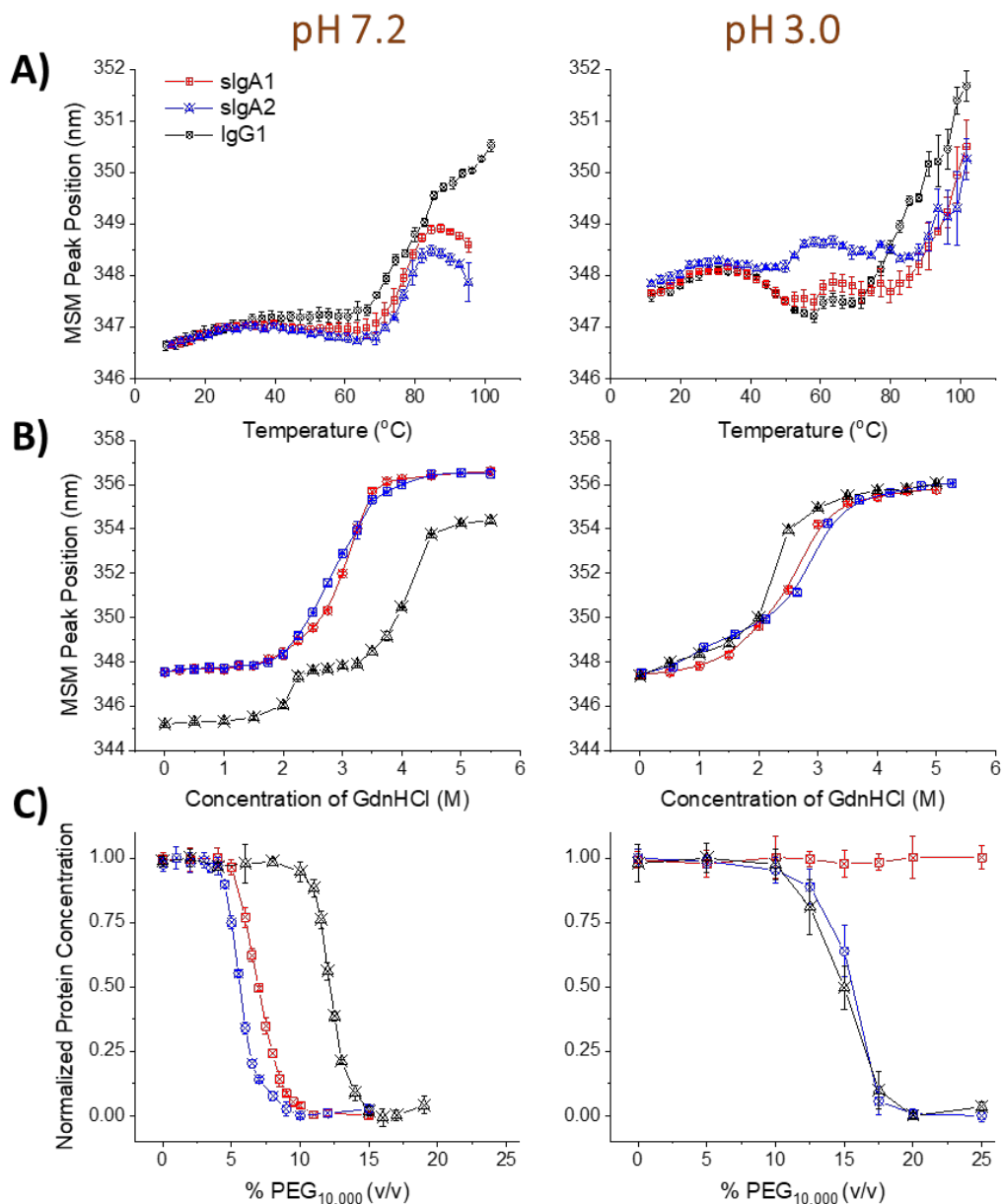


**Figure 4.10.** Comparison and rank ordering of desirable physical properties and stability profiles of sIgA1, sIgA2 and IgG1 mAbs (“relative stability indexes”) including (A) physical properties at pH 7.2, (B) physical properties at pH 3.0, and (C) relative stability after incubation at 37°C, pH 3.5 with pepsin in the *in vitro* gastric digestion model. See Figure 6 and Supplemental Figure S1 for data sets used in (A) and (B). See Figures 7-9 for data sets used to rank order mAbs in (C).





**Supplemental Figure 4.1.** Replotting of conformational stability and relative apparent solubility data sets for the three anti-LT mAbs in Figure 6 including intrinsic fluorescence peak emission maximum (MSM) values for each protein vs (A) temperature, and (B) GdnHCl concentration. (C) Relative mAb concentration in solution vs. amount of added PEG 10,000. Data sets compare and provide relative rank-ordering of the three mAbs at both pH 7.2 and 3.0 as shown in Figure 10. All data are presented as mean  $\pm$  SD;  $n = 3$ .

**Supplemental Table 4.1.** Estimation of molecular weight values of various species in solutions of the three anti-LT mAbs as determined from (A) sedimentation coefficient measurements from SV-AUC, and (B) retention time measurements from SE-HPLC (standard curve established using gel filtration molecular weight standards). Nomenclature of SV-AUC species (peaks 1-4) and SE-HPLC (peaks A-C) correspond to peaks from corresponding S values and retention times, respectively, as shown in Figure 5 (from left to right). Duplicate and triplicate measurements were performed for SV-AUC and SE-HPLC, respectively.

**A) SV-AUC**

<b>Molecule</b>		<b>Sedimentation Coefficient (Svedberges)</b>	<b>MW Estimation (kDa)</b>
<b><i>slgA1</i></b>	Peak 1	10.8	414
	Peak 2	12.9	544
	Peak 3	14.8	667
	Peak 4	16.9	817
<b><i>slgA2</i></b>	Peak 1	11.4	430
	Peak 2	15.5	686
	Peak 3	18.7	908
<b><i>IgG1</i></b>	Peak 1	6.2	149
	Peak 2	9.4	277

**B) SE-HPLC**

<b>Molecule</b>		<b>Retention Time (min)</b>	<b>MW Estimation (kDa)</b>
<b><i>slgA1</i></b>	Peak A	16.8	1032
	Peak B	18.4	441
	Peak C	21.3	95
<b><i>slgA2</i></b>	Peak A	17.5	711
	Peak B	18.5	418
	Peak C	21.4	90
<b><i>IgG1</i></b>	Peak A	8.1	833
	Peak B	10.3	340
	Peak C	12.3	151

## **Chapter 5**

Summary, Discussions, and Future Directions

## 5.1. Overview

The first major part of this Ph.D. thesis project focused on the systematic characterization of solution properties and molecular behaviors of two different human IgG1 mAbs at high protein concentrations in the absence/presence of excipients using both biophysical analytical techniques combined with HX-MS studies. Subcutaneous (SC) administration of mAb therapeutic drugs is an increasingly common and convenient route for patients to be able to do home-based treatments.<sup>1</sup> Due to small injection volume limitation, it necessitates the development of high-concentration mAb formulations, which can possess many pharmaceutical challenges during manufacturing, storage, and delivery,<sup>2,3</sup> including increasing solution viscosity and turbidity, decreasing solubility and protein physical stability, and even promoting phase separation.<sup>2,4,5</sup> Although protein engineering of mAbs by point mutations can efficiently reduce PPI propensity leading to RSA at high protein concentrations, such changes in sequence can alter other properties such as conformational stability or biological affinity to different extents.<sup>6,7</sup> As an alternative strategy, formulation approaches can significantly mitigate RSA without dramatically affecting these other desirable properties of mAbs through application of specific excipients and/or solution conditions. By understanding the predominant molecular regions of interaction and non-covalent forces responsible for IgG1 RSA, based on hydrogen exchange-mass spectrometry (HX-MS) studies, particular excipients were selected and then examined on their effects of promoting or disrupting reversible protein-protein associations at high protein concentrations.

In comparison, the second major part of this thesis project focused two different classes of immunoglobulins (secretory IgA and IgG) for potential use for passive

immunization by oral delivery to infants. The model system for this work evaluated mAbs against enterotoxigenic *Escherichia coli* (ETEC), a bacterium which is a major cause of diarrheal disease in developing countries, especially among children and infants <5.<sup>8,9</sup> The potential advantages of oral delivery to infants in the developing world not only include disease treatment, but also reduced cost, simplicity of administration and “instant protection” by localized treatment within the GI tract. One major challenge of this approach is the instability of such therapeutic mAb molecules during both oral delivery (in the digestive tract) and in solution during long-term storage.<sup>10</sup> In this work, heat labile toxin (LT) was used as the target antigen, which is one of the major virulence factors of ETEC, playing key roles of inducing water and electrolytes loss in the gastrointestinal (GI) tract of infected subjects.<sup>11,12</sup> Two main types of immunoglobulins (secretory IgA and IgG) against LT antigen were used as model therapeutic mAbs for developing analytical techniques and assessing stability (physicochemical as well as *in vitro* immunological binding) under various conditions. A combination of biochemical and biophysical methods were employed to comprehensively characterize and compare three mAbs (sIgA1, sIgA2 and IgG1) including primary structure, post translational modifications (i.e., N-linked glycans), size, higher order structural integrity, conformational stability, apparent relative solubility, and *in vitro* antigen binding activity. In this work, we also monitored and compared the stability profiles of these three mAbs using an *in vitro* oral digestion model (to mimic *in vivo* degradation conditions due to gastric acid).

## **5.2. Chapter Summaries and Future Work**

### **5.2.1. Chapter 2**

This chapter describes the solution and molecular properties of an IgG1 antibody (mAb-J) that undergoes extensive RSA, and the effects that different excipients have on altering mAb-J RSA propensity especially at high protein concentrations. Based on a previous work of mAb-J,<sup>2</sup> RSA sites and potential non-covalent interaction forces have been determined. Based on these results, five different ionic excipients, including salt (NaCl) as well as positively and negatively charged amino acids, were chosen and examined for their ability to disrupt the RSA of mAb-J driven primarily by electrostatic interactions. Among the five excipients, all of which followed a concentration-dependent pattern, Arg had the greatest effects of mitigating mAb-J RSA. All of the five additives affected mAb-J at high concentration (to varying extents) resulting in decreasing solution viscosity and opalescence, reducing mAb hydrodynamic size (increasing monomer fraction) and improving relative solubility while minimizing or even preventing phase separation. However, according to HX-MS results, a small protection was still observed at CDR L2 when comparing high vs. low protein concentrations in the presence of Arg, indicating potential residual RSA interactions involved with Fab domain. Based on the biophysical studies, such protection is potentially a signature of the difference between mAb-J dimeric and monomeric forms. Similar observations were found with Lys, but the RSA-disrupting efficiency was to a lesser extent. The other three excipients, including Glu, Asp, and NaCl, demonstrated even less efficacy on RSA disruption than positively-charged amino acids, even though they all improved mAb-J colloidal stability and solution properties. This study illustrated that although electrostatic interactions are probably the dominant force responsible for mAb-J RSA, other non-covalent forces, such as hydrophobic or dipole-dipole interactions, could also contribute to protein-protein

interactions leading to RSA of mAb-J. For example, the RSA-disrupting efficiency of Arg with mAb-J could be due to, in addition to electrostatic charge, its zwitterionic as well as chaotropic properties.

In terms of future work, although several five different ionic excipients have been studied and measured in terms of their ability to mitigate mAb-J RSA, more classes of excipients and more charge-induced self-associating mAbs could be investigated to better understand the applicability and usability of formulation strategy regarding minimization (or elimination) of RSA at high mAb protein concentration. In addition, solution pH and buffering agents also play important roles in affecting protein properties, especially the charge profile, which would be of high interest to explore in this context. Furthermore, phase separation is an important phenomenon induced by protein-protein associations at high protein concentrations, which not only can have critical biological functions inside cell, but in addition, in terms of developing protein therapeutic products, phase separation leads to notably reduced protein physical stability.<sup>13,14</sup> Therefore, it will be interesting to study protein liquid-liquid phase separation, including reversibility, solution viscosity, potential molecular mechanisms and interaction site, and effect of temperature and excipients with additional mAbs. Last but not least, long-term. real-time storage stability studies could be performed at high protein concentrations in the absence/presence of the same excipients in order to determine how such observations (of excipient effects on solution and molecular properties of mAb-J) predict the aggregation profile of over time, especially when these excipients have potential impacts on both the conformational and colloidal properties of a mAb-J protein.

### **5.2.2. Chapter 3**

In a companion study, Chapter 3 also focused on RSA of a human IgG1, but with a different mAb called mAb-C, which has been identified previously to undergo reversible self-associated by primarily intermolecular hydrophobic interactions.<sup>15</sup> Different from previous research on mAb-C performed at pH 7.0, more regions on mAb-C in this study were involved in protein-protein interactions at pH 7.5 because of probably differences in charge interactions at relatively higher pH. These regions of RSA interactions in mAb-C, consistent with previous work, are in rich of aromatic or hydrophobic amino acids, further confirming the hydrophobic interactions as the dominant force for mAb-C associations. In this work, a set of additives were selected to examine their effects on promoting or disrupting mAb-C RSA, including chaotropic, kosmotropic, and hydrophobic salts, aromatic amino acid derivative, and addition of a less polar solvent (in comparison to water). As a result, varying effects were found among these additives, where sodium sulfate promoted mAb-C RSA, while others demonstrated their ability to disrupt protein-protein interactions, albeit to notably different extents. Specifically, sodium sulfate, enhanced solution viscosity, hydrodynamic size (and fraction of oligomeric species). By HX-MS analysis, sodium sulfate induced enhanced and more extensive protections (i.e., sites of PPIs). However, in terms of relative solubility, sodium sulfate (150 mM) showed positive effects probably due to the salting-in effects, while 0.5 M of sodium sulfate decreased relative solubility likely via salting-out effects. In comparison, the other remaining additives reduced RSA propensity for mAb-C, and thus improved solution properties especially at high protein concentrations, with guanidine hydrochloride (0.5 M) showing the highest efficiency. Furthermore, in HX-MS studies, not all protected regions were disrupted in the presence of these additives, and divergent regions within mAb-C



were affected between different additives. In addition, homology modeling and patch analysis were performed in this study, showing consistent results with biophysical and analytical measurements, which further confirmed the molecular properties of mAb-C and potential RSA mechanism. Therefore, in this study, behavior of mAb-C RSA varied significantly depending on the type and amount of additives, temperature, and buffer pH.

As for possible future plans for this research, although guanidine hydrochloride had the biggest disrupting effects on mAb-C RSA, the amount used was also the highest (0.5 M). Therefore, relative efficacy of lower-amounts guanidine hydrochloride, such as 150 mM, or concentration-activity relationship would be of great interest to investigate in the future. Furthermore, additional hydrophobic salts or aromatic amino acids could be examined for their effects on both mitigating mAb-C reversible self-associations and improving solution or molecular properties. Such additional studies should lead to elucidation of some potential relationships between additive hydrophobicity and RSA-disrupting properties. In addition, unlike mAb-J, no phase separation was observed for mAb-C even with sodium sulfate in solution. As a result, knowledge of the causes and mechanisms of why RSA results in phase separation in some cases, and not in others, will provide more information for helping to better formulate and stabilize RSA-intensive mAb therapeutics. Finally, additional studies on additive-induced protein conformational and colloidal stability profiles, including for example during long-term, real-time stability studies of mAb-C, would be an important attribute to further investigate in order to assess the effect of hydrophobic additives when developing stable formulations of therapeutic protein candidates.

### **5.2.3. Chapter 4**

With the long term goal to develop a low-cost, orally delivered mAb drug product to treat ETEC-induced diarrheal disease in infants in the developing world, the work in this chapter compared two secretory IgAs (sIgAs) and an IgG1 mAbs (against the same molecular antigen) in terms of sample heterogeneity, protein primary sequence, post-translational modifications, physical stability and stability in an *in vitro* digestion model to mimic oral delivery *in vivo*. Based on the results of SDS-PAGE, SE-HPLC, and SV-AUC analyses, both sIgAs had relatively large amounts of higher molecular weight species in solution, especially sIgA2, while high monomeric content was detected for IgG1. Since such observations were found in during analysis under denaturing and non-denaturing conditions, some covalent connections such as non-native disulfide bonds, may have led to heterogeneous, oligomeric nature of the sIgA samples. Furthermore, high percentage coverage of primary sequence was found for each chain of three immunoglobulins by tryptic peptide mapping, except the heavy chain of sIgA1, which may be due to the O-linked glycosylation on the hinge region (needs to be confirmed in future work). In addition, very different amounts of total carbohydrate and N-glycan oligosaccharide composition profiles were determined for sIgAs and IgG1. Both sIgA1 and sIgA2 contained >18% (w/w) total carbohydrate and showed  $\geq 23$  various types of N-glycans on heavy chain, secretory component, and J chains. In comparison, IgG1 had ~2% (w/w) total carbohydrates with only 5 different N-linked glycan types on the heavy chain. Furthermore, higher physical stability and lower relative solubility were observed for all three mAbs at pH 7.2 vs. pH 3.0 based on the results of thermal melting, isothermal chemical denaturation, and PEG-induced precipitation assays, respectively. Comparing these three molecules, sIgA1 demonstrated the highest stability at both pHs, and sIgA2

was the second, while IgG1 displayed the least stable profile. Protease digestion stability, as measured by means of an *in vitro* gastric model, was performed on the three mAbs by three techniques, including SDS-PAGE, SE-HPLC, and ELISA, to characterize their digestion products and corresponding antigen-binding affinity. It was observed that sIgAs had relatively greater pepsin-resistant properties than IgG1, demonstrating a time course difference of 3 hours (sIgAs) vs. 5 minutes (IgG1) for complete digestion of intact proteins at low pH and 37°C. Although the major protease digestion byproduct was F(ab')<sub>2</sub> for all three mAbs, antigen-binding affinity varied notably between that coming from sIgAs or IgG1. Specifically, the F(ab')<sub>2</sub> of sIgAs were observed to bind antigen to a greater extent in comparison to that of IgG1 (needs to be further evaluated in future work). In summary, although the physicochemical and antigen binding differences in stability profile of sIgA1 and sIgA2 were not notable based on in-solution and in vitro digestion studies, both sIgA molecules displayed greater stability properties than IgG1, indicating the superiority of sIgA as potential mAb drug candidate for oral delivery.

In terms of future work, more mAbs, including additional sIgAs, IgGs, and even VHHs, targeting a different ETEC antigen such as CfaE, will be studied. For these studies, an intestinal phase *in vitro* digestion model, addition to the gastric phase model described in this work, is required and thus needs to be developed in the future to fully assess the overall *in vitro* digestion stability profile of various mAbs in the GI tract. Lead sIgA candidates will also be further studied and examined in terms of formulation development including determining the molecular mechanisms of degradation due to exposure to environmental stresses encountered manufacturing and storage as well as during oral delivery (the latter including acidic pH, elevated temperature and proteases) using a

variety of physicochemical and *in vitro* binding assays. In addition, analytical characterization methods will be used for excipient screening assays to identify specific pharmaceutical excipients that stabilize the mAbs during storage and during oral delivery. Optimized liquid formulations will therefore be not only be developed to improve the physicochemical and storage stability of sIgAs as potential drug candidates, but also for their ability to maintain the potency of these molecules during *in vivo* conditions of oral delivery.

### 5.3. References

1. Liu J, Nguyen MD, Andya JD, Shire SJ 2005. Reversible self-association increases the viscosity of a concentrated monoclonal antibody in aqueous solution. *Journal of pharmaceutical sciences* 94(9):1928-1940.
2. Arora J, Hu Y, Esfandiary R, Sathish HA, Bishop SM, Joshi SB, Middaugh CR, Volkin DB, Weis DD. *MAbs*, 2016, pp 1561-1574.
3. Arora J. 2016. Towards a greater mechanistic understanding of reversible protein-protein interactions and irreversible aggregation of IgG1 monoclonal antibodies. ed.: University of Kansas.
4. Neergaard MS, Kalonia DS, Parshad H, Nielsen AD, Møller EH, van de Weert M 2013. Viscosity of high concentration protein formulations of monoclonal antibodies of the IgG1 and IgG4 subclass– Prediction of viscosity through protein–protein interaction measurements. *European Journal of Pharmaceutical Sciences* 49(3):400-410.
5. Whitaker N, Xiong J, Pace SE, Kumar V, Middaugh CR, Joshi SB, Volkin DB 2017. A formulation development approach to identify and select stable ultra–high-concentration monoclonal antibody formulations with reduced viscosities. *Journal of pharmaceutical sciences* 106(11):3230-3241.
6. Geoghegan JC, Fleming R, Damschroder M, Bishop SM, Sathish HA, Esfandiary R. *MAbs*, 2016, pp 941-950.
7. Shan L, Mody N, Sormani P, Rosenthal KL, Damschroder MM, Esfandiary R 2018. Developability assessment of engineered monoclonal antibody variants with a complex self-association behavior using complementary analytical and in silico tools. *Molecular pharmaceutics* 15(12):5697-5710.
8. Zhang W, Sack DA 2015. Current progress in developing subunit vaccines against enterotoxigenic *Escherichia coli* (ETEC) associated diarrhea. *Clinical and Vaccine Immunology:CVI*. 00224-00215.
9. Giuntini S, Stoppato M, Sedic M, Ejemel M, Pondish JR, Wisheart D, Schiller ZA, Thomas WD, Barry EM, Cavacini LA 2018. Identification and Characterization of Human Monoclonal Antibodies for Immunoprophylaxis Against Enterotoxigenic *Escherichia coli* Infection. *Infection and immunity:IAI*. 00355-00318.
10. Wang J, Yadav V, Smart AL, Tajiri S, Basit AW 2015. Toward oral delivery of biopharmaceuticals: an assessment of the gastrointestinal stability of 17 peptide drugs. *Molecular pharmaceutics* 12(3):966-973.
11. Norton EB, Branco LM, Clements JD 2015. Evaluating the A-subunit of the heat-labile toxin (LT) as an immunogen and a protective antigen against enterotoxigenic *Escherichia coli* (ETEC). *PloS one* 10(8):e0136302.
12. Toprani VM, Sahni N, Hickey JM, Robertson GA, Middaugh CR, Joshi SB, Volkin DB 2017. Development of a candidate stabilizing formulation for bulk storage of a double mutant heat labile toxin (dmLT) protein based adjuvant. *Vaccine* 35(41):5471-5480.
13. Kastelic M, Vlachy V 2018. Theory for the Liquid–Liquid Phase Separation in Aqueous Antibody Solutions. *The Journal of Physical Chemistry B* 122(21):5400-5408.
14. Shin Y, Brangwynne CP 2017. Liquid phase condensation in cell physiology and disease. *Science* 357(6357):eaaf4382.
15. Arora J, Hickey JM, Majumdar R, Esfandiary R, Bishop SM, Samra HS, Middaugh CR, Weis DD, Volkin DB. *MAbs*, 2015, pp 525-539.